UNIVERSITY OF NAPLES FEDERICO II

Doctorate School in Molecular Medicine

Doctorate Program in
Genetics and Molecular Medicine
Coordinator: Prof. Lucio Nitsch
XXVII Cycle

Epigenetic and proteomic characterization in human morbid obesity

Valentina Capobianco

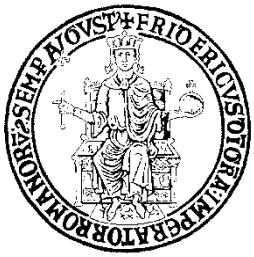

Napoli 2015

“Epigenetic and proteomic characterization in human morbid obesity”

TABLE OF CONTENTS

List of publications

1. M. Capuano; L. Iaffaldano; N. Tinto; D. Montanaro; V. Capobianco; V. Izzo; F. Tucci; G. Troncone; L. Greco; L. Sacchetti, "MicroRNA-449 overexpression reduced NOTCH1 signals and scarce goblet cells characterize the small intestine of celiac patients". PLoS One; 6(12): e29094; 2011. ISSN: 1932-6203

2. V. Capobianco; C. Nardelli; M. Ferrigno; L. Iaffaldano, V. Pilone; Pietro Forestieri; N. Zambrano; L. Sacchetti. miRNA and Protein Expression Profiles of Visceral Adipose Tissue Reveal miR-141/YWHAG and miR-520e/RAB11A as Two Potential miRNA/Protein Target Pairs Associated with Severe Obesity. J Proteome Res.; 11 (6): pp 3358–3369; 2012. ISSN: 1535-3893.

3. M. Capuano; C.M. Garcia-Herrero; N. Tinto; C. Carluccio; V. Capobianco; I. Coto; A. Cola; D. Iafusco; A. Franzese; A. Zagari; M.A. Navas; L. Sacchetti. Glucokinase (GCK) Mutations and Their Characterization in MODY2 Children of Southern Italy. PLoS One ; 7 (6): e38906; 2012. ISSN: 1932-6203.

4. C. Nardelli, G. Labruna, R. Liguori, C. Mazzaccara, M. Ferrigno, V. Capobianco, M. Pezzuti, G. Castaldo, E. Farinaro, F. Contaldo, P. Buono, L. Sacchetti, F. Pasanisi. Haplogroup T is an obesity risk factor: mitochondrial DNA haplotyping in a morbid obese population from southern Italy. Biomed Res Int., 2013; Article ID: 631082, 5 pages; 2013. ISSN: 2314-6133.

5. C. Nardelli, L. Iaffaldano, M. Ferrigno, G. Labruna, GM. Maruotti, F. Quaglia, V. Capobianco, R. Di Noto, L. Del Vecchio, P. Martinelli, L. Pastore, L. Sacchetti. Characterization and predicted role of the microRNA expression profile in amnion from obese pregnant women. Int J Obes (Lond); 2: pp.1–4; 2013. ISSN: 0307-0565

6. L. Iaffaldano, C. Nardelli, M. Raia, E. Mariotti, M. Ferrigno, F. Quaglia, G. Labruna, V. Capobianco, A. Capone, GM. Maruotti, L. Pastore, R. Di Noto, P. Martinelli, L. Sacchetti, L. Del Vecchio. High Aminopeptidase N/CD13 levels characterize human amniotic mesenchymal stem cells and drive their increased adipogenic potential in obese women. Stem Cells Dev.; 22(16): 2287-97; 2013. ISSN: 1547-32871.

Abstract

Obesity is an epidemic health problem worldwide associated with increased risk of cardiovascular disease, metabolic syndrome, and cancer. Its incidence increased in pregnant women in the last two decades as well as observed in the general population. Maternal obesity is related to offspring obesity, and there is an increased risk of adverse outcomes for both mother and child. Visceral adipose tissue (VAT) is an important risk factor for metabolic imbalance in human subjects, also during pregnancy. So, our aim was to study epigenetic regulation and proteomic signature of obesity in morbid obese women with and without pregnancy. The first aim of this study was to investigate the miRNA-expression profile and the proteomic signature in VAT from obese women to identify miRNA/protein target pairs associated with obesity. Notably, most miRNAs were down-expressed in obese tissues, whereas most of the proteins from the investigated spots were up-expressed. Bioinformatics integration of miRNA expression and proteomic data highlighted two potential miRNA/protein target pairs: miR-141/YWHAG (tyrosine 3-monooxygenase/tryptophan 5-monooxygenase activation protein, gamma polypeptide) and miR-520e/RAB11A (Ras-related protein RAB-11A); the functional interaction between these miRNAs and their target sequences on the corresponding mRNAs was confirmed by luciferase assays. Both RAB11A and YWHAG proteins are involved in glucose homeostasis; YWHAG is also involved in lipid metabolism. Hence, the identified miRNA/protein target pairs are potential players in the obese phenotype. The second aim of this study was to investigate the effects of maternal pre-pregnancy obesity in placental tissue and in human amniotic mesenchymal stem cells (hA-MSCs) from morbidly obese women to highlight differential expression patterns to correlate with the obese phenotype. The miRNA-expression profile was studied in amnion from obese and control women. Seven miRNAs were expressed only in amnion from obese women, whereas 13 miRNAs were up-expressed and 12 miRNAs down-expressed in amnion from obese women compared to controls. Target genes of these miRNAs and miRNA-regulated pathways were predicted by bioinformatics. MiRNAs significantly down-regulated the neurotrophin, cancer/ErbB, mammalian target of rapamycin, insulin, adipocytokine, actin cytoskeleton and mitogen-activated protein kinase signaling pathways. In conclusion, this study shows that the miRNA profile is altered in amnion during obesity and we hypothesize that this could affect pathways important for placental growth and function, thereby contributing to an increase in the newborn's risk of future metabolic diseases. In hA-MSCs from obese (Ob-) and non-obese (Co-) pregnant women were studied both the miRNA and

protein expression profiles to highlight differential expression patterns to correlate with the obese phenotype. Among the tested miRNAs 11 were up-expressed and 14 were down-expressed in Ob- compared to Co-hA-MSCs. Interestingly, 7 miRNAs were obesity-specific, being expressed only in Ob-hA-MSCs. Bioinformatics showed that differently expressed miRNAs significantly regulated genes belonging to several metabolic pathways, i.e. MAPK signalling, actin cytoskeleton, focal adhesion, axon guidance, insulin signaling, etc. Proteomic signature showed 40 differently expressed protein spots, 62% were increased and 38% were decreased in Ob- compared to Co-hA-MSCs. Globally, a total of 41 proteins were identified in these spots. They were involved into 5 pathways: Focal adhesion, Processing in endoplasmic reticulum, Metabolic pathways, Regulation of actin cytoskeleton, MAPK signaling. Further investigations are needed to validate proteomic data and to identify miRNA/protein target pairs in hA-MSCs. In conclusion, these data highlight in Ob-hA-MSCs altered pathways that were relevant for both metabolic function and structural integrity. Interestingly, these pathways were previously found to be altered in whole placenta or in adipose tissue from obese women, so supporting that cellular dysfunctions are present in utero during obesity and likely contribute to increase the newborns' risk for metabolic diseases in adult life.

KEYWORDS: obesity, pregnancy, visceral adipose tissue, miRNAs, 2D-DIGE

1. BACKGROUND

Obesity definition and epidemiology

Obesity is currently considered an epidemic in developed and developing countries causing a major health concern that has a priority in public health policies (Pardo et al. 2012). More than one in three adults is obese in the United States, Mexico, and New Zealand, and more than one in four in Australia, Canada, and Chile. Rates grew rapidly in some countries since the 1990s, while they grew slower in other countries. A positive note is that the overweight rate has almost stabilized in Italy in the past ten years (Figure 1). However, in Italy, more than 30% of 15-year-olds are overweight or obese (OECD obesity update, 2014). Obesity is responsible for 1% to 3% of total health expenditure in most countries (5% to 10% in the USA) (OECD obesity update, 2014). This phenomenon is worrying, since it implies an increased risk of premature death from related disease, such as diabetes, cardiovascular disease, and certain forms of cancer (Pardo et al. 2012). A growing number of countries have adopted policies to prevent obesity from spreading further (OECD obesity update. 2014).

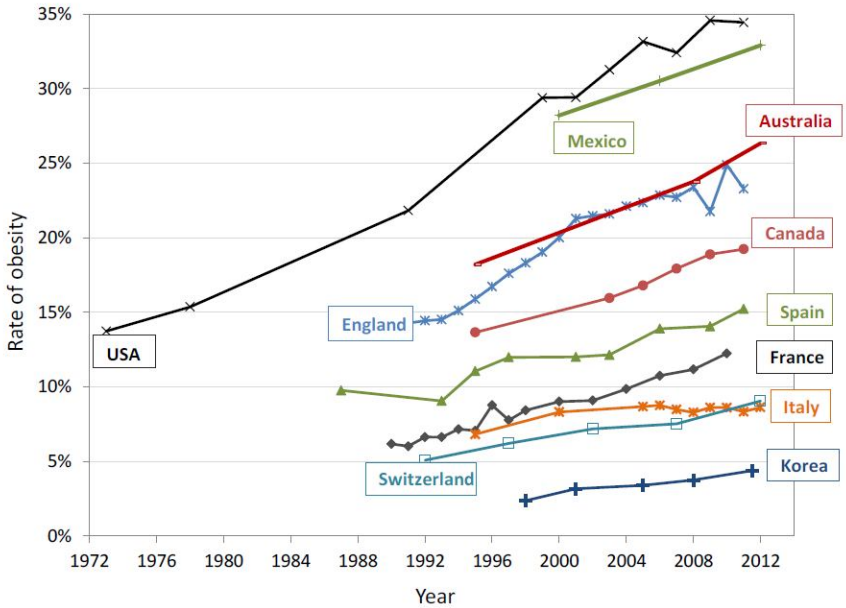

Figure 1. Obesity rates. Since 1990s rates grew rapidly in Australia, England and United States, while in other countries they grew slowly (from OECD obesity update 2014).

Obesity insurgence is characterized by an increased body weight due to an altered imbalance between energy intake and energy expenditure. The energy balance is regulated by a physiological complex, including afferent and efferent signals to the central nervous system (Woods and D'Alessio 2008). The signals coming from the periphery are constituted by gastrointestinal

hormones (ghrelin, GLP-1, Peptide Y, cholecystokinin, pancreatic polypeptide, etc.), and peptidic products released from adipose tissue and hormones, such as insulin, produced by other tissues.

One of the major players in body weight regulation is leptin. This protein was the first to be identified among a long series of products secreted by adipose tissue that today is considered a true endocrine organ. The molecules synthesized and secreted by adipose tissue are called 'adipokines'. Different cell types contribute to the secretion of these molecules; for example, a considerable number of adipokines related to inflammation was found in the vascular-stromal fraction and in the matrix of adipose tissue, which is rich in cells of the immune system.

Leptin produces the major peripheral signals that regulate the sense of satiety by acting on the melanocortin circuit. Leptin acts through its receptors (ObRb) in two different subpopulations of neurons in the arcuate nucleus. One of this expresses both orexigenic neuropeptides: Neuripeptide Y (NPY) and Agouti Related Protein (AgRP), whose expression is reduced by leptin (Schwartz et al. 2000); the other population expresses both anorexigenic neuropeptides: Cocaine and Amphetamine Related Transcript (CART) and α-melanocyte stimulating hormone (α-MSH), derived from the proteolytic processing of the POMC gene (pro-opiomelanocortin), operated by enzymes pro-convertasi (PC1 and PC2). The expression of POMC is induced by leptin (Schwartz et al. 2000). AgRP and α-MSH compete, at hypothalamic level, to binding to melanocortin receptors (MC-Rs), in particular for subtype 4 (MC4R). Under normal conditions, the interaction between the central circuits and peripheral signals produces a coordinated response to any change in nutritional status. Generally, monogenic obesity in humans is associated with mutations in POMC, PC1, PC2, and MC4R genes (Bellisari 2008, Chen and Garg 1999, Farooqi et al. 2000, Krude et al. 1998, Raffin-Sanson et al. 2003, Echwald et al. 1999, Challis et al. 2002, Miraglia del Giudice et al. 2001). These observations suggest that this pathway is important for energy homeostasis and that it is strictly regulated. In parallel, leptin also acts on the central nervous system, by inducing release of noradrenaline. Noradrenaline exerts its action on adipose tissue by binding to β3-adrenergic receptors, activating lipolysis and thermogenesis in the adipose tissue. The latter mechanism is responsible for the increase in energy expenditure.

Serum leptin concentration and its expression in adipose tissue are directly proportional to the levels of adiposity and changes in body weight, making the hormone a good indicator of the deposits of fat in the body (Vázquez-Vela et al. 2008).

Adiponectin is another protein secreted from adipose tissue. It is a protein of 30 kDa secreted by adipocytes whose circulating levels are decreased in presence of obesity and insulin resistance. Adiponectin is present in the blood in different isoforms: trimeric (low-molecular weight LMW), hexameric (two homotrimers), and multimeric (from 12 to 18 monomers, high molecular weight-HMW) which have different biological functions. The HMW

form has an insulin-sensitizing effect, while the LMW form exerts its effects centrally (Galic et al. 2010).

Adiponectin binds to its receptors ubiquitously expressed, AdipoR1 and AdipoR2, so activating AMP dependent kinase. The first receptor is expressed primarily in skeletal muscle, the second is more expressed in the liver, both are also present in the hypothalamus where they co-localize with the leptin receptor. In hypothalamus, adiponectin has opposite effects to leptin, through the activation of orexigenic genes and the silencing of anorexigenic ones. At the peripheral level, the adiponectin is involved in the phosphorylation of the insulin receptor and its substrate, a necessary mechanism for the translocation of GLUT4 transporter to the cell membrane of muscles and liver (Vázquez-Vela et al. 2008). In humans, adiponectin levels inversely correlate with insulin resistance and the metabolic syndrome and are also decreased in the presence of obesity. Adiponectin also counteracts the effects of TNF-α (Tumor necrosis factor-α), a pro-inflammatory molecule, inhibiting the expression of adhesion molecules in endothelial cells, thereby diminishing the atherogenic risk (Galic et al. 2010).

The grade of obesity is evaluated by the body mass index (BMI), defined as the weight in kilograms divided by the height in square meters (kg/m^2). It is the most used index from the World Health Organization (WHO). This classification provides that a person is overweight when the BMI is greater or equal to 25 and obese when the BMI is greater or equal to 30 (WHO. Fact sheet No 311. 2011). BMI is a strong predictor of overall mortality; above the optimum BMI range of about 22.5–25 kg/m^2 the progressive excess mortality is due to vascular disease (Huda et al. 2010; Lievense et al. 2002).

Obesity is a multifactorial disease that involves interactions between environmental and genetic factors. Studies of families, twins, and adopted children, indicate that obesity is in part heritable (Miller et al. 2004). Monogenic form of obesity results from mutations in genes involved in the central pathways of food intake regulation, such as leptin and POMC (pro-opiomelanocortin) genes (Clement and Ferrè 2003). These cases are few exceptions because obesity is a complex disease, and inter-individual variations of this phenotype are due to the action of multiple genes and environmental factors (Bellisari et al. 2008). The environmental/behavioral component is believed to affect the etiopathogenesis of obesity for the 60-70%, while the remaining 30-40% is due to alteration in the genetic counterpart. Studies in children and adolescents showed that the obesity insurgence is mostly the result of periods if overfeeding rather than a defect in basal energy expenditure (Clement and Ferrè 2003). While stored fat served as an energy reservoir during times of famine, in the modern commercialized world of continuous and ubiquitous food abundance and persistent physical inactivity, the energy conserving function of these genes has become a liability by promoting continuous fat storage (Bellisari et al. 2008).

Adipose tissues

In mammals, it is possible recognize two distinct adipose tissues: white adipose tissue (White Adipose Tissue, WAT) and brown adipose tissue (Brown Adipose Tissue, BAT).

WAT contains adipocytes characterized by the presence within the cell cytoplasm a single large vacuole of lipids, which occupies about 80% of the cell volume, confining the nucleus and the other organelles to the periphery of the cell. BAT instead contains adipocytes characterized by the presence within cells of numerous lipid droplets of small size and several mitochondria.

WAT contains in addition to mature adipocytes, several multipotent mesenchymal stem cells (MSCs) and pre-adipocytes. The increase of the deposits of triglycerides (TG), in conditions of positive caloric balance, produces a hypertrophy of the adipose cell. When these cells reach a critical volume, the differentiation of mesenchymal cells is subsequently stimulated (adipogenesis). Adipocyte differentiation is an important component of hyperplasia of adipose tissue (Vázquez-Vela et al. 2008). WAT has key functions in the control of the metabolism through energy homeostasis, adipocyte differentiation, and insulin sensitivity. Besides, it affects inflammation, through a control mechanism mediated by anti-inflammatory molecules and the activation of anti-inflammatory metabolic and immune pathways (Balistreri et al. 2010).

BAT provides energy expenditure from non-oxidative phosphorylation in form of heat largely for cold adaptation. The uncoupling of phosphorylation in BAT is due to the activity of uncoupling protein-1, expressed on the internal mitochondrial membrane, which by creating a proton leak exhausts the electrochemical gradient needed for oxidative phosphorylation. As consequence, BAT affects energy use by producing heat from uncoupled oxidative phosphorylation (Balistreri et al.2010).

Based on the localization of WAT, it is possible to identify a subcutaneous adipose tissue (SAT) and a visceral adipose tissue (VAT).

SAT deposits cover the whole body surface: in women they are particularly developed in gluteal-femoral region and breast, while in men they are present mainly in the abdomen and around the muscles of the limbs. VAT is largely localized in the mesenteric and omental regions, while smaller deposits are also present in the epicardial region and in the mediastinum. VAT represents up to 10−20% of total fat in men and 5−8% in females. In both genders, the amount of visceral fat increases with age (Ibrhaim 2010).

The risk of morbidity associated with obesity is related more to body fat distribution rather than total body fat. Fat accumulated in VAT is the major risk factor for obesity-related disorders. Because of its anatomical position, visceral fat venous blood is drained directly to the liver through the portal vein. This characteristic allows the direct access of the free fatty acids and adipokines

released from fat to the liver. Adipokines activate hepatic immune mechanisms with production of inflammatory mediators such as C-reactive protein (CRP).
There are biological differences between VAT and SAT. In fact, compared with SAT, VAT contains more large and insulin-resistant adipocytes and inflammatory cells such as macrophages that secrete pro-inflammatory cytokines (TNF-α, IL-6, and CRP). Visceral adipocytes are more metabolically active and have a greater lipolytic activity than SAT adipocytes. VAT is more sensible to the catecholamine-induced lipolysis and less to the anti-lipolytic action of insulin. VAT shows a higher insulin-stimulated glucose uptake compared with SAT (Ibrhaim 2010).

In addition, adipose tissues show selective gene expression patterns. Characterization of differences in gene expression between human subcutaneous adipose tissue and visceral adipose tissue also suggest genetic developmental heterogeneity. Particularly, they show different expression of genes involved in embryonic development that could play potentially important roles in adipocyte development and fat distribution (Gesta et al. 2006).

Obesity in pregnancy

The prevalence of obesity in women of child-bearing age (20-34 years old) has reached 28.6% in the United States population and continues to increase (Ma et al. 2010).

Maternal obesity is associated with adverse consequences, both in mother and child (Catalano et al. 2007, Huda et al. 2010) because obesity and pregnancy are independently associated with insulin resistance and inflammation status, which may be exacerbated when combined.

All women increase maternal fat stores during pregnancy irrespective of pre-pregnancy adiposity. Obese women, who have more saturated subcutaneous fat stores, accumulate fat more centrally than lean women. This visceral adiposity appears correlated more strongly to adverse metabolic outcomes in pregnancy including gestational diabetes mellitus, gestational hypertension, and preeclampsia (Huda et al. 2010; Bartha et al. 2007).

Maternal obesity is also accompanied by alterations in glucose metabolism and by perturbation in inflammatory markers, adipokines, and vascular dysfunction.

In normal pregnancies, insulin secretion increases, while insulin sensitivity is unchanged to facilitate provision of fuel substrate for the fetus. The ability of insulin to suppress lipolysis is also reduced during late pregnancy, contributing to greater postprandial increases in free fatty acids, increased gluconeogenesis, and insulin-resistance (IR). Obese women are four times more likely to develop gestational diabetes mellitus than lean women, because they have a loss of the reduction in fasting glucose in early pregnancy and significant enhancement of peripheral and hepatic IR. In this mechanism are potentially implicated the release of inflammatory mediators, such as TNF-α, the low release of adiponectin, an insulin-sensitizing hormone, and reduction in the lipogenic

transcription factor peroxisome proliferator activated receptor-γ (PPAR-γ) resulting in reduced adipose tissue insulin sensitivity and increased lipolysis (Huda et al. 2010).

Recently reports showed that at birth, term infants of overweight and obese women have increased fat mass in comparison with those of lean weight women (Sewell et al. 2006). The fetuses of the obese mothers were more insulin resistant than the fetuses of lean mothers and there was also a positive correlation between foetal insulin resistance and foetal adiposity (Catalano et al, 2009). Moreover, the risk of childhood obesity is quadrupled if the mother was obese before pregnancy, which suggests that the in utero environment is obesogenic (Li et al. 2005). The mechanisms whereby maternal obesity and nutrient excess in utero increased risk for future metabolic disease are poorly understood, but likely include changes in foetal nutrient supply in combination with genetic and epigenetic mechanism. The in utero environment can modify the gene expression of foetal genome and exerts stimulatory and inhibitory effects on foetal growth and adiposity (Heerwagen et al. 2010). The primary mechanisms that could contribute to foetal programming of obesity are neuronal regulation of appetite and food intake, adipose tissue physiology, and inflammation (Figure 2).

During fetus development, the nucleus accumbens and the hypothalamus are the two areas in the brain established to link maternal diet and offspring feeding behavior. Animal studies showed that maternal obesity affects the expression of hypothalamic neuropeptides in offspring and also disrupts the development of hypothalamic neural projections important for the regulation of energy homeostasis. However additional research is needed to elucidate these mechanisms (Sen et al. 2012).

Maternal over-nutrition affects the expression of genes involved in adipogenesis, particularly PPAR-γ and AMP-activated protein kinase (AMPK). PPAR-γ is a transcription factor that enhances the adipocyte differentiation; AMPK is a key enzyme in biosynthesis of fatty acids and represses the transcriptional activity of PPAR-γ. Animal studies showed that in adipose tissue from rats and sheep of obese mothers, PPAR-γ is increased and AMPK activity is repressed. These evidences suggest a role of PPAR-γ and AMPK in the increased adiposity reported in offspring of obese mother.

The inflammatory state of obese mothers could contribute to greater offspring adiposity as showed in studies on pregnant rats treated with TNF-α and IL-6. Body weight and fat mass were increased in their offspring respect to control animals. Maternal obesity also induces macrophage accumulation and increased inflammatory cytokine expression in placenta. The role of these inflammatory mediators in the programming of obesity is not fully understood and remains to be established how the in utero environment induces long term changes predisposing the offspring of obesity (Sen et al. 2012).

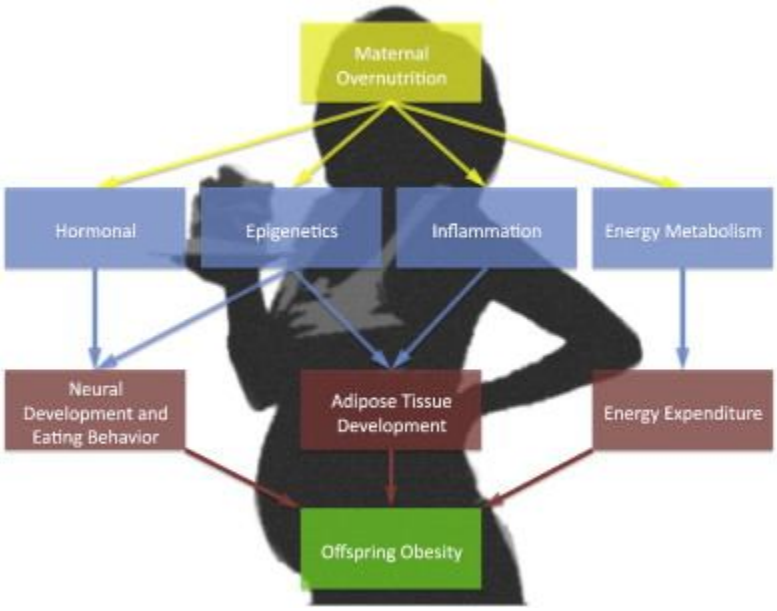

Figure 2. Mechanisms involved in transgestational obesity. The molecular mechanisms that contribute to in utero programming of obesity are complex and not yet fully understood. The primary mechanisms are neuronal regulation of appetite and food intake, adipose tissue physiology, altered energy metabolism and inflammation (from Sen et al. 2012).

Epigenetics: MicroRNAs

The term epigenetic refers to heritable changes in gene expression that cannot be explained by changes in DNA sequence. There is evidence on the impact of different nutrients, environmental compounds, and metabolic situations on the epigenome. Recently studies demonstrated that maternal undernutrition and overnutrition can alter the foetal epigenome.

As epigenetic changes are modulated by environmental exposures, epigenetics is considered the interface between genetics and the environment. In this sense, only environmental factors, including nutritional habits are able to explain the phenotypical and epigenetic differences reported in monozygotic twins. In fact, epigenetic mechanisms are good candidates for explaining the role of the diet and other environmental conditions of parents and grandparents, or the influence of perinatal dietary exposures as determinants of later health outcomes. Altered epigenetic marks are extensively studied in cancer and in chronic non-communicable metabolic diseases such as obesity, diabetes and cardiovascular diseases (Milagro et al. 2013).

Epigenetic processes play a crucial role in determining when and where specific genes are expressed. Alteration in these mechanisms could lead to profound changes in phenotype. The principal epigenetic mechanisms are: DNA methylation, histone modification, and microRNAs (miRNAs).

A common modification in mammalian genomes is the methylation at the 5’ position of cytosine in DNA CpG dinucleotide. Hypermethylation of these regions is associated with transcriptional repression, whereas their

hypomethylation is associated with transcriptional activation. DNA methylation is a stable epigenetic mark that is transmitted through DNA replication and cell division.

Histone modification, such as acetylation, methylation, phosphorylation, occurs by histone-modifying enzymes that acts on amino acid residues in the histone N-terminals.

Acetylation of histones is generally associated with active gene transcription. Consequently, removal of acetyl group from a histone residue by histone deacetylases (HDACs) represses gene transcription. The precise mode of action of the modified histone tails is not yet known. However, positive charges of lysine tails are neutralized by acetylation causing the attraction between DNA and histones resulting in opening of chromatin structure. An alternative hypothesis to the functionality of histone tail modifications is that specific proteins recognize and interact with the histone modifications. Other modifications of histones, such as methylation, can be either activating or repressing depending on degree of modification and specific site of the modification (Milagro et al. 2013).

Among the known epigenetic mechanisms, microRNAs have recently emerged as an important class mRNA expression regulators. MiRNAs are found in all multicellular organisms, from plants to humans, and in many instances are highly conserved through evolution. For this reason, they are likely to be important for normal cellular function.

MiRNAs have a peculiar biogenesis (Figure 3) a primary miRNA of several thousands of bases long is transcribed by RNA polymerase II, which is cleaved in the nucleus by a protein complex containing the enzyme Drosha to give a precursor miRNA of around 70 nucleotides in a stem-loop structure. This is then transported into the cytoplasm and further processed by the enzyme Dicer to give a short double-stranded miRNA complex, which contains the mature miRNA strand and a passenger strand (miRNA*), which is normally degraded. The mature miRNA is incorporated the RNA-induced silencing complex (miRISC) by associating with the Argonaute subfamily. In this complex, the mature miRNA is able to regulate gene expression, binding through partial complementary generally, for the most part to the 3'-untranslated region (3'-UTR) of target mRNAs, and leading at the same time to some degree of mRNA degradation and translation inhibition (Inui et al. 2010). The most stringent requirement for this interaction is a contiguous and perfect Watson-Crick basepairing of the miRNA 5'nucleotides 2-8, representing the "seed region" nucleating the interaction (Rottiers and Naar 2012).

MiRNAs are likely to be predominantly fine tuners of gene expression, but there is some evidence that on reaching a critical threshold, they may highly repress protein production, and in so doing act as 'switches'.

Each miRNA may fine-tune the expression of hundreds or even thousands of proteins, and it is estimated that over 60% of mammalian mRNAs are conserved targets for miRNAs. Additionally, each mRNA may be targeted

by many miRNAs. This system therefore potentially has enormous regulatory capacity, but also possesses a complexity that can make it difficult to clarify.

MiRNAs act as node of signaling networks essential for wide array of biological processes involved in regulation of a variety of biological processes, including appetite regulation, adipocyte differentiation, and insulin secretion (Heneghan et al. 2010; Ortega et al. 2010).

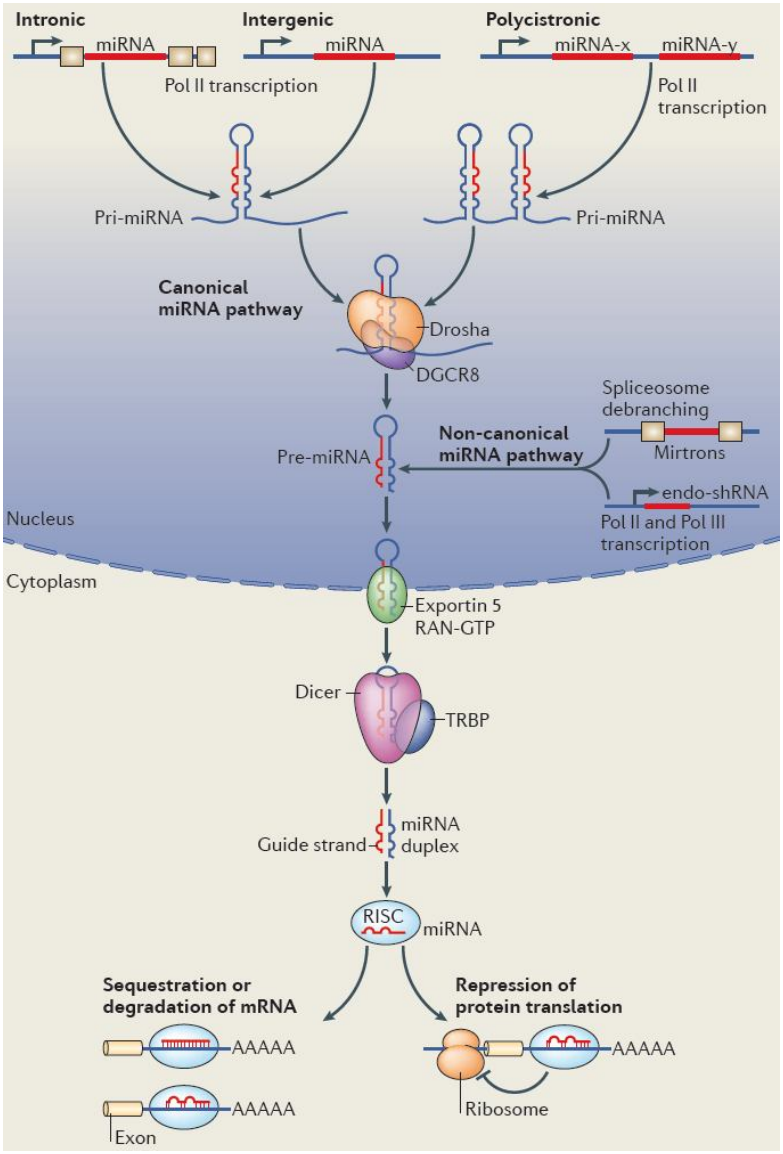

Figure 3. Biogenesis of microRNAs. MicroRNAs (miRNAs) are transcribed as precursor RNAs from intergenic, intronic or polycistronic genomic loci by RNA polymerase II (Pol II). The primary miRNA (pri-miRNA) transcript forms a stem–loop structure that is recognized and processed by the Drosha/DGCR8 complex or the spliceosome in the nucleus. The precursor (pre-miRNA) hairpins from both canonical and non-canonical miRNA pathways are then transported by an exportin 5 and RAN-GTP-dependent process to the cytosol, where they are processed by the Dicer/TRBP RNase III enzyme complex to form the mature double-stranded ~22‑nucleotide miRNA. Argonaute proteins unwind the miRNA duplex and facilitate incorporation of the miRNA-targeting strand into the AGO-containing RNA-induced silencing complex (RISC). The RISC–miRNA assembly is then guided to specific target sequences in mRNAs (Image from Mol Cell Biol 2012).

Placenta

The placenta is generally recognized for important functions such as nutrition, respiration, and excretion as well as maintenance of feto-maternal tolerance. It maintains foetal homeostasis by carrying out a wide range of physiological functions. Therefore, placental perturbations, by affecting one or more aspects of placental structure and function, may determine long-term health outcomes into adulthood (Murphy et al. 2010). For example, placental weight correlates with foetal weight, and since foetal growth is related to adult outcomes, placental weight and low birth weight could predict adult diseases as obesity, diabetes 2, and hypertension (Barker 2005, Godfrey 2002, Osmond and Barker 2000, Lewis et al. 2006). In addition, changes in placental structure (thicker placental exchange barrier and increased placental vascular resistance) are directly involved in the foetal programming of cardiovascular diseases (Thornburg and Louey 2010). The placenta could act as a nutrient sensor, in fact it could modify nutrient and hormone availability to foeto-placental tissues in relation to environmental conditions in a manner that maximizes foetal growth (Jansson and Powell 2007).

The term *placenta* is discoid in shape with a diameter of 15–20 cm and a thickness of 2–3 cm. From the margins of chorionic disc extend the foetal membrane, amnion and chorion, and the endometrial decidua (Parolini et al. 2008). The foetal component includes the amniotic and chorionic foetal membranes which separates fetus from the endometrium, enclosing the fetus in the amniotic cavity. The amnio-chorionic membrane forms the outer limits of the sac that encloses the foetus, while the innermost layer of the sac is the amniotic membrane (AM). The AM thickness varies from 0.02 mm to 0.5 mm and consists of an epithelial monolayer, a thick basement membrane, and an avascular stroma (Figure 4).

The layer nearest to the foetus is the amniotic epithelium and consists of a single layer of cells uniformly arranged on the basement membrane. The basement membrane is one of the thickest membranes found in all human tissue. The support provided to the foetus by the basement membrane throughout gestation stands testimony to the structural integrity of this remarkable membrane. The compact layer of stromal matrix adjacent to the basement membrane forms the main fibrous skeleton of the AM. The collagens of the compact layer are secreted by mesenchymal cells situated in the fibroblast layer. Interstitial collagens (types I and III) predominate and form parallel bundles that maintain the mechanical integrity of AM. Collagens type V and VI form filamentous connections between interstitial collagens and the epithelial basement membrane. The intermediate layer (spongy layer or zona spongiosa) of the stromal matrix sits adjacent to the chorionic membrane. Its abundant content of proteoglycans and glycoproteins produces a spongy appearance in histologic preparations, and it contains a non fibrillar meshwork of mostly type III collagen. The spongy layer is loosely connected to the

chorionic membrane; hence, the AM is easily separated from the chorion by means of blunt dissection. AM is not just a simple avascular structure (no blood vessels or nerves); it has multiple metabolic functions, such as the transport by diffusion out of the amniotic fluid and/or from the underlining decidua of water and soluble materials and the production of bioactive factors, including vasoactive peptides, growth factors, and cytokines. The AM provides protection to the developing embryo against desiccation and an environment of suspension, in which the embryo can grow free from pressures of the structures that surround its body (NiKnejad et al. 2008). Foetal membranes facilitate gas and waste exchange and play a critical role as defensive barriers. AM also has an important role during birth, because the substances produced by the epithelium of AM allow the initiation and maintenance of uterine contractility.

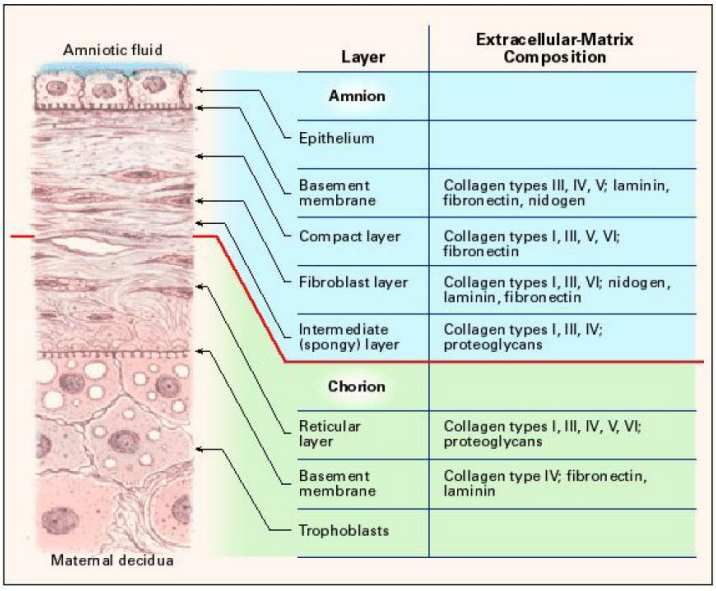

Figure 4. Structure of foetal membrane at term. Amniotic membrane consists of a foetal (chorion plate) and maternal (deciduas) component. In the figure are reported the extracellular matrix component of each layer (from NiKnejad et al. 2008).

Amniotic mesenchymal stem cells (hA-MSCs)

Human placenta draws great interest because represent a reserve of stem cells. Current source of stem cells are embryonic stem cells and adult type stem cells, but these pose many ethically and technically problems. The use of placenta as source of mesenchymal stem cell does not raise ethical problems and also has many advantages, as placenta is a tissue readily available, easily accessible, large number of cells can be isolated from the membranes (Mihu et al. 2009). The plasticity, self-renewal, and multi-lineage potential of mesenchymal stem cells have generated growing interest in their use in a constantly expanding variety of experimental regenerative applications (Klein and Fauza 2011). Four regions of placenta can be distinguished: amniotic epithelial, amniotic mesenchymal, chorionic mesenchymal, and chorionic

trophoblastic. From each region, different cell populations are isolated: from the amniotic mesenchymal region of foetal placenta are isolated: human amniotic mesenchymal stromal cells (hA-MSC) (Parolini et al. 2008). Cells from each layer demonstrate variable plasticity. Because of their plasticity, the term *stem cell* has been used in the literature to describe a number of cells isolated from placenta. Self- renewal and "hierarchy", which are normally considered a hallmark of stem cells, have not been clearly demonstrated in the different placenta derived cell types, and therefore the term "stem cell" at this time is not always appropriate. However, it may be interesting to mention that recent reports propose an alternative stem cell concept whereby plasticity is essential to define stemness, and self-renewal and hierarchy are optional characteristics (Parolini et al. 2008). According to criteria recently proposed by Dominici et al. for bone marrow-derived mesenchymal stromal cells (Parolini et al. 2008), mesenchymal cells isolated from foetal membranes should be termed *mesenchymal stromal cells* (hA-MSC). Minimal criteria for defining hA-MSCs are the following:

- Adherence to plastic;
- Formation of fibroblast colony-forming units;
- A particular pattern of surface antigen expression;
- Capacity to differentiate in more lineages, such as osteogenic, adipogenic, chondrogenic, and vascular/endhotelial;
- Foetal origin.

The hA-MSCs are isolated from the mesoderm of the amnion; the isolation is generally performed from term amnion dissected from the deflected part of the foetal membrane to minimize the presence of maternal cells. The surface markers expressed by hA-MSC are specific markers for mesehncymal stem cells such as CD90, CD29, CD105, CD73, CD49e, but they don't express hematopoietic (CD45 and CD34) and monocyte markers (CD14) (Parolini et al. 2008). Mihu and colleagues had characterized them phenotipically and genotipically. They have observed that hA-MSC expressed Oct-3/4, SSEA-4, Nanog and Sox-2. Oct-3/4 and Nanog are markers of pluripotency and self-regeneration capacity and they are essential in the formation of internal cell mass. SSEA-4 is a glycoprotein expressed in early embryonic development and it plays a role in maintenance of the non-differentiation state of stem cells. Another important characteristic, with crucial implication in the immunological tolerance of maternal organism towards the foetal organism, is the absence of HLA-DRα transcript (Mihu et al. 2009).

2. AIMS OF THE STUDY

Etiopathogenesis of obesity is still poorly known, thus, recent evidence suggests that epigenetic mechanisms could play a key role in its insurgence. Our aim was to study both epigenetic regulation and proteomic signature of VAT and foetal component of placenta in morbid obese women, in order to identify different metabolic pattern compared to control women.

Particularly, the first aim of this study was to investigate miRNA and protein signatures in VAT from obese women, to identify metabolic pathways miRNA-regulated during obesity. For this purpose, the objectives are:

1) To identify differently expressed miRNAs in VAT from obese patients compared with non-obese patients and to find predicted targets using bioinformatic tools;

2) To identify differently expressed proteins in VAT from obese patients compared with non-obese patients using 2D-DIGE (Two-Dimensional Fluorescence Difference Gel Electrophoresis) followed by tandem mass spectrometry;

3) To integrate data obtained by transcriptomic and proteomic approaches, to highlight miRNA-regulated proteins.

The second aim of this research project is to investigate, the role of epigenetic mechanisms of gene regulation in obese pregnant women, as risk factors in foetal programming of obesity. For this purpose, the objectives are the following:

1) To identify differently expressed miRNAs in amnion from obese pregnant women compared with non-obese pregnant women and to find predicted targets using bioinformatics;

2) To identify metabolic pathways that could be silenced or switched on by a miRNA-mediated mechanism (using bioinformatics);

3) To identify differently expressed miRNAs in Ob-hA-MSCs compared with Co-hA-MSCs and to find predicted targets using bioinformatic tools;

4) To identify differently expressed proteins in Ob-hA-MSCs compared to CO-hA-MSCs using 2D-DIGE (Two-Dimensional Fluorescence Difference Gel Electrophoresis) followed by tandem mass spectrometry.

3. MATERIALS AND METHODS

Obese women

Fifteen obese women (age range: 19−65 years old, BMI [mean ±SEM] 42.2 ± 1.6 kg/m^2) and ten non-obese women (age range: 19−57 years old, BMI [mean ± SEM] 23.7 ± 1.2 kg/m^2) were enrolled in the study. During surgery (gastric banding or laparoscopic cholecystectomy for obese and non-obese women, respectively), VAT biopsy samples were collected and frozen in liquid nitrogen until their use. The main anamnestic, clinical, and general characteristics of the enrolled subjects were recorded at admission. The day before surgery, a fasted blood sample was collected from all subjects and tested for the main biochemical parameters (glucose, cholesterol, triglycerides, AST, ALT, ALP, GGT) by routine methods. Written informed consent was obtained from all recruited subjects, and the study was approved by the Ethics Committee of the Faculty of Medicine of the "Federico II" University of Naples (Italy) .

Obese pregnant women

Sixteen obese (age range: 26–39 years old) and seven control pregnant women (age range: 26–38 years old), pre-pregnancy BMI (mean/SEM) 40.3/1.8 kg/m^2 and 22.4/1.0 kg/m^2, respectively) have been recruited at the Dipartimento of Neuroscienze and Scienze Riproduttive and Odontostomatologiche, University of Naples Federico II. The exclusion criteria were neoplasia, viral infection, diabetes, and drug assumption. The clinical, personal, and family histories of the twenty three women were recorded during a medical interview conducted by an expert upon hospitalization. Data relative to each pregnancy follow-up and delivery were also recorded. The general characteristics of the newborn and clinical data (birth weight, length, head circumference, Apgar score) were recorded at birth. All patients and controls gave their informed consent to the study and both parents gave consent for their newborns. The study was performed according to the Helsinki II Declaration and was approved by the Ethics Committee of our Faculty. Two fasting peripheral blood samples were collected at delivery from all enrolled pregnant women. One blood sample was used for DNA extraction, whereas the other was centrifuged at 2,500 rpm for 15 min was stored at -80°C until processing. At delivery, placentas were collected by C-section from each enrolled women and immediately processed.

Biochemical evaluations

The main serum biochemical parameters were evaluated by routine assays. Leptin and adiponectin were measured in maternal serum and in cord plasma with Luminex xMAP Technology on a BioRad Multiplex Suspension Array System (Bio-Rad, Hemel Hempstead, Herts., UK), in compliance with

the manufacturer's instructions. The ratio leptin/adiponectin (L/A) was also calculated.

Cell isolation from placenta tissue

Placentas were collected and immediately processed, following Parolini et al. After removal of the maternal decidua, the amnion was manually separated from the chorion and extensively washed 5 times in 40 mL of phosphate-buffered saline (PBS) containing 100 U/mL penicillin, 100 μg/mL streptomycin and 250 μg/mL amphotericin B (all from Sigma-Aldrich) after which it was mechanically minced into small pieces (Parolini et al. 2008). Amnion fragments were digested overnight at 4°C in ACCUMAX® reagent (Innovative Cell Technology, San Diego), a combination of DNase, protease, and collagenolytic enzymes, containing 100 U/mL penicillin, 100 μg/mL streptomycin, and 250 μg/mL amphotericin B. The next day, digestion enzymes were inactivated with complete culture medium constituted by low glucose D-MEM (Sigma-Aldrich) supplemented with 10% of heat-inactivated bovine serum (FBS), 1% of non-essential amino acids and 2% of Ultraglutamine (all from Lonza, Basel, Switzerland). After centrifugation at 300g for 10 min, cell pellets and digested tissue fragments were seeded in a cell culture dish (BD Falcon, New York) in complete culture medium and incubated at 37°C in 5% CO2. One week later, digested tissue pieces were removed from the dish and discarded, and isolated cells formed distinct fibroblast colony-forming units. When the colonies reached 70% confluence, they were washed with PBS and detached with trypsin/EDTA (Sigma-Aldrich), counted, and reseeded in complete medium for expansion at a concentration of about 5,000/cm2 (Parolini et al. 2008).

Cell preparation

hA-MSCs were expanded for several passages. Absence of mycoplasma contamination was assessed as described previously (Mariotti et al. 2008). The population-doubling level was calculated for each subcultivation with the following equation: population doubling= [log10 (NH) ─ log10 (NI)]/ log10 (2), where NI is the cell inoculum number and NH is cell harvest number (Bieback et al. 2004). The increase in population doubling was added to the population doubling levels of the previous passages, to yield the cumulative population doubling level. When 70%-80% confluent cultures had reached about 4 population doublings, they were detached with trypsin/EDTA, resuspended in PBS with 10% FBS, and processed for flow cytometry, and DNA, RNA, and protein extraction. Cellular viability was assessed by both Trypan blue dye exclusion and the analysis of light scatter proprieties in flow cytometry, and it was never lower than 90%.

DNA typing

The foetal origin of both amnion and hA-MSCs was verified by DNA typing. Genomic DNA was extracted from the mother's peripheral blood, from amnion samples and from hA-MSCs using the Nucleon BACC2 extraction kit (Illustra DNA Extraction Kit BACC2, GE Healthcare, Calfont St. Giles, Bucks, UK). DNA concentration was evaluated using the NanoDrop® ND-1000 UV-Vis spectrophotometer (NanoDrop Technologies, Wilmington, DE). Genomic DNA (1 ng) was amplified in a final volume of 25 µL using the AmpFlSTR® Identifiler™ PCR Amplification Kit (Applied Biosystems, Foster City). The AmpFlSTR® Identifiler™ PCR Amplification Kit is a short tandem repeat (STR) multiplex assay that amplifies 15 repeat loci and the Amelogenin gender determining marker in a single PCR amplification using a primer set labeled with four fluorescent molecules. The amplification was performed with the GeneAmp PCR System 9700 (Applied Biosystems) instrument. PCR products were then analyzed by capillary electrophoresis on the ABI Prism 3130 Genetic Analyzer (Applied Biosystems) together with an allelic ladder,which contained all the most common alleles for the analyzed loci that were present in Caucasian populations and both a negative- and a positive-quality control sample. Typically, 1µL of each sample was diluted in 18.7µL of deionized formamide; each sample was supplemented with 0.3µL of an internal size standard (LIZ 500 Applied Biosystems) labeled with an additional fluorophore. The samples were denatured at 95 °C for 4 min and then placed in the auto sampler tray (maximum of 96 samples) on the ABI Prism 3130 for automatic injection in the capillaries. The data were analyzed with the Gene Mapper Software (Applied Biosystems).

Immunophenotyping of hA-MSCs by flow cytometry

The expression of 38 hematopoietic, mesenchymal, endothelial, epithelial, and no-lineage membrane antigens was analyzed on the surface of hA-MSCs by four-color flow cytometry (Table 1). All monoclonal antibodies (MoAbs) were from Becton Dickinson (San José) except anti-CD338-APC, which was from R&D (Minneapolis), anti-CD-133-PE and anti-CD271-APC MoAbs, which were from Milenyi Biotec (Bergisch Gladbach, Germany). For all antibody staining experiments, at least 1x105 hA-MSCs isolated from each placenta sample were incubated at 4°C for 20 min with the appropriate amount of MoAbs, washed twice with PBS, and finally analyzed with an unmodified Becton-Dickinson FACSCanto II flow cytometer (Becton-Dickinson, San Jose), that was set up according to published guidelines (Perfetto et al. 2006). For each sample, the respective control was prepared in order to determine the level of background cellular autofluorescence without antibody staining. CaliBRITE beads (Becton-Dickinson) were used as quality controls across the study according to the manufacturer's instructions. Daily control of CaliBRITE intensity showed no change in instrument sensitivity throughout the study. The relative voltage range for each detector was assessed una tantum at the

beginning of the study, using the "eight-peak" technology (Rainbow Calibration Particles, Becton-Dickinson, catalog no. 559123). Compensation was set in the FACS-DiVa (Becton-Dickinson) software, and compensated samples were analyzed. Samples were acquired immediately after staining using the FACSCanto II instrument, and at least 10,000 events were recorded for each monoclonal combination. Levels of CD antigen expression were displayed as median fluorescence intensity (MFI). The FACS-DiVa software (Becton-Dickinson) was used for cytometric analysis.

RNA isolation

Total RNA (including miRNAs) was purified from VAT, amnion, and hA-MSCs using the mirVanaTM miRNA isolation kit (Ambion). RNA concentration was evaluated by NanoDrop® ND-1000 UV-Vis spectrophotometer (NanoDrop Technologies, Wilmington, DE, USA). The total RNA isolated from VAT, amnion and hA-MSCs from non-obese females was pooled to serve as control in the comparison of the miRNA expression profiles of the obese females.

MiRNAs expression profile

TaqMan low density arrays (TLDA) micro-fluidic cards were used to detect and quantify mature miRNAs according to manufacturer's instructions. Each TLDA Human MicroRNA Panel v1.0 card contained 365 preloaded human miRNA targets and two endogenous controls (small nucleolar RNAs: RNU48 and RNU44). TLDAs were prepared in two-steps. In the first step, 640 ng of total RNA were reverse transcribed in eight multiplex reverse transcriptase (RT) reaction pools using stem loop RT primers specific for mature miRNA species. Then, each of the resulting eight cDNA pools was diluted, mixed with TaqMan Universal PCR master mix, and loaded into one of the eight fill ports on the TLDA microfluidic card. The card was centrifuged for 2 min at 1200 rpm to distribute samples to the multiple wells of the fill ports and sealed to prevent well-to-well contamination. Finally, the cards were processed on a 7900 HT Real-Time PCR System (Applied Biosystems). The miRNA expression values were normalized to RNU48 (endogenous control), and relative expression values were obtained using the ΔΔCT method (Relative Quantification, $RQ=2^{-\Delta\Delta CT}$) with Sequence Detection System (SDS) v2.3 and RQ Manager 1.2 software (Applied Biosystems). To normalize the miRNA data and to reduce inter-individual variability, were considered differently expressed miRNAs whose mean RQ levels were < 0.5 (down-expressed) or > 2.0 (up-expressed) in most of the samples from obese compared to normal weight women.

Quantitative Real-Time Polymerase Chain Reaction (qRT-PCR) of miRNAs and mRNAs

The expression levels of some selected miRNAs in VAT (miR-141, miR-200c, miR-520e, and miR-520d), and some selected miRNAs in amnion (miR-422b, miR-23b, miR-338, miR-449bb, and miR-139) were also validated by TaqMan miRNA assays (Applied Biosystems), in accordance with the manufacturer's instructions on the 7900 HT real-time PCR system (Applied Biosystems). The expression of one of these selected miRNAs in VAT, namely, miR-141, was preliminarily tested in each non-obese control, and after ensuring that the expression was comparable among these individuals, we pooled their RNAs to obtain a control against which to compare miRNA levels in obese women.

The expression levels of the selected miRNAs were first normalized to the endogenous control (RNU48), and then the relative expression values were obtained versus the non-obese control pool, using the ΔΔCT method (relative quantification, $RQ = 2^{-\Delta\Delta CT}$) with SDS v2.3 and RQ Manager 1.2 software (Applied Biosystems).

Real-time RT-PCR of RAB11A and YWHAG mRNAs was performed using gene-specific primers (RAB11a, forward: AACATCAGCATATTATCGTGGA and reverse: GATCACTCTTATTGCCCACA; YWHAG, forward: AGACCCAGCCCCGCGAAGAT and reverse: TCTGTCACGTTCTTCATGGCCGC), the Power SYBR Green PCR Master Mix (Applied Biosystems), and the PRISM 7900HT sequence detection system (Applied Biosystems).

Preparation of Protein Extracts

hA-MSCs isolated from placentas of obese women were pooled in group of two, so we have 6 samples of Ob-hA-MSCs and 6 samples of Co-hA-MSCs.

Protein extracts from hA-MSCs samples were prepared using a lysis buffer containing 7M urea, 2M thiourea, 4% CHAPS (3-[(3-cholamidopropyl)dimethylammonium]-1-propane sulfonate) in 30mM Tris-HCl, and the GeHealthcare cocktail of protease inhibitors. The suspensions were solubilized by sonicator. Then, the samples were centrifuged at max speed for 45 min at 4 °C. The clear interface of each sample was recovered and was transferred to a clean tube. The samples were precipitated using the 2D-Clean-up kit (Amersham) according to the manufacturer's instructions. Briefly, equal amount (300 µl) of precipitant and co-precipitant were added to each sample. The samples were mixed well for 15 minutes and then centrifuged at maximum speed for 5 minutes to obtain the pellet. The supernatant was removed from each sample and 25µl of de-ionized water was added on top of each pellet. The samples were rapidly vortexed, after 1mL of cool wash buffer

and 5µl of wash additive were added on each sample. The pellets were incubated at -20°C ON. The day after, the samples were centrifuged at maximum speed at 4°C for 30 minutes. The supernatant were carefully removed and each pellet was solubilized in 300 µl of lysis buffer. The pH of each samples were adjusted to 8.5 using 1M NaOH.

Protein extracts from VAT samples were prepared using a lysis buffer containing 2% SDS, 10% glycerol, 6.25 mM Tris-HCl pH 6.8, 0.5 mM EDTA, 20 mM NaF, 1 mM Na3VO4 (Santa Cruz Biotechnology, Santa Cruz, CA), and the Sigma-Aldrich cocktail of protease inhibitors. The suspensions were shaken in Tissue Lyser II (Qiagen) for 4 min at maximum frequency. After 30 min on ice, samples were centrifuged at 15000g for 10 min at 4 °C. The clear interface of each sample was recovered and was transferred to a clean tube.

Protein concentrations were determined after precipitation by using BioRad protein reagent. Proteins extracted from VAT samples used for proteomic analysis were precipitated for 16 h at −20 °C with 9 volumes of a mix composed of acetone and methanol (9:1) and then centrifuged at 15000g for 30 min at 4 °C. Then, protein pellets were solubilized in a buffer, UTC, containing 7 M urea, 2 M thiourea, 4% CHAPS (3-[(3cholamidopropyl)dimethylammonium]-1-propane sulfonate) in 30 mM Tris-HCl. Protein concentrations were re-determined after precipitation by using BioRad protein reagent.

Two-Dimensional Fluorescence Difference Gel Electrophoresis (2D-DIGE)

Protein extracts were labeled with 240 pmol of Cy3 or Cy5 fluorescent dye on ice, in the dark, for 30 min. To exclude preferential binding of a label to a set of proteins, the samples were dye-swapped. The internal standard containing equal amounts of proteins from each sample was labeled with Cy2. The same internal standard was run in all gels to normalize the experiments and to reduce gel-to-gel variations. Labeling reactions were stopped by adding 1 mM lysine. Sample pairs labeled with Cy3 and Cy5 and the internal standard were combined and used to passively hydrate individual strips as follows: each mix of labeled samples was diluted in UTC solution containing 130 mM DTT, 2% IPG Buffer pH 3−10 NL (GE Healthcare, Buckinghamshire, UK), 2.8% DeStreak reagent (GE Healthcare) in a final volume of 400 µL. The mixtures were used to hydrate 24 cm IPG strips pH 3−10NL required for protein separation in the first dimension. Isoelectric focusing (IEF) was run in an IPGphor II apparatus (GE Healthcare) according to this voltage protocol: 300 V for 3 h, linear gradient to 600 V in 3 h, linear gradient to 1000 V in 3 h, linear gradient to 8000 V in 5 h, 8000 V for 6 h. After the first dimension, the strips were equilibrated in equilibration buffer (100 mM Tris-HCl, 6 M urea, 30% (v/v) glycerol, 2% (w/v) SDS, and trace of bromophenol blue, pH 8.0) containing 0.5% (w/v) DTT for 15 min and thereafter in equilibration buffer containing 4.5% (w/v) iodoacetamide for a further 15 min. The equilibrated strips were transferred onto 12% polyacrylamide gels for the second dimension

(Ettan Dalt six electrophoresis system, GE Healthcare). The SDS-PAGE electrophoresis was run using a Peltier-cooled DALT II Electrophoresis unit (GE Healthcare) at 30W. After the electrophoresis, the gels were scanned with a Typhoon 9400 variable mode imager (GE Healthcare) at 100 μm resolution, using appropriated individual excitation/emission wavelengths: 488/520 for Cy2, 532/580 for Cy3 and 633/670 for Cy5. The images were captured with Image Quant software and analyzed with DeCyder software (GE Healthcare). The most representative gel was chosen as a master gel to compare results obtained from other samples.

Globally, two 2D-DIGE experiments were performed: the first to analyze VAT samples from 6 randomly selected obese and 3 non-obese females; the second to analyze 12 Ob-hA-MSCs and 6 Co-hA-MSCs. The Student's t test was used to determine the fold change between the analyzed groups. Only protein spots with a $p < 0.05$ were investigated further.

Protein Identification with Liquid Chromatography−Tandem Mass Spectrometry (LC−MS/MS)

Two preparative gels were carry out: the first gel using 250 μg of proteins from VAT and the second gel using 450 μg of proteins from hA-MSCs. After 2D-electrophoresis, performed under the conditions reported for the analytical experiment, the gel was stained with SYPRO Ruby ready-to-use formula or Comassie Brillant protein stain, and the spot map so obtained was matched with the analytical reference gel. The spots differentially expressed in samples from obese and non-obese females were excised from the preparative gel using the Ettan Spot Picker robotic system (GE Healthcare). The excised spots were analyzed with LC−MS/MS (Functional and Structural Proteomics Facility, CEINGE−Biotecnologie Avanzate, Italy). The excised spots were washed in 50 mM ammonium bicarbonate pH 8.0 in 50% acetonitrile to a complete destaining. The gel pieces were resuspended in 50 mM ammonium bicarbonate pH 8.0 containing 100 ng of trypsin and incubated for 2 h at 4 °C and overnight at 37 °C. The supernatant containing the resulting peptide mixtures was removed, and the gel pieces were re-extracted with acetonitrile. The two fractions were then collected and freeze-dried. The peptide mixtures were further analyzed by LC−MS/MS using the LC−MSD Trap XCT Ultra apparatus (Agilent Technologies, Palo Alto, CA, USA) equipped with a 1100 HPLC system and a chip cube (Agilent Technologies). After loading, the peptide mixture (8 μL in 0.5% TFA) was first concentrated at 4 μL/min in 40 nL enrichment column (Agilent Technologies chip), with 0.1% formic acid as eluent. The sample was then fractionated on a C18 reverse-phase capillary column (75 μm × 43 mm in the Agilent Technologies chip) at a flow rate of 300 nL/min, with a linear gradient of eluent B (0.1% formic acid in acetonitrile) in eluent A (0.1% formic acid) from 7 to 50% in 35 min. Elution was monitored on the mass spectrometer without a splitting device. Peptide analysis was performed using data-dependent acquisition of one MS scan (m/z

range from 400 to 2000 Da/e) followed by MS/MS scans of the three most abundant ions in each MS scan. Dynamic exclusion was used to acquire a more complete survey of the peptides by automatic recognition and temporary exclusion (2 min) of ions from which definitive mass spectral data had previously been acquired. A permanent exclusion list of the most frequent peptide contaminants (keratins and trypsin peptides) was included in the acquisition method, in order to focus on significant data. Mass spectral data obtained from the LC−MS/ MS analysis were used to search a non-redundant protein database using an in-house version of the Mascot v. 2.1 (Matrix Science, Boston, MA, USA) software and NCBI database (221,338 human sequences, timestamp: March and April, 2009). Peptide mass values and sequence information from the LC−MS/MS experiments were used in the MS/MS ion search taking into account the Carbamidomethyl-Cys as fixed modification, Met oxidized, Pyro-Carbamidomethyl-Cys (with N-term Carbamidomethyl-Cys) and Pyro-Glu (with N-term E) as variable modifications. The maximum missed cleavage of 1, and a precursor ion and fragment ion mass tolerance of ±600 ppm and 0.6 Da, respectively, were used.

Bioinformatics Analysis

Biological targets of miRNAs differently expressed in VAT, amnios, and hA-MSCs from obese compared to non-obese females were predicted using the TargetScan Release 5.0 (http://www.targetscan.org) algorithm. This algorithm assigns a “total context score” for each predicted target. Target genes with a “total context score” < −0.30 were further analyzed using the KEGG database (http://www.genome.ad. jp/kegg/) to identify the pathways that involve the target genes of miRNAs and then using the Gene Ontology (GO) database (http://www.geneontology.org/ontologies) to identify the biological processes in which the proteins identified by DIGE participate. Gene ontology classification of the differentially expressed proteins revealed by 2D-DIGE analysis was performed in the web-accessible DAVID (v 6.7) annotation system (http://david.abcc.ncifcrf.gov/home.jsp) and in STRING: functional protein annotation networks (v 9.1) (http://string-db.org/).

Western Blot

Protein evaluation by Western blot was performed with 35 μg of total proteins separated by SDS-PAGE (13% polyacrylamide gel) and electroblotted onto hydrophobic polyvinylidene difluoride (PVDF) membranes (Amersham) for 19 h at 33 V. Blots were blocked with 5% BSA in TBS buffer with 0.1% Tween 20 for 2 h at room temperature. Immunoblotting was performed with the specific polyclonal antibody: rabbit anti-14-3-3γ (dilution 1:800), rabbit anti-RAB11A (1 μg/mL), and rabbit antiactin (dilution 1:800) (Abcam, Cambridge, UK) for 4 h. For the following incubation with primary antibody, membrane was washed in TBS buffer with 0.1% Tween 20 and incubated for

45 min IgG-HRP-conjugated secondary antibody (dilution 1:10000 for anti-14-3-3γ and antiactin; 1:50000 for antiRAB11A). Immunoreactive bands were visualized with the chemiluminescence reagent kit (ECL Western blotting detection reagents, GE Healthcare). We used the same membrane for each immunoblot, washing it in TBS buffer with 0.1% Tween 20 for 10 min after each experiment. After each immunoblot, the membrane was exposed to X-ray film (Amersham) for different times. The images of three different exposures were captured by Gel Doc XR (Bio-Rad) and quantitated with the Quantity One software (Bio-Rad). Each protein band was contained within a rectangular area, identical for each sample, and background values were subtracted from each band. The triplicate sample values were normalized to the corresponding triplicate actin values. Then, the mean values from the different ratio calculations were calculated for each sample. The data were expressed as percent relative expression, the sample with the highest expression of either RAB11A or YWHAG having been set as 100%. The data obtained were used to obtain the corresponding box plots and p-values (Student's t test) in the Microsoft Excel software.

Oligonucleotides and Plasmids

Chemically modified double-stranded RNA molecules (microRNA precursor molecules: pre-miR-520e and pre-miR-141) and pre-miR-negative control were purchased from Ambion (Austin, TX, USA). The final concentration of pre-miR molecules and the corresponding pre-miR negative control were 100 nM each. The plasmids used were pGL3-control (Promega Corp., Madison, WI, USA) encoding for firefly luciferase and pRL-CMV encoding for Renilla luciferase (Promega Corp., Madison, WI, USA). The 3′UTRs of RAB11A (1258−1264 bp 3′UTR) and of YWHAG (2489− 2495 bp 3′UTR) genes, containing respectively the miR-520e and miR-141 binding sites, as well as the mutated 3′UTRs of these two genes (three bases of each seed region were changed by complementary bases), were obtained from genomic DNA by PCR with a sense and antisense primers carrying a XbaI restriction site and cloned downstream to Renilla luciferase gene in pRL-CMV vector in XbaI site.

Cell Culture, Transfection, and Luciferase Assay

Human embryonic kidney (HEK) 293 cells were cultured in DMEM (Invitrogen) supplemented with 2 mM glutamine (Invitrogen), 100 U/mL penicillin/streptomycin (Invitrogen), and 10% FBS (Invitrogen). The day before transfection, cells were plated in 24-well plates to allow adherence and to reach 70−90% confluence at the time of transfection. Transfection of plasmids, carrying wild-type or mutant 3′UTRs, with pGL3control and each pre-miRNAs or pre-miR negative control (Ambion, Austin, TX, USA) in HEK293 was performed using Lipofectamine 2000, following the

manufacturer's instructions. Firefly and Renilla luciferase activities were measured 48 h after transfection, with the dual-luciferase reporter system (Promega) in a Sirius Luminometer (Berthold Detection Systems, Huntsville, AL, USA). All transfection experiments were done in triplicate.

Statistical Analysis

The investigated parameters were expressed as mean ± standard error of the mean (SEM) (parametric distribution) or as median value and interquartile range (nonparametric distributions). Student's *t* test was used to compare group means, and a p level < 0.05 was considered statistically significant. Statistical analyses were carried out with the PASW package for Windows (Ver.18; SPSS Inc. Headquarters, Chicago, Ill).

Table 1. Surface immunophenotypic profile investigated in hA-MSCs by flow cytometry

Fluorochrome	CD Antigen	Other Names	Molecular Weigth (kDa)	Cell expression	Function
FITC	**CD9**	Tspan-29	24-26	Platelets, pre-B, activated T	Adhesion, migration, platelet activation
APC	**CD10**	CALLA	100	B/T precursors, stromal cells	Endopeptidase
PE	**CD13**	APN	150	Granulocytes, monocytes and their precursors, endothelial, epithelial cells, mesenchymal stem cells	Metalloproteinase
PE	**CD14**	LPS-R	53-55	Monocytes, macrophages	Receptor for LPS/LPB complex
APC	**CD15**	Lewis X	_	Granulocyte, monocyte, epithelial cells	Cell adhesion
PE	**CD16**	FCγRIIIa	50-65	Neutrophils, NK, macrophages	Low affinity with FCγ receptor, mediates phagocytosis
APC	**CD19**	Bgp95	95	B, not on plasma cells	Signal transduction
FITC	**CD26**	DPP IV	110	Mature thymocytes, T, B, NK cells	Exoprotease, costimulation
APC	**CD28**	Tp44	44	Most T, thymocyte,NK and plasma cells	Costimulation
APC	**CD29**	VLA β1-chain	130	T, B, Granulocytes, monocytes, fibroblast, endothelial, NK , platelet	Adhesion activation, embryogenesis and development
FITC	**CD31**	PECAM-1	130-140	Monocytes, platelets, granulocytes and endothelial cells	Cell adhesion
APC	**CD33**	My9	67	Monocytes, granulocytes, masocytes and myeloid progenitors	Cell adhesion
APC	**CD34**	My10	105-120	Hematopoietic stem cells and progenitors, endothelial cells	Cell adhesion
APC	**CD36**	Platelet GPIV	85	Platelets, monocytes, macrophages, endothelial cells, erythroid precursors	Adhesion and phagocytosis
FITC	**CD40**	Bp50	48	Monocytes, macrophage, B, endothelial, fibroblast cells, keratinocytes	Costimulation to B cells, growth, differentiation and isotype switching
APC	**CD44**	H-CAM	90	Leukocytes, erythrocytes and epithelial cells	Rolling, homing and aggregation
Per Cp	**CD45**	LCA	180-220	hematopoietic cells, except erythrocyte and platelet	Critical for T and B cell receptor mediated activation
FITC	**CD47**	IAP I	50-55	Hematopoietic, epithelial, endothelial, brain mesenchymal cells	Adhesion
FITC	**CD49d**	VLA-4	150	B and T , monocytes, eosinophils, basophils, NK, dendritic cells	Adhesion, migration, homing, activation
APC	**CD54**	ICAM-1	80-114	Epithelial and endothelial cells monocyte. Low on resting lymphocyte, upregulate on activated	T cell activation
PE	**CD56**	NCAM	175-220	Neural, tumors, embryonic tissue, NK	Homophilic and heterophilic adhesion
PE	**CD58**	LFA-3	40-70	Leucocyte, erythrocyte, epithelial endothelial cells and fibroblast	Costimulation
FITC	**CD71**	Transferrin recepor	95	Reticulocytes, erythroid precursor	Controls iron intake during cell proliferation
APC	**CD81**	TAPA-1	26	B, T, monocytes, endothelial cells	Signal transduction
FITC	**CD90**	Thy-1	25-35	Hematopoietic stem cells, neurons, mesenchymal stem cells	Inhibition of hematopoietic stem cells and neurons differentiation
PE	**CD99**	MIC2	32	Leucocyte, NK, monocytes, endothelial and epithelial cells	Leucocyte migration, T cell activation,cell adhesion
PE	**CD105**	Endoglin	90	Endothelia and mesenchymal stem cells erythroid precursors, monocytes	Angiogenesis, modulates cellular response to TGFβ1
PE	**CD117**	c-kit	145	Hematopoietic stem cells and progenitors	Crucial for hematopoietic stem cells
PE	**CD133**	Prominin-1	120	Hematopoietic stem cell, endothelial, epithelial and neural precursors	Unknown function, stem cells marker
PE	**CD151**	PETA-3	32	Endothelial and epithelial cells, megakaryocye, platelets	Adhesion
PE	**CD166**	ALCAM	100-105	Neurons, activated T cells, epithelial cells, MSC	Adhesion, T cells activation
PE	**CD200**	OX-2	33	B , activated T, Thymocytes, neurons endothelium	Down regulatory signal for myeloid cell functions
FITC	**CD243**	MDR-1	170	Stem cells, multi drug resistant tumours	Influences the up-take, distribution, elimination of drugs
APC	**CD271**	NGFR	75	Neurons, stromal and dendritic follicular cells	Low affinity for NGF receptor
APC	**CD324**	E-cadherin	120	Epithelial, keratinocytes, platelet	Adhesion, growth, differentiation
APC	**CD338**	ABCG-2	72	Hematopoietic stem cells, liver, kidney, intestine, side population of stem cells	Absorbition and excretion of xenobiotics
FITC	**HLA-ABC**	Class I MHC	46	All nucleated cells and platelets	Antigen presentation
FITC	**HLA-DR**	Class II MHC	30	B cells, monocytes, myeloid progenitors, activated T and dendritic cells	Antigen presentation

4. RESULTS

Patients

Table 2 reports the clinical and biochemical characteristics of obese and non-obese women. The two groups differ statistically for weight and BMI ($p<0.0001$). The cardiac frequency and glucose level were higher in obese compared to non-obese women ($p=0.01$ and $p=0.03$, respectively).

Table 2. General characteristics of the obese (n=15) and non-obese (n=10) women

	Women	
	Obese	**Non-obese**
Subjects (n)	15	10
Age (years)	41.6 (4.4)	38.0 (3.5)
Weight (kg) [a]	115.2 (6.3)	62.5 (2.6)
Height (m)	1.7 (0.04)	1.6 (0.01)
BMI (kg/m²) [a]	42.2 (1.6)	23.7 (1.2)
Systolic blood pressure (mmHg)	133.6 (6.7)	115 (4.5)
Diastolic blood pressure (mmHg) [b]	80.0 (80.0-90.0)	80.0 (70.0-80.0)
Cardiac frequency [c]	80.0 (2.2)	67.6 (3.7)
Glucose (mmol/L) [d]	4.9 (0.2)	4.3 (0.2)
Cholesterol (mmol/L)	5.9 (0.5)	5.8 (0.6)
Tryglicerides (mmol/L)	1.4 (0.1)	0.9 (0.1)
AST (U/L) [b]	18.5 (16.0-21.0)	18.0 (13.5-19.0)
ALT (U/L) [b]	17.0 (13.0-28.5)	14.0 (12.0-21.0)
ALP (U/L)	79.3 (5.8)	89.2 (19.5)
GGT (U/L)	28.5 (4.7)	17.3 (3.5)

Data are expressed as Mean (SEM) value and interquartile range (nonparametric distributions).
[a] Statistically significant differences at Student's t-test $p<0.0001$
[b] Data are expressed as median value
[c] $p=0.01$
[d] $p=0.03$

The clinical and biochemical characteristics of pregnant mothers and their newborns are summarized in Table 3 (A and B, respectively). Weight gain was significantly lower ($P<0.05$) and diastolic blood pressure was higher ($P<0.05$) in obese than in control pregnant women. Both the leptin concentration and the L/A ratio were higher ($P<0.0001$) in obese than in control pregnant women at delivery. Biometric characteristics did not differ significantly between newborns of obese and control women.

Table 3. Clinical and biochemical characteristics of obese and normal weight control pregnant women at delivery and their newborns

A		
Mother's parameters	**Ob-pregnant women (n=16)**	**Co-pregnant women (n=7)**
Age (years)	32.6 (0.9)	30.7 (1.5)
Weight (kg) [a]	110.1 (5.4)	65.2 (3.6)
Height (m)	163.3(1.6)	169.0 (1.7)
BMI pre-pregnancy (kg/m^2) [a]	40.3 (1.8)	22.4 (1.0)
Weight gain in pregnancy [b]	8.4 (1.3)	14.3 (1.8)
Systolic blood pressure (mmHg)	124.3 (2.7)	117.1 (5.1)
Diastolic blood pressure (mmHg) [b]	82.5 (2.2)	74.2 (2.0)
Frequency cardiac.	79.6 (1.7)	79.0 (3.7)
Gestational age	38.4 (0.3)	38.7 (0.2)
Glucose (mmol/L)	4.3 (0.1)	4.0 (0.3)
Total cholesterol (mmol/L)	6.9 (0.4)	7.3 (0.1)
Triglycerides (mmol/L)	2.8 (0.2)	2.3 (0.3)
AST (U/L)	15 [d] (12.2-26.5[d])	14.8 (0.7)
ALT (U/L)	13 [d] (9.2-17.7[d])	12.1 (1.1)
ALP (U/L)	124.2 (11.1)	115.0 (12.6)
GGT (U/L)	11.0 (1.7)	8.8 (1.5)
Leptin (L)(ng/ml) [a]	38.5 (2.2)	15.2 (3.3)
Adiponectin (A)(μg/ml)	6.0 (0.7)	7.5 (1.4)
L/A [a]	7.7 (0.6)	2.6 (0.5)
B		
Newborn's parameters	**Ob-newborns (n=16)**	**Co-newborns (n=7)**
Birth weight (kg)	3162 (0.1)	3401 (0.1)
Length (cm)	49.6 (0.7)	50.8 (0.7)
Head circumference (cm)	34.0 (0.4)	34.8 (0.3)
Apgar 1'	7.0 [d] (7.0-8.0 [c])	7.8 (0.2)
Apgar 5'	9.0 [d] (8.5-9.0 [c])	8.7 (0.1)

Data are expressed as mean (SEM) (parametric distributions).
Statistically significant difference at the Student's *t* test.
[a] P<0.0001.
[b] P<0.05.
[c] Median value and 25th-75th percentiles (nonparametric distribution).

miRNAs expression signature in VAT from obese women

MiRNAs expression profile performed in VAT from 10/15 obese and 4/10 non-obese females showed that a large set of the tested miRNAs was expressed in VAT both obese and non-obese women (243/365, 66%). A small set (50/365, 14%) was not expressed, whereas 72/365 (20%) miRNAs were expressed only in VAT from obese women. On the basis of the normalization criteria reported above, namely, miRNAs whose expression levels versus controls were up- or down-expressed (respectively, RQ > 2 or < 0.5) in at least 6/10 obese females, we found that 61/243 (25%) miRNAs were down-expressed, and 10/243 (4.1%) miRNAs were up-expressed (Table 4). The search for gene targets of these differentially expressed miRNAs was

performed by TargetScan 5.0 algorithm and their assembly in metabolic pathways by Kegg database. The main significant ($p < 0.01$) pathways predicted to be affected by miRNAs in VAT samples during obesity are considered.

Table 4. Differentially Expressed miRNAs in VAT from Obese Vs Non-obese Women

Down-expressed miRNAs	RQ value	
	Mean	SEM
hsa-miR-514	0,007	0,002
hsa-miR-520e	0,014	0,005
hsa-miR-520f	0,029	0,010
hsa-miR-184	0,030	0,010
hsa-miR-518d	0,057	0,021
hsa-miR-196a	0,059	0,019
hsa-miR-337	0,065	0,025
hsa-miR-520d	0,066	0,022
hsa-miR-490	0,067	0,025
hsa-miR-508	0,069	0,022
hsa-miR-519c	0,073	0,026
hsa-miR-369-3p	0,075	0,025
hsa-miR-202	0,078	0,027
hsa-miR-141	0,079	0,025
hsa-miR-562	0,080	0,030
hsa-miR-591	0,085	0,028
hsa-miR-580	0,086	0,029
hsa-miR-380-5p	0,086	0,029
hsa-miR-518a	0,092	0,035
hsa-miR-618	0,096	0,034
hsa-miR-494	0,097	0,037
hsa-miR-624	0,099	0,035
hsa-miR-519b	0,102	0,032
hsa-miR-185	0,113	0,043
hsa-miR-219	0,120	0,042
hsa-miR-509	0,124	0,039
hsa-miR-548d	0,125	0,047
hsa-miR-206	0,126	0,042
hsa-miR-200c	0,130	0,041
hsa-miR-196b	0,166	0,055
hsa-miR-653	0,168	0,068
hsa-miR-493	0,178	0,059
hsa-miR-629	0,181	0,074
hsa-miR-198	0,187	0,062
hsa-miR-450	0,199	0,070
hsa-miR-375	0,202	0,071
hsa-miR-518b	0,208	0,069
hsa-miR-137	0,222	0,091
hsa-miR-649	0,224	0,079
hsa-miR-189	0,226	0,080
hsa-miR-489	0,240	0,085
hsa-miR-451	0,242	0,099
hsa-miR-615	0,248	0,083
hsa-miR-335	0,250	0,088
hsa-miR-215	0,264	0,088
hsa-miR-422b	0,271	0,090
hsa-miR-500	0,271	0,111
hsa-miR-601	0,285	0,108
hsa-miR-203	0,298	0,122
hsa-miR-410	0,298	0,122
hsa-miR-330	0,320	0,121
hsa-miR-30a-5p	0,324	0,122
hsa-miR-486	0,327	0,133
hsa-miR-22	0,332	0,125
hsa-miR-181c	0,332	0,117
hsa-miR-30d	0,334	0,126
hsa-miR-101	0,346	0,141
hsa-miR-376a	0,372	0,152
hsa-miR-191	0,386	0,146
hsa-miR-99a	0,393	0,161
Up-expressed miRNAs	**RQ**	
	Mean	**SEM**
hsa-miR-7	0,396	0,162
hsa-miR-433	21,563	7,624
hsa-miR-520h	13,617	5,559
hsa-miR-153	12,447	4,705
hsa-miR-579	12,047	4,553
hsa-miR-520b	9,400	3,553
hsa-miR-616	3,954	1,495
hsa-miR-296	3,872	1,463
hsa-miR-517c	3,342	1,365
hsa-miR-501	3,068	1,160
hsa-miR-594	2,714	1,108

Protein expression signature in VAT from obese women

The protein expression signature of VAT samples from 6/15 obese and 3/10 non-obese subjects was carried out using 2D-DIGE analysis. Figure 5A shows the master gel used to match the whole set of 2-DE profiles obtained.

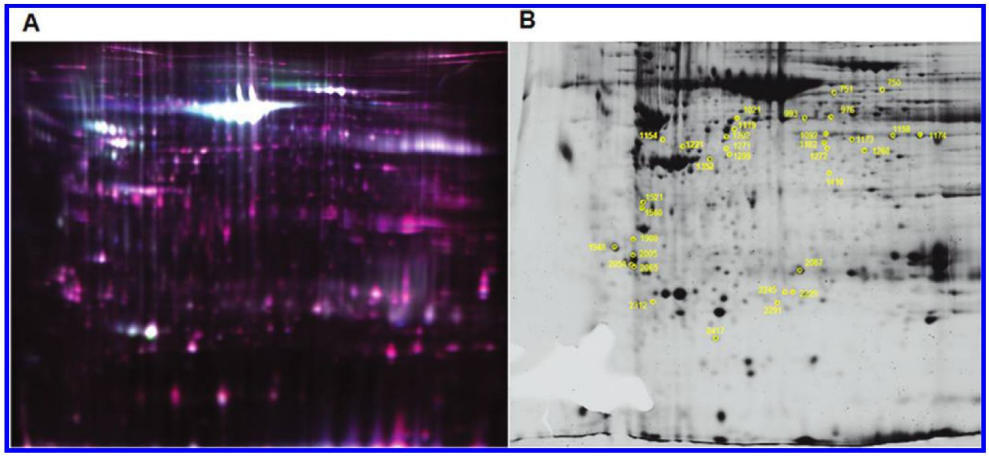

Figure 5. 2D-DIGE of VAT proteins. Panel A shows scan of master gel used for the proteomic analysis. This gel is constituted by three overlapped images: (1) VAT proteins of a nonobese female labeled with Cy3 (green), (2) VAT proteins of an obese female labeled with Cy5 (red), and (3) VAT proteins from a mixture of the random selected samples (used for normalization) labeled with Cy2 (blue). Panel B shows scan of preparative gel of VAT proteins. Numbers correspond to differentially expressed protein spots.

The analysis performed with DeCyder Software detected approximately 2700 protein spots per gel in a 3−10 pH range, with a molecular mass of 10−120 kDa. Approximately 1500 spots were matched throughout the gels. The DeCyder statistical analysis revealed 172 spots differentially expressed in obese vs non-obese VAT samples with an average ratio ≥ 1.50 for up-expressed protein spots and ≤ -1.50 for down-expressed spots ($p < 0.05$). Some spots were excluded from further evaluation, i.e., those at the extreme right and left sides of the gel and those (30 spots) representing contaminating serum proteins. Furthermore, many spots were not objected to further investigation, because of their low abundance on the analytical gel or on the preparative gel. As a result, we focused on 33 spots with optimal features. Figure 4B shows the position of the 33 selected spots on the preparative gel. The latter was stained with SYPRO Ruby protein stain and used for automated spot picking. The isolated spots were digested with trypsin and then analyzed by LC− MS/MS, followed by database search. The relative expression ratios (in obese vs non-obese VAT) for each of the 33 spots and their statistical values are listed in Table 5. Interestingly, most of the spots (32/33) were increased, and only 1 spot (number 2312) was decreased. Globally, a total of 67 proteins were identified in these spots. Most of these proteins were predicted by bioinformatics (DAVID database) to be functionally annotated in two main clusters (Figure 6). Annotation cluster 1 (Figure 6 panel A) was constituted by

the following: (i) 5 members of the 14.3.3 family of proteins, namely, YWHAB, YWHAE, YWHAG, YWHAH, and YWHAZ; (ii) 9 proteins (YWHAB, YWHAE, YWHAZ, RAB11A, RAB7A, ANXA7, ARCN1, FLOT1, and SERPINF1) involved in the GOTERM_CC_FAT vesicle pathway, on the basis of their subcellular localization; and (iii) 7 regulated proteins involved in intracellular protein transport (YWHAB, YWHAE, YWHAH, YWHAG, YWHAZ, RAB11A, and ARCN1). Annotation cluster 2 (Figure 5 panel B) was constituted by a predominance of metabolic enzymes clustered in the KEGG pathways: valine, leucine, and isoleucine degradation (6 members, ACAT2, ACADS, ALDH2, BCKDHA, ECHS1, and HADHB), butanoate metabolism (5 members, ACAT2, ACADS, ALDH2, ECHS1, and PDHAD1) and fatty acid metabolism (5 members, ACAT2, ACADS, ALDH2, ECHS1, and HADHB).

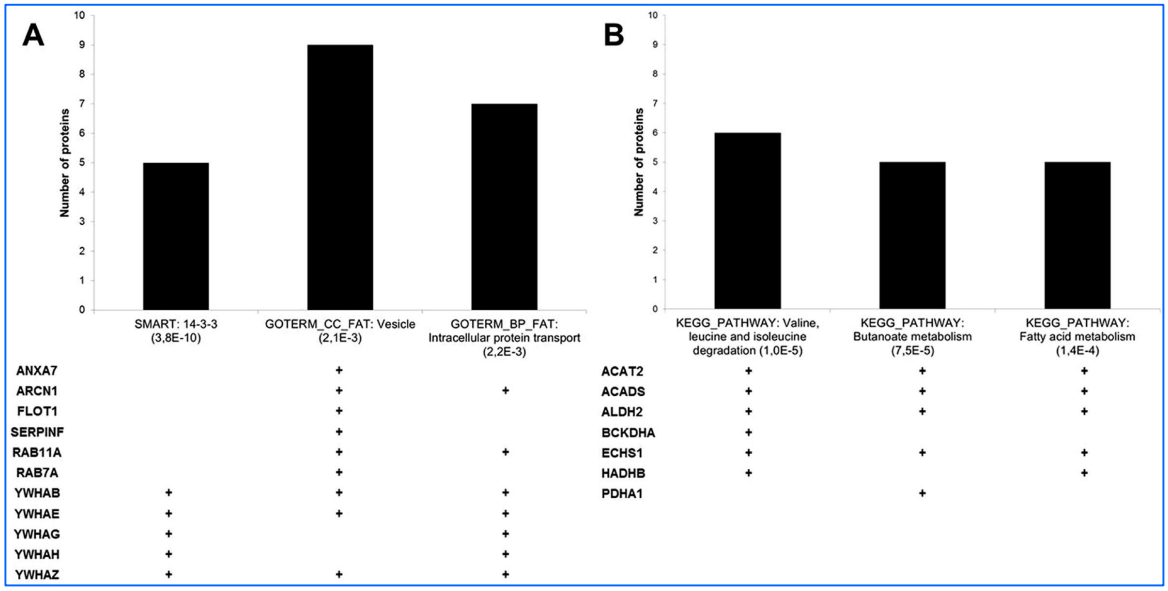

Figure 6. Functional annotation of VAT proteins. Overexpressed proteins in obese females were predicted by bioinformatics (DAVID database) to be functionally annotated in two main clusters: (A) annotation cluster 1 and (B) annotation cluster 2.

Table 5. Identification and characterization of proteins differently expressed in visceral adipose tissue from obese vs non-obese females, by 2D-DIGE analysis followed by LC-MS/MS

Spot number[a]	DIGE (p-value)[b]	DIGE Obese /control[C]	Accession No.[d]	Protein name	MW (Da)[e]	p*I*[f]	Nr. of Qualified Peptides / Coverage [g]	Score[h]	Gene symbol [i]	miRNA[l]
B1_750	0.035	1.7	gi/5031875	Lamin A/C isoform 2	65153	6.40	13/25%	743	LMNA	
			gi/20127454	5-aminoimidazole-4-carboxamide ribonucleotide formyltransferase/IMP cyclohydrolase	65089	6.27	7/16.5%	440	ATIC	
			gi/5803181	Stress induced phosphoprotein 1	63227	6.40	4/9%	228	STIP1	
C1_751	0.023	1.73	gi/55960506	Chaperonin containing TCP1, subunit 3 (gamma)	58505	6.46	17/43%	1043	CCT3	
			gi/4503377	Dihydropyrimidinase –like 2	62711	5.95	7/19%	465	DPYSL2	
			gi/11863154	**Archain isoform 1**	57630	5.89	9/19%	503	**ARCN1***	**mir-206**
			gi/189926	Phosphoglucomutase 1	61674	6.35	4/9%	208	PGM1*	mir-30a, -30d
			gi/6009626	Brain carboxylesterase hBr1	47100	6.02	3/8%	189	CES1	
D1_ 976	0.004	1.67	gi/5453603	Chaperonin containing TCP1, subunit 2	57794	6.01	17/50%	1271	CCT2	
			gi/178390	Aldehyde dehydrogenase	56858	7.00	6/15%	387	ALDH2	
			gi/2183299	Aldehyde dehydrogenase 1	55427	6.30	5/12%	319	ALDH1	
			gi/5771523	3-phosphoglycerate dehydrogenase	57370	6.29	4/9%	225	PHGDH	
E1_993	0.011	1.78	gi/16306550	Selenium binding protein 1	52928	5.93	13/37%	711	SELENBP1	
F1_1021	0.008	2.01	gi/15620780	Glutamate carboxypeptidase	53161	5.71	3/7%	143	CNDP2	
G1_1092	0.039	1.88	gi/5174529	Methionine adenosyltransferase II, alpha	43975	6.05	2/7%	143	MAT2A*	mir-30a,-30d,-22
H1_1119	0.007	1.43	gi/4504169	Glutathione synthetase	52523	5.67	7/23%	458	GSS	
			gi/1049219	Gamma-aminobutyraldehyde dehydrogenase	54410	6.01	5/11%	306	E3	
			gi/21410323	Perilipin	56216	5.82	2/5%	112	PLIN	
A2_1154	0.003	1.61	gi/21361144	Proteasome 26S ATPase subunit 3	49458	5.13	15/50%	843	PSMC3	
			gi/340219	Vimentin	53738	5.03	4/9%	273	VIM	
			gi/7106299	Ataxin 10	54196	5.12	4/4%	241	ATXN10	
B2_1158	0.011	1.48	gi/4503571	Enolase 1	47481	7.01	13/46%	906	ENOI	
			gi/40068518	Phosphogluconate dehydrogenase	53619	6.8	6/17%	427	PGD	
C2_1173	0.003	1.87	gi/4503481	Eukaryotic translation elongation factor 1 gamma	50429	6.25	10/34%	576	EEF1G	
			gi/496902	Translation initiation factor	47088	6.08	5/7%	297	E2F1	
			gi/4504327	Mitochondrial trifunctional protein, beta subunit precursor	51547	9.45	4/9%	207	HADHB*	mir-203
D2_1174	0.006	2.08	gi/5031699	Flotillin 1	47554	7.08	4/12%	265	FLOT1	
E2_1182	0.002	2.01	gi/4502111	Annexin VII isoform 1	50569	6.25	9/24%	526	ANXA7	
			gi/7546384	Chain A, Human branched- chain Alpha- Keto Acid Dehydrogenase	45770	6.32	4/11%	213	BCKDHA	
			gi/4099506	ErbB3 binding protein EBP1	38321	7.15	4/15%	211	PA2G4	
			gi/18379349	Vesicle amine transport protein 1	42122	5.88	2/8%	121	VAT1	
F2_1202	0.012	1.85	gi/39725934	Serine (or cysteine) proteinase inhibitor, clade F member 1	46454	5.97	11/38%	695	SERPINF1	
			gi/9836652	BSCv	47887	5.78	5/13%	305	C20ORF3	
			gi/285975	Human rab GDI	51088	5.94	2/5%	116	GDI	
			gi/515634	Ubiquinol-cytochrome C reductase core I protein	53270	5.94	2/4%	122	UQCRC1	

			gi/338695	Beta–tubulin	50240	4.75	2/5%	121	TUBB	
G2_1221	0.045	2.61	gi/4503529	Eukaryotic translation initiation factor 4A isoform 1	46353	5.32	8/27%	487	EIF4A1	
H2_1268	0.013	1.6	gi/181914	DNA-binding protein	36086	9.20	2/7%	122		
A3_1271	0.002	1.54	gi/33415057	Transformation-related protein 14	43248	5.49	5/19%	309	TRG14	
B3_1272	0.010	1.99	gi/4557809	Ornithine aminotransferase precursor	48846	6.57	7/23%	435	OAT	
			gi/387011	Pyruvate dehydrogenase E1-alpha precursor	47098	8.79	4/9%	265	PDHA1*	mir-203
			gi/3641398	NADP-dependent isocitrate dehydrogenase	46944	6.34	2/7%	86	IDH1*	mir-30a,-30d
C3_1299	0.004	1.81	gi/24308406	Secernin 2	46989	5.44	4/16%	231	SCRN2	
			gi/6678271	TAR DNA binding protein	45053	5.85	2/7%	162	TARDBP*	mir-137, -203
D3_1352	0.006	1.67		Not identified						
E3_1410	0.023	1.59	gi/4557233	Acyl-Coenzyme A dehydrogenase, C-2 to C-3 short chain precursor	44611	8.13	8/30%	436	ACADS	
			gi/148539872	Acetyl-Coenzyme A acetyltransferase 2	41783	6.47	2/8%	99	ACAT2	
F3_1521	0.006	1.64	gi/7661704	Osteoglycin preprotein	34243	5.46	5/18%	307	OGN*	mir-22
			gi/25453472	Eukaryotic translation elongation factor 1delta	31217	4.90	4/17%	277	EFF1D	
G3_1560	0.033	1.69	gi/194373515	Unnamed protein product (Corrisp. in Sprot a P68363 Tubulin alpha-1B chain)	33856	4.88	2/8%	151	DNAJB2	
			gi/157833780	Chain A, human Annexin V with Proline substitution by thioproline	36041	4.94	3/11%	153	ANXA5	
H3_1908	0.001	1.67	gi/24119203	Tropomyosin 3 isoform 2	29243	4.75	11/40%	598	TPM3	
			gi/4507651	Tropomyosin 4	28619	4.67	2/9%	104	TPM4	
			gi/13236577	Thiamine triphosphatase	25721	4.75	3/15%	165	THTPA	
A4_1948	0.001	1.68	gi/5803225	Tyrosine 3/tryptophan 5-monooxygenase activation protein, epsilon polypeptide	29326	4.63	15/65%	943	YWHAE	
B4_2005	0.001	1.91	gi/21464101	**Tyrosine 3-monooxygenase /tryptophan 5-monooxygenase activation protein, gamma polypeptide**	28456	4.80	5/21%	329	**YWHAG***	**mir-141, -200c**
			gi/119598039	Tropomyosin 1 (alpha), isoform Cra_m	28730	4.78	4/17%	215	TPM1	
C4_2054	0.010	1.64	gi/4507953	**Tyrosine 3 /tryptophan 5-monooxygenase activation protein, zeta polypeptide**	27899	4.73	9/52%	629	**YWHAZ***	**mir-206,** -30a, -30d, -22
D4_2065	0.001	1.72	gi/4507949	Tyrosine 3 /tryptophan 5-monooxygenase activation protein, beta polypeptide	28179	4.76	5/29%	310	YWHAB	
			gi/4507951	Tyrosine 3 /tryptophan 5-monooxygenase activation protein, eta polypeptide	28372	4.76	3/15%	225	YWHAH	
E4_2087	0.038	1.7	gi/4504517	Heat shock protein beta-1	22826	5.98	6/27%	330	HSPB1	
			gi/1922287	EnoylCoA hydratase	31807	8.34	5/23%	330	ECHS1	
F4_ 2229	0.007	1.64	gi/4758984	**Ras-related protein Rab-11A**	24492	6.12	2/11%	99	**RAB11A***	**mir-520e, -520d**
G4_2245	0.039	1.51	gi/2204207	Glutathione S-transferase	23595	5.43	6/38%	372	GSTP1	
			gi/1174149	Small GTP binding protein Rab 7	23732	6.40	2/12%	101	RAB7A*	mir-30a, -30d
H4_2291	0.008	1.65	gi/14249382	Abhydrolase domain containing 14B	22446	5.94	5/32%	264	ABHD14B	
A5_2312	>0.001	-2.12	gi/5020074	Glyoxalase-I	20934	5.24	3/16%	166	GLO I	
			gi/17986273	Fast skeletal myosin alkali light chain 1 isoform 1f	21189	4.97	3/18%	215	MYL1	
B5_2417	0.024	2.27		Not identified						

[a] Spot numbering as shown in 2-DE gel in Figure 4. [b] p-value at "Student t" test. [c] Average abundance ratio (obeses/controls) as calculated by DeCyder Analysis. [d] Protein accession number from NCBI. [e] Theoretical molecular weight (Da). [f] Theoretical pI. [g] According to the Proposed Guidelines for the Analysis and Documentation of Peptide and Protein Identifications (Paris consensus) we included in this table the complete figures of merit regarding the MS identification as: number of identified peptides whose individual ion score (as provided by Mascot) was higher than the designated confidence level (95%)/Protein sequence coverage (%); [h] Identification score (Score) indicating a probabilistic measure of the goodness of the MS protein identification.[i] Gene symbol from NCBI. [l] Down-expressed miRNAs in at least 6/10 obese females, which targeted 3'UTR-mRNA regions of asterisk genes. In bold are indicated down-expressed miRNAs in VAT from 9 or 10/10 obese females and their targeted proteins.

miRNA/Protein target pairs in VAT from obese women

To find potential miRNA/protein target pairs, miRNA expression and proteomic data were integrated. Specifically, the list of the identified protein spots was combined with the miRNAs predicted to possess the ability to target the proteins. The last column of Table 5 shows the potential miRNA counterparts of the identified proteins, as revealed by bioinformatics tools (TargetScan). Among the potential miRNA/protein target pairs deriving from this analysis, were selected those including miRNAs down-expressed in almost all VAT samples (9/10 or 10/10): miR-206/ARCN1 (spot 751); miR-141/YWHAG and miR-200c/YWHAG (spot 2005); miR206/YWHAZ (spot 2054); miR-520d/RAB11A and miR-520e/ RAB11A (spot 2229) (bold characters in Table5). The expression levels of the above miRNAs (miR-206, miR141, miR-200c, miR-520e, and -520d) were further validated by qRT-PCR. The qRT-PCR results, except slight differences due to the two different methodologies, were in close agreement with those obtained by TaqMan array (respectively, mean RQ ± SEM): miR-206 (0.209 ± 0.066 vs 0.126 ± 0.042), miR-141 (0.099 ± 0.032 vs 0.079 ± 0.025), miR-200c (0.138 ± 0.044 vs 0.130 ± 0.041), miR-520e (0.554 ± 0.175 vs 0.014 ± 0.005), except for miR-520d, whose results did not differ from controls in the qRT-PCR validation (0.944 ± 0.299 vs 0.066 ± 0.022). Consequently the miR-520d was discarded in our following evaluations. All the miRNA/protein target pairs reported above warrant further investigation.

Pathways deregulated in VAT

Functional annotation clustering in the DAVID database revealed that ARCN1, YWHAG, YWHAZ, and RAB11A are present in the annotation cluster intracellular protein transport (Figure 5 panel A), which may be involved in the physiopathology of the adipose tissue. Among the miRNAs associated to these targets, miR-141 and miR-520e were accordingly regulated in the complete set of RNA samples (10/10) from obese VAT. Thus, the functional pairs miR-141/YWHAG and miR-520e/RAB11A were selected for further analysis.

mRNA and Western blot

Since the effects of miRNA down-regulations may result in increased mRNA stability and/or mRNA translation, the transcript levels for RAB11A and YWHAG by qRT-PCR were tested. Both mRNAs were more abundantly expressed in VAT of obese women (RQ ± SEM: 6.1 ± 2.6 and 4.8 ± 0.7, respectively) compared to control VAT mRNA samples. Next, YWHAG and RAB11A protein expression were tested by Western blot in VAT from a subset of obese (8/15) and non-obese (7/10) females. These samples were also probed with an actin antibody for protein normalization. As shown in Figure 7, both

YWHAG and RAB11A proteins were significantly more ($p = 0.001$ and $p = 0.00001$, respectively) up-expressed in obese than in non-obese VAT tissues.

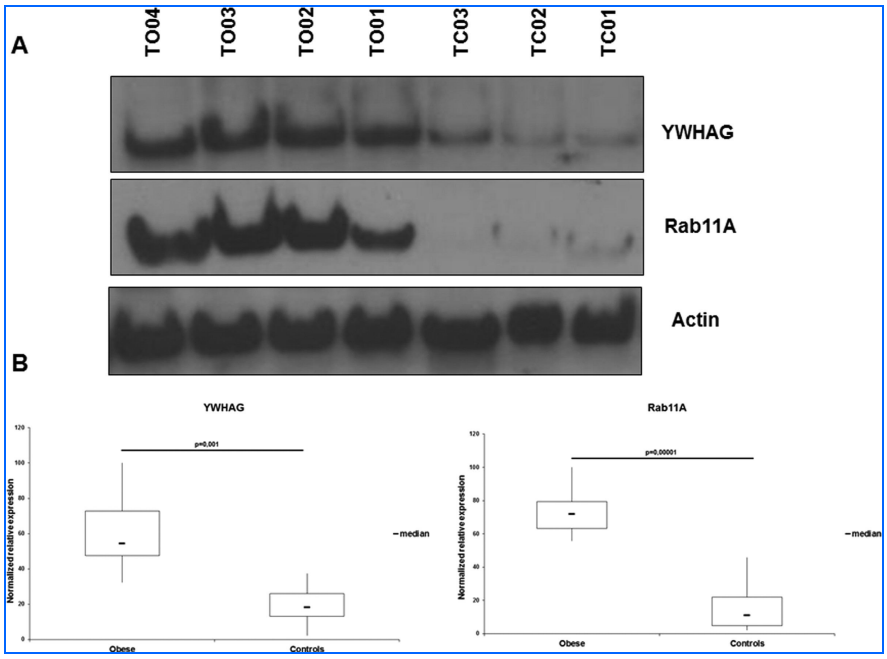

Figure 7. Western blot for YWHAG and Rab11a evaluation. (A) An example of the Western blot evaluation of YWHAG and RAB11A proteins from VAT of randomly selected obese females (TO01, TO02, TO03, TO04) and controls (TC01, TC02, TC03). (B) The box plots of the data normalized to actin content, after densitometric analysis of YWHAG and RAB11A immunoblots. The data are expressed as percent relative expression, the sample with the highest expression of either RAB11A ($p = 0.00001$) or YWHAG ($p = 0.001$) having been set as 100%. The bottom and top of each box represent the 25th and 75th percentile, respectively; the thick band inside each box shows the 50th percentile (the median). The ends of the whiskers represent the minimum and maximum values of each group of data.

Taken together, these data suggest that in VAT from obese females, there is a functional interplay between the mRNAs of two up-expressed proteins (YWHAG and RAB11A, as emerged from 2D-DIGE analysis, qRT-PCR, and Western blot validations) and two down-expressed miRNAs (miR-141 and miR-520e, respectively, as revealed by the transcriptomic screening and qRT-PCR analysis).

Luciferase Assay

To determine whether the mRNAs of YWHAG and RAB11A are targets of miR-141 and miR-520e respectively, the regions encompassing the 3′UTRs of the two mRNAs were cloned downstream the Renilla luciferase gene, under the transcriptional control of the cytomegalovirus promoter. The constructs were co-transfected with the pre-miRNAs for miR-141 or miR-520e, and as a transfection control, were used a pGL3-control expressing firefly luciferase. As shown in Figure 8, both pre-miR-520e (A) and pre-miR-141 (B) significantly reduced the normalized Renilla luciferase activities of the constructs containing respectively the RAB11A ($p = 0.004$) and the YWHAG

3′UTRs (p = 0.02). No inhibition was observed in mutant 3′UTR of RAB11A (A) and YWHAG (B) constructs. These data are consistent with a functional interaction between the selected miRNAs and the 3′UTRs of their mRNA targets, thereby suggesting that changes in the levels of these two miRNAs may modulate the expression of RAB11A and YWHAG.

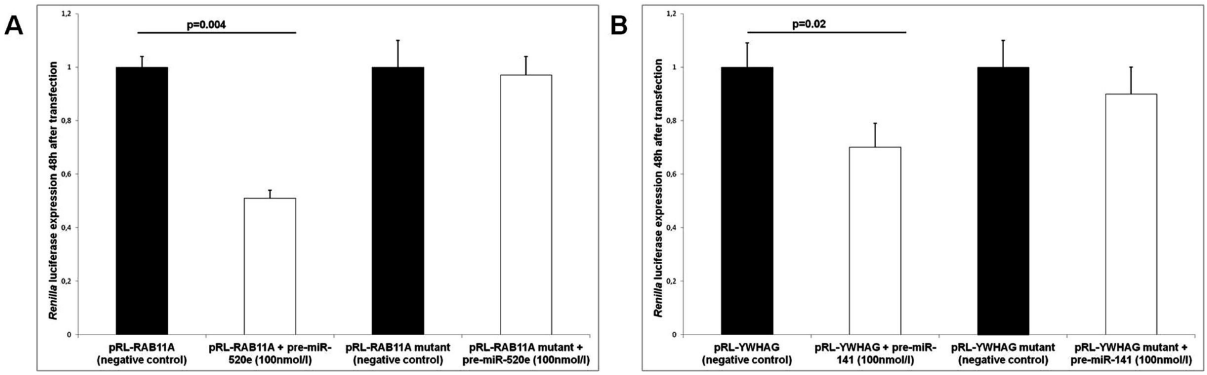

Figure 8. Validation of interaction between selected miRNAs and proteins. To validate the interaction between miR-520e and miR-141 with respectively wild-type or mutant 3′UTR of RAB11A or YWHAG. HEK-293 cells were transfected with wild-type or mutant 3′UTR of RAB11A, pGL3-control, pre-miR-520e, or pre-miR-negative control (A) and with wild-type or mutant 3′UTR of YWHAG, pGL3-control, pre-miR-141, or pre-miR-negative control (B). Pre-miR-520e and the pre-miR-141 significantly inhibited the expression of a Renilla luciferase-expressing construct that contains the 3′UTR region of the RAB11A (p = 0.004) and YWHAG (p = 0.02), respectively. No inhibition was observed in mutant 3′UTR of RAB11A (A) and YWHAG (B) constructs. All experiments were done in triplicate. Error bars denote SEM.

miRNA expression profile in amnion

The miRNA expression profiles were evaluated in the amnion from 10 obese and 5 normal weight pregnant women. A large percentage (74%) of the analyzed miRNAs was expressed (271/365), whereas 26% was not (94/365). Most of the expressed miRNAs (90%, 243/271) did not differ between obese and control women and were not further investigated. On the contrary, 4.8% of miRNAs (13/271) were higher and 4.4% (12/271) were lower in obese than normal weight control (Figure 9). Interestingly, 7/271 miRNAs were obesity specific being expressed only in amnion from obese women (miR-422b, miR-219, miR-575, miR-523, miR-579, miR-618 and miR-659). The expression levels of these miRNAs were further validated by quantitative real-time polymerase chain reaction and were in close agreement with those obtained with TaqMan array, except for the slight differences because of the two different methodologies. The mean RQ values in obese respect to control are the following: miR-422b=6.4; miR-23b=1.19; miR-338=1.25; miR-139=0.68; and miR-449b=0.9.

Pathways deregulated in the amnion

Bioinformatics showed that differently expressed miRNAs had a significant probability ($p<0.01$) of deregulating several genes and metabolic pathways (Figure 9 panel c and d). Among pathways regulated by differently

expressed miRNAs, the most represented pathway is cancer regulation (including 17 genes regulated by up-expressed miRNAs and 11 genes regulated by down-expressed miRNAs) following by focal adhesion (including 10 genes regulated by down-expressed miRNAs) and MAPK signaling (including 9 genes regulated by up-expressed miRNAs). Moreover, there are many miRNA-regulated genes involved in different pathways related to cell-cell interaction and cell structure maintenance.

The obesity-specific miRNAs regulate 7 metabolic pathways, the most representative are MAPK and Cancer/Erb signaling (including 10 genes respectively) (Figure 10).

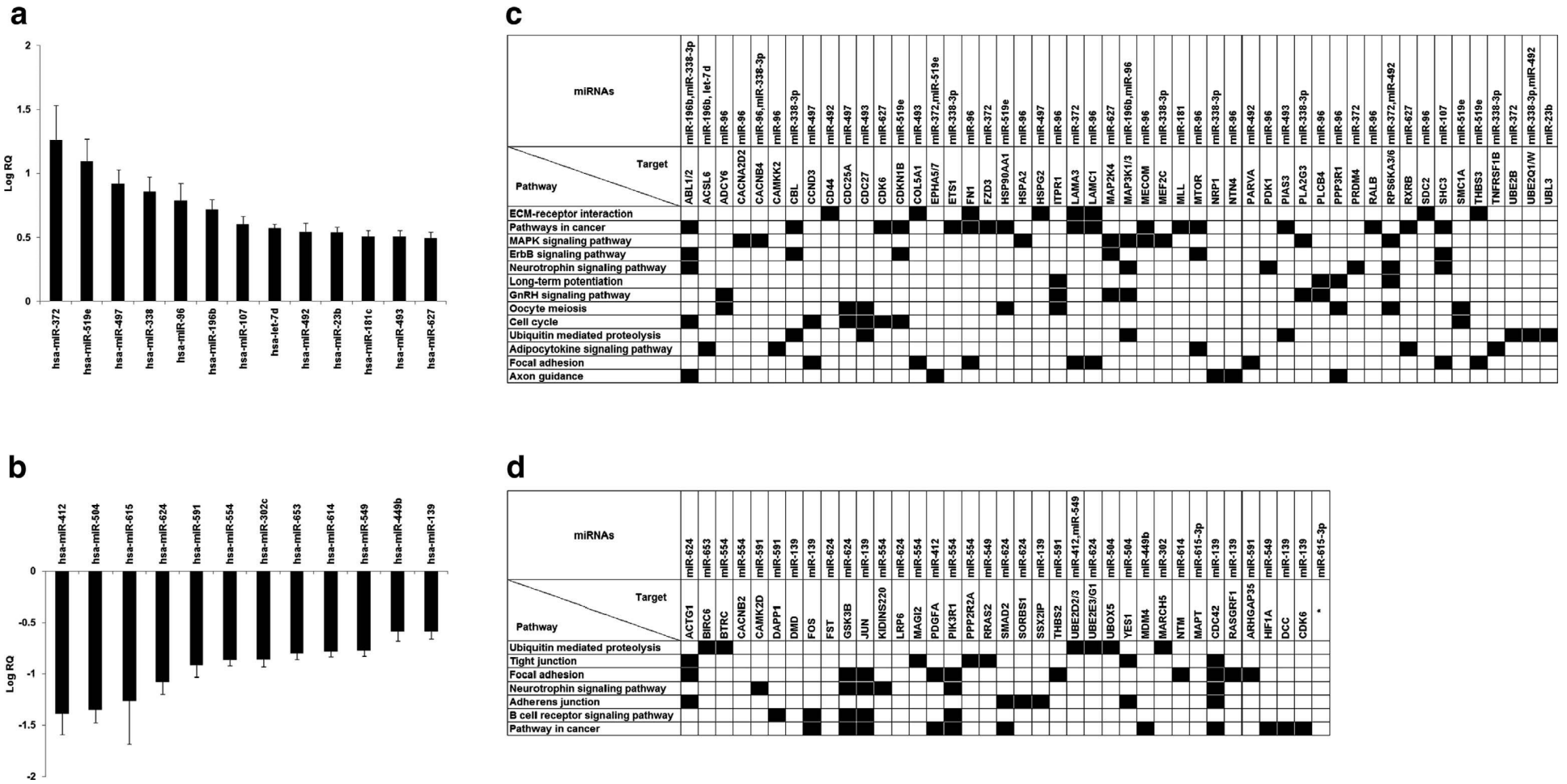

Figure 9. Differently expressed miRNAs in amnion from obese and control women and their predicted target genes. Panels (a) and (b) depict miRNAs up-expressed and down-expressed, respectively. miRNA expression levels are shown as Log RQ mean and s.e.m. (The miRNA expression values were first normalized to RNU48, after which, the relative quantification was calculated as: $RQ=2^{-\Delta\Delta Ct}$, where $\Delta\Delta Ct=(Ct_{obese}(miRNA)-Ct_{obese}\ (RNU48))-(Ct_{calibrator}\ (miRNA)-Ct_{calibrator}\ (RNU48))$). Panels (c) and (d) show metabolic pathways (black squares) and genes targeted by miRNAs ($P<0.01$) up-expressed and down-expressed, respectively. *Pathways significantly regulated by target genes of miR-615-3p were not reported by TargetScan.

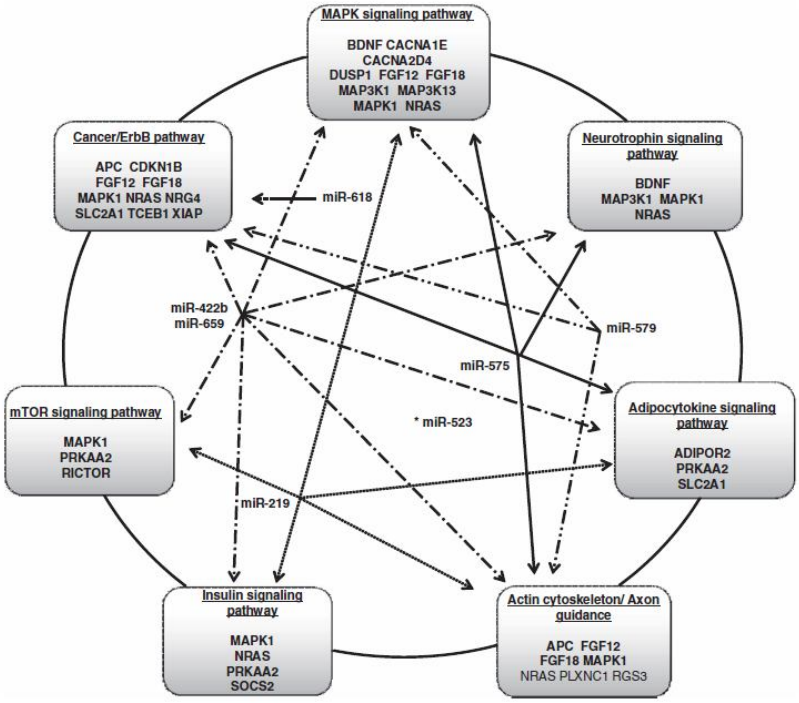

Figure 10. Pathways and genes predicted by bioinformatics to be regulated by obesity-specific miRNAs in amnion. The metabolic pathways and genes targeted by obesity-specific miRNAs (miR-422b, miR-219, miR-575, miR-579, miR-618 and miR-659) are reported in boxes . The arrows connect miRNAs to target genes in each pathway. *Conserved target genes of miR-523 were not predicted by TargetScan.

Characterization of hA-MSCs

The hA-MSCs were isolated from the mesenchymal layer of amniotic membranes obtained from all enrolled women at delivery. The foetal origin of isolated hA-MSCs was confirmed by STR typing of the mother's DNA and of the hA-MSCs. All isolated hA-MSCs were collected after four population doublings. The mesenchymal origin of the isolated cells was confirmed evaluating morphology and immunophenotype. Cultured Ob- and Co-hA-MSCs showed a similar fibroblastic-like morphology (Figure 11). The immunophenotype showed that isolated hA-MSCs expressed on the surface the following mesenchymal markers: CD9, CD10, CD13, CD26, CD29, CD44, CD47, CD49d, CD54, CD56, CD58, CD71, CD81, CD90, CD99, CD105, CD151, CD166, CD200. But they didn't express on the surface hematopoietic antigens (CD14, CD15, CD16, CD19, CD28, CD33, CD34, CD45, and CD117), the endothelial marker PECAM-1/CD31, and non-lineage markers (thrombospondin receptor/CD36, Bp50/CD40, Prominin-1/CD133, MDR-1/CD243, NGFR/CD271, ABCG-2/CD338, and HLA-DR).

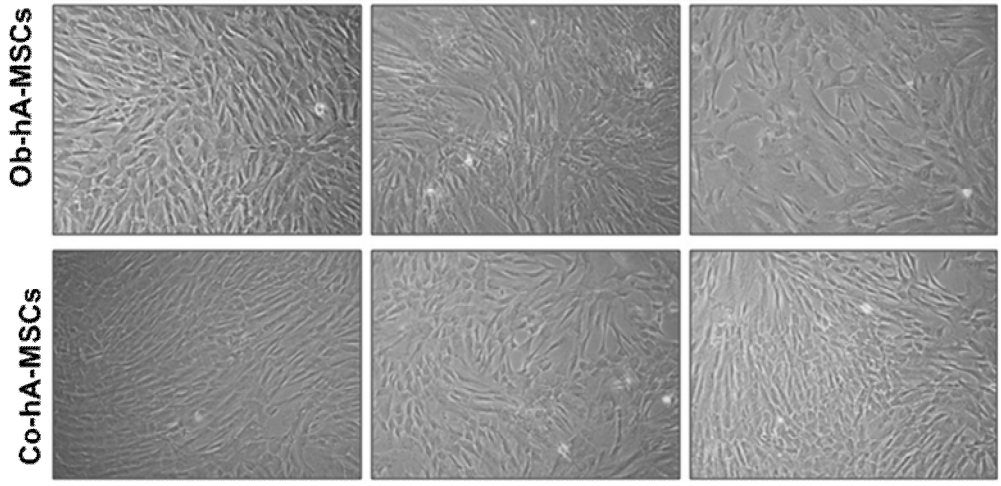

Figure 11. Morphological characterization of isolated hA-MSC. The MSCs isolated from the amnion showed a similar fibroblastic-like morphology after four population doublings.

miRNA expression profile in hA-MSCs

The miRNA expression profiles were evaluated in hA-MSCs isolated from amnion of 16 obese and 7 control women. A large set of the tested miRNAs was expressed in Ob- and Co-hA-MSCs (61.4% corresponding to 232 miRNAs), whereas a small set (38.6%) was not expressed. Most of the expressed miRNAs (89.2%, 207/232) did not differ between Ob- and Co-hA-MSCs and were not further investigated. Conversely, 4.8% of miRNAs (11/232) was higher and 6.0% (14/232) was lower in Ob- vs Co-hA-MSCs (Figure 12, panel A and B respectively). Interestingly, 7/232 miRNAs (miR-365-3p, miR-155, miR-199b, miR-22, miR-542-5p, miR-597, and miR-629) were obesity-specific, being expressed only in hA-MSCs isolated from obese women (Figure 12, panel C). Among miRNAs differently expressed, miR-449b was down-expressed both in hA-MSCs and in amnion from obese compared normal weight control.

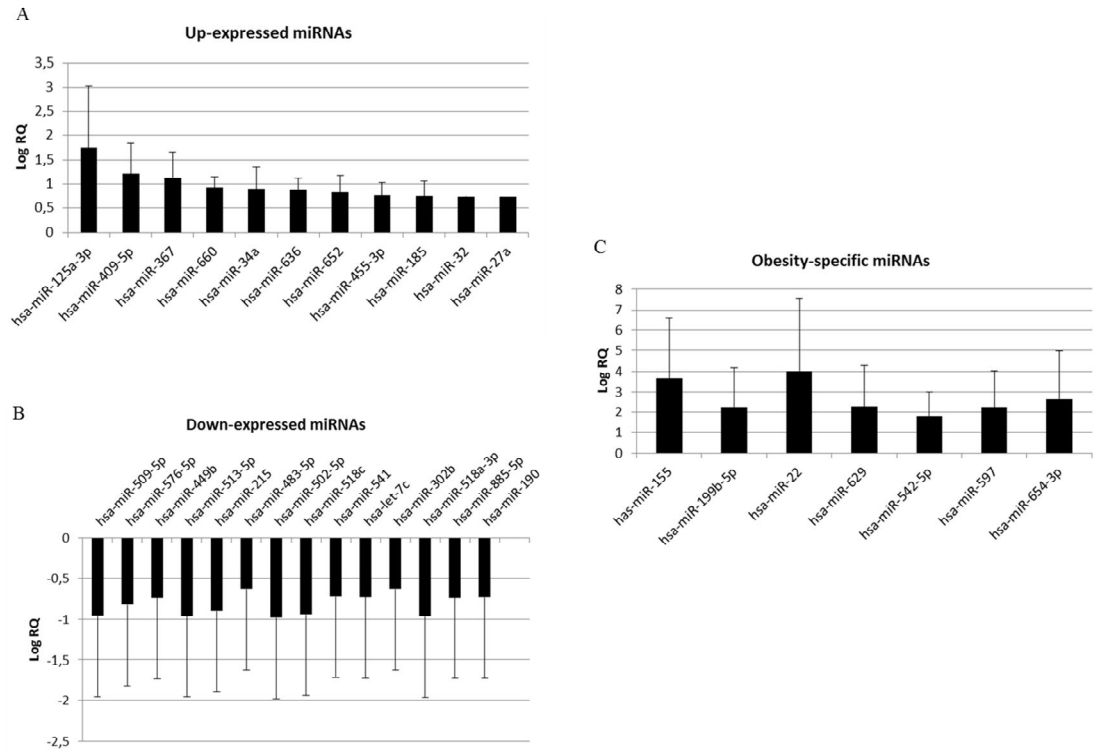

Figure 12. Differently expressed miRNAs in Ob-hA-MSCs compared to Co-hA-MSCs. Panels A and B show up- and down-expressed miRNAs, respectively; panel C shows miRNA expressed only in Ob-hA-MSCs. MiRNAs expression levels are shown as LogRQ mean and sem.

Pathways deregulated in hA-MSCs

Bioinformatics showed that differently expressed miRNAs had a significant probability ($p<0.001$) of deregulating several genes and biological pathways (Table 6, Table 7, Table 8). The most represented pathway was composed by genes involved in metabolic pathways (including 57 genes regulated by up-expressed miRNA), followed by cancer regulation (including 35 genes regulated by up-expressed miRNAs and 22 genes regulated by down-expressed miRNAs) and MAPK signaling (including 26 genes targeted by up-expressed and 15 genes by down-expressed miRNAs). The pathways potentially deregulated both up- and down-expressed miRNAs targeted different genes.

The obesity-specific miRNAs in hA-MSCs regulate 2 pathways: endocytosis and cancer singalling.

Up-expressed miRNAs in Ob- respect to Co-hA-MSCs were involved in the same pathways resulted also regulated by miRNAs in amnios from obese women, such as: pathways in cancer, MAPK signalling, ErbB signaling pathway, Neurotrophin signaling pathway, GnRH signaling pathway, focal adhesion, and axon guidance.

Table 6. Pathways deregulated by up-expressed miRNAs

Patways in cancer	APPL1	adaptor protein, phosphotyrosine interaction, PH domain and leucine zipper containing 1
	CAMK2A	calcium/calmodulin-dependent protein kinase II alpha
	CCDC6	coiled-coil domain containing 6
	CCNE2	cyclin E2
	CREB1	cAMP responsive element binding protein 1
	CSF1R	colony stimulating factor 1 receptor
	DCC	deleted in colorectal carcinoma
	E2F3	E2F transcription factor 3
	EGFR	epidermal growth factor receptor
	ELK1	ELK1, member of ETS oncogene family
	EPAS1	endothelial PAS domain protein 1
	FGF23	fibroblast growth factor 23
	GAB1	GRB2-associated binding protein 1
	GRB2	growth factor receptor-bound protein 2
	ITGAV	integrin, alpha V
	KITLG	KIT ligand
	KRAS	v-Ki-ras2 Kirsten rat sarcoma viral oncogene homolog
	LEF1	lymphoid enhancer-binding factor 1
	MAP2K1	mitogen-activated protein kinase kinase 1
	MAPK10	mitogen-activated protein kinase 10
	MET	met proto-oncogene (hepatocyte growth factor receptor)
	PAK6	p21 protein (Cdc42/Rac)-activated kinase 6
	PAK7	p21 protein (Cdc42/Rac)-activated kinase 7
	PDGFRA	platelet-derived growth factor receptor, alpha polypeptide
	PIK3R3	phosphoinositide-3-kinase, regulatory subunit 3 (gamma)
	PPARG	peroxisome proliferator-activated receptor gamma
	PRKCB	protein kinase C, beta
	PTEN	phosphatase and tensin homolog
	RALGDS	ral guanine nucleotide dissociation stimulator
	RUNX1	runt-related transcription factor 1
	SHC4	SHC (Src homology 2 domain containing) family, member 4
	VEGFA	vascular endothelial growth factor A
	VEGFC	vascular endothelial growth factor C
Erb signalling pathways	SHC4	SHC (Src homology 2 domain containing) family, member 4
	PAK7	p21 protein (Cdc42/Rac)-activated kinase 7
	MAP2K1	mitogen-activated protein kinase kinase 1
	KRAS	v-Ki-ras2 Kirsten rat sarcoma viral oncogene homolog
	ELK1	ELK1, member of ETS oncogene family
	SRC	v-src sarcoma (Schmidt-Ruppin A-2) viral oncogene homolog (avian)
	EGFR	epidermal growth factor receptor
	GRB2	growth factor receptor-bound protein 2
	PAK6	p21 protein (Cdc42/Rac)-activated kinase 6
	ABL2	v-abl Abelson murine leukemia viral oncogene homolog 2
	AREG	Amphiregulin
	PRKCB	protein kinase C, beta
	PIK3R3	phosphoinositide-3-kinase, regulatory subunit 3 (gamma)
	MAPK10	mitogen-activated protein kinase 10
	MAP2K4	mitogen-activated protein kinase kinase 4
	GAB1	GRB2-associated binding protein 1
	CAMK2A	calcium/calmodulin-dependent protein kinase II alpha

MAPK signalling pathways	GNG12	guanine nucleotide binding protein (G protein), gamma 12
	RRAS	related RAS viral (r-ras) oncogene homolog
	RAPGEF2	Rap guanine nucleotide exchange factor (GEF) 2
	CACNA1E	calcium channel, voltage-dependent, R type, alpha 1E subunit
	CACNA1A	calcium channel, voltage-dependent, P/Q type, alpha 1A subunit
	MAP2K1	mitogen-activated protein kinase kinase 1
	NLK	nemo-like kinase
	PRKX	protein kinase, X-linked
	KRAS	v-Ki-ras2 Kirsten rat sarcoma viral oncogene homolog
	ELK1	ELK1, member of ETS oncogene family
	CACNA2D3	calcium channel, voltage-dependent, alpha 2/delta subunit 3
	RPS6KA5	ribosomal protein S6 kinase, 90kDa, polypeptide 5
	PDGFRA	platelet-derived growth factor receptor, alpha polypeptide
	DUSP5	dual specificity phosphatase 5
	EGFR	epidermal growth factor receptor
	HSPA1B	heat shock 70kDa protein 1B
	GRB2	growth factor receptor-bound protein 2
	PRKCB	protein kinase C, beta
	DUSP10	dual specificity phosphatase 10
	RPS6KA4	ribosomal protein S6 kinase, 90kDa, polypeptide 4
	PPM1A	protein phosphatase, Mg2+/Mn2+ dependent, 1A
	CACNB3	calcium channel, voltage-dependent, beta 3 subunit
	FGF23	fibroblast growth factor 23
	MAP3K12	mitogen-activated protein kinase kinase kinase 12
	MAPK10	mitogen-activated protein kinase 10
	CACNA1I	calcium channel, voltage-dependent, T type, alpha 1I subunit
	MAP2K4	mitogen-activated protein kinase kinase 4
Fochal adhesion	VEGFC	vascular endothelial growth factor C
	SHC4	SHC (Src homology 2 domain containing) family, member 4
	PAK7	p21 protein (Cdc42/Rac)-activated kinase 7
	MAP2K1	mitogen-activated protein kinase kinase 1
	ITGA5	integrin, alpha 5 (fibronectin receptor, alpha polypeptide)
	RELN	reelin
	VEGFA	vascular endothelial growth factor A
	ELK1	ELK1, member of ETS oncogene family
	PDGFRA	platelet-derived growth factor receptor, alpha polypeptide
	SRC	v-src sarcoma (Schmidt-Ruppin A-2) viral oncogene homolog (avian)
	EGFR	epidermal growth factor receptor
	GRB2	growth factor receptor-bound protein 2
	PAK6	p21 protein (Cdc42/Rac)-activated kinase 6
	FYN	FYN oncogene related to SRC, FGR, YES
	PRKCB	protein kinase C, beta
	PTEN	phosphatase and tensin homolog
	PIK3R3	phosphoinositide-3-kinase, regulatory subunit 3 (gamma)
	COL1A2	collagen, type I, alpha 2
	ITGAV	integrin, alpha V
	MET	met proto-oncogene (hepatocyte growth factor receptor)
	MAPK10	mitogen-activated protein kinase 10

Table 6. Continues

Metabolic pathways	NDUFC2	NADH dehydrogenase (ubiquinone) 1, subcomplex unknown, 2, 14.5kDa
	FUK	Fucokinase
	PPCS	phosphopantothenoylcysteine synthetase
	DGKZ	diacylglycerol kinase, zeta
	UGP2	UDP-glucose pyrophosphorylase 2
	PAPSS2	3'-phosphoadenosine 5'-phosphosulfate synthase 2
	SDHC	succinate dehydrogenase complex, subunit C, integral membrane protein, 15kDa
	ATP6V1A	ATPase, H+ transporting, lysosomal 70kDa, V1 subunit A
	XYLT1	xylosyltransferase I
	SGMS1	sphingomyelin synthase 1
	ADO	2-aminoethanethiol (cysteamine) dioxygenase
	SLC33A1	solute carrier family 33 (acetyl-CoA transporter), member 1
	ASAH1	N-acylsphingosine amidohydrolase (acid ceramidase) 1
	MGAT5B	mannosyl (alpha-1,6-)-glycoprotein beta-1,6-N-acetyl-glucosaminyltransferase, isozyme B
	INPP1	inositol polyphosphate-1-phosphatase
	PGAP1	post-GPI attachment to proteins 1
	BCAT2	branched chain amino-acid transaminase 2, mitochondrial
	CDS1	CDP-diacylglycerol synthase (phosphatidate cytidylyltransferase) 1
	NDUFS4	NADH dehydrogenase (ubiquinone) Fe-S protein 4, 18kDa (NADH-coenzyme Q reductase)
	ALDH4A1	aldehyde dehydrogenase 4 family, member A1
	GNS	glucosamine (N-acetyl)-6-sulfatase
	FUT9	fucosyltransferase 9 (alpha (1,3) fucosyltransferase)
	NMNAT2	nicotinamide nucleotide adenylyltransferase 2
	MGAT4A	mannosyl (alpha-1,3-)-glycoprotein beta-1,4-N-acetylglucosaminyltransferase, isozyme A
	ALG13	asparagine-linked glycosylation 13 homolog (S. cerevisiae)
	FUT8	fucosyltransferase 8 (alpha (1,6) fucosyltransferase)
	MAN2A1	mannosidase, alpha, class 2A, member 1
	ATP6V0A2	ATPase, H+ transporting, lysosomal V0 subunit a2
	ACSL4	acyl-CoA synthetase long-chain family member 4
	DGKB	diacylglycerol kinase, beta 90kDa
	MMAB	methylmalonic aciduria (cobalamin deficiency) cblB type
	DNMT1	DNA (cytosine-5-)-methyltransferase 1
	CTH	cystathionase (cystathionine gamma-lyase)
	ALG9	asparagine-linked glycosylation 9, alpha-1,2-mannosyltransferase homolog (S. cerevisiae)
	PGM1	phosphoglucomutase 1
	GCNT2	glucosaminyl (N-acetyl) transferase 2, I-branching enzyme (I blood group)
	GALNT5	UDP-N-acetyl-alpha-D-galactosamine:polypeptide N-acetylgalactosaminyltransferase 5 (GalNAc-T5)
	LDHA	lactate dehydrogenase A
	AK4	adenylate kinase 4
	ST6GALNAC3	ST6 (alpha-N-acetyl-neuraminyl-2,3-beta-galactosyl-1,3)-N-acetylgalactosaminide alpha-2,6-sialyltransferase 3
	GALNT7	UDP-N-acetyl-alpha-D-galactosamine:polypeptide N-acetylgalactosaminyltransferase 7 (GalNAc-T7)
	IDH1	isocitrate dehydrogenase 1 (NADP+), soluble
	SPTLC2	serine palmitoyltransferase, long chain base subunit 2
	PDHX	pyruvate dehydrogenase complex, component X
	DGKE	diacylglycerol kinase, epsilon 64kDa
	GLCE	glucuronic acid epimerase
	UAP1	UDP-N-acteylglucosamine pyrophosphorylase 1
	ATP6V1F	ATPase, H+ transporting, lysosomal 14kDa, V1 subunit F
	DGKI	diacylglycerol kinase, iota
	GCH1	GTP cyclohydrolase 1
	ALDOA	aldolase A, fructose-bisphosphate
	B3GALT2	UDP-Gal:betaGlcNAc beta 1,3-galactosyltransferase, polypeptide 2
	PAFAH1B2	platelet-activating factor acetylhydrolase 1b, catalytic subunit 2 (30kDa)
	GPAM	glycerol-3-phosphate acyltransferase, mitochondrial
	B4GALT3	UDP-Gal:betaGlcNAc beta 1,4- galactosyltransferase, polypeptide 3
	PGAM1	phosphoglycerate mutase 1 (brain)
	ST6GAL2	ST6 beta-galactosamide alpha-2,6-sialyltranferase 2
	PIP5K1B	phosphatidylinositol-4-phosphate 5-kinase, type I, beta
Regulation of actin cytoskeleton	GNG12	guanine nucleotide binding protein (G protein), gamma 12
	RRAS	related RAS viral (r-ras) oncogene homolog
	WASF1	WAS protein family, member 1
	SSH1	slingshot homolog 1 (Drosophila)
	PAK7	p21 protein (Cdc42/Rac)-activated kinase 7
	MAP2K1	mitogen-activated protein kinase kinase 1
	ITGA5	integrin, alpha 5 (fibronectin receptor, alpha polypeptide)
	KRAS	v-Ki-ras2 Kirsten rat sarcoma viral oncogene homolog
	ENAH	enabled homolog (Drosophila)
	PDGFRA	platelet-derived growth factor receptor, alpha polypeptide
	EGFR	epidermal growth factor receptor
	PAK6	p21 protein (Cdc42/Rac)-activated kinase 6
	WASL	Wiskott-Aldrich syndrome-like
	LIMK1	LIM domain kinase 1
	CHRM5	cholinergic receptor, muscarinic 5
	PIK3R3	phosphoinositide-3-kinase, regulatory subunit 3 (gamma)
	ITGAV	integrin, alpha V
	PIKFYVE	phosphoinositide kinase, FYVE finger containing
	FGF23	fibroblast growth factor 23
	PIP5K1B	phosphatidylinositol-4-phosphate 5-kinase, type I, beta
Phosphatydilinositol signaling	DGKZ	diacylglycerol kinase, zeta
	PTEN	phosphatase and tensin homolog
	PRKCB	protein kinase C, beta
	DGKI	diacylglycerol kinase, iota
	ITPR1	inositol 1,4,5-trisphosphate receptor, type 1
	PIK3R3	phosphoinositide-3-kinase, regulatory subunit 3 (gamma)
	PIKFYVE	phosphoinositide kinase, FYVE finger containing
	DGKB	diacylglycerol kinase, beta 90kDa
	INPP1	inositol polyphosphate-1-phosphatase
	DGKE	diacylglycerol kinase, epsilon 64kDa
	CDS1	CDP-diacylglycerol synthase (phosphatidate cytidylyltransferase) 1
	PIP5K1B	phosphatidylinositol-4-phosphate 5-kinase, type I, beta
Calcium signaling pathways	CACNA1E	calcium channel, voltage-dependent, R type, alpha 1E subunit
	CACNA1A	calcium channel, voltage-dependent, P/Q type, alpha 1A subunit
	P2RX7	purinergic receptor P2X, ligand-gated ion channel, 7
	PRKX	protein kinase, X-linked
	ADORA2B	adenosine A2b receptor
	PDGFRA	platelet-derived growth factor receptor, alpha polypeptide
	EGFR	epidermal growth factor receptor
	GRM5	glutamate receptor, metabotropic 5
	PTGER3	prostaglandin E receptor 3 (subtype EP3)
	ATP2A2	ATPase, Ca++ transporting, cardiac muscle, slow twitch 2
	PRKCB	protein kinase C, beta
	ITPR1	inositol 1,4,5-trisphosphate receptor, type 1
	CHRM5	cholinergic receptor, muscarinic 5
	ADRB1	adrenoceptor beta 1
	ADCY3	adenylate cyclase 3
	CACNA1I	calcium channel, voltage-dependent, T type, alpha 1I subunit
	CAMK2A	calcium/calmodulin-dependent protein kinase II alpha
N-Glycan biosynthesis	ALG9	asparagine-linked glycosylation 9, alpha-1,2-mannosyltransferase homolog (S. cerevisiae)
	MGAT4A	mannosyl (alpha-1,3-)-glycoprotein beta-1,4-N-acetylglucosaminyltransferase, isozyme A
	ALG13	asparagine-linked glycosylation 13 homolog (S. cerevisiae)
	FUT8	fucosyltransferase 8 (alpha (1,6) fucosyltransferase)
	MAN2A1	mannosidase, alpha, class 2A, member 1
	MGAT5B	mannosyl (alpha-1,6-)-glycoprotein beta-1,6-N-acetyl-glucosaminyltransferase, isozyme B
	B4GALT3	UDP-Gal:betaGlcNAc beta 1,4- galactosyltransferase, polypeptide 3
	ST6GAL2	ST6 beta-galactosamide alpha-2,6-sialyltranferase 2

Table 6. Continues

GnRH signaling pathway	GRB2	growth factor receptor-bound protein 2
	PRKCB	protein kinase C, beta
	ITPR1	inositol 1,4,5-trisphosphate receptor, type 1
	MAP2K1	mitogen-activated protein kinase kinase 1
	PRKX	protein kinase, X-linked
	ADCY3	adenylate cyclase 3
	KRAS	v-Ki-ras2 Kirsten rat sarcoma viral oncogene homolog
	ELK1	ELK1, member of ETS oncogene family
	MAPK10	mitogen-activated protein kinase 10
	MAP2K4	mitogen-activated protein kinase kinase 4
	SRC	v-src sarcoma (Schmidt-Ruppin A-2) viral oncogene homolog (avian)
	CAMK2A	calcium/calmodulin-dependent protein kinase II alpha
	EGFR	epidermal growth factor receptor
Gap junction	GRB2	growth factor receptor-bound protein 2
	PRKCB	protein kinase C, beta
	ITPR1	inositol 1,4,5-trisphosphate receptor, type 1
	MAP2K1	mitogen-activated protein kinase kinase 1
	ADRB1	adrenoceptor beta 1
	PRKX	protein kinase, X-linked
	ADCY3	adenylate cyclase 3
	KRAS	v-Ki-ras2 Kirsten rat sarcoma viral oncogene homolog
	PDGFRA	platelet-derived growth factor receptor, alpha polypeptide
	SRC	v-src sarcoma (Schmidt-Ruppin A-2) viral oncogene homolog (avian)
	EGFR	epidermal growth factor receptor
	GRM5	glutamate receptor, metabotropic 5
Neurotrophin signaling pathways	GRB2	growth factor receptor-bound protein 2
	IRS1	insulin receptor substrate 1
	SHC4	SHC (Src homology 2 domain containing) family, member 4
	NGFRAP1	nerve growth factor receptor (TNFRSF16) associated protein 1
	MAP2K1	mitogen-activated protein kinase kinase 1
	YWHAQ	tyrosine 3-monooxygenase/tryptophan 5-monooxygenase activation protein, theta polypeptide
	PIK3R3	phosphoinositide-3-kinase, regulatory subunit 3 (gamma)
	RPS6KA4	ribosomal protein S6 kinase, 90kDa, polypeptide 4
	KRAS	v-Ki-ras2 Kirsten rat sarcoma viral oncogene homolog
	PSEN1	presenilin 1
	MAPK10	mitogen-activated protein kinase 10
	RPS6KA5	ribosomal protein S6 kinase, 90kDa, polypeptide 5
	GAB1	GRB2-associated binding protein 1
	CAMK2A	calcium/calmodulin-dependent protein kinase II alpha
Axon Guidance	PAK6	p21 protein (Cdc42/Rac)-activated kinase 6
	SRGAP2	SLIT-ROBO Rho GTPase activating protein 2
	FYN	FYN oncogene related to SRC, FGR, YES
	EPHB2	EPH receptor B2
	SEMA4C	sema domain, immunoglobulin domain (Ig), transmembrane domain (TM) and short cytoplasmic domain, (semaphorin) 4C
	SEMA4F	sema domain, immunoglobulin domain (Ig), transmembrane domain (TM) and short cytoplasmic domain, (semaphorin) 4F
	PAK7	p21 protein (Cdc42/Rac)-activated kinase 7
	DCC	deleted in colorectal carcinoma
	LIMK1	LIM domain kinase 1
	RGS3	regulator of G-protein signaling 3
	SEMA7A	semaphorin 7A, GPI membrane anchor (John Milton Hagen blood group)
	KRAS	v-Ki-ras2 Kirsten rat sarcoma viral oncogene homolog
	MET	met proto-oncogene (hepatocyte growth factor receptor)
	EFNB1	ephrin-B1

Insulin signaling pathways	GRB2	growth factor receptor-bound protein 2
	PRKAA2	protein kinase, AMP-activated, alpha 2 catalytic subunit
	PPP1R3B	protein phosphatase 1, regulatory subunit 3B
	IRS1	insulin receptor substrate 1
	TSC1	tuberous sclerosis 1
	SHC4	SHC (Src homology 2 domain containing) family, member 4
	MAP2K1	mitogen-activated protein kinase kinase 1
	PIK3R3	phosphoinositide-3-kinase, regulatory subunit 3 (gamma)
	PRKX	protein kinase, X-linked
	KRAS	v-Ki-ras2 Kirsten rat sarcoma viral oncogene homolog
	ELK1	ELK1, member of ETS oncogene family
	FLOT2	flotillin 2
	MAPK10	mitogen-activated protein kinase 10
	PRKAR2A	protein kinase, cAMP-dependent, regulatory, type II, alpha
Dorso-ventral axis formation	GRB2	growth factor receptor-bound protein 2
	KRAS	v-Ki-ras2 Kirsten rat sarcoma viral oncogene homolog
	NOTCH1	notch 1
	EGFR	epidermal growth factor receptor
	FMN2	formin 2
	MAP2K1	mitogen-activated protein kinase kinase 1
Bacterial invasion of epithelial cells	SHC4	SHC (Src homology 2 domain containing) family, member 4
	WASF1	WAS protein family, member 1
	WASL	Wiskott-Aldrich syndrome-like
	ITGA5	integrin, alpha 5 (fibronectin receptor, alpha polypeptide)
	PIK3R3	phosphoinositide-3-kinase, regulatory subunit 3 (gamma)
	MET	met proto-oncogene (hepatocyte growth factor receptor)
	GAB1	GRB2-associated binding protein 1
	SRC	v-src sarcoma (Schmidt-Ruppin A-2) viral oncogene homolog (avian)
	ARHGEF26	Rho guanine nucleotide exchange factor (GEF) 26
Endocytosis	EPN2	epsin 2
	VPS37A	vacuolar protein sorting 37 homolog A (S. cerevisiae)
	RNF41	ring finger protein 41
	VPS37B	vacuolar protein sorting 37 homolog B (S. cerevisiae)
	ADRB1	adrenoceptor beta 1
	MET	met proto-oncogene (hepatocyte growth factor receptor)
	FAM125B	family with sequence similarity 125, member B
	PDGFRA	platelet-derived growth factor receptor, alpha polypeptide
	GIT2	G protein-coupled receptor kinase interacting ArfGAP 2
	SRC	v-src sarcoma (Schmidt-Ruppin A-2) viral oncogene homolog (avian)
	PARD6B	par-6 partitioning defective 6 homolog beta (C. elegans)
	EGFR	epidermal growth factor receptor
	NEDD4	neural precursor cell expressed, developmentally down-regulated 4, E3 ubiquitin protein ligase
	HSPA1B	heat shock 70kDa protein 1B
	PIP5K1B	phosphatidylinositol-4-phosphate 5-kinase, type I, beta
	CSF1R	colony stimulating factor 1 receptor

Table 7. Pathways deregulated by down-expressed miRNAs

Pathways in cancer	CASP3	caspase 3, apoptosis-related cysteine peptidase
	CEBPA	CCAAT/enhancer binding protein (C/EBP), alpha
	COL4A6	collagen, type IV, alpha 6
	CTNNB1	catenin (cadherin-associated protein), beta 1, 88kDa
	DVL3	transforming growth factor, beta receptor 1
	EDN1	endothelin 1
	EDNRB	endothelin receptor type B
	FAS	Fas (TNF receptor superfamily, member 6)
	FZD3	frizzled family receptor 3
	FZD4	frizzled family receptor 4
	FZD6	frizzled family receptor 6
	IGF1R	insulin-like growth factor 1 receptor
	LAMA3	laminin, alpha 3
	NRAS	neuroblastoma RAS viral (v-ras) oncogene homolog
	RELA	v-rel reticuloendotheliosis viral oncogene homolog A (avian)
	SMAD2	SMAD family member 2
	STK4	serine/threonine kinase 4
	TGFBR1	transforming growth factor, beta receptor 1
	TGFBR2	transforming growth factor, beta receptor II (70/80kDa)
	WNT11	wingless-type MMTV integration site family, member 11
	WNT4	wingless-type MMTV integration site family, member 4
MAPK signalling pathways	CASP3	caspase 3, apoptosis-related cysteine peptidase
	NRAS	neuroblastoma RAS viral (v-ras) oncogene homolog
	RAP1B	RAP1B, member of RAS oncogene family
	TGFBR1	transforming growth factor, beta receptor 1
	MAP4K3	mitogen-activated protein kinase kinase kinase kinase 3
	NGF	nerve growth factor (beta polypeptide)
	TGFBR2	transforming growth factor, beta receptor II (70/80kDa)
	FAS	Fas (TNF receptor superfamily, member 6)
	MAP3K2	mitogen-activated protein kinase kinase kinase 2
	CACNB2	calcium channel, voltage-dependent, beta 2 subunit
	RELA	v-rel reticuloendotheliosis viral oncogene homolog A (avian)
	PLA2G3	phospholipase A2, group III
	RASGRP1	RAS guanyl releasing protein 1 (calcium and DAG-regulated)
	RPS6KA3	ribosomal protein S6 kinase, 90kDa, polypeptide 3
	MAP3K1	mitogen-activated protein kinase kinase kinase 1, E3 ubiquitin protein ligase
	STK4	serine/threonine kinase 4

Table 8. Pathways deregulated by obesity specific miRNAs

Endocytosis	SMAD2	SMAD family member 2
	RAB11FIP2	RAB11 family interacting protein 2 (class I)
	STAMBP	STAM binding protein
	CLTC	clathrin, heavy chain (Hc)
	USP8	ubiquitin specific peptidase 8
	ARRB1	arrestin, beta 1
	ERBB3	v-erb-b2 erythroblastic leukemia viral oncogene homolog 3 (avian)
	EHD4	EH-domain containing 4
	CAV3	caveolin 3
	TGFB2	transforming growth factor, beta 2
	FAM125B	family with sequence similarity 125, member B
	CBL	Cbl proto-oncogene, E3 ubiquitin protein ligase
	ARF6	ADP-ribosylation factor 6
	RAB5B	RAB5B, member RAS oncogene family
	ZFYVE9	zinc finger, FYVE domain containing 9
	CSF1R	colony stimulating factor 1 receptor
Pathways in cancer	SOS2	son of sevenless homolog 2 (Drosophila)
	SMAD2	SMAD family member 2
	NRAS	neuroblastoma RAS viral (v-ras) oncogene homolog
	LAMC1	laminin, gamma 1 (formerly LAMB2)
	PTEN	phosphatase and tensin homolog
	FZD4	frizzled family receptor 4
	FZD3	frizzled family receptor 3
	WNT2	wingless-type MMTV integration site family member 2
	GSK3B	glycogen synthase kinase 3 beta
	PIK3CD	phosphatidylinositol-4,5-bisphosphate 3-kinase, catalytic subunit delta
	CBL	Cbl proto-oncogene, E3 ubiquitin protein ligase
	TGFB2	transforming growth factor, beta 2
	FZD6	frizzled family receptor 6
	CSF1R	colony stimulating factor 1 receptor
	VEGFB	vascular endothelial growth factor B

Protein expression signature in hA-MSCs

The protein expression signature was performed in 12 Ob- and 6 Co-hA-MSCs using 2D-DIGE analysis. Figure 13 shows the master gel used to match the whole set of 2-DE profiles obtained. The analysis performed with DeCyder Software detected approximately 7000 protein spots per gel in a 3−10 pH range. Approximately 2384 spots were matched throughout the gels. The DeCyder statistical analysis revealed 166 spots deferentially expressed in Ob-hA-MSC, compared to Co-hA-MSC

samples with average ratio ≥ 1.2 for up-expressed protein spots and ≤ −1.2 for down-expressed spots ($p < 0.05$). Some spots were excluded from further evaluation, i.e., those at the extreme right and left sides of the gel. Furthermore, many spots were not objected to further investigation, because of their low abundance on the preparative gel. As a result, we focused on 40 spots with optimal features. The latter was stained with Comassie Brillant protein stain and used for automated spot picking. The isolated spots were digested with trypsin and then analyzed with mass spectrometry followed by database search. The relative expression ratios (in Ob- vs Co-hA-MSC) for each of the identified spots and their statistical values are listed in Table 9. Approximately 62% (25/40) of the spots were increased, and 38% of the spots (15/40) were decreased. Globally, a total of 41 proteins were identified in these spots. The identified proteins were organized by STRING database and more interconnections were showed (Figure 14). Particularly, they were clustered into 5 Kegg pathways containing at least 3 proteins: Focal adhesion (FLNA, FLNB, ACTG1 and ACTN1); Processing in endoplasmic reticulum (HSP90B1, HSPA5, RRBP1 and VCP); Metabolic pathways (ATP5B, DLST, PKM and MTAP); Regulation of actin cytoskeleton (MYH9, ACTG1, and ACTN1); and MAPK signaling (HSPB1, FLNA and FLNB).

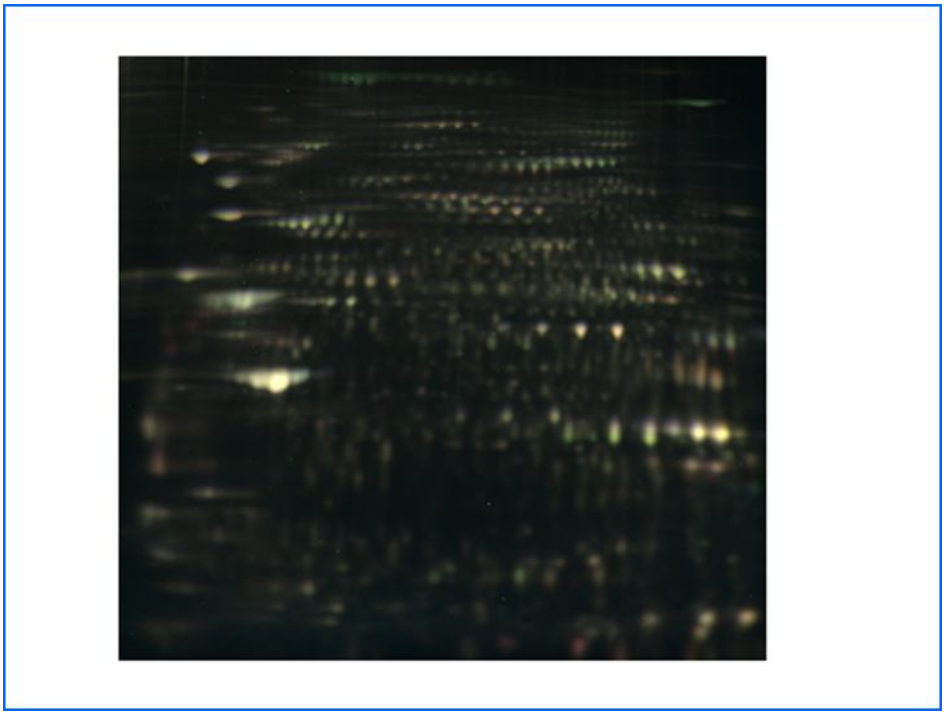

Figure 13. Image of gel chosen as master gel. This gel is constituted by three overlapped images: (1) Ob-hA-MSC labeled with Cy3 (green), (2) Co-hA-MSC proteins of labeled with Cy5 (red), and (3) proteins from a mixture of the all samples (used for normalization) labeled with Cy2 (blue).

Table 9. Identification of proteins differently expressed in Ob-hA-MSCs vs Co-hA-MSCs.

Spot no.[a]	DIGE Ob-/Co-hAMSCs [b]	DIGE (p-value)[c]	Protein name	Gene Symbol [d]	MW (Da)[e]	PI[f]	Gene ID [g]	Protein code [h]
279	1.23	0.014	Pyruvate kinase PKM	PKM	57937	7.96	5315	P14618
453	1.20	0.0069	Nodal modulator 1	NOMO1	134324	5.54	23420	Q15155
492	1.37	0.0056	Filamin-A	FLNA	280739	5.70	2316	P21333
			Filamin-B	FLNB	278164	5.47	2317	O75369
574	1.33	0.040	Ribosome-binding protein 1	RRBP1	152472	8.69	6238	Q9P2E9
660	1.47	0.0099	Programmed cell death 6-interacting protein	PDCD6IP	96023	6.13	10015	Q8WUM4
798	-1.39	0.046	Lon protease homolog, mitochondrial	LONP1	106489	6.01	9361	P36776
829	-1.30	0.028	Endoplasmin	HSP90B1	92468	4.76	7184	P14625
918	1.27	6.4e-005	Ubiquitin-like modifier-activating enzyme 1	UBA1	117849	5.49	7317	P22314
			Alpha-actinin-1	ACTN1	103057	5.25	87	P12814
			Alanine-tRNA ligase, mitochondrial	AARS2	107340	5.87	57505	Q5JTZ9
1047	1.38	0.0056	Myosin-9	MYH9	226532	5.50	4627	P35579
			Transitional endoplasmic reticulum ATPase	VCP	89265	5.14	7415	P55072
1243	-1.37	0.0038	Ran GTPase-activating protein 1	RANGAP1	63541	4.63	5905	P46060
1385	-2.05	0.019	78 kDa glucose-regulated protein	HSPA5	72332	5.07	3309	P11021
1408	-1.28	0.00018	79 kDa glucose-regulated protein	HSPA5	72332	5.07	3309	P11022
1476	1.23	0.0029	Stress-70 protein, mitochondrial	HSPA9	73680	5.87	3313	P38646
			Annexin A6	ANXA6	75873	5.41	309	P08133
1536	1.63	0.026	Myosin-9	MYH9	226532	5.50	4627	P35579
			LIM domain and actin-binding protein 1	LIMA1	85225	6.41	51474	Q9UHB6
1786	-1.22	0.0028	60 kDa heat shock protein, mitochondrial	HSPD1	61054	5.70	3329	P10809
1866	1.26	0.022	Pyruvate kinase PKM	PKM	57937	7.96	5315	P14618
1874	1.21	0.018	Pyruvate kinase PKM	PKM	57937	7.96	5315	P14618
1996	1.32	0.049	Vimentin	VIM	53651	5.05	7431	P08670
2086	-1.19	0.017	Heterogeneous nuclear ribonucleoprotein H	HNRNPH1	49229	5.89	3187	P31943
2125	-1.35	0.017	Dihydrolipoyllysine-residue succinyltransferase component of 2-oxoglutarate dehydrogenase complex, mitochondrial	DLST	48755	9.10	1743	P36957
2621	-1.23	0.049	Actin, cytoplasmic 2	ACTG1	41792	5.31	71	P63261
			COP9 signalosome complex subunit 4	COPS4	46268	5.57	51138	Q9BT78
2710	1.77	0.031	Serpin B6	SERPINB6	42621	5.18	5269	P35237
2730	1.47	0.049	Heterogeneous nuclear ribonucleoprotein A1	HNRNPA1	38746	9.17	3178	P09651
2748	1.77	0.031	Annexin A1	ANXA1	38714	6.57	301	P04083
2769	1.22	0.016	Eukaryotic translation initiation factor 3, subunit I	EIF3I	36501	5.38	8668	Q13347
2770	-6.13	0.041	Annexin A1	ANXA1	38714	6.57	301	P04083
2813	1.40	0.022	Annexin A2	ANXA2	38604	7.57	302	P07355
			LIM and SH3 domain protein 1	LASP1	29717	6.61	3927	Q14847
2879	1,47	0,0042	Elongation factor 1-delta	EEF1D	31121	4.90	1936	P29692
2861	1.26	0.049	Annexin A2	ANXA2	38604	7.57	302	P07355
2925	1.37	0.053	Annexin A2	ANXA2	38604	7.57	302	P07355
			LIM and SH3 domain protein 1	LASP1	29717	6.61	3927	Q14847
2955	1.25	0.038	LIM and SH3 domain protein 1	LASP1	29717	6.61	3927	Q14847
3114	1.96	0.029	Annexin A5	ANXA5	35936	4.93	308	P08758
3162	-3.34	0.041	Chloride intracellular channel protein 1	CLIC1	26922	5.09	1192	O00299
3248	-2.21	0.051	S-methyl-5'-thioadenosine phosphorylase	MTAP	31236	6.75	4507	Q13126
3335	1.49	0.041	Prohibitin	PHB	29804	5.57	5245	P35232
3408	1.26	0.0013	40S ribosomal protein SA	RPSA	32854	4.79	3921	P08865
3412	-1.93	0.0030	Heat shock protein beta-1	HSPB1	22782	5.98	3315	P04792
3452	-1.70	0.00024	Heat shock protein beta-1	HSPB1	22782	5.98	3315	P04792
3711	1.66	0.0037	Ubiquitin carboxyl-terminal hydrolase isozyme L1	UCHL1	24824	5.33	7345	P09936
3794	-1.59	0.031	Chain A, Three-Dimensional Structure Of Class Pi Glutathione S-Transferase From Human Placenta (Glutathione S-transferase P)	GSTP1	23355	5.43	2950	P09211

[a] Spot numbering to indicate the positions of spots in preparative gel. [b] p-value at Student's *t* test. [c] Average abundance ratio (Ob-/Co-hA-MSCs) as calculated by DeCyder Analysis. [d] Gene symbol from NCBI. [e] Theoretical molecular weight (Da). [f] Theoretical pI. [g] Gene ID from NCBI. [h] Protein code from Swiss Prot.

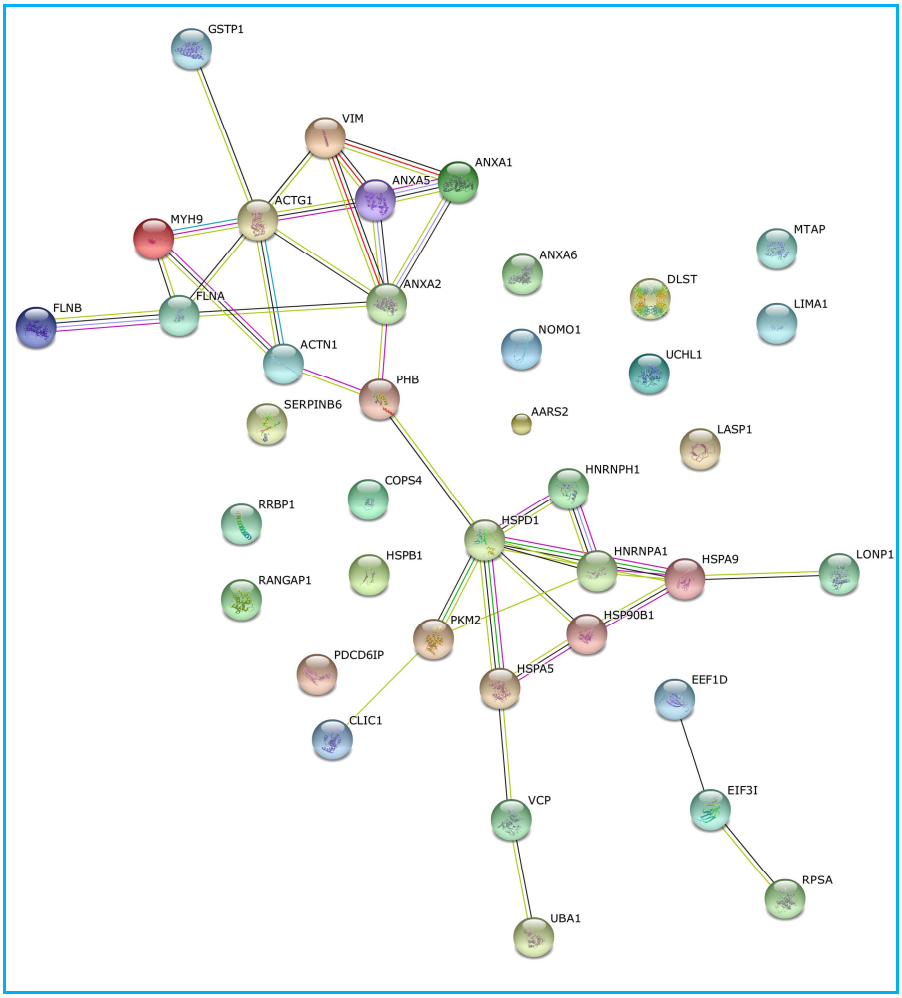

Figure 14. Representation of connection among the identified proteins. The proteins identified by mass spectrometry were organized using STRING database (v 9.1) and more interconnections were showed.

5. DISCUSSION

Understanding the molecular mechanisms underlying obesity could open the way for new therapeutic strategies to contrast obesity-related metabolic disorders. MiRNAs which have been involved in the regulation of a variety of biological processes, including appetite regulation, adipocyte differentiation, and insulin secretion (Heneghan et al. 2010), are interesting candidate molecules to be investigated in adipose tissues as potential mediators of metabolic pathway alterations in obesity. Previous study performed in SAT have reported that miRNA expression was altered in morbidly obese patients, and that up-expressed miR-519d plays a role in adipocyte lipid metabolism (Martinelli et al. 2010). The first aim of this study was to describe the miRNA and proteome VAT signatures in morbidly obese females and to show several miRNAs and proteins differentially expressed between obese and non-obese

females. Globally, the miRNA expression profile revealed that 71 miRNAs were deregulated in the VAT from obese females. Interestingly, most of these miRNAs (61/71) were down-expressed. This latter finding coincides with a report of a similar global down-expression of miRNAs in VAT from obese individuals with nonalcoholic steatohepatitis than those with nonalcoholic fatty liver disease that, moreover, was correlated with enhanced expression of inflammatory adipocytokines (Estep et al. 2010). Eleven of the 61 largely down-expressed miRNAs in the VAT of our obese females were also found in the above report; in particular, 7/11 of these miRNAs were previously reported (miR200c, miR-519b, miR-206, miR-618, miR-30a, miR-181c, and miR-7) down-expressed in SAT from the same obese females (Martinelli et al. 2010). In a mouse model, Xie et al. reported an inverse correlation of miRNA expression between adipogenesis and obesity (Xie et al. 2009). In fact, they observed that up-expressed miRNAs during adipogenesis tended to be down-expressed in the mouse epididymal fat pads, and vice versa, suggesting that these changes could be linked to the chronic local inflammation environment in the fat-mouse obese tissue. Lastly, Klöting et al. reported that miR-198, one of our down-expressed miRNAs, was inversely correlated with omental adipocyte diameter during obesity (Klöting et al. 2009).

The 2D-DIGE analysis has showed that 172 protein spots were differentially expressed in VAT from obese compared to non-obese females. Analysis of 33 of these protein spots, those with optimal features, has led to the identification of 67 proteins because most spots were related to more than one protein. Our data confirm, and also integrate, proteomic data previously obtained in VAT (Pérez-Pérez et al. 2009, Cortón et al. 2008, Pérez-Pérez et al. 2012). In particular, this study showed high levels of EIF4A1, CES1, SELENBP1, ALDH1, ALDH2, GSTP1, and HSPB1 proteins that were previously reported to be increased in the omental compared to SAT in an obese population. Furthermore, we have identified proteins that were differently expressed in VAT from obese compared to non-obese females, such as ACADS, LMNA, VIM, which indicates that VAT is not only a lipid storage site, but also a highly active metabolic tissue (Pérez-Pérez et al. 2009, Pérez-Pérez et al. 2012). Moreover, Pérez-Pérez et al. have suggested that EIF4A1 could be involved in the altered protein synthesis pathways preceding insulin resistance and/or type 2 diabetes (Pérez-Pérez et al. 2009). In agreement with another study, high levels of E2F1 have been detected, which could play a role in glucose metabolism (Fajas et al. 2010). In agreement with earlier reports, proteins involved in intracellular trafficking, i.e., ARCN1 (or COPI), PLIN, RAB11A, and RAB14 have also been identified (Beller et al. 2010, Stenmark. 2009). Furthermore, resulted up-expressed proteins involved in antioxidant activity and in apoptosis, namely, GSS, ANXA5, ANXA7, PRDX3, and GSTP1, some of which were reported by Córton and collegues in a proteomic study of VAT from obese females with or without polycystic ovary syndrome (Córton et al. 2008). A novelty of the present study is that we have evaluated simultaneously the miRNome and the proteome of VAT in obese and non-

obese women to identify potential biological mechanisms, based on the concerted action of miRNA and protein targets, associated with obesity. To this aim, the list of the bioinformatically predicted protein targets of the deregulated miRNAs were intersected with the whole set of identified proteins from the experimental comparison of the VAT proteomes. Thus, using this approach a potential miRNA-based mechanism for the up-expression of some proteins was identified, in particular YWHAG and RAB11A, which was associated with down-expression of miR-141 and miR-520e, respectively. The functional luciferase assay has confirmed the binding of these miRNAs to the 3′UTRs of the YWHAG and RAB11A transcripts. We investigated YWHAG and RAB11A because they are involved in glucose homeostasis (Cartee et al. 2009, Ramm et al. 2006, Chen et al. 2011) and YWHAG also in lipid metabolism, and hence are potential actors in the obese phenotype (Péterfy et al. 2010, Reue et al. 2008). Rab proteins are a large family of small GTPases that are involved in vesicular trafficking, in cytoskeleton organization, and in the control of cell proliferation and differentiation (Stenmark 2009). Members of the Rab family, which includes about 70 proteins in humans, continuously cycle between the cytosol and different membranes as inactive GDP-bound or active GTP-bound forms, assisted by different Rab-associated proteins (Mitra et al. 2011). Defects in Rab-associated proteins lead to abnormal intracellular trafficking and have been associated with several monogenic inherited disorders and multigenic conditions such as type 2 diabetes (Mitra et al. 2011, Kaddai et al. 2009). Several Rab GTPases have been implicated in GLUT4 trafficking in relation to the cell type studied; among these, RAB10, RAB11, and RAB14 have been identified in adipocytes (Larance et al. 2005). An additional player in GLUT4 trafficking is the GTPase-activating protein AS160. The latter, under basal conditions, contributes to cytosolic retention of GLUT4, whereas, upon insulin stimulation, it is phosphorylated at Thr642 by AKT kinase and inactivated, so that AS160 dissociates from GLUT4 vesicles to favor an increase in the GTP-bound form of RAB. This event facilitates the transport of GLUT4 from storage vesicles toward cell surface (Cartee et al. 2009). YWHAG (also known as 14-3-3γ) protein belongs to a seven-member protein family in mammals. These proteins, by interacting with target proteins, typically at phospho-residues, regulate a variety of functions, including subcellular redistribution (Ramm et al. 2006). Studies conducted in animal models and/or in cellular systems have shown that 14-3-3 plays a relevant role in both cellular insulin-mediated glucose transport and lipid metabolism. In fact, in mice, insulin-stimulated YWHAG binding to AS160 at phospho-Thr649 (equivalent to Thr642 in human AS160) normally regulates GLUT4 trafficking from storage vesicles to plasma membrane, thereby influencing glucose uptake (Chen et al. 2011). AS160-Thr649Ala knock-in mice (Ala: non-phosphorylable residue) display impaired glucosal and insulin sensitivity (Chen et al. 2011). Furthermore, in 3T3-L1 adipocytes, the up-expression of 14-3-3 promotes the cytoplasmic localization of Lipin1, a bifunctional protein involved in lipid metabolism (Péterfy et al. 2011). The subcellular localization of this protein is

relevant to its activities; in fact, its nuclear isoform promotes the activation of genes involved in oxidative metabolism. In the cytosol, its insulin-mediated phosphorylation leads to the conversion of phosphatidate (PA) to diacylglycerol (DAG), a precursor of triacylglycerol (TAG) (Reue et al. 2008). On the basis of the above-mentioned mechanisms, we hypothesize (Figure 15) that in VAT from obese subjects, low expression levels of some miRNAs, including miR-520e and miR-141, by modulating the up-expression of RAB11A and YWHAG proteins, respectively, may lead to increased glucose uptake and to increased triglyceride synthesis. This could then contribute to worsen the obese phenotype by increasing the accumulation of adipose tissue. Obviously, the analysis of suitable cellular systems is required to provide mechanistic details for the proposed model and clarify the role of insulin as an independent, or co-operative model, linked to the observed miRNA down-expression and protein target up-expression in obesity. Furthermore, studies on larger cohorts of obese and non-obese subjects are necessary to verify our results on the expression of miR-520e and miR-141, as well as of YWHAG and RAB11A proteins, in obesity risk assessment.

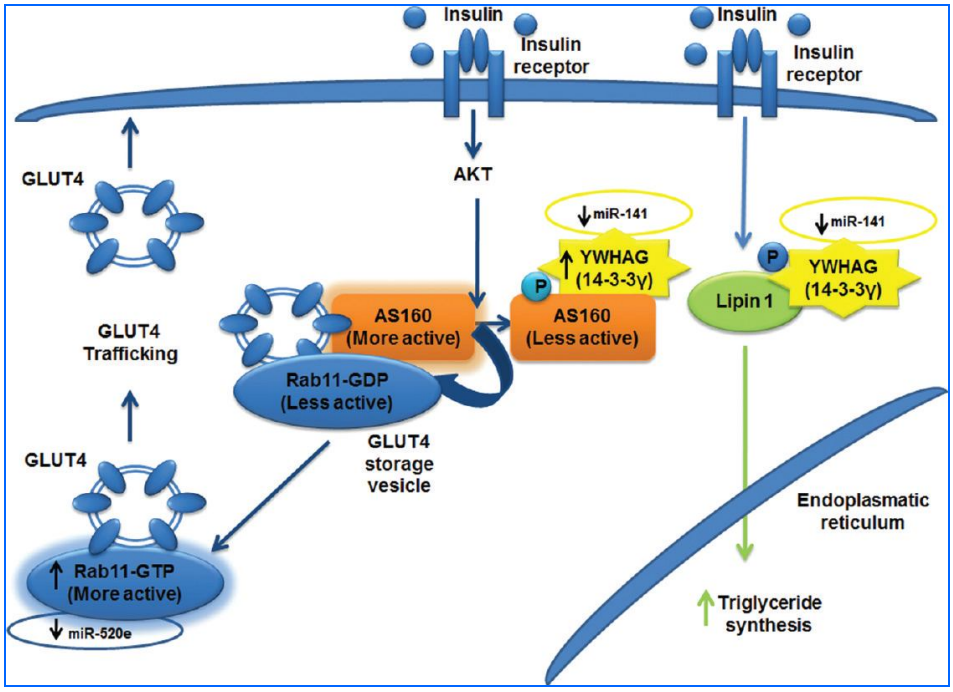

Figure 15. Hypothesized model of visceral adipose tissue (VAT) accumulation based on miR-141/YWHAG and miR-520e/RAB11A interaction. Under basal conditions, the Akt substrate of 160 kDa (AS160) binds RAB11-bound guanosine diphosphate (GDP) that retains glucose transporter protein (GLUT4) vesicles in the cytosol. After insulin stimulation, Akt phosphorylates AS160 that binds YWHAG (14-3-3γ) and catalyzes the phosphorylation of RAB11-GDP in RAB11-bound guanosine triphosphate (GTP). This process results in GLUT4 translocation toward the cell surface. In response to insulin, lipin1 is phosphorylated and interacts with YWHAG (14-3-3γ). The interaction between these two proteins induces increased synthesis of triglycerides in the endoplasmic reticulum.

Concerning the second aim of this study, miRNA expression profiles were investigated in amnion and in hA-MSCs from obese pregnant women. It is now recognized that epigenetic modifications of the foetal genome contribute

to disease development in adults (Fowden et al. 2008). The present data show that miRNAs regulate gene expression in the amnion during obesity. In particular, 25 miRNAs were differently expressed in amnion from obese compared to control women, and seven obesity-specific miRNAs were identified. The differently expressed placental miRNAs include miRNAs previously associated with endometriosis (miR-196b, let-7d, and miR-107) (Hawkins et al. 2011), preeclampsia (miR-181 and let-7d) (Mayor-Lynn et al. 2011, Yang et al. 2001), cancer (miR-422b) (Lee et al. 2009), or identified in sera from normal pregnancies (miR-23b, miR-372, and miR-519e) (Li et al. 2012, Kotlabova et al. 2011).

The predicted target genes of our miRNAs belong to pathways potentially important for placental development and/or functions. In fact, the neurotrophin pathway was regulated by three obesity-specific miRNAs (miR-422b, miR-659, and miR-575), six miRNAs up-expressed (miR-196b, miR-96, miR-338-3p, miR-372, miR-492, and miR-107) and four miRNAs down-expressed (miR-591, miR-139, miR-624, and miR-554). The brain-derived neurotrophic factor was recently implicated in placental development and foetal growth in mice and its placental expression was increased in intrauterine growth restriction and decreased in maternal type 1 diabetes (Mayeur et al. 2010). Obesity-specific miRNAs (miR-422b, miR-659, and miR-219) also down-regulated the mammalian target of rapamycin (mTOR) and the insulin signaling pathways. mTOR is highly expressed in syncytiotrophoblasts of the human placenta and exists as two complexes with distinct regulation and function based on its association with accessory proteins: raptor in Complex 1 (mTORC1) and rictor in Complex 2 (mTORC2) (Jansson et al. 2012). A multitude of upstream regulators of mTORC1, including insulin, cellular energy, and oxygen levels, could affect placental size and modulate foetal growth by regulating placental nutrient transporter function (Jansson et al. 2012). Conversely, mTORC2 is involved in lipid metabolism; in fact, in C. elegans loss of rictor function causes developmental delay, reduced size and reproduction, and increased fat accumulation (Jones et al. 2009). Here, we highlight a new potential mechanism based on miRNA down-regulation of mTOR that could impact foetal growth during obesity. Mammalian mTORC2 controls the actin cytoskeleton organization, as shown by the finding that its knockdown prevents actin polymerization (Jacinto et al. 2004). The cytoskeleton has a crucial role in basic cellular processes and in decidualization (Ihnatovych et al. 2009), and the down-regulation of placenta actin cytoskeleton signaling was observed in preeclampsia (Kang et al. 2011). In this study, the actin cytoskeleton pathway was predicted to be down-regulated by obesity-specific miR-422b, miR-659, miR-575, and miR-579, which indicates that the placental structural organization and function are also altered in human obesity.

The miRNA expression profiles of Ob-hA-MSCs compared to Co-hA-MSCs have showed 25 differently expressed miRNAs (11 up-expressed and 14 down-expressed) and 7 obesity-specific miRNAs. The miRNA expression

profiles of hA-MSCs were different from those observed in the amnion from obese women, but predicted target genes of miRNAs differently expressed in Ob-hA-MSCs are involved in the same pathways in which are involved predicted target genes of miRNAs differently expressed in the amnion. For example, predicted target genes of differently expressed miRNAs in Ob-hA-MSCs are involved in MAPK signalling, and in the regulation of actin cytoskeleton. In addition, predicted targets genes of up-expressed miRNAs in Ob-hA-MSCs are also involved in regulation of focal adhesion and Gap junction in agreement with previous reports that the signature transcriptomes of MSCs isolated from human tissues includes genes involved in regulation of the extracellular matrix and adhesion (Wang et al. 2010).

Interestingly, some pathways were regulated by both up- and down-expressed miRNAs that act on different genes, such as pathways in cancer and MAPK signalling.

In hA-MSCs obesity specific miRNAs regulate 2 pathways also regulated by up-expressed miRNAs, such as endocytosis and pathway in cancer. In amniotic epithelial cells it was demonstrated that the formation of endocytotic vesicles was an extremely active process. The activation of this pathway is essential for maintaining amniotic survival, because endocytosis plays a key role in the ability of the amnion to adapt to availability of nutrients. Shen and colleagues (Shen et al. 2008) suggests that the activation of endocytosis in amnion is also induced by nutrient limitation. Otherwise in the placenta from obese women this pathway may be suppressed due to the presence of excess nutrients and obese specific or up-expressed miRNAs could play a role in this regulation.

Comparing differently expressed miRNAs in amnios and in hA-MSCs, we observed that only miR-449b shows the same trend. It was down-expressed both in amnion and in hA-MSCs from obese women. This miRNA was found significantly down-expressed in the bovine hatched blastocysts and by luciferase assay was confirmed the functional interaction with NOTCH1. NOTCH1 is a member of the Notch trans-membrane protein family that shares structural characteristics, including an extracellular domain consisting of multiple epidermal growth factor-like repeats, and an intracellular domain consisting of multiple, different domain types. The Notch signaling pathway is an evolutionarily conserved, but very versatile pathway, operating in many cell types and at various stages during development. In mouse embryos, Notch1 is expressed during all developmental stages from fertilized eggs until the late blastocyst stage. It is also expressed in trophoblast stem cells and mouse models carrying mutations in the Notch signaling pathway display defects in the development of the placenta, suggesting that this pathway is required for placental development (Goossens et al. 2013). These findings suggest that down-regulation of miR-449b could play a central role in physiological foetal development.

The proteomic approach has showed 48 differently expressed protein spots in Ob-hA-MSCs compared to Co-hA-MSc. Most of them (62%) were up-expressed and the remaining (38%) was down-expressed.

In the last years much attention has been given to the amniotic membrane and to mesenchymal stem cells isolated from a variety of adult tissues because they represent a major hope for tissue-engineered replacement and regenerative medicine. Roche and colleagues defined a common proteomic profile that distinguished multipotent MSCs from pluripotent embryonic stem cells. They selected Annexin A1 (ANXA1), Annexin A2 (ANXA2) and Heat shock protein beta-1 (HSPB1) as proteomic markers of MSCs (Roche et al. 2009). We confirm in our hA-MSCs, the presence of these proteins between those characterizing the proteomic profile, both in Ob-hA-MSCs and in Co-hA-MSc.

Proteins identified in hA-MSCs were mainly involved in the following pathways: Focal adhesion; Processing in endoplasmic reticulum; Metabolic pathways; Regulation of actin cytoskeleton. This finding is in agreement to MSC proteome dataset previously described by Park and colleagues, in which the most abundant proteins expressed in MSC were components of cellular metabolic pathways, heat shock proteins, proteins associated with protein folding, and cellular cytoskeleton. In addition, the abundant presence of vimentin (VIM) and LIM and SH3 domain protein 1 (LASP1), cellular cytoskeleton proteins, in our Ob-hA-MSC, support data previously reported in other MSC studies (Wagner W et al. 2006, Sun KJ et al. 2006, Feldmann et a.l 2005, Park et al. 2007). VIM is the most abundant intermediate filament protein, highly expressed in mesenchymal tissues of mesodermal origin. When it is phosphorylated plays a role in cell division, differentiation, and apoptosis. Whereas, LASP1 is a focal adhesion protein involved in cell migration and survival in response to growth factors and extracellular matrix (Park et al. 2007).

VIM was also identified in adipocytes as a lipid droplets (LD) associated protein, where it forms a scaffold around LD (Brasaemle et al. 2004). Recently, it has been shown that VIM participates in lipolysis through hormonally regulated interaction with lipase hormone sensible (HSL). In vimentin null mice lipolysis is less efficient than in wild type mice (Shen et al. 2010). Moreover, adipocytes from vimentin null mice were smaller than those from wild type mice, suggesting that vimentin might participate in lipid droplet formation and homeostasis (Shen et al. 2012). Similar results in cell size were described in mice with deletions of other intermediate filaments (Galarneau et al. 2007, Kim et al. 2006). VIM plays also a role in GLUT4 trafficking by binding the insulin responsive aminopeptidase (IRAP), an abundant cargo protein associated with GLUT4 storage vesicles. In knockdown for VIM 3T3-L1 adipocytes, insulin-stimulated GLUT4 insertion into membrane is completely disrupted (Hirata et al. 2011). Overall these findings suggest that VIM could play a role in homeostasis of adipocyte cells and in GLUT4 trafficking in plasmatic membrane.

The effect of pre-existing maternal obesity on the protein expression profiles was previously investigated in human placenta dissected to remove visible connective tissue and calcium deposits. In this study 8 proteins were shown to be altered. Particularly, between these proteins, the authors highlighted the lower expression of Annexin A5 (ANXA5), VIM and HSPB1 in obese compared to lean subjects (Oliva et al. 2012). Our data, in confirming the obese associated down-regulation of HSPB1 are in contrast for the expression rate of ANXA5 and VIM, that we found to be up-expressed in Ob-compared to Co-hA-MSCs, probably due to the fact that different samples were analyzed.

ANXA5, otherwise known as placenta anticoagulant protein 1, is abundantly expressed in humans placenta. It can form a shield around negatively-charged phospholipid molecules and inhibit blood coagulation. The anti-coagulation effects of ANXA5 includes competing with activated factor VIII for phosphatidylserine binding sites, inhibiting thromboplastin and blocking the binding of factor X to thrombin-stimulated platelets (Liu et al. 2012). A hypercoagulable state becomes more common during pregnancy and it was increased during pregnancy complicated with gestational diabetes mellitus (GDM). ANXA5 protein was found up-expressed in placental villi from pregnant women complicated with GDM compared to normal placenta villi. In this case, the placenta may up-regulate and secrete more ANXA5 in order to counteract the hypercoagulation state induced by GDM. ANXA5 has also anti-inflammatory and anti-apoptotic properties. In placentas from obese women an increased inflammation was demonstrated (Oliva et al. 2012). Exposure of the fetus to an intrauterine inflammatory environment may have long term consequences, including foetal programming of obesity. The high expression of ANXA5 in Ob-hA-MSCs could be a signal of pregnancy complicated with obesity, but further investigations are needed to elucidate this mechanism.

HSPB1, also know HSP27, belongs to the family of small heat shock proteins. Changes in expression of HSPB1 occurs in response to stress. The functions of HSPB1 include protein chaperone, control of apoptosis, regulation of cell glutathione levels, inhibition of actin polymerization as well as protection against heat shock, oxidative stress and mechanical stress. HSPB1 plays a role also in oxidative stress and inflammation, both features of labor.

The mechanisms that are involved in maintaining a human pregnancy to term and the changes that lead to a normal pregnancy outcome or indeed an adverse outcome such as miscarriage, preeclampsia, foetal growth restriction or preterm labor are complex but the role of the placenta is crucial to them all. When the production of reactive oxygen species overwhelms the intrinsic anti-oxidant defenses oxidative stress occurs. It can induce a range of cellular responses depending upon how severe the insult is and the cellular compartment in which reactive oxidative species are generated. However, a recent study showed that HSPB1 mRNA and protein were reduced in placenta during labor. Particularly, there was less HSPB1 in the inner compared with

both the middle and outer area of at term placenta from pregnant women delivered by cesarean section.

One reason for this may be that a fall in HSPB1 may be necessary to facilitate the inflammatory steps of labor which is, after all, a normal physiological process, not a disease (Abdulsid et al. 2013).

The low expression of HSPB1 both in placenta and in hA-MSCs from obese women could suggest a defective response to oxidative stress associated with maternal overweight.

Another protein involved in response to oxidative stress is glutathione S-transferase P (GSTP1), that was down-expressed in Ob-hA-MSCs. It is a glutathione S-transferase (GST) and belongs to a group of multigene and multifunctional detoxification enzymes, which defend cells against a wide variety of toxic insults from chemicals and metabolites. Low levels of placental GST were observed in some cases of maternal inflammatory state, such as pre-eclampsia (Johnstone et al. 2011) and in placenta from mother living in radioactivity-contaminated and chemically-polluted areas (Obolenskaya et al. 2010). In these cases the reduced GST expression or activity demonstrated defective anti-oxidative stress response and an imbalance in detoxification capacity.

Moreover, a GSTP1 gene polymorphism was associated with diabetes mellitus type 2 (T2DM). Particularly, GSTP1 variant with A to G transition in exon 5 at codon 105 leads to Ile105Val amino acid substitution, which reduces the ability to conjugate reactive electrophiles with glutathione and may therefore sensitize cells to free radical-mediated damage. The Val105 variant has been associated with susceptibility to smoking-related cancer and cardiovascular disease. In T2DM patients were found a significant association between this polymorphism, inactivating GSTP1, and BMI.

These findings suggest that in placenta from obese women could be a defective anti-oxidative stress response because there is reduced expression of glutathione S-transferase the major component of cellular protection against oxidative stress.

6. CONCLUSIONS

In conclusion, the present study provides an integrated view of both miRNAs and protein expression profiles in VAT during obesity and gives clues as to the metabolic pathways that may be involved in adipose tissue accumulation.

In addition, we have elucidate the role of epigenetic mechanisms of gene regulation as risk factors in foetal programming of obesity showing that the miRNA expression profile is altered in amnion and in hA-MSCs during obesity. The research of miRNA predicted targets allow us to hypothesize that this deregulation could affect pathways important for placental growth and function, thereby contributing to an increase in the newborn's risk of future metabolic diseases.

Finally, our data have highlighted that Ob-hA-MSCs have a different proteomic signature compared to Co-hA-MSCs. Even if some identified proteins are previously described in MSCs isolated from several adult tissues, in our study they are deregulated in association with obesity.

The data concerning hA-MSC need to further considerations, particularly the miRNA expression levels and the proteomic data should be confirmed with another method.

7. REFERENCES

Abdulsid A, Fletcher A, Lyall F. Heat shock protein 27 is spatially distributed in the human placenta and decreased during labor. PLoS One 2013;22:e71127

Barker DJ. The developmental origins of insulin resistance. Horm Res 2005; 64:2-7.

Bartha JL, Marin-Segura P, Gonzalez-Gonzalez NL, Wagner F, Aguilar-Diosdado M, Hervias-Vivancos B. Ultrasound evaluation of visceral fat and metabolic risk factors during early pregnancy. Obesity (Silver Spring) 2007;15:2233–9.

Beller M, Thiel K, Thul PJ, Jäckle H. Lipid droplets: a dynamic organelle moves into focus. FEBS Lett 2010; 584: 2176−2182.

Bellisari A. Evolutionary origins of obesity. Obes Rev. 2008;9:165-80.

Bieback K, Kern S, Klüter H and Eichler H. Critical parameters for the isolation of mesenchymal stem cells from umbilical cord blood. Stem Cells 2004;22:625-634.

Brasaemle DL, Dolios G, Shapiro L, Wang R. Proteomic analysis of proteins associated with lipid droplets of basal and lipolytically stimulated 3T3-L1 adipocytes. J Biol Chem 2004;279:46835-42.

Cartee GD, Funai K. Exercise and insulin: Convergence or divergence at AS160 and TBC1D1? Exercise Sport Sci Rev 2009;37:188−195.

Catalano PM. Increasing maternal obesity and weight gain during pregnancy: the obstetric problems of plentitude. Obstet Gynecol 2007;110:743-4.

Challis BG, Pritchard LE, Creemers JW, Delplanque J, Keogh JM, Luan J, Wareham NJ, Yeo GS, Bhattacharyya S, Froguel P, White A, Farooqi IS, O'Rahilly S. A missense mutation disrupting a dibasic prohormone processing site in pro-opiomelanocortin (POMC) increases susceptibility to early-onset obesity through a novel molecular mechanism. Hum Mol Genet 2002;11:1997-2004.

Chen D, Garg A. Monogenic disorders of obesity and body fat distribution. J Lipid Res 1999;40:1735-1746.

Chen S, Wasserman DH, MacKintosh C, Sakamoto K. Mice with AS160/TBC1D4-Thr649Ala knockin mutation are glucose intolerant with reduced insulin sensitivity and altered GLUT4 trafficking. Cell Metab 2011; 13:68−79.

Clement K and Ferré P. Genetics and pathophysiology of obesity. Pediatr Res 2003;53:721-5.

Cortón M, Botella-Carretero JI, López JA, Camafeita E, San Millán JL, Escobar-Morreale HF, Peral B. Proteomic analysis of human omental adipose tissue in the polycystic ovary syndrome using two-dimensional difference gel electrophoresis and mass spectrometry. Hum Reprod 2008;23:651−661.

Klein JD and Fauza DO. Amniotic and placental mesenchymal stem cell isolation and culture. Methods Mol Biol 2011;698:75-88.

Krude H, Biebermann H, Werner L, Rudiger H, Brabant G, Gruters Á. Severe early-onset obesity, adrenal insufficiency and red hair pigmentation caused by POMC mutations in humans. Nat Genet 1998;19:155-7.

Echwald SM, Sørensen TIA, Andersen T, Tybjaerg-Hansen A, Clausen JO, Pedersen O. Mutational analysis of the proopiomelanocortin gene in Caucasians with early onset obesity. Int J Obes Relat Metab Disord 1999;23:293-8.

Estep M, Armistead D, Hossain N, Elarainy H, Goodman Z, Baranova A, Chandhoke V, Younossi Z. M. Differential expression of miRNAs in the visceral adipose tissue of patients with non-alcoholic fatty liver disease. Aliment Pharmacol Ther 2010;32:487−497.

Fajas L, Blanchet E, Annicotte JS. The CDK4-pRB-E2F1 pathway: A new modulator of insulin secretion. Islets 2010;2:51− 53.

Farooqi IS, Yeo GS, Keogh JM. Dominant recessive and inheritance of morbid obesity associated with melanocotin 4 deficiencies. J Clin Invest 2000;106:271-279.

Feldmann RE, Bieback K, Maurer MH, Kalenka A, Bürgers HF, Gross B, Hunzinger C, Klüter H, Kuschinsky W, Eichler H. Stem cell proteomes: a profile of human mesenchymal stem cells derived from umbilical cord blood. Electrophoresis 2005;26:2749-58.

Fowden AL, Forhead AJ, Coan PM, Burton GJ. The placenta and intrauterine programming. J Neuroendocrinol 2008;20:439–450.

Galarneau L, Loranger A, Gilbert S, Marceau N. Keratins modulate hepatic cell adhesion, size and G1/S transition. Exp Cell Res 2007;313:179-94.

Galic S, Oakhill JS, Steinberg GR. Adipose tissue as an endocrine organ. Mol Cell Endocrinol 2010;316:129-39.

Gesta S, Blüher M, Yamamoto Y et al. Evidence for a role of developmental genes in the origin of obesity and body fat distribution. Proc Natl Acad Sci USA 2006;103:6676-81.

Godfrey KM. The role of the placenta in fetal programming-a review. Placenta 2002;23:S20-7.

Goossens K, Mestdagh P, Lefever S, Van Poucke M, Van Zeveren A, Van Soom A, Vandesompele J, Peelman L. Regulatory microRNA network identification in bovine blastocyst development. Stem Cell and Dev 2013;22:1907-1920.

Hawkins SM, Creighton CJ, Han DY, Zariff A, Anderson ML, Gunaratne PH et al. Functional microRNA involved in endometriosis. Mol Endocrinol 2011;25:821–832.

Heerwagen MJ, Miller MR, Barbour LA, Friedman JE. Maternal obesity and fetal metabolic programming: a fertile epigenetic soil. Am J Physiol Regul Integr Comp Physiol 2010;299:R711-22.

Heneghan HM, Miller N, Kerin MJ. Role of microRNAs in obesity and the metabolic syndrome. Obes Rev 2010;11:354− 361.

Hirata Y, Hosaka T, Iwata T, Le CT, Jambaldorj B, Teshigawara K, Harada N, Sakaue H, Sakai T, Yoshimoto K, Nakaya Y. Vimentin binds IRAP and is involved in GLUT4 vesicle trafficking. Biochem Biophys Res Commun 2011;405:96-101.

Huda SS, Brodie LE, Sattar N. Obesity in pregnancy: prevalence and metabolic consequences. Semin Fetal Neonatal Med 2010;15:70-6.

Ibrhaim MM. Subcutaneous and visceral adipose tissue: structural and functional differences. Obes Rev 2010;11:11-8.

Ihnatovych I, Livak M, Reed J, de Lanerolle P, Strakova Z. Manipulating actin dynamics affects human in vitro decidualization. Biol Reprod 2009;81:222-230.

Inui M, Martello G, Piccolo S. MicroRNA control of signal transduction. Nat Rev Mol Cell Biol 2010;11:252-63.

Jacinto E, Loewith R, Schmidt A, Lin S, Rüegg MA, Hall A, Hall MN. Mammalian TOR complex 2 controls the actin cytoskeleton and is rapamycin insensitive. Nat Cell Biol 2004; 6: 1122–1128

Jansson T, Aye IL, Goberdhan DC. The emerging role of mTORC1 signaling in placental nutrient-sensing. Placenta 2012; 33: e23–e29.

Jansson T, Powell TL. Role of the placenta in fetal programming: underlying mechanisms and potential interventional approaches. Clin. Sci 2007;113:1-13.

Johnstone ED, Sawicki G, Guilbert L, Winkler-Lowen B, Cadete VJ, Morrish DW. Differential proteomic analysis of highly purified placental cytotrophoblasts in pre-eclampsia demonstrates a state of increased oxidative stress and reduced cytotrophoblast antioxidant defense. Proteomics 2011;11:4077-84.

Jones KT, Greer ER, Pearce D, Ashrafi K. Rictor/TORC2 regulates Caenorhabditis elegans fat storage, body size, and development through sgk-1. PLoS Biol 2009;7:e60.

Kaddai V, Gonzalez T, Keslair F, Grémeaux T, Bonnafous S, Gugenheim J, Tran A, Gual P, Le Marchand-Brustel Y, Cormont M. Rab4b is a small GTPase involved in the control of the glucose transporter GLUT4 localization in adipocyte. PLoS One 2009;4:e5257.

Kang JH, Song H, Yoon JA, Park DY, Kim SH, Lee KJ et al. Preeclampsia leads to dysregulation of various signaling pathways in placenta. J Hypertens 2011;29:928–936.

Kim S, Wong P, Coulombe PA. A keratin cytoskeletal protein regulates protein synthesis and epithelial cell growth. Nature 2006;441:362-5.

Klöting N, Berthold S, Kovacs P, Schön MR, Fasshauer M, Ruschke K, Stumvoll M, Blüher M. MicroRNA expression in human omental and subcutaneous adipose tissue. PLoS One 2009;4:e4699.

Kotlabova K, Doucha J, Hromadnikova I. Placental-specific microRNA in maternal circulation—identification of appropriate pregnancy-associated microRNAs with diagnostic potential. J Reprod Immunol 2011;89:185–191.

Larance M, Ramm G, Stöckli J, van Dam EM, Winata S, Wasinger V, Simpson F, Graham M, Junutula JR, Guilhaus M, James DE. Characterization of the role of the Rab GTPase-activating protein AS160 in insulin-regulated GLUT4 trafficking. J Biol Chem 2005;280:37803−37813.

Lee CH, Subramanian S, Beck AH, Espinosa I, Senz J, Zhu SX, Huntsman D, van de Rijn M, Gilks CB. MicroRNA profiling of BRCA1/2 mutation-carrying

and non-mutation-carrying high-grade serous carcinomas of ovary. PLoS One 2009;4:e7314.

Lewis RM, Poore KR, Godfrey KM. The role of the placenta in the developmental origins of health and disease-implications for practice. Reviews in Gynaecology & Perinatal Practice 2006;6:70-9.

Li C, Kaur H, Choi WS, Huang TT, Lee ME, Walker I, Greer IA. Additive interactions of maternal prepregnancy BMI and breast-feeding on childhood overweight. Obes Res 2005;13:362-371.

Li H, Guo L, Wu Q, Lu J, Ge Q, Lu Z. A comprehensive survey of maternal plasma miRNAs expression profiles using high-throughput sequencing. Clin Chim Acta 2012;413:568–576.

Lievense AM, Bierma-Zeinstra SM, Verhagen AP, van Baar ME, Verhaar JA, Koes BW. Influence of obesity on the development of osteoarthritis of the hip: a systematic review. Rheumatology 2002;41:1155–62.

Liu B, Xu Y, Voss C, Qiu FH, Zhao MZ, Liu YD, Nie J, Wang ZL. Altered protein expression in gestational diabetes mellitus placentas provides insight into insulin resistance and coagulation/fibrinolysis pathways. PLoS One 2012;7:e44701.

Ma Y, Zhu MJ, Zhang L, Hein SM, Nathanielsz PW, Ford SP. Maternal obesity and overnutrition alter fetal growth rate and cotyledonary vascularity and angiogenic factor expression in ewe. Am J Physiol Regul Integr Comp Physiol 2010;299:R249-R258.

Mariotti E, Mirabelli P, Di Noto R, Fortunato G and Salvatore F. Rapid detection of mycoplasma in continuous cell lines using a selective biochemical test. Leuk Res 2008;32:323-326

Martinelli R, Nardelli C, Pilone V, Buonomo T, Liguori R, Castanò I, Buono P, Masone S, Persico G, Forestieri P, Pastore L, Sacchetti L. miR-519d overexpression is associated with human obesity. Obesity 2010; 18: 2170−2176.

Mayeur S, Silhol M, Moitrot E, Barbaux S, Breton C, Gabory A, Vaiman D, Dutriez-Casteloot I, Fajardy I, Vambergue A, Tapia-Arancibia L, Bastide B, Storme L, Junien C, Vieau D, Lesage J. Placental BDNF/TrkB signaling system is modulated by fetal growth disturbances in rat and human. Placenta 2010;31:785–791.

Mayor-Lynn K, Toloubeydokhti T, Cruz AC, Chegini N. Expression profile of microRNAs and mRNAs in human placentas from pregnancies complicated by preeclampsia and preterm labor. Reprod Sci 2011;18:46–56.

Mihu CM, Mihu D, Costin N, Rus Ciucă D, Suşman S, Ciortea R. Isolation and characterization of stem cells from the placenta and the umbilical cord. Rom J Morphol Embryol 2008;49:441-6.

Milagro FI, Mansego ML, De Miguel C, Martínez JA. Dietary factors, epigenetic modifications and obesity outcomes: progresses and perspectives. Mol Aspects Med 2013;34:782-812.

Miller J, Rosenbloom A, Silverstein J. Childhood obesity. J Clin Endocrinol Metab 2004;89:4211-8.

Miraglia del Giudice E, Cirillo G, Santoro N, D'Urso L, Carbone MT, Di Toro R, Perrone L. Molecular screening of the proopiomelanocortin (POMC) gene in Italian obese children: report of three new mutations. Int J Obes Relat Metab Disord 2001;25:61-7.

Mitra S, Cheng KW, Mills GB. Rab GTPases implicated in inherited and acquired disorders. Semin Cell Dev Biol 2011;22:57−68.

Murphy VE, Smith R, Giles WB, Clifton VL. Endocrine regulation of human fetal growth: the role of the mother, placenta, and fetus. Endocr Rev 2006;27:141-69.

Niknejad H, Peirovi H, Jorjani M, Ahmadiani A, Ghanavi J, Seifalian AM. Properties of the amniotic membrane for potential use in tissue engineering. Eur Cell Mater 2008;29:88-99.

Obolenskaya MY, Teplyuk NM, Divi RL, Poirier MC, Filimonova NB, Zadrozna M, Pasanen MJ. Human placental glutathione S-transferase activity and polycyclic aromatic hydrocarbon DNA adducts as biomarkers for environmental oxidative stress in placentas from pregnant women living in radioactivity- and chemically-polluted regions. Toxicol Lett 2010;196:80-6.

OECD (Organisation for Economic Co-operation and Development) Obesity update 2014;www.oecd.org/els/health-systems/Obesity-Update-2014.pdf

Oliva K, Barker G, Riley C, Bailey MJ, Permezel M, Rice GE, Lappas M. The effect of pre-existing maternal obesity on the placental proteome: two-dimensional difference gel electrophoresis coupled with mass spectrometry. J Mol Endocrinol 2012;48:139-49.

Ortega FJ, Moreno-Navarrete JM, Pardo G, Sabater M, Hummel M, Ferrer A, Rodriguez-Hermosa JI, Ruiz B, Ricart W, Peral B, Fernández-Real JM. MiRNA expression profile of human subcutaneous adipose and during adipocyte differentiation. PLoS One 2010;5:e9022.

Osmond C, Barker DJ. Fetal, infant, and childhood growth are predictors of coronary heart disease, diabetes, and hypertension in adult men and women. Environ Health Perspect 2000;108:545-53.

Parolini O, Alviano F, Bagnara GP, Bilic G, Bühring HJ, Evangelista M, Hennerbichler S, Liu B, Magatti M, Mao N, Miki T, Marongiu F, Nakajima H, Nikaido T, Portmann-Lanz CB, Sankar V, Soncini M, Stadler G, Surbek D, Takahashi TA, Redl H, Sakuragawa N, Wolbank S, Zeisberger S, Zisch A, Strom SC. Concise review: isolation and characterization of cells from human term placenta: outcome of the first international Workshop on Placenta Derived Stem Cells. Stem Cells 2008;26:300-11.

Pardo M, Roca-Rivada A, Seoane LM, Casanueva FF. Obesidomics: contribution of adipose tissue secretome analysis to obesity research. Endocrine 2012;4:374-83.

Park HW, Shin JS, Kim CW. Proteome of mesenchymal stem cells. Proteomics 2007;7:2881-94.

Pérez-Pérez R, Ortega-Delgado FJ, García-Santos E, López JA, Camafeita E, Ricart W, Fernández-Real JM, Peral B. Differential proteomics of omental and subcutaneous adipose tissue reflects their unalike biochemical and metabolic properties. J Proteome Res 2009;8:1682−1693.

Pérez-Pérez R, García-Santos E, Ortega-Delgado FJ, López JA, Camafeita E, Ricart W, Fernández-Real JM, Peral B. Attenuated metabolism is a hallmark of obesity as revealed by comparative proteomic analysis of human omental adipose tissue. J Proteomics 2012;75:783−795.

Perfetto SP, Ambrozak D, Nguyen R, Chattopadhyay P, Roederer M. Quality assurance foe polychromatic flow cytometry. Nat Protocols 2006;1:1522-1530.

Péterfy M, Harris TE, Fujita N, Reue K. Insulin-stimulated interaction with 14-3-3 promotes cytoplasmic localization of lipin-1 in adipocytes. J Biol Chem 2010;285:3857−3864.

Raffin-Sanson ML, de Keyzer Y, Bertagna X. Proopiomelanocortin, a polypeptide precursor with multiple functions: from physiology to pathological conditions. Eur J Endocrinol 2003;149:79-90.

Ramm G, Larance M, Guilhaus M, James DE. A role for 14-3-3 in insulin-stimulated GLUT4 translocation through its interaction with the RabGAP AS160. J Biol Chem 2006;281:29174−29180.

Reue K, Brindley DN. Thematic Review Series: Glycerolipids. Multiple roles for lipins/phosphatidate phosphatase enzymes in lipid metabolism. J Lipid Res 2008;49:2493−2503.

Roche S, Delorme B, Oostendorp RA, Barbet R, Caton D, Noel D, Boumediene K, Papadaki HA, Cousin B, Crozet C, Milhavet O, Casteilla L, Hatzfeld J, Jorgensen C, Charbord P, Lehmann S. Comparative proteomic analysis of human mesenchymal and embryonic stem cells: towards the definition of a mesenchymal stem cell proteomic signature. Proteomics 2009;9:223-32.

Rottiers V, Näär AM. MicroRNAs in metabolism and metabolic disorders. Nat Rev Mol Cell Biol 2012;13:239-50.

Schwartz MW, Woods SC, Porte D Jr, Seeley RJ, Baskin DG. Central nervous system control of food intake. Nature 2000;404:661-71.

Sen S, Carpenter AH, Hochstadt J, Huddleston JY, Kustanovich V, Reynolds AA, Roberts S. Nutrition, weight gain and eating behavior in pregnancy: a review of experimental evidence for long-term effects on the risk of obesity in offspring. Physiol Behav 2012;107:138-45.

Sewell MF, Huston-Presley L, Super DM, Catalano PM. Increased neonatal fat mass, and not lean body mass is associated with maternal obesity. Am J Obstet Gynecol 2006;195:1100–1103.

Shen WJ, Patel S, Eriksson JE, Kraemer FB. Vimentin is a functional partner of hormone sensitive lipase and facilitates lipolysis. J Proteome Res 2010;9:1786-1794.

Shen WJ, Zaidi SK, Patel S, Cortez Y, Ueno M, Azhar R, Azhar S, Kraemer FB. Ablation of vimentin results in defective steroidogenesis. Endocrinology 2012;153:3249-57.

Shen ZY, Xu LY, Li EM, Zhuang BR, Lu XF, Shen J, Wua XY, Li QS, YJ Lin, Chen YW, Tan LJ. Autophagy and endocytosis in the amnion. Journal of Structural Biology 2008;162: 197–204.

Stenmark H. Rab GTPases as coordinators of vesicle traffic. Nat Rev Mol Cell Biol 2009;10:513−525.

Sun HJ, Bahk YY, Choi YR, Shim JH, Han SH, Lee JW. A proteomic analysis during serial subculture and osteogenic differentiation of human mesenchymal stem cell. J Orthop Res 2006;24:2059-71.

Thornburg KL, Louey S. Fetal roots of cardiac disease. Heart 2005;91:867-8.

Vázquez-Vela ME, Torres N, Tovar AR. White adipose tissue as endocrine organ and its role in obesity. Arch Med Res 2008;39:715-28.

Wagner W, Feldmann RE Jr, Seckinger A, Maurer MH, Wein F, Blake J, Krause U, Kalenka A, Bürgers HF, Saffrich R, Wuchter P, Kuschinsky W, Ho

AD. The heterogeneity of human mesenchymal stem cell preparations-evidence from simultaneous analysis of proteomes and transcriptomes. Exp Hematol 2006;34:536-48.

Wang KH, Kao AP, Singh S, Yu SY, Kao LP, Tsai ZY, Lin SD, Li SSL. Comparative expression profiles of mRNA and microRNA among human Mesenchymal stem cells derived from breast, face, and abdominal adipose tissues. Kaohsiung J Med Sci 2010;26:113-121.

WHO-Obesity and overweight Fact Sheet 311. Update March 2011. http://www.who.int/mediacentre/factsheets/fs311/en/

Woods SC, D'Alessio DA. Central control of body weight and appetite. J Clin Endocrinol Metab 2008;93:S37-50.

Xie H, Lim B, Lodish HF. MicroRNAs induced during adipogenesis that accelerate fat cell development are downregulated in obesity. Diabetes 2009;58:1050−1057.

Yang Q, Lu J, Wang S, Li H, Ge Q, Lu Z. Application of next-generation sequencing technology to profile the circulating microRNAs in the serum of preeclampsia versus normal pregnant women. Clin Chim Acta 2011;412: 2167–2173.

OPEN ACCESS Freely available online

PLoS one

MicroRNA-449a Overexpression, Reduced NOTCH1 Signals and Scarce Goblet Cells Characterize the Small Intestine of Celiac Patients

Marina Capuano[1,2☯], Laura Iaffaldano[1,2☯], Nadia Tinto[1,2], Donatella Montanaro[1], Valentina Capobianco[3], Valentina Izzo[4], Francesca Tucci[4], Giancarlo Troncone[1,5], Luigi Greco[4], Lucia Sacchetti[1,2]*

1 CEINGE (Centro di Ingegneria Genetica) Advanced Biotechnology, s. c. a r. l., Naples, Italy, **2** Department of Biochemistry and Medical Biotechnology, University of Naples Federico II, Naples, Italy, **3** Fondazione IRCSS SDN (Istituto di Ricovero e Cura a Carattere Scientifico - Istituto di Ricerca Diagnostica e Nucleare), Naples, Italy, **4** Department of Paediatrics and European Laboratory for the Investigation of Food-Induced Diseases (ELFID), University of Naples Federico II, Naples, Italy, **5** Department of Biomorphological and Functional Sciences, University of Naples Federico II, Naples, Italy

Abstract

MiRNAs play a relevant role in regulating gene expression in a variety of physiological and pathological conditions including autoimmune disorders. MiRNAs are also important in the differentiation and function of the mouse intestinal epithelium. Our study was aimed to look for miRNA-based modulation of gene expression in celiac small intestine, and particularly for genes involved in cell intestinal differentiation/proliferation mechanisms. A cohort of 40 children (20 with active CD, 9 on a gluten-free diet (GFD), and 11 controls), were recruited at the Paediatrics Department (University of Naples Federico II). The expression of 365 human miRNAs was quantified by TaqMan low-density arrays. We used bioinformatics to predict putative target genes of miRNAs and to select biological pathways. The presence of NOTCH1, HES1, KLF4, MUC-2, Ki67 and beta-catenin proteins in the small intestine of CD and control children was tested by immunohistochemistry. The expression of about 20% of the miRNAs tested differed between CD and control children. We found that high miR-449a levels targeted and reduced both NOTCH1 and KLF4 in HEK-293 cells. NOTCH1, KLF4 signals and the number of goblet cells were lower in small intestine of children with active CD and in those on a GFD than in controls, whereas more nuclear beta-catenin staining, as a sign of the WNT pathway activation, and more Ki67 staining, as sign of proliferation, were present in crypts from CD patients than in controls. In conclusion we first demonstrate a miRNA mediated gene regulation in small intestine of CD patients. We also highlighted a reduced NOTCH1 pathway in our patients, irrespective of whether the disease was active or not. We suggest that NOTCH pathway could be constitutively altered in the celiac small intestine and could drive the increased proliferation and the decreased differentiation of intestinal cells towards the secretory goblet cell lineage.

Citation: Capuano M, Iaffaldano L, Tinto N, Montanaro D, Capobianco V, et al. (2011) MicroRNA-449a Overexpression, Reduced NOTCH1 Signals and Scarce Goblet Cells Characterize the Small Intestine of Celiac Patients. PLoS ONE 6(12): e29094. doi:10.1371/journal.pone.0029094

Editor: Hang Thi Thu Nguyen, Emory University, United States of America

Received May 23, 2011; **Accepted** November 21, 2011; **Published** December 15, 2011

Funding: Study supported from European community (PREVENT CD project: EU-FP6-2005-FOOD4B-contract no. 036383). The funder had no role in study design, data collection and analysis, decision to publish, or preparation of the manuscript.

Competing Interests: The authors have declared that no competing interests exist.

* E-mail: sacchett@unina.it

☯ These authors contributed equally to this work.

Introduction

Celiac disease (CD) is an immunomediated enteropathy and one of the most heritable complex diseases. The concordance rate in monozygotic twins is 75% [1,2]. HLA DQ2/DQ8 haplotypes confer the highest estimated heritability (~35%) [3] reported so far.

Exposure to gliadin triggers an inappropriate immune response in HLA-susceptible individuals. However, the presence of HLA-risk alleles is a necessary but not sufficient condition for the development of CD. In fact, about 30–40% of healthy subjects carry HLA-risk alleles [4,5]. Attempts at identifying non-HLA major genetic risk loci have been unsuccessful [6]. Gluten has also been shown to affect epithelial differentiation-associated genes in the small intestinal mucosa of celiac patients [7,8]. However, the role of miRNA-based regulatory mechanisms in mediating gene expression alteration in CD has not yet been investigated.

MicroRNAs (miRNAs) are small non-coding RNAs, 20–25 nt long, that modulate gene expression through canonical base pairing to complementary sequences in the 3′UTR of target mRNA [9]. Since their identification in 1993 [10], miRNAs have been found to play a relevant role in regulating gene expression in a variety of biological processes in physiological and pathological conditions [11] including autoimmune disorders [12]. They can be involved in the development of mature immune cells and in the control of their function [13–15]. MiRNAs are also important in the differentiation and function of the mouse intestinal epithelium [16].

In this study, we evaluated the miRNA expression pattern in the small intestine of children affected by active CD, children with CD on a gluten-free diet (GFD) and control children without CD. Our aim was to look for miRNA-based modulation of gene expression in celiac small intestine, and particularly for genes involved in cell intestinal differentiation/proliferation mechanisms.

Results

Clinical features of CD patients and controls

Clinical features of our CD patients and controls are reported in Table 1. Villous atrophy was subtotal or total [TIIIB: n = 3 (15%) and TIIIC: n = 17 (85%)] in all active CD patients. Only minor histological abnormalities were present in GFD patients [T0: n = 5 (56%) and TI: n = 4 (44%)] and in control patients [T0: n = 7 (64%) and TI: n = 4 (36%)].

CD children and controls have a different miRNA expression levels in small intestine

Figure 1 shows the miRNA expression in the small intestine of children with active CD (panel A) and in children on a GFD (panel B). Ninety of the 365 (25%) miRNAs tested were not expressed in small intestine. Over 50% of miRNAs were expressed at similar levels in the two groups of CD compared to controls. On the contrary, the expression levels of about 20% of miRNAs (22% in active CD and 19% in GFD) differed between CD and controls. In particular, in active CD patients 27 and 55 miRNAs were expressed respectively more (RQ≥2.0) or less (RQ≤0.5) than in controls, whereas in GFD patients 22 and 49 miRNAs were expressed respectively more (RQ≥2.0) or less (RQ≤0.5) than in controls. The miRNAs that were differently expressed in the two CD groups are listed in Table S1.

Two sets of miRNAs (one down-regulated and one up-regulated compared to controls) show similar expression levels in active and GFD CD patients, being miR-449a the highest expressed miRNA

Among the miRNAs differently expressed between CD children and controls, but with similar expression levels in active and in GFD CD, 9 were up-regulated and 21 were down-regulated (Table 2). Particularly, among the down-regulated miRNAs the set of miR-124a, miR-189, miR-299-5p and miR-379, was previously reported associated with autoimmune disorders [17]. Among the up-regulated miRNAs the miR-449a was expressed at very high levels in all active CD (55.18±16.45 mean RQ±SEM) and GFD children (15.43±7.69 mean RQ±SEM). qRT-PCR confirmed the expression levels both of miR-449a (active CD: 2.8±0.9 mean RQ±SEM) and of 2 other tested miRNAs, the down-regulated miR-124a (active CD:0.6±0.1 mean RQ±SEM) and the similar to control expressed miR-564 (active CD:1.4±0.3 mean RQ±SEM vs 1.2±0.1 at array).

Table 1. General characteristics of studied celiac patients (active CD and GFD) and control children (CTRL).

Characteristics[#]	Subjects		
	Active CD (n = 20)	GFD[^] (n = 9)	CTRL (n = 11)
Sex Female (%)	55	55	45
Age (Years)	4.3±1.3	7.6±2.5	6.1±1.0
Clinical presentation:			
Gastrointestinal symptoms (%)	80	22	82
Villous atrophy % (Marsh stage)[‡]	TIIIB 15	T0 56	T0 64
	TIIIC 85	TI 44	TI 36
Positive tTG or EMA (IgA)[§]	19	3	0
Familiarity for:			
CD (%)	20	22	0
Other autoimmune diseases (%)	5	11	0

[#]Data are expressed as percentage (%) or as mean ± standard error of the mean (SEM)

[^]At gluten free diet from at least 2 years.

[‡]According to [41].

[§]Only 1 active CD patient was negative for these antibodies but was positive for both AGA IgG/IgA antibodies. Borderline tTG values in 3/9 GFD patients were attributed to reported sporadic gluten ingestion.

doi:10.1371/journal.pone.0029094.t001

Bioinformatic prediction of the target genes of miR-449a

Six of the 11 programs [Target Scan 5.1, PicTar, Miranda 1.9, MirTarget2 (v2.0), PITA (Catalog version 3) and RNAhybrid (v2.2)], which we used to predict putative target genes of miR-449a, identified several proteins that are present in relevant biological pathways. The biological pathways predicted to be deregulated by miR-449a and sorted in functional groups are reported in Figure S1 (http://mirecords.biolead.org/interactions.php?species=Homo+sapiens&mirna_acc=hsa-miR449a&targetgene_type=refseq_acc&targetgene_info=&v=yes&search_int=Search (http://www.targetscan.org/cgi-bin/targetscan/vert_50/targetscan.cgi?species=Human&gid=&mir_sc=&mir_c=&mir_nc=&mirg=hsa-miR-449a). Among putative target genes the programs identified NOTCH1, Krueppel-like factor 4 (KLF4), delta-like 1 (DLL1), lymphoid enhancer-binding factor 1 (LEF1) and numb homolog-like (NUMBL) proteins, which are all involved in the Notch pathway. As this pathway plays a relevant role in the control of intestinal cell fate in animal models we further examined the interaction of miR-449a with Notch pathway [18].

MiR-449a binds to the 3′ UTR of NOTCH1 and KLF4 and inhibits their expression. We verified the interaction between miR-449a and the 3′ UTR of NOTCH1 and of KLF4 using the luciferase reporter assay. In cells co-transfected with pRL-NOTCH1 vector and pre-miR-449a or with pRL-KLF4 vector, a pre-miR-449a concentration of 100 nmol/L was sufficient to significantly reduce (respectively, $p = 0.001$ and $p = 0.002$) *Renilla* luciferase activity versus control values after 48 h (Figure S2A and S2B).This finding confirms the interaction between miR-449a and the 3′ UTR of both NOTCH1 and KLF4.

The direct interaction between miR-449a and the 3′UTRs of both NOTCH1 and KLF4 was further confirmed after mutating the putative target sites in 3′UTR of the two genes (See Materials and Methods S1).

NOTCH1 and HES1 mRNAs are expressed in the small intestine of CD patients

NOTCH1 and HES1 mRNA levels, tested by qRT-PCR, were expressed in the small intestine of active CD patients (RQ±SEM: 3.4±1.3 and 1.4±0.2, respectively *vs* controls) and of GFD patients (RQ±SEM: 6.5±4.7 and 0.7±0.1, respectively vs controls).

NOTCH1 and HES1 proteins are underexpressed in the small intestine of CD patients

We next investigated the protein expression of NOTCH1 and of HES1, which is a well known target gene of the Notch receptor family, in small intestinal biopsies from CD patients and controls. Figure 2 shows the results obtained for NOTCH1. NOTCH1 was homogeneously distributed in the intestinal villi and crypts of controls and higher expressed in crypts of controls than in crypts of active and GFD CD patients (panel A, B).

In Figure 2 (panel C) are also the images converted for automated analysis (white: unstained cells, yellow/orange: low/moderately stained cells, brown: intensely stained cells). Significantly more intensely stained and less unstained cells ($p = 0.02$)

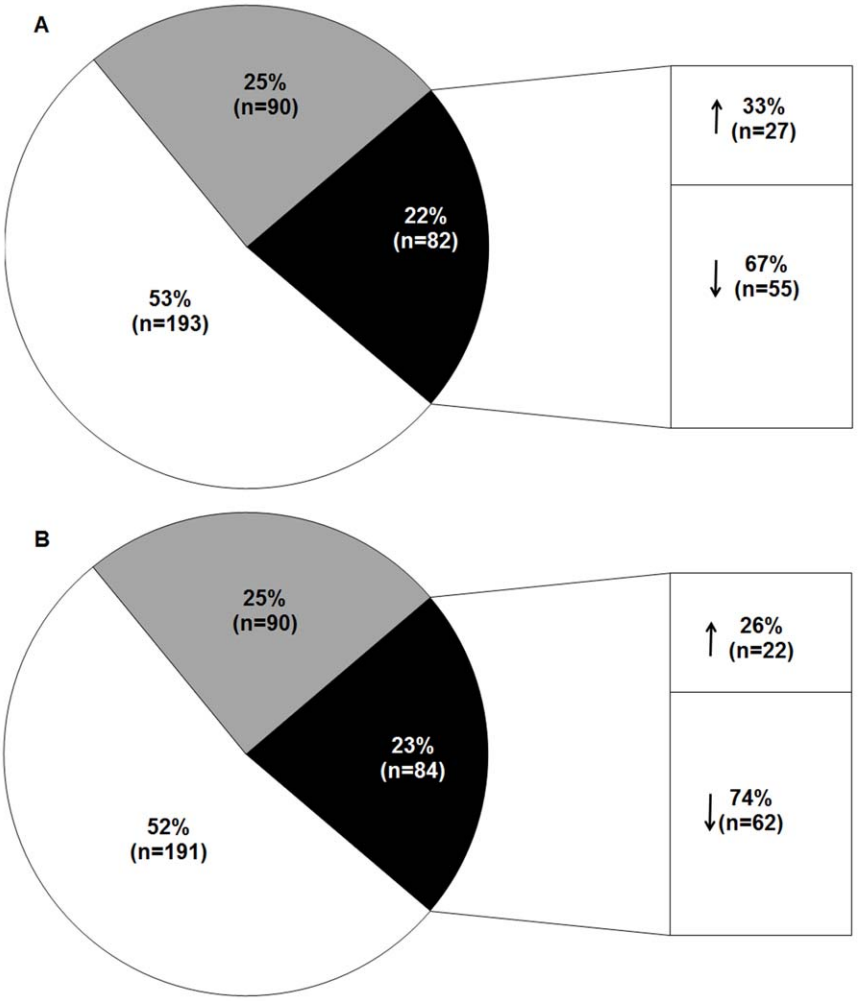

Figure 1. miRNA expression pattern in small intestine of CD patients. miRNA expression in the small intestine of patients with active CD (Panel A) and of CD patients on a GFD (Panel B). Data are expressed as percentage of miRNAs tested (n = 365). White areas, miRNAs whose expression levels were similar in the two CD groups and controls; gray areas, miRNAs not expressed; black areas, miRNAs whose expression levels differed between CD patients and controls (up-regulated ↑ (RQ≥2.0) or down-regulated ↓ (RQ≤0.5)).
doi:10.1371/journal.pone.0029094.g001

were detected in controls than in the two groups of CD patients, whereas no statistical significant difference was observed between the two CD groups (Figure S3, panel A and Figure S4). These results indicate that NOTCH1 is less expressed in the small intestine of active and GFD CD patients than in controls. Figure 3 shows the results obtained for HES1. HES1 was homogeneously distributed in the intestinal villi and crypts of controls and higher expressed in crypts of controls than in crypts of active and GFD CD patients (panels A and B). In Figure 3 (panel C) are also the images converted for automated analysis (white: unstained cells, yellow/orange: low/moderately stained cells, brown: intensely stained cells). Significantly more intensely stained cells were detected in controls than in CD patients ($p = 0.02$) and significantly less unstained cells were detected in controls than in active CD patients ($p = 0.03$), whereas no statistical significant difference was observed between the two CD groups (Figure S3, panel B and Figure S5). These results indicate that HES1 is less expressed in the small intestine of active and GFD CD patients with respect to controls. The above findings confirm that NOTCH1 signaling is reduced in patients affected by CD.

KLF4 protein is reduced and the number of goblet cells is significantly lower in the small intestine of CD patients versus controls

We also investigated the protein expression of KLF4, another selected target gene of miR449a, in small intestinal villi from GFD patients and controls, lacking the villous architecture in active CD patients. We found that the levels of this protein (mean±SEM) were significantly lower in villi from GFD patients vs controls, respectively 29.0±5.0 vs 79.0±3.0 ($p<0.0001$) (Figure S6, panel A). Since KLF4 negatively regulates cellular proliferation, we examined the effect of inhibition of KLF4 on the proliferation of intestinal crypts with the proliferation marker Ki67. The results show that the number of Ki67 positive cells is higher in the crypts of CD patients than in controls (Figure S6, panel B). Because KLF4 is also involved in the differentiation and maturation of secretory goblet cells we examined these cells by immunohistochemistry and using anti-MUC-2 antibodies. We detected statistically fewer MUC-2-stained cells (mean±SEM) in the crypts of active CD patients (18.0±1.6) and GFD patients (15.0±3.0) than in controls (35.0±7.7) ($p = 0.04$) (Figure 4A and B). Moreover, there were fewer goblet cells in the villi of GFD

Table 2. List of miRNAs (n = 30) differently expressed in CD patients and controls but with similar expression levels both in active CD and GFD children.

MiRNA	Active CD	GFD
up-regulated miRNAs		
miR-449a	55.18±16.45	15.43±7.69
miR-492	48.88±14.56	26.86±9.00
miR-644	47.80±8.80	37.53±18.85
miR-503	19.84±2.36	20.55±8.07
miR-196a	11.06±2.84	8.45±1.01
miR-504	5.54±0.83	8.02±2.86
miR-500	5.49±0.70	7.88±1.56
miR-330	3.84±0.45	2.48±0.11
miR-182	2.95±0.42	2.75±0.13
down-regulated miRNAs		
miR-105	0.37±0.03	0.25±0.03
miR-409-5p	0.35±0.04	0.31±0.05
miR-631	0.34±0.03	0.27±0.04
miR-659	0.33±0.03	0.30±0.05
miR-379	0.30±0.05	0.23±0.10
miR-566	0.29±0.02	0.23±0.03
miR-512-3p	0.27±0.03	0.26±0.04
miR-614	0.26±0.02	0.21±0.02
miR-380-5p	0.25±0.03	0.28±0.04
miR-135a	0.21±0.05	0.38±0.05
miR-124a	0.20±0.02	0.21±0.05
miR-600	0.19±0.02	0.22±0.06
miR-618	0.18±0.03	0.32±0.07
miR-616	0.17±0.04	0.11±0.03
miR-189	0.15±0.05	0.21±0.06
miR-576	0.15±0.04	0.40±0.10
miR-412	0.13±0.03	0.18±0.01
miR-202	0.12±0.06	0.17±0.08
miR-299-5p	0.11±0.01	0.15±0.05
miR-323	0.11±0.01	0.23±0.08
miR-219	0.10±0.01	0.27±0.08

Data are reported as RQ[#] levels (mean±SEM).
[#]RQ = $2^{-\text{delta deltaCT}}$ represents miRNA fold change in CD patients vs mean value obtained in control patients.
doi:10.1371/journal.pone.0029094.t002

patients (7.0±1.8) than in controls (20.0±4.9) (p = 0.04) (data not shown). This finding demonstrates that the differentiation of the secretory goblet cells is impaired in small intestine of CD patients.

Expression of beta-catenin

Because NOTCH1 and also KLF4 interact with the WNT pathway to influence the intestinal stem cell fate, we investigated the WNT pathway using beta-catenin antibodies. By counting the beta-catenin positive nuclei/crypt for each patient we observed higher even if not statistical significant mean percentage beta-catenin positive nuclei/crypt in active CD and GFD patients than in controls, respectively 57.0±11.5 and 37.0±4.6 *vs* 27.0±4.6 (Figure S7). This finding suggests that cellular proliferation is increased in the small intestine of CD patients.

Discussion

A very recent study established the importance of miRNAs in the differentiation and function of the mouse intestinal epithelium [16], whereas there are no data about miRNAs expression in human CD small intestine. Our study reveals that the expression of about 20% of miRNAs tested in the small intestine differed among CD and control children irrespective of whether the disease was active or not. Particularly, the miR-449a showed the highest expression level in CD patients than in controls. The miR-449 (a and b) cluster is embedded into an intronic sequence of the mRNA-encoding gene *CDC20B* on Chr 5q11.2 [17]. MiR-449a seems to be regulated through activation of its host gene, *CDC20B*, and both were induced by the cell cycle regulator E2F1 [19]. The mature miR-449a sequence is evolutionarily conserved across a variety of species (monkey, horse, rodents, and dogs) and therefore it probably exerts an important function [20]. The bioinformatics search for putative target genes of miR-449a revealed about one hundred proteins, among these several belonged to the Notch pathway, i.e., NOTCH1, KLF4 (a NOTCH1 transcription factor) [21], DLL1, LEF1 and NUMBL. Our strategy to choose NOTCH1 gene among the other putative miRNA-target genes was based on many studies highlighting that cellular formation of the villi in small and large intestine is affected by signaling pathways such as Notch, Wnt and BMP [22–25]. Notably, deregulation of the intestinal epithelial formation has been reported in several intestinal diseases such as Crohn, ulcerative colitis and colon cancer [26]. Further, NOTCH1 and KLF4 genes are both involved in the control of mouse intestinal epithelial homeostasis [18,27]. In fact, in mouse intestine, also in cooperation with WNT signals, NOTCH1 guides cell proliferation and differentiation [18] and KLF4 inhibition by NOTCH1 or KLF4 deletion was shown to reduce the differentiation and maturation of goblet cells [21,27–29]. The Notch family is constituted by single transmembrane receptors that, in mammals, after interaction with ligands (DLL1,3,4 and Jagged 1–2) undergo proteolytic cleavage and finally translocate into the nucleus where they activate target gene transcription [30].

After confirmed the interaction between miR-449a and both NOTCH1 and KLF4 mRNA, we measured the NOTCH1 and KLF4 protein levels in small intestinal biopsies of CD children. NOTCH1-positive cells were significantly fewer in biopsies from active and GFD CD patients versus controls. Similar results were also obtained for HES1, a target gene of NOTCH1 [31]. Globally, these data indicate that the NOTCH1 pathway is deregulated in intestinal epithelium of CD children, irrespective of whether the disease is active or not, and that this alteration could be related to the very high miR-449a expression. Accordingly, in a very recent report miR449 by repressing the Delta/Notch pathway was elegantly shown to control the human airway epithelium and vertebrate multilciliogenesis [32]. In our patients we also observed fewer KLF4-positive cells in small intestinal villi from GFD patients than in controls, and, moreover, Ki67 signals were higher in crypts from CD patients versus controls. These two results are in agreement with data very recently reported in a mouse $KLF4^{DELTAIS}$ model [27] and indicate a higher proliferation rate in our CD patients in the presence of reduced KLF4 expression [27]. In parallel the number of goblet cells was significantly lower in the two CD groups than in control children. Ciacci et al [33] previously reported fewer goblet cells/mm^2 in untreated (29.1) and in treated CD patients (42.2) than in controls (50.5), although the differences were statistically significant only in untreated patients ($p<0.02$).

The WNT pathway in the small intestine of our CD patients, evaluated based on beta-catenin expression level, did not differ

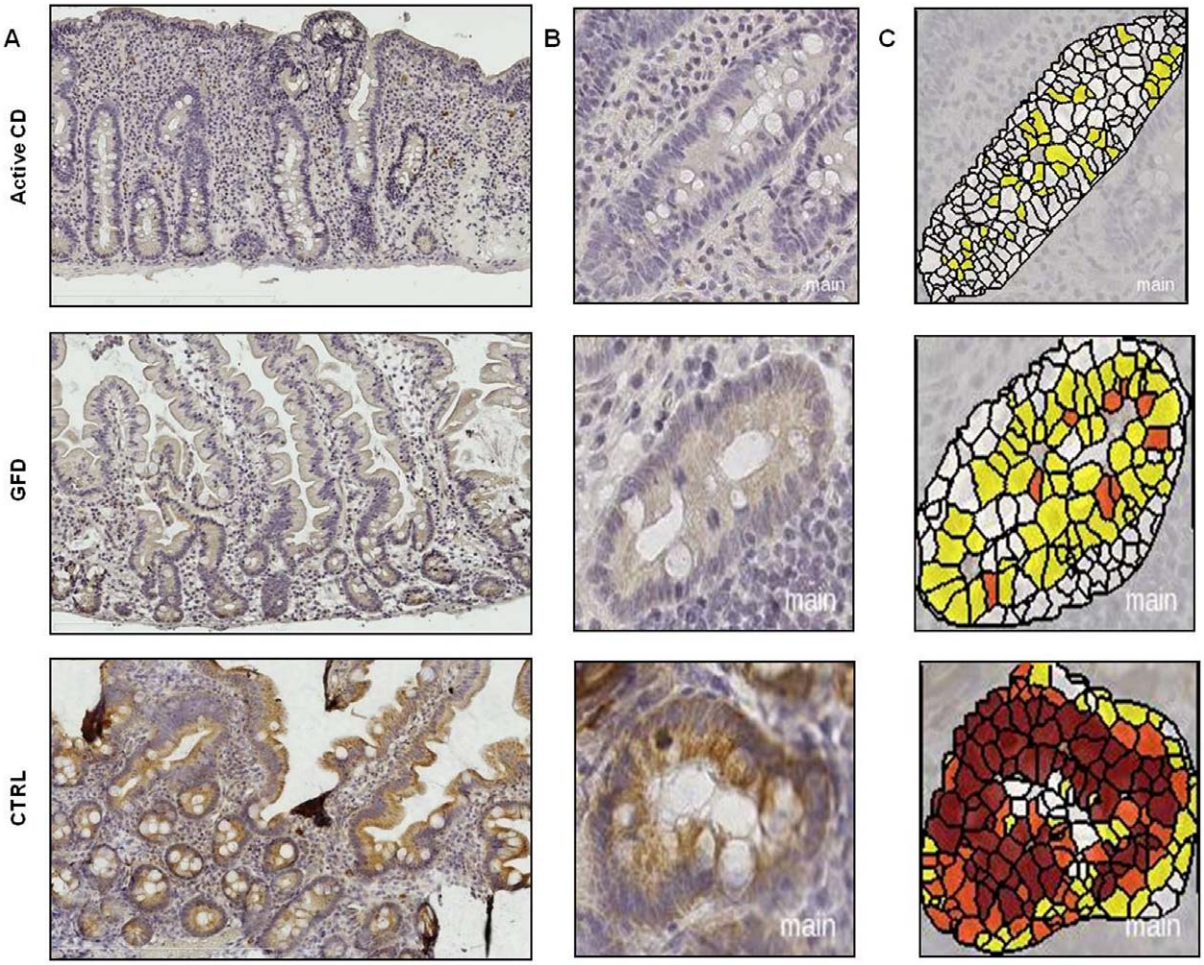

Figure 2. Decreased expression of NOTCH1 in small intestine of CD patients compared with controls. An example of NOTCH1 immunohistochemistry in small intestine. **A.** Low magnification picture of the intestinal sections (Original magnification 10×). **B.** Intestinal crypts (Original magnification 40×). Note the homogeneous distribution of NOTCH1 in crypts and along the villi in control sample, whereas in active CD and GFD samples the signals were prevalently detected in the crypts. Higher levels of NOTCH1 were detected in the intestinal crypts of controls than in crypts of active and GFD CD samples. **C.** Images converted for automated analysis (white: unstained cells, yellow/orange: low/moderately stained cells, brown: intensely stained cells). These results indicate that NOTCH1 is less expressed in the small intestine of active and GFD CD samples compared with controls. (CTRL: controls; GFD: gluten free diet; CD: celiac disease).
doi:10.1371/journal.pone.0029094.g002

from that of control children. This result is in agreement with the western blot data reported by Ciccocioppo et al [34] and by Juuti-Uusitalo et al [7]. However, we observed a more evident nuclear localization of beta-catenin, albeit not statistically significant, in the small intestinal crypts from our active and GFD CD patients than in controls, which suggests activation of the WNT pathway. The latter finding is in agreement with a previous study of human CD [7] and with the increased mRNA levels of the genes in the WNT pathway, including beta-catenin, observed in the $KLF4^{DELTAIS}$ mouse [27]. Globally, our data support increased cellular proliferation in the small intestinal epithelium in CD patients. As it is well known, active CD is characterized by an inversion of the differentiation/proliferation program of the intestine with a reduction in the differentiated compartment, up to complete villous atrophy, and an increase of the proliferative compartment, with crypt hyperplasia [7,8]. Furthermore, although GFD intestinal mucosa is characterized by an apparently normal mucosal architecture, it can also be associated with increased crypt cell proliferation (Barone M. V. et al., personal communication). Our data are in contrast with those obtained in mouse models, in which NOTCH1 activation resulted in a reduction of goblet cells consequent to HES-1 dependent repression of Math1 (intestinal secretory cell differentiation factor) [18] and in which NOTCH1 inhibited the expression of KLF4 [35]. However, our data are in agreement with a recent report of increased proliferation, reduced differentiation and goblet cells maturation associated with down-regulation of the expression of components of the Notch pathway (HES1, DLL1, JAG1) in the small intestine of the $KLF4^{DELTAIS}$ mouse [27]. The authors for the latter article hypothesized that KLF4 was involved in a feed-back loop by positively regulating Notch signaling. Our results are suggestive that an altered NOTCH1 and KLF4 expression could lead to the reduction of goblet cells in the small intestine of CD patients. The maintenance of a correct number of functional goblet cells is required for the homeostasis of the intestinal mucosal environment, and deficiencies in the mucin composition renders the mucosa more susceptible to damaging agents in the lumen [36–38]. In fact, loss of goblet cell function leads to spontaneous colitis in mice [39]. Moreover, an altered mucous layer and increased rod-shaped bacteria and interferon-gamma mRNA levels were found in

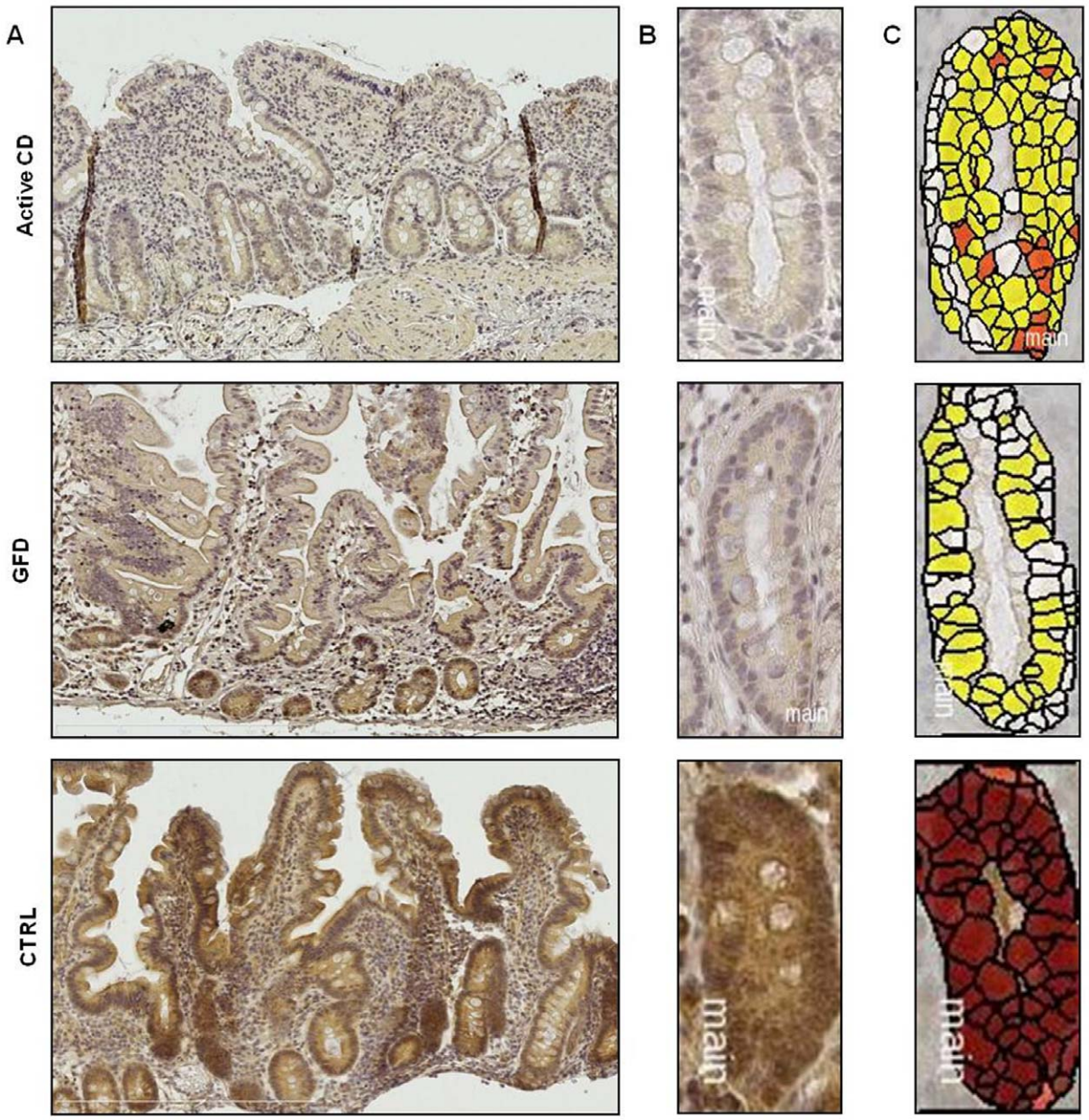

Figure 3. Decreased expression of HES1 in small intestine of CD patients compared with controls. An example of HES1 immunohistochemistry in small intestine. **A.** Low magnification picture of the examined intestinal sections (Original magnification 10×). **B.** Intestinal crypts (Original magnification 40×). Note the homogeneous distribution of HES1 in crypts and along the villi in control sample, whereas the signals were prevalently detected in the crypts of active CD and GFD samples. Higher levels of HES1 were detected in the intestinal crypts of controls than in crypts of active and GFD CD samples. **C.** Images converted for automated analysis (white: unstained cells, yellow/orange: low/moderately stained cells, brown: intensely stained cells). These results indicate that HES1 is less expressed in the small intestine of active and GFD CD samples compared with controls. (CTRL: controls; GFD: gluten free diet; CD: celiac disease).
doi:10.1371/journal.pone.0029094.g003

intestine from CD patients [40]. Based on these experimental data, we suggest that the mucus layer in our CD children could be altered so deranging the protective function of the mucosal barrier that interfaces with the environment. In our study, the observed small intestine alterations are not related to inflammation; in fact, they occurred in both the active CD and GFD patients. The major criticism in our work is the gap between the results of the miRNA array with NOTCH1 gene in *a vivo* system, however the lack of a celiac animal model at moment, prevent us from this further validation of our data. Nevertheless, our first description of miRNA pattern in celiac disease and of the correlation of miRNA 449a over expression with NOTCH pathway could pave the way for further research in this field. However, our choice to study Notch pathway doesn't exclude that other relevant biological pathways in addition to it could be miRNA-deregulated in the celiac intestine. Further deeper investigation are necessary to test this hypothesis.

In conclusion we first demonstrate a miRNA mediated gene regulation in small intestine of CD patients. We also highlighted a reduced NOTCH1 pathway in our patients, irrespective of whether

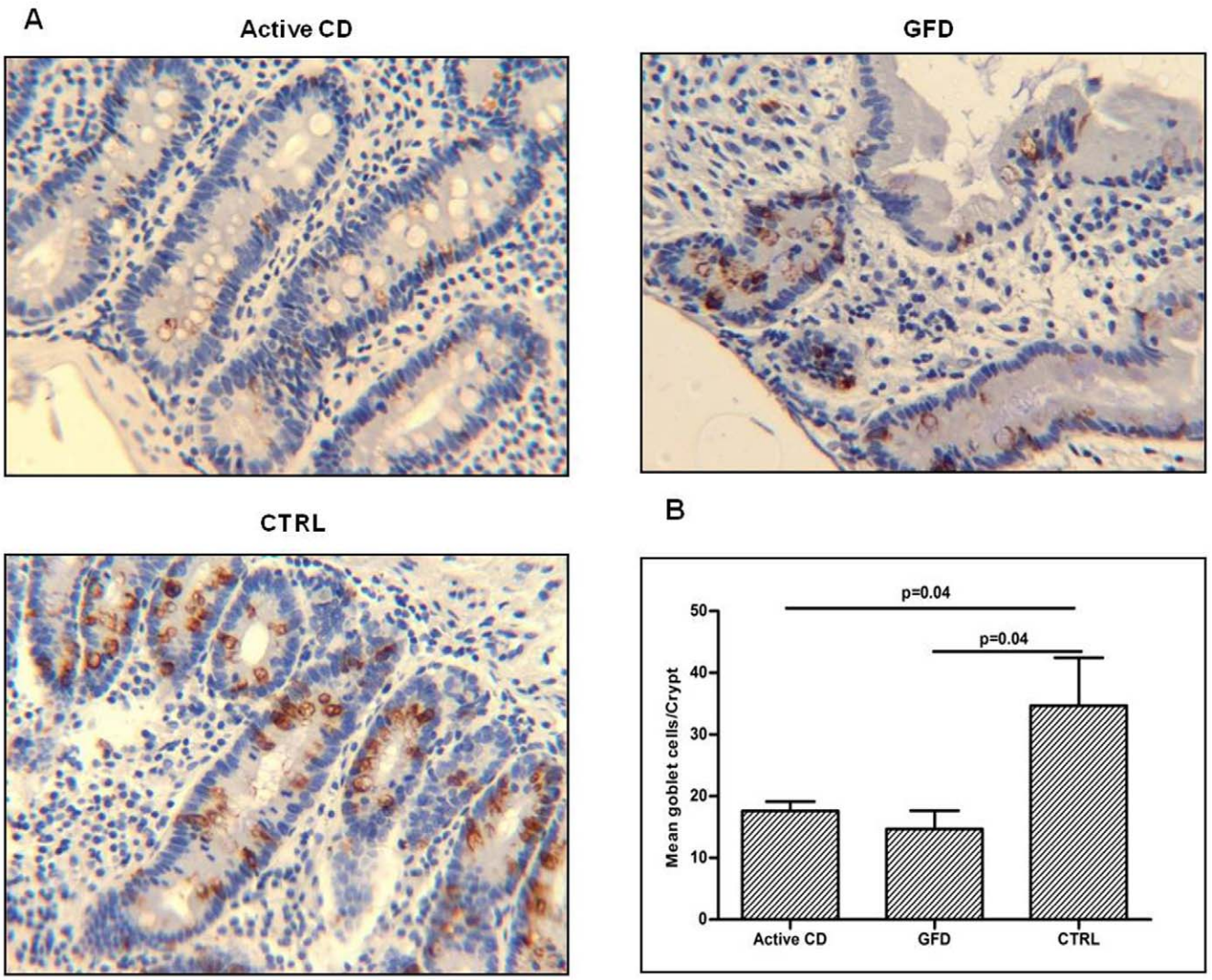

Figure 4. Decreased expression of MUC2 in small intestine of CD patients compared with controls. Immunohistochemistry of goblet cells in small intestine. **A.** An example of staining for MUC-2 shows fewer MUC-2 stained cells in active and in GFD CD samples than in controls. (Original magnification 20×). **B.** MUC2 stained cells evaluated in CD patients (6 active CD and 6 GFD patients) and in controls (n = 4). Data are expressed as mean of the number of goblet cells/crypt measured in 10 crypts/children. Significantly fewer stained cells were detected in active and GFD CD samples than in controls (p = 0.04). These results indicate that MUC2 is less expressed in small intestine of active and GFD CD patients compared with controls. (CTRL: controls; GFD: gluten free diet; CD: celiac disease).
doi:10.1371/journal.pone.0029094.g004

the disease was active or not. We suggest that NOTCH pathway could be constitutively altered in the celiac small intestine and could drive the increased proliferation and the decreased differentiation of intestinal cells towards the secretory goblet cell lineage.

Materials and Methods

Ethics approval

The study was conducted according to the Helsinki II declaration and it was approved by the Ethics Committee of the School of Medicine Federico II, Naples, Italy.

Written informed consent was obtained from the parent/guardian of all children involved in our study before their enrollment.

Patients and controls

Forty-four children were recruited, in a two months period, among patients attending the Department of Paediatrics of the University of Naples Federico II where the European Laboratory for the Investigation of Food-Induced Diseases (ELFID) is also present. In our center about 40 biopsies are monthly performed and about 50% of them are usually indicative of CD. Twenty/44 children were diagnosed celiacs according to the criteria established by the European Society for Paediatric Gastroenterology, Hepatology and Nutrition (ESPGHAN) [41]; the CD was excluded based on both absence of CD antibodies and slight or no abnormalities in the mucosal architecture in 15/44 children. In four of these latter children (4/15) the final diagnoses were IgA deficiency (2 cases), De George syndrome (1 case) and autoimmune thyroiditis (1 case), these subjects were excluded from the study to avoid potentially confounding diseases. In the other 11/15 CD-negative children the final diagnoses were: *Helicobacter pylori* infection, recurrent vomiting, food refusal or reflux esophagitis, they were our enrolled controls. Nine out 44 children were CD patients on gluten free diet for at least 2 years undergoing CD

follow-up in the same study period of the active CD patients and controls. There was no statistically significant difference in mean age at diagnosis among the groups evaluated (4.3±1.3 years old in active CD subjects, 7.6±2.5 in GFD subjects, and 6.1±1.0 in controls [mean±SEM]). About 50% of each group was girls. From all participants, we collected a fasting serum sample, a blood sample with EDTA, and a small intestine biopsy sample.

Biochemical parameters

Anti-Endomysium IgA were detected by indirect immunofluorescence on rhesus monkey esophagus substrate (Eurospital, Trieste, Italy); tTG IgA, anti-gliadin (AGA) IgA/IgG were analyzed by ELISA with human recombinant tTG as antigen (DIA Medix Corp., Miami, FL, USA).

Histopathological analysis

Architectural abnormalities were classified according to the modified Marsh classification: normal mucosa (T0), intraepithelial lymphocytosis (TI), intraepithelial lymphocytosis and crypt hyperplasia (TII), intraepithelial lymphocytosis, crypt hyperplasia and villous atrophy (partial TIIIA, subtotal TIIIB, total TIIIC) [42].

DNA and RNA extraction

Genomic DNA was extracted using the Nucleon BACC 2 kit (Amersham Biosciences Europe, Milan, Italy). Total RNA, including miRNAs, was extracted from small intestinal biopsy samples using the Mirvana extraction kit (Applied Biosystems, Foster City, CA, USA).

HLA typing

DQ2/DQ8 HLA CD-associated molecules were identified by using primers and the PCR conditions of a commercial kit (BAG Health care GmbH, Lich, Germany), which allows to identify the HLA-alleles coding DQ2/DQ8 molecules.

MiRNAs evaluation

TaqMan low density arrays (TLDA), micro fluidic cards were used to detect and quantify mature miRNAs (Applied Biosystems' 7900HT) according to manufacturer's instructions (see Materials and Methods S1 for details). We considered differently expressed in CD vs controls, the miRNAs whose mean RQ levels were ≤ 0.5 (down-regulated) or ≥ 2.0 (up-regulated).

Bioinformatic approach

The prediction of putative target genes of miRNAs was determined using miRecords (http://mirecords.biolead.org/), which is an integration of 11 established miRNA target prediction programs. The lists of target genes that were predicted by two or more programs were then combined and analyzed using the Gene Ontology Tree Machine (GOTM) (http://bioinfo.vanderbilt.edu/gotm/) and KEGG database (http://www.genome.ad.jp/kegg/). Finally, we identified the biological pathways that contained at least two up- or down-regulated genes with a statistically significant probability ($p<0.01$).

Quantitative real-time polymerase chain reaction (qRT-PCR) of miRNAs and mRNAs

The levels of a group of deregulated miRNAs (up-regulated miR-449a, down-regulated miR-124a, and similar to controls expressed miR-564) were also evaluated with TaqMan miRNA assays (Applied Biosystems) to validate the array results.

mRNA expression levels of neurogenic locus notch homolog protein 1 (NOTCH1) and of hairy and enhancer of split 1 (HES1) were measured in small intestinal tissues by qRT-PCR using single TaqMan mRNA assays (Applied Biosystems) according to the manufacturer's instructions and using the housekeeping gene beta-actin as control. Reverse transcription reactions were performed with the High Capacity cDNA Reverse Transcription Kit (Applied Biosystems). The expression levels of miRNAs and mRNAs were quantified using the ABI Prism 7900HT Sequence Detection System 2.3 software.

Transfection and inhibition experiments

The oligonucleotides, plasmids (pGL3-control, pRL-NOTCH1-encoding, pRL-KLF4-encoding and mutated pR-KLF4-encoding, firefly luciferase and Renilla luciferase, respectively) and human embryonic kidney cell lines (HEK293 cell line, ATCC number CRL-1573, supplied by the Centre for Applied Microbiology and Research, Salisbury, Wiltshire, UK) used for cell transfection experiments are described in detail in the online Materials and Methods S1.

Forty-eight hours after transfection, we measured firefly and *Renilla* luciferase activities using a dual luciferase assay according to the manufacturer's instructions (Promega, Naples, Italy).

Protein evaluation by immunohistochemistry

Given the small amount of sample available for each patient (1–2 mg of intestinal tissue/patient) we tested the expression of selected proteins by immunohistochemistry instead of by western blotting. The NOTCH1, HES1, MUC-2, KLF4, Ki67 and beta-catenin proteins were identified on formalin-fixed paraffin-embedded small intestinal tissue blocks in CD patients and in controls. We randomly selected six active CD, six GFD and four controls (see Materials and Methods S1 for details). We also tested the specificity of our NOTCH1 and HES1 signals evaluating two different human tissue samples where it is known NOTCH1 and HES1 be present or absent respectively, that are colon cancer and endothelial wall (Figure S8).

Scanning and automated image analysis of NOTCH1 and HES1

To increase precision, we automated the quantification of the immunohistochemical signals. Sections of the small intestine were scanned with the NanoZoomer 2.0 system (Hamamatsu, Japan), equipped with a 20×, 0.7 Numerical Aperture Plan-Apochromat lens, using a lens of 0.23 mm pixel size. The compressed jpeg files were transferred to the Definiens Analyst LS5.0 system (Definiens AG, Germany) that counted the NOTCH1, HES1 and beta-catenin -positive and -negative cells and quantified the staining signal (see materials and methods S1 for Definiens Analyst software details). The Definiens Analyst software (Definiens AG, Germany) is based on cognition network technology that is a semantic network of objects and their mutual relationships. Two rule sets, using cognition network language, were specifically written for this evaluation to automatically detect and measure the small intestinal area and to count positive and negative crypt cells. The signal was classified as intensely stained, low/moderate stained and unstained. Thus, both the percentage and intensity of labeled cells were taken into account. The detection and exclusion of areas not belonging to crypt were visually checked for all image files. Ten crypts/patient were counted.

Immunohistochemical analysis of MUC-2, KLF4 and beta-catenin

Because the MUC-2 staining of goblet cells was patchy, we picked ten crypts from each slide and manually counted the

number of goblet cells stained in each crypt. We also evaluated MUC-2 staining of villi, when possible, i.e., in GFD patients and controls. We also evaluated KLF4-positive villi (in GFD patients) and both beta-catenin- and Ki67-positive nuclei/crypt in each subject. Two independent observers evaluated the immunohistochemical slides.

Statistics

All variables were expressed as mean±standard error of the mean (SEM). Student t's test and ANOVA were used to compare group means and p values<0.05 were considered significant. Statistically significant ($p<0.01$) miRNA-regulated pathways were selected by the GOTM program.

Supporting Information

Materials and Methods S1
(DOC)

Figure S1 Bioinformatics analysis of miR-449a putative target genes. miR-449a putative target genes with most favorable context score, selected by bioinformatics, were sorted into pathways using GOTM(http://bioinfo.vanderbilt.edu/webgestalt/) and then combined into functional groups. (http://mirecords.biolead.org/interactions.php?species=Homo+sapiens&mirna_acc=hsa-miR-449a&targetgene_type=refseq_acc&targetgene_info=&v=yes&search_int=Search) (http://www.targetscan.org/cgibin/targetscan/vert_50/targetscan.cgi?species=Human&gid=&mir_sc=&mir_c=&mir_nc=&mirg=hsa-miR-449a). In each functional group are reported the genes belonging to NOTCH pathway/total gene number.
(TIF)

Figure S2 The luciferase assay confirms that miR-449a inhibits the expression of NOTCH1 and KLF4. In HEK293 cells co-transfected or with pRL-NOTCH1 vector (panel A) or with pRL-KLF4 vector (panel B), a pre-miR-449a concentration of 100 nmol/L was sufficient to significantly reduce (respectively, $p = 0.001$ and $p = 0.002$) *Renilla* luciferase activity versus control values. No inhibition of the *Renilla* luciferase expression was observed in mutant 3′UTR of KLF4-mRNA with miR-449a, so confirming the miR-449a/3′UTR KLF4-mRNA direct interaction (panel B). We didn't verify the interaction miR-449a/3′UTR NOTCH1 being this latter recently validated by Marcet B et al [32].
(TIF)

Figure S3 Automated Counts of NOTCH1 and HES1 stained/unstained cells. A. Automated counts of NOTCH1 stained/unstained cells (reported in Figure 2) in small intestine from CD patients (6 active CD and 6 GFD patients) and from controls ($n = 4$). Data are expressed as mean percent of intensely stained, low-moderately stained and unstained cells of the total intraepithelial cells (IECs) counted in ten crypts. The numbers of intensely stained and unstained cells were significantly ($p = 0.02$) higher and lower, respectively, in CTRL than in active CD and in GFD patients. **B.** Automated counts of HES1 stained/unstained cells (reported in Figure 3) in small intestine from CD patients (6 active CD and 6 GFD patients) and from controls ($n = 4$). Data are expressed as mean percent of intensely stained, low-moderately stained and unstained cells of the total intraepithelial cells (IECs) counted in ten crypts. The number of intensely stained cells was significantly higher in controls versus CD and GFD patients ($p = 0.02$) and the number of unstained cells was significantly lower in CTRL than in active CD patients ($p = 0.03$). (CTRL: controls; GFD: gluten free diet; CD: celiac disease).
(TIF)

Figure S4 Other examples of NOTCH1 immunohistochemistry in CD patients. Examples of NOTCH1 immunohistochemistry in 4 CD patients (2 active CD: TIII Marsh stage and 2 GFD: TI and T0 Marsh stage) and 2 controls (T0 Marsh stage). The images show that the low expression levels of NOTCH1 in intestinal mucosa from CD patients were always present from TIII to T0 Marsh stage. (CTRL: controls; GFD: gluten free diet; CD: celiac disease).
(TIF)

Figure S5 Other examples of HES1 immunohistochemistry in CD patients. Examples of HES1 immunohistochemistry in 4 CD patients (2 active CD: TIII Marsh stage and 2 GFD: TI and T0 Marsh stage) and 2 controls (T0 Marsh stage). The images show that the low expression levels of HES1 in intestinal mucosa from CD patients were always present from TIII to T0 Marsh stage. (CTRL: controls; GFD: gluten free diet; CD: celiac disease).
(TIF)

Figure S6 Decreased KLF4 and increased Ki67 expression in small intestine from CD patients compared with controls. A. KLF4 staining of small intestinal villi in GFD patients and Controls (Original magnification 20×). A statistically significant reduced KLF4-positive cells/villi were counted in GFD patients than in controls, respectively 29.0±5.0 vs 79.0±3.0 (mean±SEM) ($p<0.0001$). **B.** Increased Ki67 signal is present in small intestinal crypts of active CD, GFD patients than in controls (Original magnification 20×). (CTRL: controls; GFD: gluten free diet; CD: celiac disease).
(TIF)

Figure S7 Increased expression of beta-catenin in small intestine from CD patients compared with controls. Immunostaining with beta-catenin in small intestinal crypts from active CD, GFD and controls. We counted the beta-catenin labeled nuclei. Similar counts of beta-catenin labelled nuclei were detected in the crypts of the small intestine in all groups. However, higher even if not statistical significant mean percentage counts (beta-catenin positive nuclei/crypt) were obtained in active CD and GFD than in controls, respectively 57.0±11.5 and 37.0±4.6 vs 27.0±4.6 (Original magnification 63×). (CTRL: controls; GFD: gluten free diet; CD: celiac disease).
(TIF)

Figure S8 Specificity of NOTCH1 and HES1 signals by immunohistochemistry. Specificity controls of NOTCH1 and HES1 antibodies. Positive NOTCH1 (**A**) and HES1 (**B**) immunostaining signals obtained in human colon cancer and negative NOTCH1 (**C**) and HES1 (**D**) immunostaining signals obtained in human endothelial wall.
(TIF)

Table S1 MiRNAs differently expressed in active and GFD CD patients.
(DOC)

Acknowledgments

Jean Ann Gilder (Scientific Communication srl) provided writing assistance.

Provenance and peer review not commissioned; externally peer reviewed.

This paper is dedicated to Prof. Salvatore Auricchio. He has promoted research in celiac disease in Naples for 40 years and kindly read and commented on this study. We are grateful to M. V. Barone for helpful discussion and to Carolina Tarantino for skilled technical assistance.

Author Contributions

Conceived and designed the experiments: LS. Performed the experiments: MC LI NT LS. Analyzed the data: LS MC LI NT VC GT DM. Contributed reagents/materials/analysis tools: LG VI FT DM. Wrote the paper: LS MC LI.

References

1. Nisticò L, Fagnani C, Coto I, Percopo S, Cotichini R, et al. (2006) Concordance, disease progression, and heritability of coeliac disease in Italian twins. Gut 55: 803–808.
2. Greco L, Romino R, Coto I, Di Cosmo N, Percopo S, et al. (2002) The first large population based twin study of coeliac disease. Gut 50: 624–628.
3. Schuppan D, Junker Y, Barisani D (2009) Celiac disease: from pathogenesis to novel therapies. Gastroenterology 137: 1912–1933.
4. Hunt KA, van Hell DA (2009) Recent advances in celiac disease genetics. Gut 58: 473–476.
5. Sacchetti L, Calcagno G, Ferrajolo A, Sarrantonio C, Troncone R, et al. (1998) Discrimination between celiac and other gastrointestinal disorders in childhood by rapid human lymphocyte antigen typing. Clin Chem 44: 1755–1757.
6. Van Heel DA, Franke L, Hunt KA, Gwilliam R, Zhernakova A, et al. (2007) A genome-wide association study for celiac disease identifies risk variants in the region harboring IL2 and IL21. Nat Genet 39: 827–829.
7. Juuti-Uusitalo K, Mäki M, Kainulainen H, Isola J, Kaukinen K (2007) Gluten affects epithelial differentiation-associated genes in small intestinal mucosa of coeliac patients. Clin Exp Immunol 150: 294–305.
8. Diosdado B, Wapenaar MC, Franke L, Duran KJ, Goerres MJ, et al. (2004) A microarray screen for novel candidate genes in coeliac disease pathogenesis. Gut 53: 944–951.
9. Inui M, Martello G, Piccolo S (2010) MicroRNA control of signal transduction. Nature review 11: 252–263.
10. Lee RC, Feinbaum RL, Ambros V (1993) The C. elegans heterochronic gene lin-4 encodes small RNAs with antisense complementarity to lin-14. Cell 75: 843–854.
11. Pauley KM, Chan EKL (2008) MicroRNAs and their emerging roles in immunology. Ann NY Acad Sci 1143: 226–239.
12. Pauley KM, Cha S, Chan EKL (2009) MicroRNA in autoimmunity and autoimmune diseases. J Autoimmun 32: 189–194.
13. Neilson JR, Zheng GXY, Burge CB, Sharp PA (2007) Dynamic regulation of miRNA expression in ordered stages of cellular development. Genes Dev 21: 578–589.
14. Wu H, Neilson JR, Kumar P, Manocha M, Shankar P, et al. (2007) miRNA profiling of naïve, effector and memory CD8 T cells. PLoS One 10;2(10): e1020.
15. Zhou B, Wang S, Mayr C, Bartel DP, Lodish HF (2007) miR-150, a microRNA expressed in mature B and T cells, blocks early B cell development when expressed prematurely. Proc Natl Acad Sci U S A 104: 7080–7085.
16. McKenna LB, Schug J, Vourekas A, McKenna JB, Bramswig NC, et al. (2010) MicroRNAs control intestinal epithelial differentiation, architecture, and barrier function. Gastroenterology 139: 1654–1664.
17. Iborra M, Bernuzzi F, Invernizzi P, Danese S (2010) MicroRNAs in autoimmunity and inflammatory bowel disease: Crucial regulators in immune response. Autoimmun Rev;doi:10.1016/j.autrev.2010.07.002.
18. Fre S, Pallavi SK, Huyghe M, Laé M, Janssen KP, et al. (2009) Notch and Wnt signals cooperatively control cell proliferation and tumorigenesis in the intestine. Proc Natl Acad Sci 106: 6309–6314.
19. Lizé M, Pilarski S, Dobbelstein M (2010) E2F1-inducible microRNA 449a/b suppresses cell proliferation and promotes apoptosis. Cell Death Differ 17: 452–458.
20. Noonan EJ, Place RF, Pookot D, Basak S, Whitson JM, et al. (2009) miR-449a targets HDAC-1 and induces growth arrest in prostate cancer. Oncogene 28: 1714–1724.
21. McConnell BB, Ghaleb AM, Nandan MO, Yang VW (2007) The diverse functions of Krüppel-like factors 4 and 5 in epithelial biology and pathobiology. Bioessays 29: 549–557.
22. Clevers H (2006) Wnt/beta-catenin signaling in development and disease. Cell 127(3): 469–480.
23. Fre S, Huyghe M, Mourikis P, Robine S, Louvard D, et al. (2005) Notch signals control the fate of immature progenitor cells in the intestine. Nature 435(7044): 964–968.
24. Oshima S, Nakamura T, Namiki S, Okada E, Tsuchiya K, et al. (2004) Interferon regulatory factor 1 (IRF-1) and IRF-2 distinctively up-regulate gene expression and production of interleukin-7 in human intestinal epithelial cells. Mol Cell Biol 24(14): 6298–6310.
25. Crosnier C, Stamataki D, Lewis J (2006) Organizing cell renewal in the intestine: stem cells, signals and combinatorial control. Nat Rev Genet 7(5): 349–359.
26. Okamoto R, Tsuchiya K, Nemoto Y, Akiyama J, Nakamura T, et al. (2009) Requirement of Notch activation during regeneration of the intestinal epithelia. Am J Physiol Gastrointest Liver Physiol 296(1): G23–G35.
27. Ghaleb AM, McConnell BB, Kaestner KH, Yang VW (2011) Altered intestinal epithelial homeostasis in mice with intestine-specific deletion of the Krüppel-like factor 4 gene. Developmental Biology 349: 310–320.
28. Zheng H, Pritchard DM, Yang X, Bennett E, Liu G, et al. (2009) KLF4 gene expression is inhibited by the notch signaling pathway that controls goblet cell differentiation in mouse gastrointestinal tract. Am J Physiol Gastrointest Liver Physiol 296(3): G490–G498.
29. Katz JP, Perreault N, Goldstein BG, Lee CS, Labosky PA, et al. (2002) The zinc-finger transcription factor Klf4 is required for terminal differentiation of goblet cells in the colon. Development 129: 2619–2628.
30. Kopan R, Ilagan MXG (2009) The canonical Notch signaling pathway: unfolding the activation mechanism. Cell 137: 216–233.
31. Yin L, Velazquez OC, Liu ZJ (2010) Notch signaling: emerging molecular targets for cancer therapy. Biochem Pharmacol 80: 690–701.
32. Marcet B, Chevalier B, Luxardi G, Curaux C, Zaragosi LE, et al. (2011) Control of vertebrate multiciliogenesis by miR-449 through direct repression of the Delta/Notch pathway. Nat Cell Biol 6: 693–699.
33. Ciacci C, Di Vizio D, Seth R, Insabato G, Mazzacca G, et al. (2002) Selective reduction of intestinal trefoil factor in untreated coeliac disease. Clin Exp Immunol 130: 526–531.
34. Ciccocioppo R, Finamore A, Ara C, Di Sabatino A, Mengheri E, et al. (2006) Altered Expression, Localization, and Phosphorylation of Epithelial Junctional Proteins in Celiac Disease. Am J Clin Pathol 125: 502–511.
35. Ghaleb AM, Aggarwal G, Bialkowska AB, Nandan MO, Yang VW, et al. (2008) Notch inhibits expression of the Krüppel-like factor 4 tumor suppressor in the intestinal epithelium. Mol Cancer Res 6(12): 1920–1927.
36. McAuley JL, Linden SK, Png CW, King RM, Pennington HL, et al. (2007) MUC1 cell surface mucin is a critical element of the mucosal barrier to infection. J Clin Invest 2007;117: 2313–2324.
37. Corfield AP, Myerscough N, Longman R, Sylvester P, Arul S, et al. (2000) Mucins and mucosal protection in the gastrointestinal tract: new prospects for mucins in the pathology of gastrointestinal disease. Gut 2000;47: 589–594.
38. Festen EA, Szperl AM, Weersma RK, Wijmenga C, Wapenaar MC, et al. (2009) Inflammatory bowel disease and celiac disease: overlaps in the pathology and genetics, and their potential drug targets. Endocr Metab Immune Disord Drug Targets 9: 199–218.
39. Van der Sluis M, De Koning BA, De Bruijn AC, Velcich A, Meijerink JP, et al. (2006) Muc2-deficient mice spontaneously develop colitis, indicating that MUC2 is critical for colonic protection. Gastroenterology 131: 117–129.
40. Forsberg G, Fahlgren A, Hörstedt P, Hammarström S, Hernell O, et al. (2004) Presence of bacteria and innate immunity of intestinal epithelium in childhood celiac disease. Am J Gastroenterol 99(5): 894–890.
41. Report of Working Group of European Society of Paediatric Gastroenterology and Nutrition (1990) Revised criteria for diagnosis of coeliac disease. Arch disease child 65: 909–911.
42. Marsh MN, Crowe PT (1995) Morphology of the mucosal lesion in gluten sensitivity. Baillieres Clin Gastroenterol 9(2): 273–293.

Journal of proteome research

Article

pubs.acs.org/jpr

miRNA and Protein Expression Profiles of Visceral Adipose Tissue Reveal miR-141/YWHAG and miR-520e/RAB11A as Two Potential miRNA/Protein Target Pairs Associated with Severe Obesity

Valentina Capobianco,[†] Carmela Nardelli,[‡,§] Maddalena Ferrigno,[§] Laura Iaffaldano,[‡,§] Vincenzo Pilone,[∥] Pietro Forestieri,[∥] Nicola Zambrano,[‡,§] and Lucia Sacchetti*[,‡,§]

[†]Fondazione IRCCS SDN, Istituto di Ricerca Diagnostica e Nucleare, Via Gianturco 113, 80143 Naples, Italy

[‡]Dipartimento di Biochimica e Biotecnologie Mediche, Università degli Studi di Napoli Federico II, Via Pansini 5, 80131 Naples, Italy

[§]CEINGE Biotecnologie Avanzate S.C. a R.L., Via Gaetano Salvatore 486, 80145, Naples, Italy

[∥]Dipartimento di Chirurgia Generale, Geriatrica, Oncologica e Tecnologie Avanzate, Università degli Studi di Napoli Federico II, Via Pansini 5, 80131 Naples, Italy

Supporting Information

ABSTRACT: Adipose tissues show selective gene expression patterns, to whom microRNAs (miRNAs) may contribute. We evaluated in visceral adipose tissue (VAT) from obese and nonobese females, both miRNA and protein expression profiles, to identify miRNA/protein target pairs associated with obesity (metabolic pathways miRNA-deregulated during obesity). Obese and nonobese females [BMI 42.2 ± 1.6 and 23.7 ± 1.2 kg/m^2 (mean ± SEM), respectively] were enrolled in this study. Notably, most miRNAs were down-expressed in obese tissues, whereas most of the proteins from the investigated spots were up-expressed. Bioinformatics integration of miRNA expression and proteomic data highlighted two potential miRNA/protein target pairs: miR-141/YWHAG (tyrosine 3-monooxygenase/tryptophan 5-monooxygenase activation protein, gamma polypeptide) and miR-520e/RAB11A (Ras-related protein RAB-11A); the functional interaction between these miRNAs and their target sequences on the corresponding mRNAs was confirmed by luciferase assays. Both RAB11A and YWHAG proteins are involved in glucose homeostasis; YWHAG is also involved in lipid metabolism. Hence, the identified miRNA/protein target pairs are potential players in the obese phenotype.

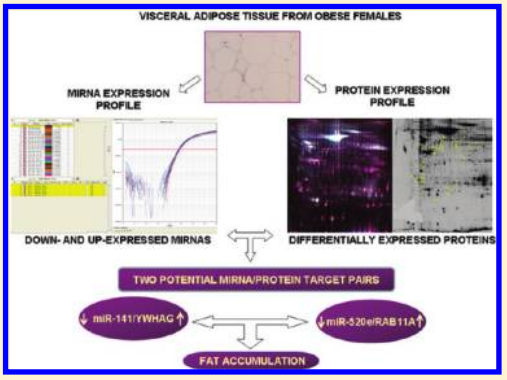

KEYWORDS: *obesity, visceral adipose tissue, miRNAs, 2D-DIGE*

INTRODUCTION

Obesity is an epidemic health problem worldwide that causes morbidity and mortality associated with increased risk of cardiovascular disease, metabolic syndrome, and cancer.[1,2] In particular, central obesity, i.e., fat accumulated in visceral adipose tissue (VAT), is the major risk factor for obesity-related disorders.[3,4] VAT represents up to 10−20% of total fat in men and 5−8% in females. It is anatomically present in the mesentery and omentum, and it drains directly to the liver through the portal vein. This characteristic allows the direct access of the free fatty acids and of adipokines released from fat to the liver.[4] In addition, adipose tissues show selective gene expression patterns,[2,3,5,6] to whom microRNAs (miRNAs) may contribute.[7] miRNAs are small noncoding RNAs ∼21 nucleotides long that bind specific regions of mRNA targets to mediate their cleavage or translational repression, and they regulate about 50% of human genes.[8] In mammals, miRNAs have been also shown to modulate adipocyte differentiation.[9] Previous work from our laboratory showed that up-expression of miR-519d in subcutaneous adipose tissue (SAT) from obese patients was associated with down-expression of the PPARA protein.[10] There are biological differences between VAT and SAT. In fact, compared with SAT, VAT contains more large and insulin-resistant adipocytes and inflammatory cells such as macrophages that secrete pro-inflammatory cytokines (TNF-α, IL-6, and CRP).[4]

In the present study, we evaluated miRNA and protein signatures using transcriptomic and proteomic approaches, respectively, in VAT from the women studied previously. Our aim was to investigate for metabolic pathways miRNA-regulated in VAT that could be altered during obesity. Our results indeed show that VAT from obese females is characterized by peculiar miRNA and protein expression signatures. Most of the tested miRNAs are down-expressed in VAT from obese females. Accordingly, most of proteins in VAT from the obese group showed increased levels by proteomic profile. Finally, the functional association of the transcriptomic and proteomic profiles revealed two potential miRNA/protein

Received: February 15, 2012
Published: April 27, 2012

target pairs in VAT, namely, miR-141/YWHAG (tyrosine 3-monooxygenase/tryptophan 5-monooxygenase activation protein, gamma polypeptide) and miR-520e/RAB11A (Ras-related protein RAB-11A), which may contribute to altered gene expression in obesity.

EXPERIMENTAL SECTION

Subjects and Experimental Design

Fifteen obese females (age range: 19−65 years, BMI [mean ± SEM] 42.2 ± 1.6 kg/m^2) and 10 nonobese females (age range: 19−57 years, BMI [mean ± SEM] 23.7 ± 1.2 kg/m^2) were enrolled in the study. During surgery (gastric banding or laparoscopic cholecystectomy for obese and nonobese females, respectively), a bioptic sample of VAT was collected and frozen in liquid nitrogen. The main anamnestic, clinical, and general characteristics of the enrolled subjects were recorded at admission. The day before surgery, a fasted blood sample was collected from all subjects and tested for the main biochemical parameters (glucose, cholesterol, triglycerides, AST, ALT, ALP, GGT) by routine methods (Table 1). Written informed consent was obtained from all recruited subjects, and the study was approved by the Ethics Committee of our Faculty of Medicine.

Table 1. General Characteristics of the Obese (n = 15) and Nonobese (n = 10) Females Enrolled in the Study[a]

	females	
	obese	nonobese
subjects (n)	15	10
age (years)	41.6 (4.4)	38.0 (3.5)
weight (kg)†[b]	115.2 (6.3)	62.5 (2.6)
height (m)	1.7 (0.04)	1.6 (0.01)
BMI (kg/m^2)‡[b]	42.2 (1.6)	23.7 (1.2)
systolic blood pressure (mmHg)	133.6 (6.7)	115 (4.5)
diastolic blood pressure (mmHg)[c]	80.0 (80.0−90.0)	80.0 (70.0−80.0)
cardiac frequency[d]	80.0 (2.2)	67.6 (3.7)
glucose (mmol/L)[e]	4.9 (0.2)	4.3 (0.2)
cholesterol (mmol/L)	5.9 (0.5)	5.8 (0.6)
triglycerides (mmol/L)	1.4 (0.1)	0.9 (0.1)
AST (U/L)[c]	18.5 (16.0−21.0)	18.0 (13.5−19.0)
ALT (U/L)[c]	17.0 (13.0−28.5)	14.0 (12.0−21.0)
ALP (U/L)	79.3 (5.8)	89.2 (19.3)
GGT (U/L)	28.5 (4.7)	17.3 (3.5)

[a]Data are expressed as mean (SEM) value (unless specified otherwise) and interquartile range (nonparametric distributions). [b]Statistically significant differences (designated by † and ‡) at Student's t test $p < 0.0001$. [c]Data are expressed as median value. [d]$p = 0.01$. [e]$p = 0.03$.

RNA Isolation

Total RNA (including miRNAs) was isolated from the VAT of all subjects using the mirVana miRNA isolation kit (Ambion, Austin, TX, USA) according to the manufacturer's instructions. RNA concentration was evaluated using the NanoDrop ND-1000 UV−vis spectrophotometer (NanoDrop Technologies, Wilmington, DE, USA).

The total RNA isolated from nonobese females was pooled to serve as control in the comparison of the miRNA expression profiles of the obese females.

miRNA Expression Profile

We used the commercially available TaqMan Array Human MicroRNA Panel v1.0 (Applied Biosystems Inc., Foster City, CA, USA) to measure miRNA expression profile in 10/15 obese and 4/10 nonobese females. The panel contains 365 different human miRNA assays in addition to two small nucleolar RNAs (snoRNAs) that function as endogenous controls for data normalization. We used 80 ng of total RNA for reverse transcription. RT-PCR was performed using the 7900 HT real-time PCR system (Applied Biosystems). The miRNA expression values were normalized to RNU48 (endogenous control), and relative expression values were obtained using the ΔΔCT method (relative quantification, RQ = $2^{-\Delta\Delta CT}$) with sequence detection system (SDS) v2.3 and RQ Manager 1.2 software (Applied Biosystems). To further normalize our miRNA data and to minimize interindividual variability, we considered differently expressed the miRNAs whose mean RQ levels were <0.5 (down-expressed) or >2.0 (up-expressed) in at least 6/10 obese females.

Quantitative Real-Time Polymerase Chain Reaction (qRT-PCR) of miRNAs and mRNAs

The expression levels of some selected miRNAs (miR-141, miR-200c, miR-520e, and miR-520d) were also validated by TaqMan miRNA assays (Applied Biosystems) in accordance with the manufacturer's instructions on the 7900 HT real-time PCR system (Applied Biosystems). The expression of one of these selected miRNAs, namely, miR-141, was preliminarily tested in each nonobese control, and after ensuring that the expression was comparable among these individuals, we pooled their RNAs to obtain a control against which to compare miRNA levels in obese females.

The expression levels of the selected miRNAs (miR-141, miR-200c, miR-520e, and miR-520d) were first normalized to the endogenous control (RNU48), and then the relative expression values were obtained versus the nonobese control pool using the ΔΔCT method (relative quantification, RQ = $2^{-\Delta\Delta CT}$) with SDS v2.3 and RQ Manager 1.2 software (Applied Biosystems).

Real-time RT-PCR of RAB11A and YWHAG mRNAs was performed using gene- specific primers (**RAB11a**, forward: AACATCAGCATATTATCGTGGA and reverse: GATCACTCTTATTGCCCACA; **YWHAG**, forward: AGACCCAGCCCCGCGAAGAT and reverse: TCTGTCACGTTCTTCATGGCCGC), the Power SYBR Green PCR Master Mix (Applied Biosystems) and the PRISM 7900HT sequence detection system (Applied Biosystems).

Bioinformatic Analysis

Biological targets of miRNAs differently expressed in obese vs nonobese females were predicted using the TargetScan Release 5.0 algorithm (http://www.targetscan.org). This algorithm assigns a "total context score" for each predicted target. Target genes with a "total context score" < −0.30 were further analyzed using the KEGG database (http://www.genome.ad.jp/kegg/) to identify the pathways that involve the target genes of miRNAs and then using the Gene Ontology (GO) database (http://www.geneontology.org/ontologies) to identify the biological processes in which the proteins identified by DIGE participate. Gene ontology classification of the differentially expressed proteins revealed by 2D-DIGE analysis was performed in the web-accessible DAVID (v 6.7) annotation system (http://david.abcc.ncifcrf.gov/home.jsp).[11,12]

dx.doi.org/10.1021/pr300152z | J. Proteome Res. 2012, 11, 3358−3369

Preparation of Protein Extracts and Two-Dimensional Fluorescence Difference Gel Electrophoresis (2D-DIGE) Analysis

Protein extracts from VAT samples of 6/15 obese and 3/10 nonobese females were prepared using a lysis buffer containing 2% SDS, 10% glycerol, 6.25 mM Tris-HCl pH 6.8, 0.5 mM EDTA, 20 mM NaF, 1 mM Na_3VO_4 (Santa Cruz Biotechnology, Santa Cruz, CA), and the Sigma-Aldrich cocktail of protease inhibitors. The suspensions were shaken in Tissue Lyser II (Qiagen) for 4 min at maximum frequency. After 30 min on ice, samples were centrifuged at 15000*g* for 10 min at 4 °C. The clear interface of each sample was recovered and was transferred to a clean tube. Protein concentrations were determined by the Bradford method using BioRad protein reagent (Bio-Rad Laboratories, Hercules, CA). For 2D-DIGE analysis, proteins extracted from VAT were precipitated for 16 h at −20 °C with 9 volumes of a mix composed of acetone and methanol (9:1) and then centrifuged at 15000*g* for 30 min at 4 °C; protein pellets were solubilized in a buffer, UTC, containing 7 M urea, 2 M thiourea, 4% CHAPS (3-[(3-cholamidopropyl)dimethylammonium]-1-propane sulfonate) in 30 mM Tris-HCl. Protein concentrations were redetermined after precipitation by using BioRad protein reagent. Thirty micrograms of each protein extract were labeled with 240 pmol of Cy3 or Cy5 fluorescent dye on ice, in the dark for 30 min. To exclude preferential binding of a label to a set of proteins, we dye-swapped the samples. The internal standard containing equal amounts of proteins from each sample was labeled with Cy2. The same internal standard was run in all gels to normalize the experiments and to reduce gel-to-gel variations. Labeling reactions were stopped by adding 1 mM lysine. Sample pairs labeled with Cy3 and Cy5 and the internal standard were combined and used to hydrate passively individual strips as follows: each mix of labeled samples was diluted in UTC solution containing 130 mM DTT, 2% IPG Buffer pH 3−10 NL (GE Healthcare, Buckinghamshire, UK), 2.8% DeStreak reagent (GE Healthcare) in a final volume of 400 μL. The mixtures were used to hydrate 24 cm IPG strips pH 3−10NL required for protein separation in the first dimension. Isoelectric focusing (IEF) was run in an IPGphor II apparatus (GE Healthcare) according to this voltage protocol: 300 V for 3 h, linear gradient to 600 V in 3 h, linear gradient to 1000 V in 3 h, linear gradient to 8000 V in 5 h, 8000 V for 6 h. After the first dimension, the strips were equilibrated in equilibration buffer (100 mM Tris-HCl, 6 M urea, 30% (v/v) glycerol, 2% (w/v) SDS, and trace of bromophenol blue, pH 8.0) containing 0.5% (w/v) DTT for 15 min and thereafter in equilibration buffer containing 4.5% (w/v) iodoacetamide for a further 15 min. The equilibrated strips were transferred onto 12% polyacrylamide gels for the second dimension (Ettan Dalt six electrophoresis system, GE Healthcare). The SDS-PAGE electrophoresis was run using a Peltier-cooled DALT II Electrophoresis unit (GE Healthcare) at 30W. After the electrophoresis, the gels were scanned with a Typhoon 9400 variable mode imager (GE Healthcare) at 100 μm resolution, using appropriated individual excitation/emission wavelengths: 488/520 for Cy2, 532/580 for Cy3 and 633/670 for Cy5. The images were captured with Image Quant software and were analyzed with DeCyder software (GE Healthcare). We chose the most representative gel as master gel to compare results obtained from other samples. Globally we analyzed VAT samples from 6 randomly selected obese (mean BMI 38.7) and 3 nonobese females (mean BMI 23.5). We used the Student's *t* test to determine the fold change between obese and nonobese females. Only protein spots with a $p < 0.05$ were investigated further.

Protein Identification with Liquid Chromatography−Tandem Mass Spectrometry (LC−MS/MS)

We used 250 μg of protein sample for the preparative gel. After 2D-electrophoresis, performed under the conditions reported for the analytical experiment, the gel was stained with SYPRO Ruby ready-to-use formula (BIORAD), and the spot map so obtained was matched with the analytical reference gel. The spots differentially expressed in obese and nonobese females were excised from the preparative gel using the Ettan Spot Picker robotic system (GE Healthcare). The excised spots were analyzed with LC−MS/MS (Functional and Structural Proteomics Facility, CEINGE−Biotecnologie Avanzate, Italy).

The excised spots were washed in 50 mM ammonium bicarbonate pH 8.0 in 50% acetonitrile to a complete destaining. The gel pieces were resuspended in 50 mM ammonium bicarbonate pH 8.0 containing 100 ng of trypsin and incubated for 2 h at 4 °C and overnight at 37 °C. The supernatant containing the resulting peptide mixtures was removed, and the gel pieces were re-extracted with acetonitrile. The two fractions were then collected and freeze-dried. The peptide mixtures were further analyzed by LC−MS/MS using the LC−MSD Trap XCT Ultra apparatus (Agilent Technologies, Palo Alto, CA, USA) equipped with a 1100 HPLC system and a chip cube (Agilent Technologies). After loading, the peptide mixture (8 μL in 0.5% TFA) was first concentrated at 4 μL/min in 40 nL enrichment column (Agilent Technologies chip), with 0.1% formic acid as eluent. The sample was then fractionated on a C18 reverse-phase capillary column (75 μm × 43 mm in the Agilent Technologies chip) at a flow rate of 300 nL/min, with a linear gradient of eluent B (0.1% formic acid in acetonitrile) in eluent A (0.1% formic acid) from 7 to 50% in 35 min. Elution was monitored on the mass spectrometer without a splitting device. Peptide analysis was performed using data-dependent acquisition of one MS scan (m/z range from 400 to 2000 Da/e) followed by MS/MS scans of the three most abundant ions in each MS scan. Dynamic exclusion was used to acquire a more complete survey of the peptides by automatic recognition and temporary exclusion (2 min) of ions from which definitive mass spectral data had previously been acquired. A permanent exclusion list of the most frequent peptide contaminants (keratins and trypsin peptides) was included in the acquisition method in order to focus on significant data. Mass spectral data obtained from the LC−MS/MS analyses were used to search a nonredundant protein database using an in-house version of the Mascot v. 2.1 (Matrix Science, Boston, MA, USA) software and NCBI database (221,338 human sequences, timestamp: March and April, 2009). Peptide mass values and sequence information from the LC−MS/MS experiments were used in the MS/MS ion search taking into account the Carbamidomethyl-Cys as fixed modification, Met oxidized, Pyro-Carbamidomethyl-Cys (with N-term Carbamidomethyl-Cys) and Pyro-Glu (with N-term E) as variable modifications. The maximum missed cleavage of 1, and a precursor ion and fragment ion mass tolerance of ±600 ppm and 0.6 Da, respectively, were used. In agreement with the proposed Guidelines for the Analysis and Documentations of Peptide and Protein Identifications (Paris Consensus), we report the number of identified peptides whose individual ion

dx.doi.org/10.1021/pr300152z | J. Proteome Res. 2012, 11, 3358−3369

score (as provided by Mascot) was higher than the designated confidence level (95%)/protein sequence coverage (%). The sequences and charge state of the peptides used for protein identification of each DIGE spot obtained by LC−MS/MS are reported in Supporting Information Table S1.

Western Blot

Protein evaluation by Western blot was performed in 8/15 obese and 7/10 nonobese females with 35 μg of total proteins separated by SDS-PAGE (13% polyacrylamide gel) and electroblotted onto hydrophobic polyvinylidene difluoride (PVDF) membranes (Amersham) for 19 h at 33 V. Blots were blocked with 5% BSA in TBS buffer with 0.1% Tween 20 for 2 h at room temperature. Immunoblotting was performed with the specific polyclonal antibody: rabbit anti-14-3-3γ (dilution 1:800), rabbit anti-RAB11A (1 μg/mL), and rabbit antiactin (dilution 1:800) (Abcam, Cambridge, UK) for 4 h. For the following incubation with primary antibody, membrane was washed in TBS buffer with 0.1% Tween 20 and incubated for 45 min IgG-HRP-conjugated secondary antibody (dilution 1:10000 for anti-14-3-3γ and antiactin; 1:50000 for anti-RAB11A). Immunoreactive bands were visualized with the chemiluminescence reagent kit (ECL Western blotting detection reagents, GE Healthcare). We used the same membrane for each immunoblot, washing it in TBS buffer with 0.1% Tween 20 for 10 min after each experiment.

After each immunoblot, the membrane was exposed to X-ray film (Amersham) for different times. The images of three different exposures were captured by Gel Doc XR (Bio-Rad) and quantitated with the Quantity One software (Bio-Rad). Each protein band was contained within a rectangular area, identical for each sample, and background values were subtracted from each band. The triplicate sample values were normalized to the corresponding triplicate actin values. Then, the mean values from the different ratio calculations were calculated for each sample. The data were expressed as percent relative expression, the sample with the highest expression of either RAB11A or YWHAG having been set as 100%. The data obtained were used to obtain the corresponding box plots and *p*-values (Student's *t* test) in the Microsoft Excel software.

Oligonucleotides and Plasmids

Chemically modified double-stranded RNA molecules (microRNA precursor molecules: pre-miR-520e and pre-miR-141) and pre-miR-negative control were purchased from Ambion (Austin, TX, USA). The final concentration of pre-miR molecules and the corresponding pre-miR negative control were 100 nM each. The plasmids used were pGL3-control (Promega Corp., Madison, WI, USA) encoding for firefly luciferase and pRL-CMV encoding for *Renilla* luciferase (Promega Corp., Madison, WI, USA). The 3′UTRs of RAB11A (1258−1264 bp 3′UTR) and of YWHAG (2489−2495 bp 3′UTR) genes, containing respectively the miR-520e and miR-141 binding sites, as well as the mutated 3′UTRs of these two genes (three bases of each seed region were changed by complementary bases), were obtained from genomic DNA by PCR with a sense and antisense primers carrying a XbaI restriction site and cloned downstream to *Renilla* luciferase gene in pRL-CMV vector in XbaI site.

Cell Culture, Transfection, and Luciferase Assay

Human embryonic kidney (HEK) 293 cells were cultured in DMEM (Invitrogen) supplemented with 2 mM glutamine (Invitrogen), 100 U/mL penicillin/streptomycin (Invitrogen), and 10% FBS (Invitrogen). The day before transfection, cells were plated in 24-well plates to allow adherence and to reach 70−90% confluence at the time of transfection. Transfection of plasmids, carrying wild-type or mutant 3′UTRs, with pGL3-control and each pre-miRNAs or pre-miR negative control (Ambion, Austin, TX, USA) in HEK293 was performed using Lipofectamine 2000 following the manufacturer's instructions. Firefly and *Renilla* luciferase activities were measured 48 h after transfection, with the dual-luciferase reporter system (Promega) in a Sirius Luminometer (Berthold Detection Systems, Huntsville, AL, USA). All transfection experiments were done in triplicate.

Statistical Analysis

The investigated parameters were expressed as mean ± standard error of the mean (SEM) (parametric distribution) or as median value and interquartile range (nonparametric distributions). Student's *t* test was used to compare group means, and a *p*-level < 0.05 was considered statistically significant. Statistical analyses were carried out with the PASW package for Windows (Ver.18; SPSS Inc. Headquarters, Chicago, Ill).

RESULTS

miRNA Expression Signature in Visceral Adipose Tissue from Obese Females

Expression profile showed that a large set of the tested miRNAs was expressed in VAT from both obese and nonobese females (243/365, 66%). A small set (50/365, 14%) was not expressed, whereas 72/365 (20%) miRNAs were expressed only in VAT from one or more obese females. On the basis of the normalization criteria reported above (see the Experimental Section), namely, miRNAs whose expression levels versus controls were up- or down-expressed (respectively, RQ > 2 or < 0.5) in at least 6/10 obese females, we found that 61/243 (25%) miRNAs were down-expressed, and 10/243 (4.1%) miRNAs were up-expressed (Table 2). The search for gene targets of these differentially expressed miRNAs was performed by TargetScan 5.0 algorithm and their assembly in metabolic pathways by Kegg database. The main significant ($p < 0.01$) pathways predicted to be affected by miRNAs in VAT samples during obesity are reported in Supplementary Figure 1.

Protein Expression Signature in VAT from Obese Females

We studied the protein expression signature of VAT samples from obese and nonobese subjects using 2D-DIGE analysis. Figure 1A shows the master gel used to match the whole set of the 2-DE profiles obtained. The analysis performed with DeCyder Software detected approximately 2700 protein spots per gel in a 3−10 pH range, with a molecular mass of 10−120 kDa. Approximately 1500 spots were matched throughout the gels. The DeCyder statistical analysis revealed 172 spots differentially expressed in obese vs nonobese VAT samples with average ratio ≥ 1.50 for up-expressed protein spots and ≤ −1.50 for down-expressed spots ($p < 0.05$). Some spots were excluded from further evaluation, i.e., those at the extreme right and left sides of the gel and those (30 spots) representing contaminating serum proteins. Furthermore, many spots were not objected to further investigation, because of their low abundance on the analytical gel or on the preparative gel. As a result, we focused on 33 spots with optimal features.

Figure 1B shows the position of the 33 selected spots on the preparative gel. The latter was stained with SYPRO Ruby protein stain and used for automated spot picking. The isolated

dx.doi.org/10.1021/pr300152z | J. Proteome Res. 2012, 11, 3358−3369

Table 2. Differentially Expressed miRNAs in Visceral Adipose Tissue from Obese Vs Nonobese Females Identified with the TaqMan Array Human MicroRNA Panel v1.0[a]

	RQ value	
down-expressed miRNAs	mean	SEM
hsa-miR-514-4373240	0.007	0.002
hsa-miR-520e-4373255	0.014	0.005
hsa-miR-520f-4373256	0.029	0.010
hsa-miR-184-4373113	0.030	0.010
hsa-miR-518d-4373248	0.057	0.021
hsa-miR-196a-4373104	0.059	0.019
hsa-miR-337-4373044	0.065	0.025
hsa-miR-520d-4373254	0.066	0.022
hsa-miR-490-4373215	0.067	0.025
hsa-miR-508-4373233	0.069	0.022
hsa-miR-519c-4373251	0.073	0.026
hsa-miR-369-3p-4373032	0.075	0.025
hsa-miR-202-4378075	0.078	0.027
hsa-miR-141-4373137	0.079	0.025
hsa-miR-562-4380939	0.080	0.030
hsa-miR-591-4380955	0.085	0.028
hsa-miR-580-4381024	0.086	0.029
hsa-miR-380-5p-4373021	0.086	0.029
hsa-miR-518a-4373186	0.092	0.035
hsa-miR-618-4380996	0.096	0.034
hsa-miR-494-4373219	0.097	0.037
hsa-miR-624-4380964	0.099	0.035
hsa-miR-519b-4373250	0.102	0.032
hsa-miR-185-4373181	0.113	0.043
hsa-miR-219-4373080	0.120	0.042
hsa-miR-509-4373234	0.124	0.039
hsa-miR-548d-4381008	0.125	0.047
hsa-miR-206-4373092	0.126	0.042
hsa-miR-200c-4373096	0.130	0.041
hsa-miR-196b-4373103	0.166	0.055
hsa-miR-653-4381012	0.168	0.068
hsa-miR-493-4373218	0.178	0.059
hsa-miR-629-4380969	0.181	0.074
hsa-miR-198-4373101	0.187	0.062
hsa-miR-450-4373208	0.199	0.070
hsa-miR-375-4373027	0.202	0.071
hsa-miR-518b-4373246	0.208	0.069

	RQ value	
down-expressed miRNAs	mean	SEM
hsa-miR-137-4373174	0.222	0.091
hsa-miR-649-4381005	0.224	0.079
hsa-miR-189-4378067	0.226	0.080
hsa-miR-489-4373214	0.240	0.085
hsa-miR-451-4373209	0.242	0.099
hsa-miR-615-4380991	0.248	0.083
hsa-miR-335-4373045	0.250	0.088
hsa-miR-215-4373084	0.264	0.088
hsa-miR-422b-4373016	0.271	0.090
hsa-miR-500-4373225	0.271	0.111
hsa-miR-601-4380965	0.285	0.108
hsa-miR-203-4373095	0.298	0.122
hsa-miR-410-4378093	0.298	0.122
hsa-miR-330-4373047	0.320	0.121
hsa-miR-30a-5p-4373061	0.324	0.122
hsa-miR-486-4378096	0.327	0.133
hsa-miR-22-4373079	0.332	0.125
hsa-miR-181c-4373115	0.332	0.117
hsa-miR-30d-4373059	0.334	0.126
hsa-miR-101-4373159	0.346	0.141
hsa-miR-376a-4373026	0.372	0.152
hsa-miR-191-4373109	0.386	0.146
hsa-miR-99a-4373008	0.393	0.161
hsa-miR-7-4373014	0.396	0.162
	RQ value	
up-expressed miRNAs	mean	SEM
hsa-miR-433-4373205	21.563	7.624
hsa-miR-520 h-4373258	13.617	5.559
hsa-miR-153-4373125	12.447	4.705
hsa-miR-579-4381023	12.047	4.553
hsa-miR-520b-4373252	9.400	3.553
hsa-miR-616-4380992	3.954	1.495
hsa-miR-296-4373066	3.872	1.463
hsa-miR-517c-4373264	3.342	1.365
hsa-miR-501-4373226	3.068	1.160
hsa-miR-594-4380958	2.714	1.108

[a]The normalization criteria are detailed in the Experimental Section. Data are expressed as RQ. RQ value was calculated as $2^{-\Delta\Delta Ct}$ (see the Experimental Section for details), and it is reported as mean and SEM.

spots were digested with trypsin and then analyzed by LC–MS/MS, followed by database search. The relative expression ratios (in obese vs nonobese VAT) for each of the 33 spots and their statistical values are listed in Table 3. Interestingly, most (32/33) of the spots were increased, and only 1 spot (number 2312) was decreased.

Globally, a total of 67 proteins, after the exclusion of very abundant proteins that we considered not informative, were identified in these spots (http://pubs.acs.org/paragonplus/submission/jprobs/jprobs_proteomics_guidelines.pdf) (Table 3). Most of these proteins were bioinformatically predicted by DAVID database to be functionally annotated in two main clusters (Figure 2). Annotation cluster 1 (Figure 2A) was constituted by the following: (i) 5 members of the 14.3.3 family of proteins, namely, YWHAB, YWHAE, YWHAG, YWHAH, and YWHAZ; (ii) 9 proteins (YWHAB, YWHAE, YWHAZ, RAB11A, RAB7A, ANXA7, ARCN1, FLOT1, and SERPINF1) involved in the GOTERM_CC_FAT *vesicle* pathway, on the basis of their subcellular localization; and (iii) 7 regulated proteins involved in *intracellular protein transport* (YWHAB, YWHAE, YWHAH, YWHAG, YWHAZ, RAB11A, and ARCN1). Annotation cluster 2 (Figure 2B) was constituted by a predominance of metabolic enzymes clustered in the KEGG pathways: *valine*, *leucine*, and *isoleucine* degradation (6 members, ACAT2, ACADS, ALDH2, BCKDHA, ECHS1, and HADHB), *butanoate metabolism* (5 members, ACAT2, ACADS, ALDH2, ECHS1, and PDHAD1) and *fatty acid metabolism* (5 members, ACAT2, ACADS, ALDH2, ECHS1, and HADHB).

miRNA/Protein Target Pairs in VAT from Obese Females

To find potential miRNA/protein target pairs, we integrated miRNA expression and proteomic data. Specifically, we combined the list of the identified protein spots with the miRNAs predicted to possess the ability to target the proteins we identified. The last column of Table 3 shows the potential miRNA counterparts of the identified proteins, as revealed by bioinformatics tools (TargetScan). Among the potential miRNA/protein target pairs deriving from this analysis, we

dx.doi.org/10.1021/pr300152z | J. Proteome Res. 2012, 11, 3358–3369

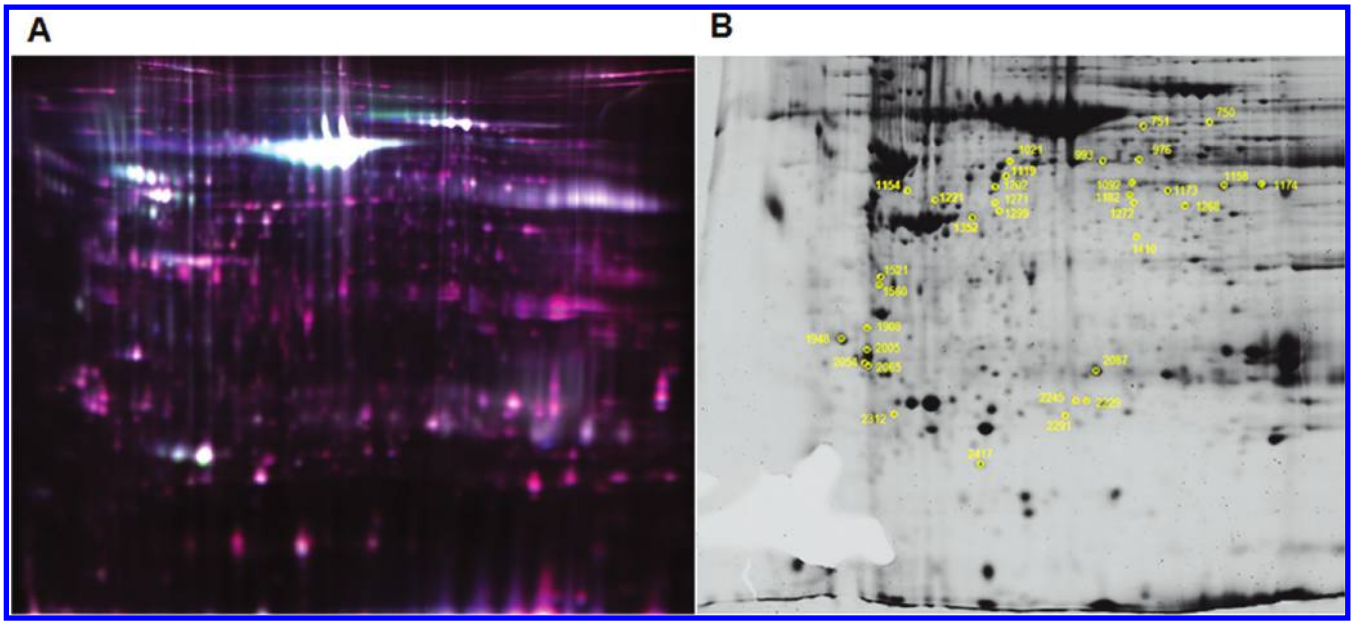

Figure 1. 2D-DIGE of visceral adipose tissue (VAT) proteins. (A) Scan of master gel used to match protein spots from the different gels used for the analysis. This gel is constituted by three overlapped images: (1) VAT proteins of a nonobese female labeled with Cy3 (green), (2) VAT proteins of an obese female labeled with Cy5 (red), and (3) VAT proteins from a mixture of the random selected samples (used for normalization) labeled with Cy2 (blue). (B) Scan of preparative gel of VAT proteins from a mixture of samples stained with SYPRO Ruby protein stain. Numbers correspond to differentially expressed protein spots as indicated in Table 3.

selected those including miRNAs down-expressed in almost all VAT samples (9/10 or 10/10): miR-206/ARCN1 (spot 751); miR-141/YWHAG and miR-200c/YWHAG (spot 2005); miR-206/YWHAZ (spot 2054); miR-520d/RAB11A and miR-520e/RAB11A (spot 2229) (bold characters in Table 3).

The expression levels of the above miRNAs (miR-206, miR-141, miR-200c, miR-520e, and -520d) were further validated by qRT-PCR. The qRT-PCR results, except slight differences due to the two different methodologies, were in close agreement with those obtained by TaqMan array (respectively, mean RQ ± SEM): miR-206 (0.209 ± 0.066 vs 0.126 ± 0.042), miR-141 (0.099 ± 0.032 vs 0.079 ± 0.025), miR-200c (0.138 ± 0.044 vs 0.130 ± 0.041), miR-520e (0.554 ± 0.175 vs 0.014 ± 0.005), except for miR-520d, whose results did not differ from controls in the qRT-PCR validation (0.944 ± 0.299 vs 0.066 ± 0.022). Consequently the miR-520d was discarded in our following evaluations.

All the miRNA/protein target pairs reported above warrant further investigation. However, functional annotation clustering in the DAVID database revealed that ARCN1, YWHAG, YWHAZ, and RAB11A are present in the annotation cluster *intracellular protein transport* (Figure 2A), which may be involved in the physiopathology of the adipose tissue. Among the miRNAs associated to these targets, miR-141 and miR-520e were accordingly regulated in the complete set of RNA samples (10/10) from obese VAT. Thus, we selected the functional pairs miR-141/YWHAG and miR-520e/RAB11A for further analysis.

Since the effects of miRNA down-regulations may result in increased mRNA stability and/or mRNA translation, we tested the transcript levels for RAB11A and YWHAG by qRT-PCR. We indeed observed that both mRNAs were more abundantly expressed in VAT of obese women (RQ ± SEM: 6.1 ± 2.6 and 4.8 ± 0.7, respectively) compared to control VAT mRNA samples (data not shown). Next, we tested YWHAG and RAB11A protein expression by Western blot in VAT from a subset of obese (8/15) and nonobese (7/10) females whose samples were available. These samples were also probed with an actin antibody for protein normalization. As shown in Figure 3, both YWHAG and RAB11A proteins were significantly (p = 0.001 and p = 0.00001, respectively) up-expressed in obese than in nonobese VAT tissues.

Taken together, our data suggest that in VAT from obese females, there is a functional interplay between the mRNAs of two up-expressed proteins (YWHAG and RAB11A, as emerged from 2D-DIGE analysis, qRT-PCR, and Western blot validations) and two down-expressed miRNAs (miR-141 and miR-520e, respectively, as revealed by the transcriptomic screening and qRT-PCR analysis). Thus, to determine whether the mRNAs of YWHAG and RAB11A are targets of miR-141 and miR-520e, respectively, we cloned the regions encompassing the 3′UTRs of the two mRNAs downstream the *Renilla* luciferase gene, under the transcriptional control of the cytomegalovirus promoter. The constructs were cotransfected with the pre-miRNAs for miR-141 or miR-520e, and as a transfection control, we used a pGL3-control that expresses firefly luciferase. As shown in Figure 4, both pre-miR-520e (A) and pre-miR-141 (B) significantly reduced the normalized *Renilla* luciferase activities of the constructs containing respectively the RAB11A (p = 0.004) and the YWHAG 3′UTRs (p = 0.02). No inhibition was observed in mutant 3′UTR of RAB11A (A) and YWHAG (B) constructs. These data are consistent with a functional interaction between the selected miRNAs and the 3′UTRs of their mRNA targets, thereby suggesting that changes in the levels of these two miRNAs may modulate the expression of RAB11A and YWHAG.

■ DISCUSSION

Understanding the molecular mechanisms underpinning obesity could pave the way for new therapeutic strategies to contrast obesity-related metabolic disorders. miRNAs, which

dx.doi.org/10.1021/pr300152z | *J. Proteome Res.* 2012, 11, 3358−3369

Table 3. Identification and Characterization of Proteins Differently Expressed in Visceral Adipose Tissue from Obese Vs Nonobese Females by 2D-DIGE Analysis Followed by LC−MS/MS

spot no.[a]	DIGE (p-value)[b]	DIGE obese/ control[c]	accession no.[d]	protein name	MW (Da)[e]	pI[f]	no. of qualified peptides/ coverage (%)[g]	score[h]	gene symbol[i]	miRNA[j]
B1_750	0.035	1.7	gi/5031875	Lamin A/C isoform 2	65153	6.40	13/25	743	LMNA	
			gi/20127454	5-aminoimidazole-4-carboxamide ribonucleotide formyltransferase/IMP cyclohydrolase	65089	6.27	7/16.5	440	ATIC	
			gi/5803181	Stress induced phosphoprotein 1	63227	6.40	4/9	228	STIP1	
C1_751	0.023	1.73	gi/55960506	Chaperonin containing TCP1, subunit 3 (gamma)	58505	6.46	17/43	1043	CCT3	
			gi/4503377	Dihydropyrimidinase −like 2	62711	5.95	7/19	465	DPYSL2	
			gi/11863154	**Archain isoform 1**	57630	5.89	9/19	503	**ARCN1***	**mir-206**
			gi/189926	Phosphoglucomutase 1	61674	6.35	4/9	208	PGM1*	mir-30a, -30d
			gi/6009626	Brain carboxylesterase hBr1	47100	6.02	3/8	189	CES1	
D1_ 976	0.004	1.67	gi/5453603	Chaperonin containing TCP1, subunit 2	57794	6.01	17/50	1271	CCT2	
			gi/178390	Aldehyde dehydrogenase	56858	7.00	6/15	387	ALDH2	
			gi/2183299	Aldehyde dehydrogenase 1	55427	6.30	5/12	319	ALDH1	
			gi/5771523	3-phosphoglycerate dehydrogenase	57370	6.29	4/9	225	PHGDH	
E1_993	0.011	1.78	gi/16306550	Selenium binding protein 1	52928	5.93	13/37	711	SELENBP1	
F1_1021	0.008	2.01	gi/15620780	Glutamate carboxypeptidase	53161	5.71	3/7	143	CNDP2	
G1_1092	0.039	1.88	gi/5174529	Methionine adenosyltransferase II, alpha	43975	6.05	2/7	143	MAT2A*	mir-30a, -30d,-22
H1_1119	0.007	1.43	gi/4504169	Glutathione synthetase	52523	5.67	7/23	458	GSS	
			gi/1049219	Gamma-aminobutyraldehyde dehydrogenase	54410	6.01	5/11	306	E3	
			gi/21410323	Perilipin	56216	5.82	2/5	112	PLIN	
A2_1154	0.003	1.61	gi/21361144	Proteasome 26S ATPase subunit 3	49458	5.13	15/50	843	PSMC3	
			gi/340219	Vimentin	53738	5.03	4/9	273	VIM	
			gi/7106299	Ataxin 10	54196	5.12	4/4	241	ATXN10	
B2_1158	0.011	1.48	gi/4503571	Enolase 1	47481	7.01	13/46	906	ENOI	
			gi/40068518	Phosphogluconate dehydrogenase	53619	6.8	6/17	427	PGD	
C2_1173	0.003	1.87	gi/4503481	Eukaryotic translation elongation factor 1 gamma	50429	6.25	10/34	576	EEF1G	
			gi/496902	Translation initiation factor	47088	6.08	5/7	297	E2F1	
			gi/4504327	Mitochondrial trifunctional protein, beta subunit precursor	51547	9.45	4/9	207	HADHB*	mir-203
D2_1174	0.006	2.08	gi/5031699	Flotillin 1	47554	7.08	4/12	265	FLOT1	
E2_1182	0.002	2.01	gi/4502111	Annexin VII isoform 1	50569	6.25	9/24	526	ANXA7	
			gi/7546384	Chain A, Human branched- chain Alpha-Keto Acid Dehydrogenase	45770	6.32	4/11	213	BCKDHA	
			gi/4099506	ErbB3 binding protein EBP1	38321	7.15	4/15	211	PA2G4	
			gi/18379349	Vesicle amine transport protein 1	42122	5.88	2/8	121	VAT1	
F2_1202	0.012	1.85	gi/39725934	Serine (or cysteine) proteinase inhibitor, clade F member 1	46454	5.97	11/38	695	SERPINF1	
			gi/9836652	BSCv	47887	5.78	5/13	305	C20ORF3	
			gi/285975	Human rab GDI	51088	5.94	2/5	116	GDI	
			gi/515634	Ubiquinol-cytochrome C reductase core I protein	53270	5.94	2/4	122	UQCRC1	
			gi/338695	Beta-tubulin	50240	4.75	2/5	121	TUBB	
G2_1221	0.045	2.61	gi/4503529	Eukaryotic translation initiation factor 4A isoform 1	46353	5.32	8/27	487	EIF4A1	
H2_1268	0.013	1.6	gi/181914	DNA-binding protein	36086	9.20	2/7	122		
A3_1271	0.002	1.54	gi/33415057	Transformation-related protein 14	43248	5.49	5/19	309	TRG14	
B3_1272	0.010	1.99	gi/4557809	Ornithine aminotransferase precursor	48846	6.57	7/23	435	OAT	
			gi/387011	Pyruvate dehydrogenase E1-alpha precursor	47098	8.79	4/9	265	PDHA1*	mir-203
			gi/3641398	NADP-dependent isocitrate dehydrogenase	46944	6.34	2/7	86	IDH1*	mir-30a, -30d
C3_1299	0.004	1.81	gi/24308406	Secernin 2	46989	5.44	4/16	231	SCRN2	
			gi/6678271	TAR DNA binding protein	45053	5.85	2/7	162	TARDBP*	mir-137, -203
D3_1352	0.006	1.67		not identified						
E3_1410	0.023	1.59	gi/4557233	Acyl-Coenzyme A dehydrogenase, C-2 to C-3 short chain precursor	44611	8.13	8/30	436	ACADS	
			gi/148539872	Acetyl-Coenzyme A acetyltransferase 2	41783	6.47	2/8	99	ACAT2	
F3_1521	0.006	1.64	gi/7661704	Osteoglycin preprotein	34243	5.46	5/18	307	OGN*	mir-22

dx.doi.org/10.1021/pr300152z | J. Proteome Res. 2012, 11, 3358−3369

Table 3. continued

spot no.[a]	DIGE (*p*-value)[b]	DIGE obese/ control[c]	accession no.[d]	protein name	MW (Da)[e]	pI[f]	no. of qualified peptides/ coverage (%)[g]	score[h]	gene symbol[i]	miRNA[j]
			gi/25453472	Eukaryotic translation elongation factor 1delta	31217	4.90	4/17	277	EFF1D	
G3_1560	0.033	1.69	gi/194373515	Unnamed protein product (Corrisp. in Sprot a P68363 Tubulin alpha-1B chain)	33856	4.88	2/8	151	DNAJB2	
			gi/157833780	Chain A, human Annexin V with Proline substitution by thioproline	36041	4.94	3/11	153	ANXA5	
H3_1908	0.001	1.67	gi/24119203	Tropomyosin 3 isoform 2	29243	4.75	11/40	598	TPM3	
			gi/4507651	Tropomyosin 4	28619	4.67	2/9	104	TPM4	
			gi/13236577	Thiamine triphosphatase	25721	4.75	3/15	165	THTPA	
A4_1948	0.001	1.68	gi/5803225	Tyrosine 3/tryptophan 5-monooxygenase activation protein, epsilon polypeptide	29326	4.63	15/65	943	YWHAE	
B4_2005	0.001	1.91	gi/21464101	**Tyrosine 3-monooxygenase/tryptophan 5-monooxygenase activation protein, gamma polypeptide**	28456	4.80	5/21	329	**YWHAG***	**mir-141, -200c,**
			gi/119598039	Tropomyosin 1 (alpha), isoform Cra_m	28730	4.78	4/17	215	TPM1	
C4_2054	0.010	1.64	gi/4507953	**Tyrosine 3/tryptophan 5-monooxygenase activation protein, zeta polypeptide**	27899	4.73	9/52	629	**YWHAZ***	**mir-206,** -30a, -30d, -22
D4_2065	0.001	1.72	gi/4507949	Tyrosine 3/tryptophan 5-monooxygenase activation protein, beta polypeptide	28179	4.76	5/29	310	YWHAB	
			gi/4507951	Tyrosine 3/tryptophan 5-monooxygenase activation protein, eta polypeptide	28372	4.76	3/15	225	YWHAH	
E4_2087	0.038	1.7	gi/4504517	Heat shock protein beta-1	22826	5.98	6/27	330	HSPB1	
			gi/1922287	EnoylCoA hydratase	31807	8.34	5/23	330	ECHS1	
F4_ 2229	0.007	1.64	gi/4758984	**Ras-related protein Rab-11A**	24492	6.12	2/11	99	**RAB11A***	**mir-520e, -520d,**
G4_2245	0.039	1.51	gi/2204207	Glutathione S-transferase	23595	5.43	6/38	372	GSTP1	
			gi/1174149	Small GTP binding protein Rab 7	23732	6.40	2/12	101	RAB7A*	mir-30a, -30d
H4_2291	0.008	1.65	gi/14249382	Abhydrolase domain containing 14B	22446	5.94	5/32	264	ABHD14B	
A5_2312	>0.001	−2.12	gi/5020074	Glyoxalase-I	20934	5.24	3/16	166	GLO I	
			gi/17986273	Fast skeletal myosin alkali light chain 1 isoform 1f	21189	4.97	3/18	215	MYL1	
B5_2417	0.024	2.27		not identified						

[a]Spot numbering as shown in 2-DE gel in Figure 1. [b]*p*-value at Student's *t* test. [c]Average abundance ratio (obeses/controls) as calculated by DeCyder Analysis. [d]Protein accession number from NCBI. [e]Theoretical molecular weight (Da). [f]Theoretical p*I*. [g]According to the Proposed Guidelines for the Analysis and Documentation of Peptide and Protein Identifications (Paris consensus), we included in this table the complete figures of merit regarding the MS identification as the number of identified peptides whose individual ion score (as provided by Mascot) was higher than the designated confidence level (95%)/protein sequence coverage (%). [h]Identification score indicating a probabilistic measure of the goodness of the MS protein identification. [i]Gene symbol from NCBI. [j]Down-expressed miRNAs in at least 6/10 obese females, which targeted 3′UTR-mRNA regions of asterisk genes. In bold are indicated down-expressed miRNAs in VAT from 9 or 10/10 obese females and their targeted proteins.

have been involved in the regulation of a variety of biological processes, including appetite regulation, adipocyte differentiation, and insulin secretion,[13] are interesting candidate molecules to be investigated in adipose tissues as potential mediators of metabolic pathway alterations in obesity. We previously reported that miRNA expression was altered in SAT from morbidly obese patients, and that up-expressed miR-519d plays a role in adipocyte lipid metabolism.[10] We now describe the miRNA and proteome VAT signatures in morbidly obese females and show several miRNAs and proteins differentially expressed between obese and nonobese females.

Globally, our miRNA expression profile revealed that 71 miRNAs were deregulated in the VAT from obese females. Interestingly, most of these miRNAs (61/71) were down-expressed. This latter finding coincides with a report of a similar global down-expression of miRNAs in VAT from obese individuals with nonalcoholic steatohepatitis than those with nonalcoholic fatty liver disease that, moreover, was correlated with enhanced expression of inflammatory adipocytokines.[14] Eleven of the 61 largely down-expressed miRNAs in the VAT of our obese females were also found in the above report;[14] in particular, we previously reported 7/11 of these miRNAs (miR-200c, miR-519b, miR-206, miR-618, miR-30a, miR-181c, and miR-7) down-expressed in SAT from the same obese females.[10]

In a mouse model, Xie et al.[15] reported an inverse correlation of miRNA expression between adipogenesis and obesity.[15] In fact, they observed that up-expressed miRNAs during adipogenesis tended to be down-expressed in the mouse epididymal fat pads, and vice versa, and suggested that these changes could be linked to the chronic local inflammation environment in the fat mouse obese tissue. Lastly, Kloting et al.[7] reported that miR-198, one of our down-expressed miRNAs, was inversely correlated with omental adipocyte diameter during obesity.[7]

Our 2D-DIGE analysis showed that 172 protein spots were differentially expressed in VAT from obese vs nonobese females. Analysis of 33 of these protein spots, those with optimal features, led to the identification of 67 proteins because most spots were related to more than one protein. Our data confirm, and also integrate, proteomic data previously obtained in VAT.[3,16,17] In particular, we detected high levels of EIF4A1, CES1, SELENBP1, ALDH1, ALDH2, GSTP1, HSPB1 proteins that were previously reported to be increased in the omental vs

dx.doi.org/10.1021/pr300152z | J. Proteome Res. 2012, 11, 3358−3369

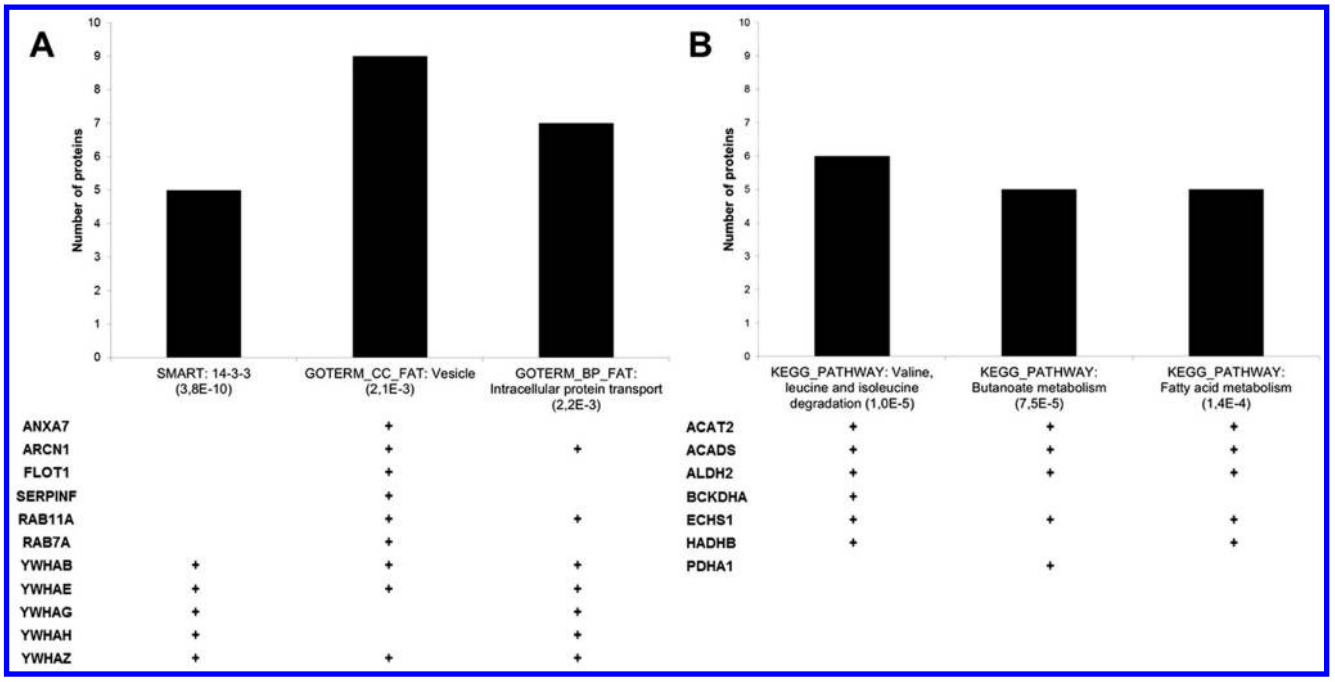

Figure 2. VAT proteins, overexpressed in obese females and identified by LC−MS/MS, were bioinformatically predicted by DAVID database to be functionally annotated in two main clusters: (A) annotation cluster 1 and (B) annotation cluster 2.

SAT in an obese population, or proteins that were differently expressed in VAT from obese vs nonobese females, such as ACADS, LMNA, VIM,[17] which indicates that VAT is not only a lipid storage site, but also a highly active metabolic tissue.[3] Furthermore, Pérez-Pérez et al.[3] suggested that EIF4A1 could be involved in the altered protein synthesis pathways preceding insulin resistance and/or type 2 diabetes.[3] In agreement with another study,[18] we detected high levels of E2F1, which could play a role in glucose metabolism.[18] We also identified proteins involved in intracellular trafficking, i.e., ARCN1 (or COPI), PLIN, RAB11A, and RAB14, in agreement with earlier reports.[19,20] Furthermore, we observed an up-expression of proteins involved in antioxidant activity and in apoptosis, namely, GSS, ANXA5, ANXA7, PRDX3, and GSTP1, some of which were reported by Córton et al.[16] in a proteomic study of VAT from obese females with or without polycystic ovary syndrome.[16]

A novelty of our study is that we evaluated simultaneously the miRNome and the proteome of VAT in obese and nonobese women to identify potential biological mechanisms, based on the concerted action of miRNA and protein targets, associated with obesity. To this aim, we intersected the list of the bioinformatically predicted protein targets of the deregulated miRNAs with the whole set of identified proteins from the experimental comparison of the VAT proteomes. This screening enabled us to identify in the obese VAT samples a potential miRNA-based mechanism for the up-expression of some proteins, in particular YWHAG and RAB11A, which was associated with down-expression of miR-141 and miR-520e, respectively. The functional luciferase assay confirmed the binding of these miRNAs to the 3′UTRs of the YWHAG and RAB11A transcripts. We investigated YWHAG and RAB11A because they are involved in glucose homeostasis,[21−23] and YWHAG also in lipid metabolism,[24,25] and hence are potential actors in the obese phenotype.

Rab proteins are a large family of small GTPases that are involved in vesicular trafficking, in cytoskeleton organization, and in the control of cell proliferation and differentiation.[20] Members of the Rab family, which includes about 70 proteins in humans, continuously cycle between the cytosol and different membranes as inactive GDP-bound or active GTP-bound forms, assisted by different Rab-associated proteins.[26] Defects in Rab-associated proteins lead to abnormal intracellular trafficking and have been associated with several monogenic inherited disorders and multigenic conditions such as type 2 diabetes.[26,27] Several Rab GTPases have been implicated in GLUT4 trafficking in relation to the cell type studied; among these, RAB10, RAB11, and RAB14 have been identified in adipocytes.[28] An additional player in GLUT4 trafficking is the GTPase-activating protein AS160. The latter, under basal conditions contributes to cytosolic retention of GLUT4, whereas, upon insulin stimulation, it is phosphorylated at Thr642 by AKT kinase and inactivated, so that AS160 dissociates from GLUT4 vesicles to favor an increase in the GTP-bound form of RAB. This event facilitates the transport of GLUT4 from storage vesicles toward cell surface.[21]

YWHAG (14-3-3γ) protein belongs to a seven-member protein family in mammals. These proteins, by interacting with target proteins, typically at phospho-residues, regulate a variety of functions, including subcellular redistribution.[22] Studies conducted in animal models and/or in cellular systems have shown that 14-3-3 plays a relevant role in both cellular insulin-mediated glucose transport and lipid metabolism. In fact, in mice, insulin-stimulated YWHAG binding to AS160 at phospho-Thr649 (equivalent to Thr642 in human AS160) normally regulates GLUT4 trafficking from storage vesicles to plasma membrane, thereby influencing glucose uptake.[23] AS160-Thr649Ala knock-in mice (Ala: nonphosphorylable residue) display impaired glucosal and insulin sensitivity.[23] Furthermore, in 3T3-L1 adipocytes, the up-expression of 14-3-3 promotes the cytoplasmic localization of Lipin1, a bifunctional protein involved in lipid metabolism.[24] The subcellular localization of this protein is relevant to its activities; in fact, its nuclear isoform promotes the activation

dx.doi.org/10.1021/pr300152z | J. Proteome Res. 2012, 11, 3358−3369

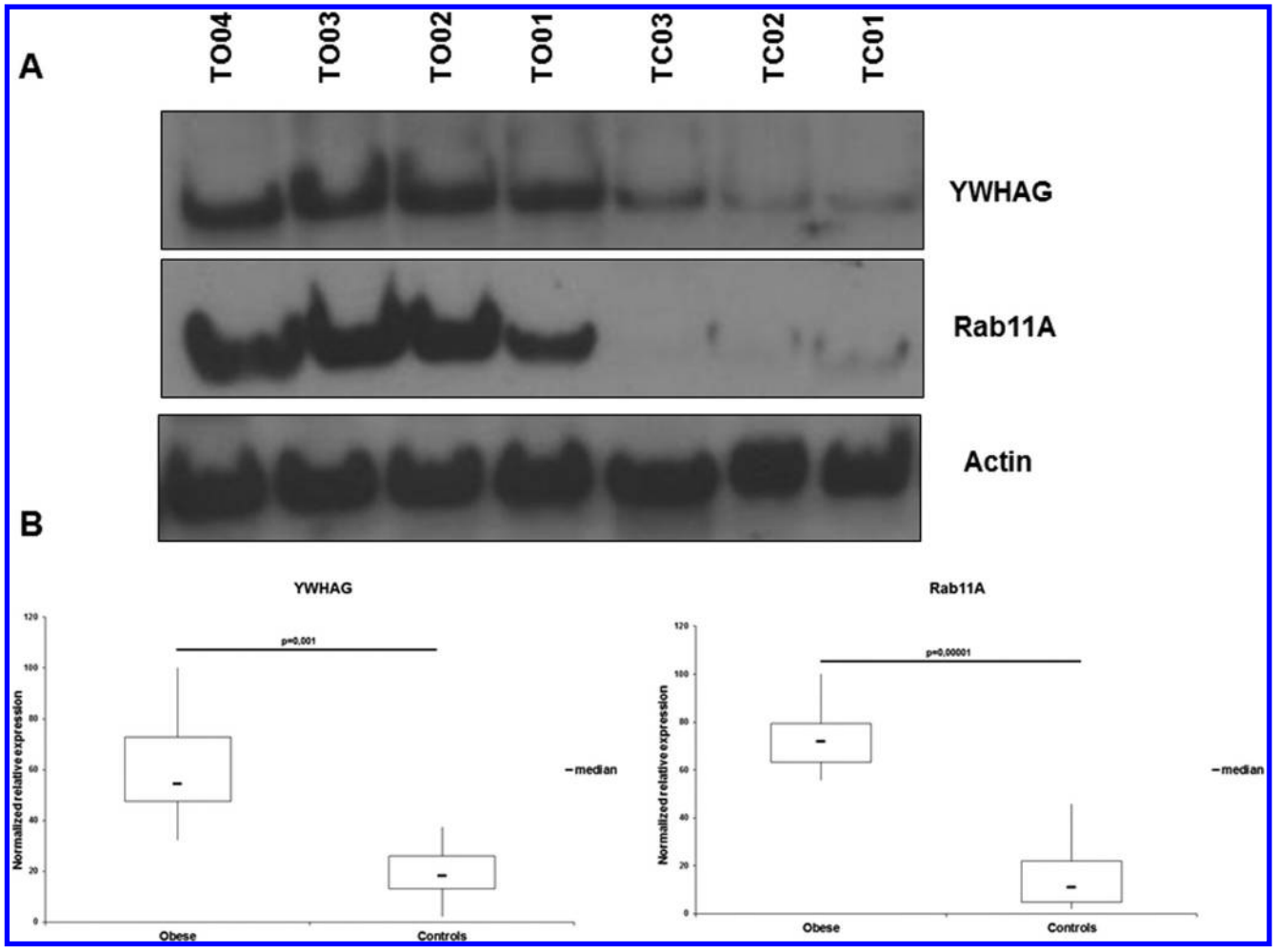

Figure 3. (A) An example of the Western blot evaluation of YWHAG and RAB11A proteins from VAT of randomly selected obese females (TO01, TO02, TO03, TO04) and controls (TC01, TC02, TC03). (B) The box plots of the data normalized to actin content, after densitometric analysis of YWHAG and RAB11A immunoblots. The data are expressed as percent relative expression, the sample with the highest expression of either RAB11A (p = 0.00001) or YWHAG (p = 0.001) having been set as 100%. The bottom and top of each box represent the 25th and 75th percentile, respectively; the thick band inside each box shows the 50th percentile (the median). The ends of the whiskers represent the minimum and maximum values of each group of data.

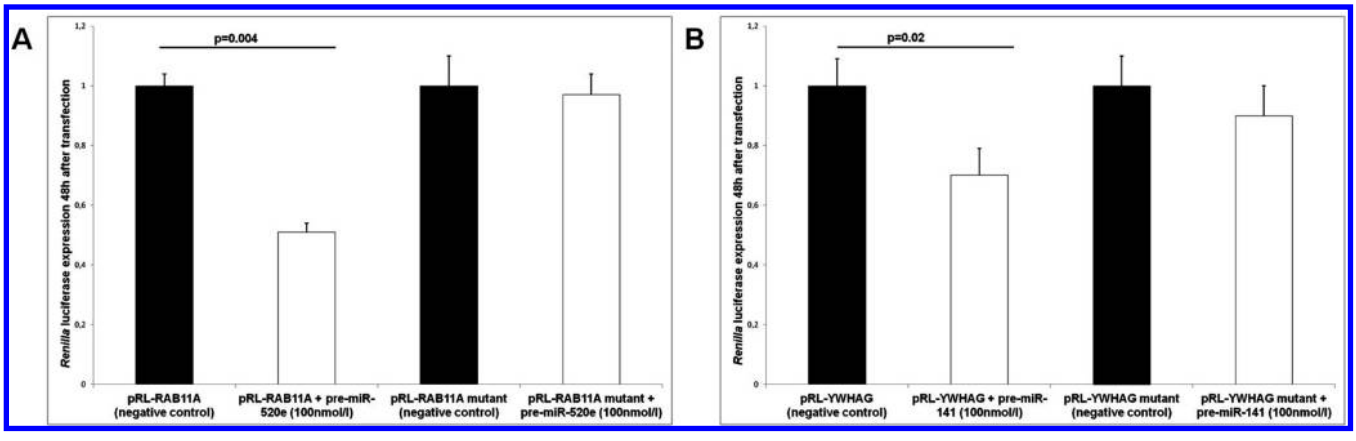

Figure 4. Validation of interaction between miR-520e and miR-141 with respectively wild-type or mutant 3′UTR of RAB11A or YWHAG. HEK-293 cells were transfected with wild-type or mutant 3′UTR of RAB11A, pGL3-control, pre-miR-520e, or pre-miR-negative control (A) and with wild-type or mutant 3′UTR of YWHAG, pGL3-control, pre-miR-141, or pre-miR-negative control (B). Pre-miR-520e and the pre-miR-141 significantly inhibited the expression of a *Renilla* luciferase-expressing construct that contains the 3′UTR region of the RAB11A (p = 0.004) and YWHAG (p = 0.02), respectively. No inhibition was observed in mutant 3′UTR of RAB11A (A) and YWHAG (B) constructs. All experiments were done in triplicate. Error bars denote SEM.

of genes involved in oxidative metabolism. In the cytosol, its insulin-mediated phosphorylation leads to the conversion of phosphatidate (PA) to diacylglycerol (DAG), a precursor of triacylglycerol (TAG).[25]

dx.doi.org/10.1021/pr300152z | J. Proteome Res. 2012, 11, 3358−3369

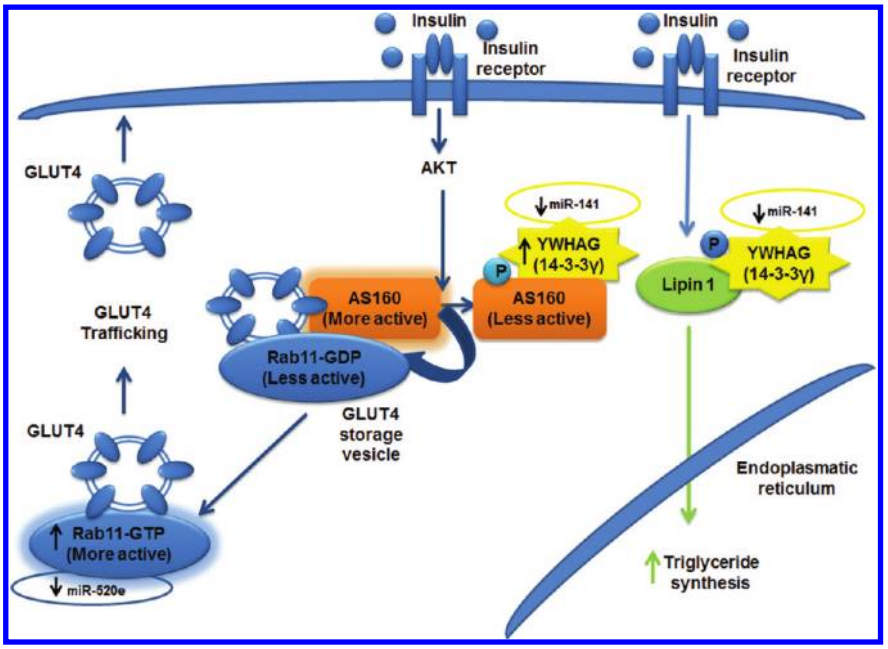

Figure 5. Proposed model of visceral adipose tissue (VAT) accumulation based on miR-141/YWHAG and miR-520e/RAB11A interaction. Under basal conditions, the Akt substrate of 160 kDa (AS160) binds RAB11-bound guanosine diphosphate (GDP) that retains glucose transporter protein (GLUT4) vesicles in the cytosol. After insulin stimulation, Akt phosphorylates AS160 that binds YWHAG (14-3-3γ) and catalyzes the phosphorylation of RAB11-GDP in RAB11-bound guanosine triphosphate (GTP). This process results in GLUT4 translocation toward the cell surface. In response to insulin, lipin1 is phosphorylated and interacts with YWHAG (14-3-3γ). The interaction between these two proteins induces increased synthesis of triglycerides in the endoplasmic reticulum. The figure also shows the down-expressed miRNAs that target RAB11A and YWHAG (14-3-3γ).

On the basis of above-mentioned mechanisms, we hypothesize (Figure 5) that in VAT from obese subjects, low expression levels of some miRNAs, including miR-520e and miR-141, by modulating the up-expression of RAB11A and YWHAG proteins, respectively, may lead to increased glucose uptake and to increased triglyceride synthesis. This could then contribute to worsening the obese phenotype by increasing the accumulation of adipose tissue. Obviously, the analysis of suitable cellular systems is required to provide mechanistic details for the proposed model and clarify the role of insulin as an independent, or co-operative model, linked to the observed miRNA down-expression and protein target up-expression in obesity.

Furthermore, studies on larger cohorts of obese and nonobese subjects are necessary to verify our results on the expression of miR-520e and miR-141, as well as of YWHAG and RAB11A proteins, in obesity risk assessment.

Lastly, we did not study the 72/365 miRNAs that were expressed only in VAT from obese females. Further investigations are necessary to test if these miRNAs may play a role in obesity insurgence and/or in the metabolic-associated alterations.

In conclusion, our study provides an integrated view of both miRNAs and protein expression profiles in VAT during obesity and gives clues as to the metabolic pathways that may be involved in adipose tissue accumulation.

■ ASSOCIATED CONTENT

Supporting Information

Figure S1: Main bioinformatically predicted pathways that are deregulated by miRNAs in VAT from obese females. Putative target genes of deregulated miRNAs in VAT from obese patients were sorted into pathways using the Kegg database. In parentheses are the number of genes targeted by miRNAs. Table S1: The sequences and charge states of each peptide used for identification of the proteins by LC−MS/MS. This material is available free of charge via the Internet at http://pubs.acs.org.

■ AUTHOR INFORMATION

Corresponding Author

*Fax: 0039-081-7462404. Tel.: 0039-081-7463541. E-mail: sacchett@unina.it.

Notes

The authors declare no competing financial interest.

■ ACKNOWLEDGMENTS

The present work was supported by grants from CEINGE Regione Campania (DGRC 1901/2009) and by MIUR-PRIN 2008. We thank the Genomics for Applied Research Consortium (GEAR) for granting full access to the 2D-DIGE platform. We thank Jean Ann Gilder (Scientific Communication srl) for revising and editing the manuscript. We thank Piero Pucci's group at the Proteomic Facility of CEINGE−Biotecnologies Avanzate for support and guidance in the production and interpretation of LC−MS/MS data.

■ REFERENCES

(1) Maury, E.; Brichard, S. M. Adipokine dysregulation, adipose tissue inflammation and metabolic syndrome. *Mol. Cell. Endocrinol.* **2010**, *314* (1), 1−16.

(2) Gesta, S.; Blüher, M.; Yamamoto, Y.; Norris, A. W.; Berndt, J.; Kralisch, S.; Boucher, J.; Lewis, C.; Kahn, C. R. Evidence for a role of developmental genes in the origin of obesity and body fat distribution. *Proc. Natl. Acad. Sci. U. S. A.* **2006**, *103* (17), 6676−6681.

(3) Pérez-Pérez, R.; Ortega-Delgado, F. J.; García-Santos, E.; López, J. A.; Camafeita, E.; Ricart, W.; Fernández-Real, J. M.; Peral, B. Differential proteomics of omental and subcutaneous adipose tissue

reflects their unalike biochemical and metabolic properties. *J. Proteome Res.* **2009**, *8* (4), 1682−1693.
(4) Ibrahim, M. M. Subcutaneous and visceral adipose tissue: structural and functional differences. *Obes. Rev.* **2010**, *11* (1), 11−18.
(5) Linder, K.; Arner, P.; Flores-Morales, A.; Tollet-Egnell, P.; Norstedt, G. Differentially expressed genes in visceral or subcutaneous adipose tissue of obese men and females. *J. Lipid Res.* **2004**, *45* (1), 148−154.
(6) van Beek, E. A.; Bakker, A. H.; Kruyt, P. M.; Hofker, M. H.; Saris, W. H.; Keijer, J. Intra- and interindividual variation in gene expression in human adipose tissue. *Pfluegers Arch.* **2007**, *453* (6), 851−861.
(7) Klöting, N.; Berthold, S.; Kovacs, P.; Schön, M. R.; Fasshauer, M.; Ruschke, K.; Stumvoll, M.; Blüher, M. MicroRNA expression in human omental and subcutaneous adipose tissue. *PLoS One* **2009**, *4* (3), e4699.
(8) Krol, J.; Loedige, I.; Filipowicz, W. The widespread regulation of microRNA biogenesis, function and decay. *Nat. Rev. Genet.* **2010**, *11* (9), 597−610.
(9) Ortega, F. J.; Moreno-Navarrete, J. M.; Pardo, G.; Sabater, M.; Hummel, M.; Ferrer, A.; Rodriguez-Hermosa, J. I.; Ruiz, B.; Ricart, W.; Peral, B.; Fernández-Real, J. M. MiRNA expression profile of human subcutaneous adipose and during adipocyte differentiation. *PLoS One* **2010**, *5* (2), e9022.
(10) Martinelli, R.; Nardelli, C.; Pilone, V.; Buonomo, T.; Liguori, R.; Castanò, I.; Buono, P.; Masone, S.; Persico, G.; Forestieri, P.; Pastore, L.; Sacchetti, L. miR-519d overexpression is associated with human obesity. *Obesity* **2010**, *18* (11), 2170−2176.
(11) Huang, D. W.; Sherman, B. T.; Lempicki, R. A. Systematic and integrative analysis of large gene lists using DAVID Bioinformatics Resources. *Nat. Protoc.* **2009**, *4* (1), 44−57.
(12) Huang, D. W.; Sherman, B. T.; Lempicki, R. A. Bioinformatics enrichment tools: paths toward the comprehensive functional analysis of large gene lists. *Nucleic Acids Res.* **2009**, *37* (1), 1−13.
(13) Heneghan, H. M.; Miller, N.; Kerin, M. J. Role of microRNAs in obesity and the metabolic syndrome. *Obes. Rev.* **2010**, *11* (5), 354−361.
(14) Estep, M.; Armistead, D.; Hossain, N.; Elarainy, H.; Goodman, Z.; Baranova, A.; Chandhoke, V.; Younossi, Z. M. Differential expression of miRNAs in the visceral adipose tissue of patients with non-alcoholic fatty liver disease. *Aliment. Pharmacol. Ther.* **2010**, *32* (3), 487−497.
(15) Xie, H.; Lim, B.; Lodish, H. F. MicroRNAs induced during adipogenesis that accelerate fat cell development are downregulated in obesity. *Diabetes* **2009**, *58* (5), 1050−1057.
(16) Cortón, M.; Botella-Carretero, J. I.; López, J. A.; Camafeita, E.; San Millán, J. L.; Escobar-Morreale, H. F.; Peral, B. Proteomic analysis of human omental adipose tissue in the polycystic ovary syndrome using two-dimensional difference gel electrophoresis and mass spectrometry. *Hum. Reprod.* **2008**, *23* (3), 651−661.
(17) Pérez-Pérez, R.; García-Santos, E.; Ortega-Delgado, F. J.; López, J. A.; Camafeita, E.; Ricart, W.; Fernández-Real, J. M.; Peral, B. Attenuated metabolism is a hallmark of obesity as revealed by comparative proteomic analysis of human omental adipose tissue. *J. Proteomics* **2012**, *75* (3), 783−795.
(18) Fajas, L.; Blanchet, E.; Annicotte, J. S. The CDK4-pRB-E2F1 pathway: A new modulator of insulin secretion. *Islets* **2010**, *2* (1), 51−53.
(19) Beller, M.; Thiel, K.; Thul, P. J.; Jäckle, H. Lipid droplets: a dynamic organelle moves into focus. *FEBS Lett.* **2010**, *584* (11), 2176−2182.
(20) Stenmark, H. Rab GTPases as coordinators of vesicle traffic. *Nat. Rev. Mol. Cell Biol.* **2009**, *10* (8), 513−525.
(21) Cartee, G. D.; Funai, K. Exercise and insulin: Convergence or divergence at AS160 and TBC1D1? *Exercise Sport Sci. Rev.* **2009**, *37* (4), 188−195.
(22) Ramm, G.; Larance, M.; Guilhaus, M.; James, D. E. A role for 14-3-3 in insulin-stimulated GLUT4 translocation through its interaction with the RabGAP AS160. *J. Biol. Chem.* **2006**, *281* (39), 29174−29180.
(23) Chen, S.; Wasserman, D. H.; MacKintosh, C.; Sakamoto, K. Mice with AS160/TBC1D4-Thr649Ala knockin mutation are glucose intolerant with reduced insulin sensitivity and altered GLUT4 trafficking. *Cell Metab.* **2011**, *13* (1), 68−79.
(24) Péterfy, M.; Harris, T. E.; Fujita, N.; Reue, K. Insulin-stimulated interaction with 14-3-3 promotes cytoplasmic localization of lipin-1 in adipocytes. *J. Biol. Chem.* **2010**, *285* (6), 3857−3864.
(25) Reue, K.; Brindley, D. N. Thematic Review Series: Glycerolipids. Multiple roles for lipins/phosphatidate phosphatase enzymes in lipid metabolism. *J. Lipid Res.* **2008**, *49* (12), 2493−2503.
(26) Mitra, S.; Cheng, K. W.; Mills, G. B. Rab GTPases implicated in inherited and acquired disorders. *Semin. Cell Dev. Biol.* **2011**, *22* (1), 57−68.
(27) Kaddai, V.; Gonzalez, T.; Keslair, F.; Grémeaux, T.; Bonnafous, S.; Gugenheim, J.; Tran, A.; Gual, P.; Le Marchand-Brustel, Y.; Cormont, M. Rab4b is a small GTPase involved in the control of the glucose transporter GLUT4 localization in adipocyte. *PLoS One* **2009**, *4* (4), e5257.
(28) Larance, M.; Ramm, G.; Stöckli, J.; van Dam, E. M.; Winata, S.; Wasinger, V.; Simpson, F.; Graham, M.; Junutula, J. R.; Guilhaus, M.; James, D. E. Characterization of the role of the Rab GTPase-activating protein AS160 in insulin-regulated GLUT4 trafficking. *J. Biol. Chem.* **2005**, *280* (45), 37803−37813.

OPEN ACCESS Freely available online

PLoS one

Glucokinase (GCK) Mutations and Their Characterization in MODY2 Children of Southern Italy

Marina Capuano[1,2☯], Carmen Maria Garcia-Herrero[3,4☯], Nadia Tinto[1,2], Carla Carluccio[2,5], Valentina Capobianco[6], Iolanda Coto[1,2], Arturo Cola[1,2], Dario Iafusco[7], Adriana Franzese[8], Adriana Zagari[2,5], Maria Angeles Navas[3,4], Lucia Sacchetti[1,2]*

1 Department of Biochemistry and Medical Biotechnology, University of Naples "Federico II", Naples, Italy, **2** Centro di Ingegneria Genetica (CEINGE) Advanced Biotechnology, s. c. a r. l., Naples, Italy, **3** Department of Biochemistry and Molecular Biology III, Faculty of Medicine, Complutense University of Madrid, Madrid, Spain, **4** Centro de Investigación Biomédica en Red de Diabetes y Enfermedades Metabólicas Asociadas (CIBERDEM), Barcelona, Spain, **5** Department of Biological Science, University of Naples "Federico II", Naples, Italy, **6** Fondazione SDN-IRCSS (Istituto di Diagnostica Nucleare-Istituto di Ricerca e Cura a Carattere Scientifico), Naples, Italy, **7** Department of Pediatrics, Second University of Naples, Naples, Italy, **8** Department of Pediatrics, University of Naples "Federico II", Naples, Italy

Abstract

Type 2 Maturity Onset Diabetes of the Young (MODY2) is a monogenic autosomal disease characterized by a primary defect in insulin secretion and hyperglycemia. It results from GCK gene mutations that impair enzyme activity. Between 2006 and 2010, we investigated GCK mutations in 66 diabetic children from southern Italy with suspected MODY2. Denaturing High Performance Liquid Chromatography (DHPLC) and sequence analysis revealed 19 GCK mutations in 28 children, six of which were novel: p.Glu40Asp, p.Val154Leu, p.Arg447Glyfs, p.Lys458_Cys461del, p.Glu395_Arg397del and c.580-2A>T. We evaluated the effect of these 19 mutations using bioinformatic tools such as Polymorphism Phenotyping (Polyphen), Sorting Intolerant From Tolerant (SIFT) and *in silico* modelling. We also conducted a functional study to evaluate the pathogenic significance of seven mutations that are among the most severe mutations found in our population, and have never been characterized: p.Glu70Asp, p.His137Asp, p.Phe150Tyr, p.Val154Leu, p.Gly162Asp, p.Arg303Trp and p.Arg392Ser. These seven mutations, by altering one or more kinetic parameters, reduced enzyme catalytic activity by >40%. All mutations except p.Glu70Asp displayed thermal-instability, indeed >50% of enzyme activity was lost at 50°C/30 min. Thus, these seven mutations play a pathogenic role in MODY2 insurgence. In conclusion, this report revealed six novel GCK mutations and sheds some light on the structure-function relationship of human GCK mutations and MODY2.

Citation: Capuano M, Garcia-Herrero CM, Tinto N, Carluccio C, Capobianco V, et al. (2012) Glucokinase (GCK) Mutations and Their Characterization in MODY2 Children of Southern Italy. PLoS ONE 7(6): e38906. doi:10.1371/journal.pone.0038906

Editor: Pal Bela Szecsi, Lund University Hospital, Sweden

Received March 12, 2012; **Accepted** May 14, 2012; **Published** June 20, 2012

Funding: Work was supported by grants from: CEINGE-Regione Campania, Italy (DGRC 1901/2009), the Instituto de Salud Carlos III, Spain (PI1000424) and the Dirección General de Universidades e investigación de la Consejería de Educación de la Comunidad de Madrid-Universidad Complutense de Madrid, Spain (CCG10-UCM/BIO-4728). C.M. García-Herrero was supported by a predoctoral FPU fellowship from the Ministerio de Ciencia e Innovación of Spain. The funders had no role in study design, data collection and analysis, decision to publish, or preparation of the manuscript.

Competing Interests: The authors have declared that no competing interests exist.

* E-mail: sacchett@unina.it

☯ These authors contributed equally to this work.

Introduction

Maturity Onset Diabetes of the Young (MODY), a monogenic diabetes inherited in an autosomal dominant mode, accounts for 1–2% of all diabetes forms in Europe [1,2]. It is a clinically heterogeneous group of diseases caused by at least eight gene defects in the pancreatic β-cell that impair insulin secretion [3]. MODY is characterized by onset before 25 years of age; patients usually lack auto-antibodies, and clinical manifestations go from slight non-ketotic hyperglycemia to severe complicated hyperglycemia [4]. Heterozygous mutations in the *glucokinase* (*GCK*) gene produce two distinct diseases, MODY type 2 (MODY2) (MIM:125851) and persistent hyperinsulinemia of infancy (MIM:601820) [5,6]. Persistent hyperinsulinemia of infancy is associated with hyperactive GCK variants, while MODY2 is associated with GCK mutations that impair its activity [7]. GCK (hexokinase IV) catalyzes the ATP-dependent phosphorylation of glucose in the first, rate-limiting step of glycolysis in pancreatic β-cells [1]. The crystal structure determination of the enzyme by Kamata et al. [8] revealed that the enzyme exists in at least two distinct forms, the super-open ligand-free form and the closed active form that is bound to glucose and ATP. The molecule consists of two domains, namely a small and large domain separated by the glucose site. In detail, amino acid residues 1–64 and 206–439 belong to the large domain, amino acid residues 72–201 and 445–465 to the small domain, and amino acid residues 65–71, 202–205 and 440–444 to the three loops connecting the domains [8]. The GCK protein switches from an inactive conformation to a close active conformation upon ligand binding. A huge conformational transition occurs through a large rotation of the small domain [8].

The heterozygous loss-of-function GCK mutations causative of MODY2 diabetes include missense, nonsense, splicing, small deletions/insertions/duplications variants, and result in stable fasting hyperglycemia from birth (>5.5 mol/L) and rare microvascular complications [1]. Over 644 *GCK* mutations have been

described, and a study of the mutational mechanisms for a number of these has shed light on GCK regulation [9].

The molecular diagnosis of MODY2 is important: to classify the type of diabetes correctly, to predict prognosis, and to initiate screening of family members [1]. It is particularly important to identify MODY2 in diabetic pregnant patients in order to start "ad hoc" treatment [10]. However, the identification of *GCK* mutations by molecular analysis will not always reveal whether a variant is really pathogenic or how serious the diabetic phenotype could be. Therefore, in this five-year study, we applied an integrated approach to investigate the effect of *GCK* mutations in the diabetic phenotype in children from southern Italy. First, we used DHPLC and mutation sequencing to identify variants, then a computational approach to predict the effect of the variants identified, and finally a functional study to determine the effect of seven candidate variants on enzyme activity and on enzyme thermo-stability.

Results

Among the 66 enrolled patients with suspected MODY2, 28/66 were diagnosed as MODY2 based on mutations in the *GCK* gene (MODY2+) and 38/66 were MODY2-negative (MODY2−). All mutated patients were unrelated, except two pairs of siblings (patient identification: MD19/20: two sisters and MD69/70: brother/sister). The mean age at diagnosis (± Standard Deviation: SD) was lower, albeit not significantly, in MODY2+ than in MODY2− patients (105±45 months vs 113±45 months). Mean triglyceride levels did not differ between the two groups (0.6±0.2 and 0.7±0.3 mmol/L, respectively). Mean Fasting Plasma Glucose (FPG) and glycosylated hemoglobin (HbA1c) concentrations were significantly higher ($p<0.003$ and $p<0.001$, respectively) in MODY2+ than in MODY2− patients (6.7±0.8 mmol/L and 6.2±0.3% vs 6.1±0.7 mmol/L and 5.5±0.5%, respectively). The Body Mass Index zeta-score (BMIz-score) of enrolled children at first admission was always in the reference range for the children's age (reference range: −1.5/+1.5), except in one patient (BMIz-score: 2.5). Two/28 MODY2+ patients were positive for only one type-1 diabetes auto antibody (glutamate decarboxylase: 8 and 18 U/mL). The patients were untreated until diagnosis.

Identification of *GCK* Mutations

We identified 19 different *GCK* mutations in 28/66 patients (Table 1). Six of them were novel: two missense mutations (p.Val154Leu and p.Glu40Asp), one splice site variant (c.580-2A>T) and three deletions (p.Lys458_Cys461del, p.Arg447Glyfs, and p.Glu395_Arg397del). We also found 13 previously reported mutations: 11 missense mutations (p.Arg303Trp, p.Gly261Arg, p.Phe150Tyr, p.Ala259Thr, p.Glu70Asp, p.Lys420Glu, p.Ala188Thr, p.Tyr289Cys, p.Asp278Glu, p.Gly223Ser, and p.Ala449Thr) and two splice site variants (c.864-1G>A and c.1019+5G>A). All the detected mutations were always present in the children's mother or father and were absent from 200 chromosomes of our euglycemic controls. Seven mutations were each present in two unrelated families: p.Arg303Trp, p.Lys458_Cys461del, p.Arg447Glyfs, p.Gly261Arg, p.Phe150Tyr, p.Lys420Glu and p.Ala259Thr, the latter was also identified in two siblings. The splice variant c.580-2A>T was present in two siblings. Table 1 shows, for each mutation (except the three splice variants c.864-1G>A, c.580-2A>T and c.1019+5G>A, the frameshift mutation p.Arg447Glyfs and the p.Lys458_Cys461del), the nucleotide position, the amino acid change (if present), the effect on the protein predicted by bioinformatics.

Bioinformatics Study of the GCK Variants

All substitutions, except p.Val154Leu and p.Glu40Asp, were predicted to be deleterious mutations by online prediction tools (Table 1, column 4). Overall, the theoretical structural models of the mutants we obtained *in silico* (Table 1, column 5), preserve the overall protein fold. In detail, however, all mutations produced local conformational alterations − in some cases, such as p.Gly162Asp, dramatic perturbations – that well account for the functional alterations we found (Table 2). **p.Arg303Trp**-Arg303 is a highly conserved residue located in the α8 helix within the large domain. Mutation p.Arg303Trp disrupts two salt-bridges between the side chain of Arg303 and the side chain of Glu300, located in the same helix. These salt-bridges may be essential for the stability of the helix and their loss could destabilize the helix structure. **p.Val154Leu**-The p.Val154Leu mutation (Figure 1) does not cause any significant change in the local structure. Indeed, Val154 is located in the β-sheet that encompasses the small domain hydrophobic core. Its substitution with a leucine residue does not affect the hydrophobic interactions. Nevertheless, Val154 is involved in the large conformational variation from the super-open to close form upon glucose binding (Figure 1A). **p.Gly261Arg**-Gly261 is located in the loop connecting the β-sheet and the α6 helix in the large domain. p.Gly261Arg is a dramatic mutation because the small, flexible hydrophobic Gly residue is replaced by a very large Arg residue that bears a positive net charge. This substitution causes a local re-arrangement that involves the nearby residues such as Leu266 and Leu270. This process results in destabilization of the local structure.

p.Phe150Tyr-Phe150 is a highly conserved residue located in the β-sheet that encompasses the small domain hydrophobic core. The p.Phe150Tyr mutation (Figure 1B, C) introduces a polar residue inside the hydrophobic core in a region rich in phenylalanine. This replacement can influence the stability of the β-sheet thereby altering the structure of the domain. **p.Ala259Thr-**Ala259 residue is located in the large domain near the glucose-binding cleft. Introduction of a larger and polar side chain of threonine in the p.Ala259Thr mutant could influence the hydrogen bond network in that area. In fact, Thr259 can compete with other residues in the formation of hydrogen bonds with two water molecules. See our previous study for a description of the **p.Glu70Asp** variant [11]. **p.Lys420Glu-**Mutation p.Lys420Glu involves an inversion from a positively charged lysine to a negatively charged glutamic acid. The substitution affects the interaction of Lys420 with surrounding residues. Indeed, Lys420 is located in the α12 helix (Figure S1) in the large domain and forms a salt bridge with Glu440 located in a connecting loop between the two domains. The loss of this bond, caused by the mutation, could destabilize the region. **p.Ala188Thr-**The p.Ala188Thr mutation alters a highly conserved amino acid. Ala188 is located in the α4 helix within the small domain. The mutation leads to the substitution of a hydrophobic residue, alanine, with a polar residue, tyrosine, on the hydrophobic side of an amphipathic helix. Thr188 can form hydrogen bonds through the hydroxyl group with the side chains of the Ser127 and Asp124 residues on the α3 helix that is on the surface of the enzyme. The introduction of the threonine can cause a different arrangement of such side chain. **p.Tyr289Cys-**Tyr289 is located in the α7 helix in the large domain. The substitution of the bulk tyrosine in position 289 with the smaller cysteine side chain leads to the formation of a cavity. The mutant disrupts a favorable interaction between Tyr289 and Met381 of the α11 helix that may be important to keep helices together. It is noteworthy that, in our model, Cys289 is not bound to the nearby Cys230 because the distance (4.1 Å) between the two sulfur atoms too long for a disulfide bond formation. **p.As-**

Table 1. GCK mutations detected in MODY2 children from South Italy.

Patient code	GCK Exon[a]	cDNA mutation[b]	Polyphen/SIFT prediction[c]	Aminoacid change[d]/Domain localization/Secondary structure	Effect on protein 3D-structure	Reference
MD01/92	8	c.907C>T	1/deleterious	p.Arg303Trp/Large domain/α8 helix	Disruption of two salt-bridges	[25]
MD05/71	10	c.1373_1385del		p.Lys458_Cys461del/Small domain/ α13 helix		NOVEL
MD10	4	c.460G>T	2/tolerated	p.Val154Leu/Small domain/β-strand 6	Severe perturbation during the transition from the super-open to closed form. Mild local structural alteration	NOVEL
MD12/89	10	c.1339delC		p.Arg447Glyfs/Small domain/α13 helix		NOVEL
MD16/75	7	c.781G>T	1/deleterious	p.Gly261Arg/Large domain/loop	Replacement of a small and flexible hydrophobic residue with a large positive residue	[26]
MD18/94	4	c.449T>A	1/deleterious	p.Phe150Tyr/Small domain/β-strand 5	Introduction of a polar residue in the hydrophobic core. Perturbation of the β-sheet	[27]
MD19[e]/20[e]/79	7	c.775G>A	3/deleterious	p.Ala259Thr/Large domain/loop	Influence on the hydrogen bond network near the glucose-binding cleft	[28]
MD25	2	c.210A>C	1/deleterious	p.Glu70Asp/Connection/Loop spatially near α13 helix	Weakness of salt bridge interaction with K458 (α13 helix)	[11]
MD26/65	10	c.1258A>G	2/deleterious	p.Lys420Glu/Large domain/α12 helix	Loss of a salt bridge between K420 and E440	[29]
MD38	Intron 7	c.864-1G>A		IVS7-1G>A		[9]
MD57	5	c.562G>A	1/deleterious	p.Ala188Thr/Small domain/α4 helix	Substitution of a hydrophobic residue with a polar residue	[30]
MD59	8	c.866A>G	1/deleterious	p.Tyr289Cys/Large domain/α7 helix	Disruption of a favorable interaction between Y289 and M381	[9]
MD68	7	c.834G>A	1/deleterious	p.Asp278Glu/Large domain/α6 helix	Mild structural alteration	[9]
MD69[e]/70 [e]	Intron 5	c.580-2A>T		IVS5-2A>T		NOVEL
MD80	6	c.667G>A	3/deleterious	p.Gly223Ser/Large domain/β-strand 9	Perturbation of the β-strand	[31]
MD86	Intron 8	c.1019+5G>A		IVS8+5G>A		[27]
MD90	2	c.120G>C	2/tolerated	p.Glu40Asp/Large domain/α2 helix	Mild structural alteration	NOVEL
MD91	10	c.1345G>C	3/deleterious	p.Ala449Thr/Small domain in the closed form/α13 helix	Introduction of a larger and polar side chain	[9]
MD95	9	c.1182_1191del		p.Glu395_Arg397del/Large domain/ last residue of α11 helix and following loop	Destabilization of the C-terminal region of the helix and shortening of loop	NOVEL

[a]GenBank: accession number (AH005826). [b]The reference cDNA sequence was obtained from GenBank (NM_000162) and +1 corresponds to the A of the ATG translation initiation codon. [c]Polyphen prediction: probably damaging (1), benign (2), possibly damaging (3). SIFT score: <0.05 deleterious variant, ≥0.05 tolerated variant. [d]Swissprot accession number: P35557. [e]Sibling pairs (MD19/20: two sisters; MD69/70: brother/sister).
doi:10.1371/journal.pone.0038906.t001

p278Glu-The p.Asp278Glu mutation affects a highly conserved amino acid. Asp278 is located on the polar side of the α6 helix in the large domain. The replacement of Asp with a Glu residue in the mutant does not seem to cause significant changes in the enzyme structure. **p.Gly223Ser-**Gly223 is a highly conserved residue located in the β-sheet of the large domain hydrophobic core. The substitution with a serine involves the serine side-chain hydrogen bonding to Cys 233, close to Gly223 in the structure of GCK and could perturb the β-strand. **p.Glu40Asp-**The pGlu40Asp mutation substitutes a conserved glutamate residue with aspartate. Glu40 is located on the polar side of the α2 helix in the large domain. These amino acids are acidic residues but the side chain of the aspartate is shorter than the side chain of the glutamate. Nevertheless, the mutation does not seem to cause significant changes in the structure of the enzyme. **p.Ala449Thr-**Ala449 is a highly conserved residue located on the C-terminal α13 helix. This helix is part of the small domain in the closed form, but it lies between the two domains in the super-open form. In the closed form, the small domain has a three-layer architecture and the α13 helix is in the inner layer. At the domain interface, the α13 helix makes favorable interactions with the α5 helix of the large domain. Because the conformational features of this region are essential for the super-open (inactive form)/closed (active form) conversion, the introduction of a larger and polar side chain of the threonine in the p.Ala449Thr mutant could influence the enzymatic activity and/or stability. **p.Glu395_Arg397del–**The p.Glu395_Arg397 deletion causes the elimination of the last residue, Glu395, of the α11 helix in the large domain and two residues of the following loop, Ser396 and Arg397. In the wild-type enzyme, Glu395 is involved, through the backbone N atom, in the formation of a hydrogen bond of the α11 helix. Its deletion in the mutant causes the lack of this bond and could destabilize the C-terminal region of the helix. Moreover, also the backbone N atom of Arg397 interacts with an oxygen atom of Arg394 thereby

Table 2. Kinetic constants of human recombinant wild type-GCK and mutant β-cell GST-GCK fusion proteins.

Preparation	Protein yield (mg/L of culture)	Kcat (s^{-1})	$S_{0.5}$ for glucose (mmol/L)	nH	Km for ATP (mmol/L)	I_a
Wild-type GST-GCK	3.12±0.91	44.10±7.50	7.20±0.40	1.40±0.08	0.40±0.00	1.0±0.07
GST-GCK(Glu70Asp]	2.35±0.55	27.40±4.80*	20.10±3.20†	1.20±0.07	0.25±0.05	0.25±0.06**
GST-GCK(His137Asp]	2.82±0.47	17.20±1.20**	18.10±3.10*	1.10±0.03**	0.23±0.03*	0.26±0.09**
GST-GCK(Phe150Tyr]	3.07±0.55	9.92±2.38*	101.40±6.20**	1.06±0.05*	3.11±0.48*	0.014±0.003*
GST-GCK(Val154Leu]	2.77±0.48	46.60±4.40	26.00±3.40*	1.54±0.01	1.62±0.16*	0.099±0.036**
GST-GCK(Gly162Asp]	2.78±0.58	Undetectable activity				
GST-GCK(Arg303Trp]	1.58±0.26	14.60±1.38**	4.62±0.10**	1.52±0.02	0.29±0.01*	0.59±0.09*
GST-GCK(Arg392Ser]	2.44±0.74	41.30±11.30	11.90±1.70*	1.30±0.03	0.63±0.03*	0.60±0.25

Data represent means ± SEM of 3 separate enzyme expressions each tested in duplicate. Note that the Hill coefficient (nH) and the relative activity index (I_a) are unit less. Kcat: GCK catalytic constant; $S_{0.5}$: affinity constant for glucose; nH: Hill coefficient; Km for ATP: affinity constant for ATP; I_a: GCK activity index. (*)$p<0.05$, *t* test; (**)$p<0.005$, *t* test.

doi:10.1371/journal.pone.0038906.t002

stabilizing the helix. In the mutant, the loop becomes shorter and the side chain of Arg394, which in the wild-type enzyme is directed towards the loop, changes the orientation because of steric interactions. This change disrupts interactions between the side chain of Arg394 and some residues of the loop. Although the interaction between the side chains of Arg394 and Ser433 in the loop following the α12 helix is conserved, the binding appears to be weakened compared with the wild-type enzyme.

Kinetic Analysis and Thermo-stability of Recombinant GCK Mutants

To select representative mutations for a functional study to evaluate their pathogenic significance, we considered all the mutations found in our population in the last decade (11 and present work) in terms of severity and location. All the selected mutations were mapped in the whole GCK structure: p.His137Asp, pPhe150Tyr, p.Val154Leu, p.Gly162Asp, in the small domain, Arg303Trp and p.Arg392Ser, in the large domain and p.Glu70Asp in a loop connecting the two domains. Three among these mutations, (p.Gly162Asp, p.His137Asp and p.Arg392Ser) were the most severe and none have been produced or characterized. Figure 2 shows the position of selected mutated residues in the structure model of the GCK enzyme. All variants displayed reduced enzyme activity versus the wild-type GST-GCK, as shown by the I_a index. The kinetic characteristics of GST-GCK-wt and GST-GCK-mutants, determined *in vitro* enzymatic assays, are shown in Table 2. Mutations p.Gly162Asp, p.Phe150Tyr and p.Val154Leu, localized in the core of the molecule, not far from the substrate binding site, produced the strongest effect. The p.Gly162Asp change is very deleterious since no enzymatic activity was detected in the mutant protein, and mutations p.Phe150Tyr and p.Val154Leu reduced enzyme activity to below 10% of the wild-type enzyme. In contrast, mutations p.Glu70Asp, p.His137Asp, p.Arg303Trp and p.Arg392Ser, localized in more peripheral positions, retained at least 25% of wild-type activity. We also evaluated the protein stability of wild-type and of mutant GST-GCK and the time-course of thermal inactivation at different temperatures (Figure 3A and B respectively). Wild-type GCK activity remained practically constant under temperatures up to 50°C, but fell abruptly at 55°C. In contrast, the enzyme activity of all mutants, except GST-GCK (p.Glu70Asp), rapidly decreased by more than 50% at 50°C (Figure 3A). The time-course analysis of GCK thermal inactivation indicated that the mutants rendered the enzyme thermo-unstable (more than 50% of GCK activity was lost within 30 min at 50°C), whereas 50% of wild-type GCK activity was present after 30 min of incubation at the critical temperature (Figure 3B).

Discussion

A correct diagnostic approach to the MODY2 patient is important to avoid useless, expensive analyses and misclassification of the diabetes. In this study, we characterized the *GCK* gene by DHPLC followed by sequence analysis in 66 patients with suspected MODY2 enrolled between 2006 and 2010. We identified 19 GCK mutations in 28 children accounting for 42.4% of suspected MODY2 children. Our data are similar to those we obtained between 2001 and 2005 [11] and are also in agreement with the high prevalence of MODY2 (up to 61% of MODY forms) found in Italy and in southern Europe [12,13]. Among the 19 GCK variants described herein, six are new (p.Lys458_Cys461del, p.Val154Leu, p.Arg447Glyfs, IVS5-2A>T, p.Glu40Asp and p.Glu395_Arg397del) and 13 previously reported. Glucokinase missense mutations are the most frequent causes of MODY2 [9]. In our study, the missense mutations (13/19: two new and 11 known), and deletions (n = 3) were distributed throughout the protein: six/16 (38%) in the small domain, nine/16 (56%) in the large domain and one/16 (6%) in the connecting region of the protein. These findings are in agreement with a study in which no hot spot mutations were reported [9].

In the attempt to understand how the detected mutations could contribute to MODY2 insurgence, we searched for structure/function correlations of the disease-causing mutated proteins. First, we evaluated the impact of each mutation (except splice variants and deletions) on the enzyme 3D-structure and then, for seven selected mutations, we carried out functional studies. All the mutations considered here are buried in the enzyme, except for p.Glu70Asp that is located on the surface of the protein, and all mutations are far from the active and ATP binding sites (Table 1). Apart from p.Val154Leu and p.Phe150Tyr that undergo large movements during the conformational transition from the super-open to the closed active form, all the mutant structures exhibit local structural alterations (Table 1) that well correlate to kinetic parameters and thermal inactivation data (Table 2, Figure 3). In all cases, the amino-acid replacement either provokes the loss of stabilizing interactions or generates unfavorable interactions that may destabilize the enzyme.

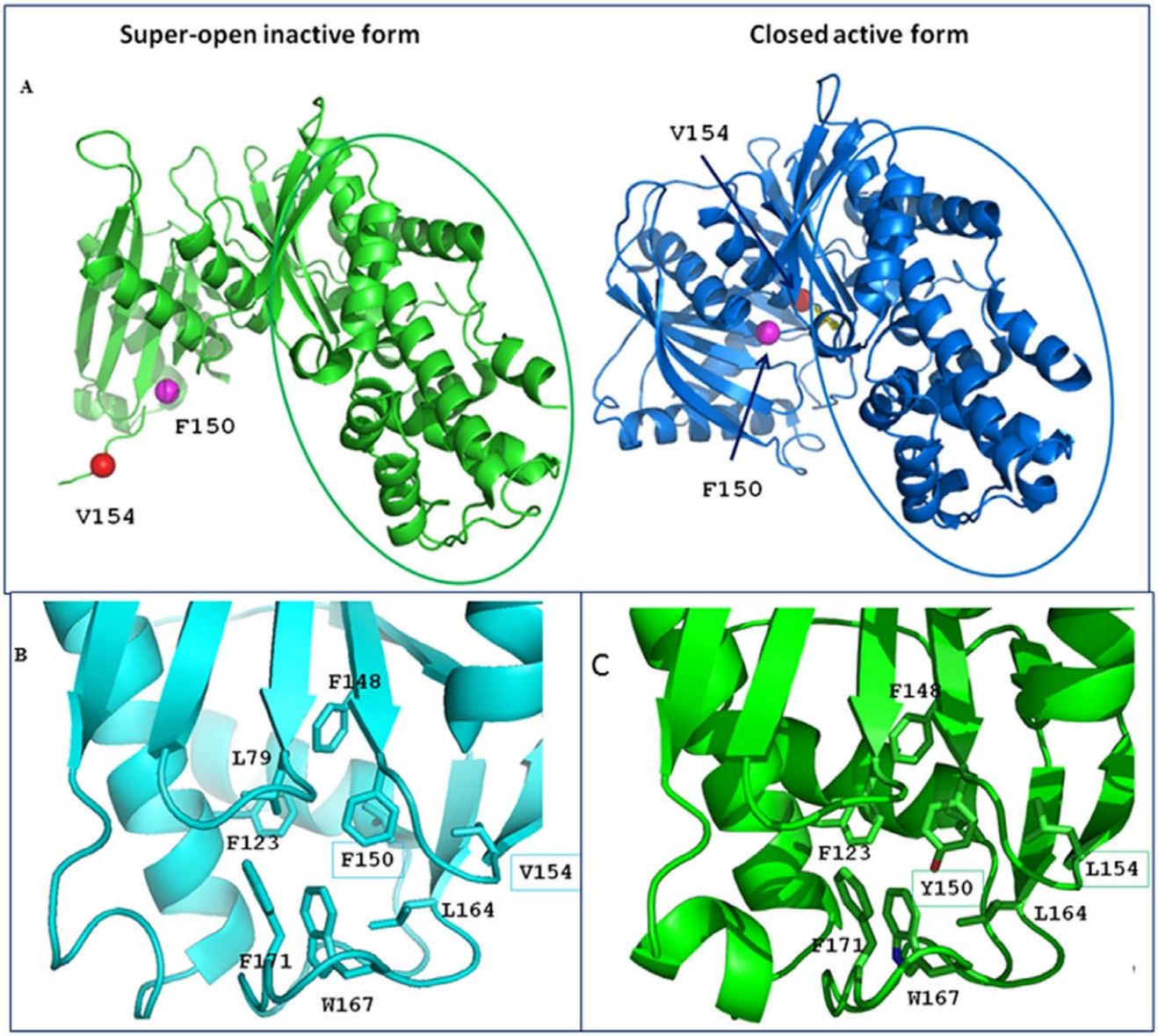

Figure 1. View of the mutations p.Phe150Tyr and p.Val154Leu in the whole structures and in their local environment. A: The structures of GCK in the super-open inactive form (PDB code code: 1v4t) and in the closed active form (PDB code code: 1v4s) are shown on the left and on the right, respectively. In the closed form (right) the sugar is shown as a yellow stick. In both panels, the large domain is in the same orientation and is circled. It is clear that the small domain undergoes a large conformational variation from the super-open to the closed form. Specifically the region embodying the residues Phe150 (blue sphere) and Val154 (red sphere) dramatically changes its orientation. **B**: Close-up view of the wild-type closed structure showing the hydrophobic core rich in aromatic/hydrophobic amino acids. Leu79, Phe123, Phe148, Phe150, Val154, Leu164, Trp167 and Phe171 form an intricate network of stabilizing hydrophobic interactions. **C**: Structure of GCK closed structure containing the both the Tyr150 and Leu154 mutated residues. Introduction of the oxydryl group (red) of Tyr150 within the hydrophobic core disrupts the interactions present in the wt-enzyme. The replacement of Val154 by leucine produces only small changes in the closed form.
doi:10.1371/journal.pone.0038906.g001

We evaluated the effects on GCK kinetics and thermo-stability of seven GCK variants distributed in different functional domains of the enzyme: three variants described in the present study (p.Phe150Tyr, p.Val154Leu, p.Arg303Trp) and four (p.Glu70Asp, p.His137Asp, p.Gly162Asp and p.Arg392Ser) previously reported [11]. The GST-GCK (p.Glu70Asp) mutant showed a GCK activity index significantly lower than the wild type (mean $I_a = 0.25$). This effect is due to discrete defects in the kinetic constants, in particular, glucose affinity was significantly reduced ($S_{0.5}$ for glucose: 20.1 ± 3.2 vs 7.2 ± 0.4 mM). Variant p.Glu70Lys displayed a similarly decreased activity index (mean $I_a = 0.31$) without significant thermo-instability [14,15]. The substitution of histidine with aspartic acid (p.His137Asp) affected GCK function (mean $I_a = 0.26$). As shown by molecular modelling, this mutation introduces a negative charge in the region that may affect the charge distribution of the protein [11]. The previously reported mutation p.His137Arg, in which His is replaced by the positively charged arginine, did not affect enzyme activity (mean $I_a = 0.92$) [15]. This finding shows that a negatively charged amino acid is not tolerated at this site. p.Phe150Tyr and the novel p.Val154Leu mutations dramatically reduced GCK activity (mean $I_a = 0.014$ and 0.099, respectively)

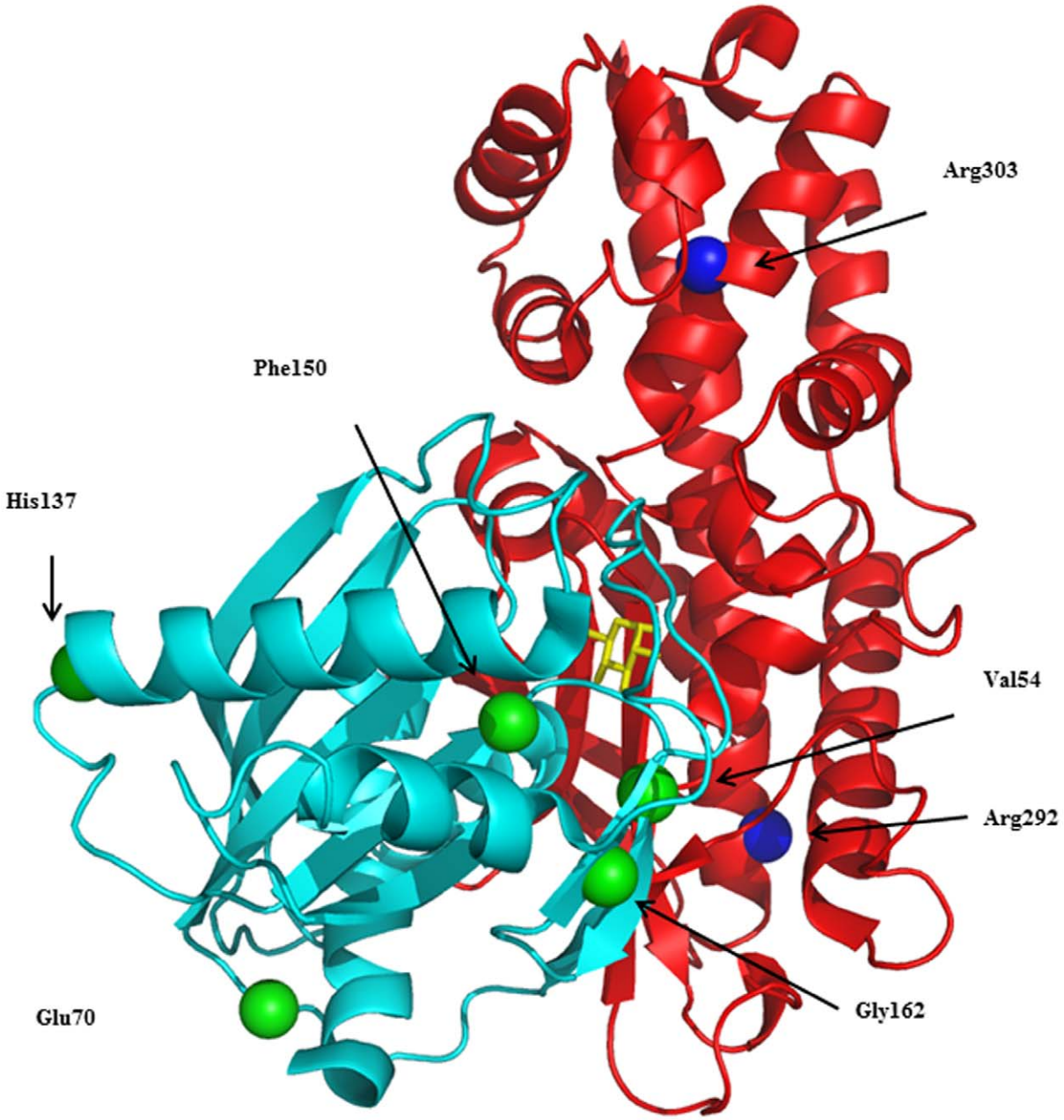

Figure 2. Distribution of the selected GCK mutations. The structure of GCK in the active closed form is shown (PDB code: 1v4s); the small and large domains are drawn in cyan and red, respectively; glucose appears as a yellow stick. Mutation sites are shown as green or blue spheres.
doi:10.1371/journal.pone.0038906.g002

and thermo-stability (<40% at 50°C/30 min than in wild-type). Both mutations displayed high $S_{0.5}$ and ATP Km values, which indicate a greatly reduced affinity for glucose and ATP. In particular, the cooperativity of p.Phe150Tyr was significantly reduced (nH = 1.06 vs 1.40, *t* test, $p = 0.038$). It is noteworthy that Val154 is one of residues that undergo large movements during the transition from the super-open to the closed form. Even though the replacement of Val by Leu provokes only small local perturbations, the latter may be relevant during the conformational transition induced by ATP and glucose binding. The substitution of glycine 162 by aspartic acid (p.Gly162Asp) affected the hydrophobic core of the enzyme and, as predicted by molecular modelling [11], markedly alters the structure and dynamics of the domain. This is one of the most dramatic mutations we identified as it introduces a net negative charge into a hydrophobic environment [11]. In fact, the enzyme activity of this mutant was undetectable. Although any reduction in the I_a below 30% of the wild type would have little further effect on the fasting plasma glucose [15], it is noteworthy that fasting glycemia was higher in the child with this mutation (10.0 mmol/L) [11] than in other MODY2 children (mean 6.7±0.8 mmol/L). Arg 303 is located in the α8 helix and molecular modelling indicates that the Arg-to-Trp change at this position would destabilize the helix structure. Mutation p.Arg303Trp caused a reduction of the activity index (mean I_a = 0.59), mainly due to a decrease in the catalytic constant, being

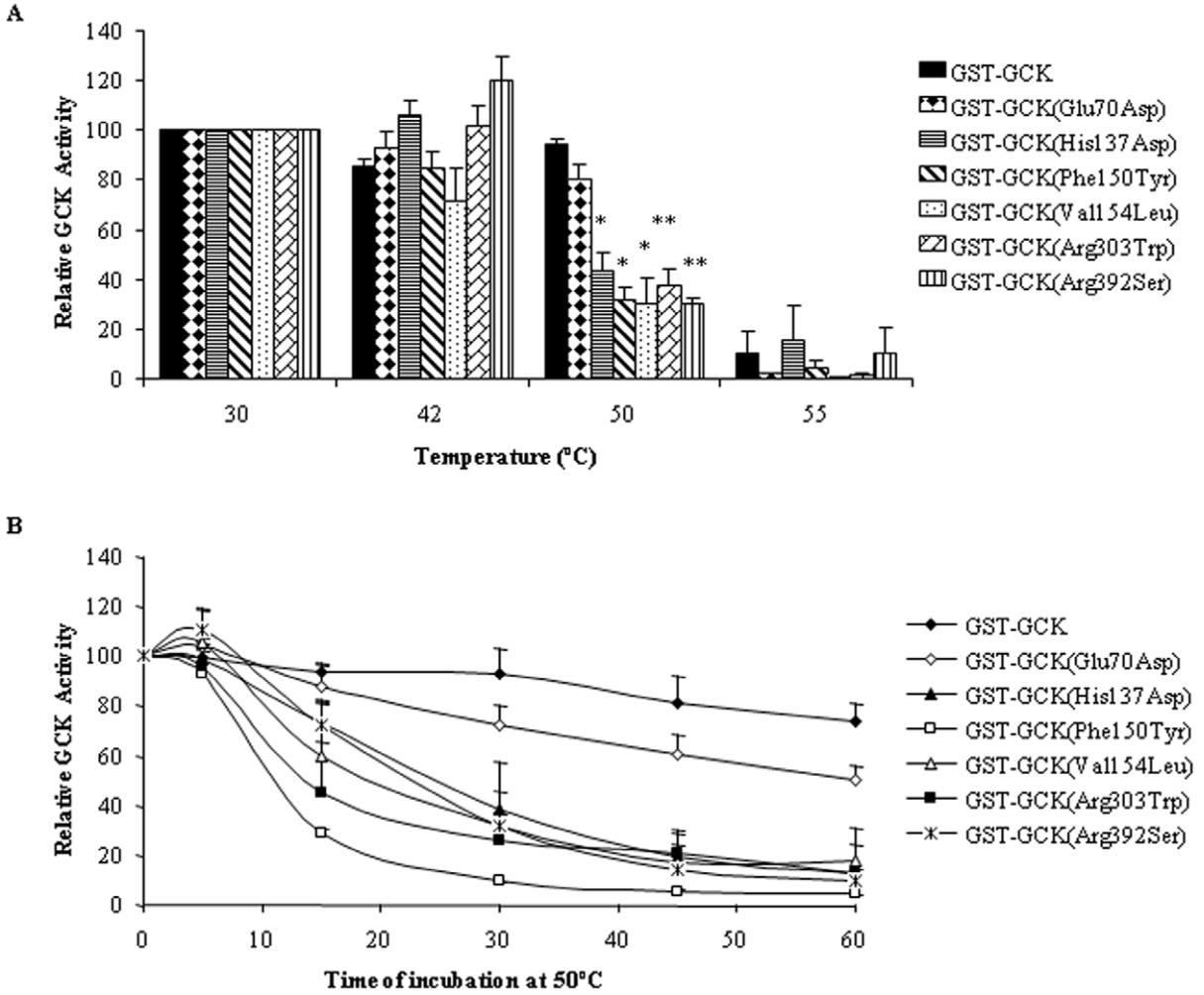

Figure 3. Effect of temperature on the stability of GST-GCK mutants. Stock enzyme solutions were diluted to 250 μg/ml in storage buffer containing 30% glycerol, 50 mM glucose, 10 mM glutathione, 5 mM DTT, 200 mM KCl and 50 mMTris/HCl, pH 8.0. Panel A: The enzyme solutions were incubated for 30 min at temperatures ranging from 30 to 55°C and then assayed at 30°C as described in the Methods section. Panel B: The enzyme solutions were incubated for periods of time from 5 to 60 min at 50°C. Results are means and SEM of three independent enzyme preparations for each mutant except for GST-GCK (Phe150Tyr) which corresponds to two independent enzyme preparations. (*) $p \leq 0.03$, (†) $p < 0.008$.
doi:10.1371/journal.pone.0038906.g003

both glucose and ATP affinities modified. Our results concord with the finding that other mutations in the same helix (p.Leu309Pro and p.Arg308Trp) increased thermal inactivation and/or modified glucose affinity [16,17]. Taken together, these results suggest that the α8 helix plays a role in the regulation of substrate affinity and protein stability. Mutation p.Arg392Ser is located in the protein periphery and, like the neighboring mutation p.Arg397Leu [17], it only slightly affected GCK activity. Thus, our mutants reduced the enzyme's catalytic activity by altering one or more kinetic parameters. Moreover, all mutants, except GCK-Glu70Asp, displayed thermal-instability, which has been implicated in hyperglycemia in MODY2 patients [17,18]. Nevertheless, additional defects caused by these mutations on other mechanisms of GCK control, such as post-translational regulation, interaction with other protein partners or organelles, cannot be excluded. Globally our evaluation of enzyme activity indicates that all seven mutants play a pathogenic role in MODY2 insurgence. In addition although altered glucose and ATP binding, and thermal stability appear to be the major causes of the disease, in a few cases mutations affected cooperativity and molecular motions, and hence impaired enzyme activity.

Although the in vitro functional evaluation of a GCK-mutant is a useful method with which to predict the effect exerted by a DNA change on enzyme activity, it is not a practical approach to the diagnosis of MODY. In our experience, taking into account all the experimental data concerning the seven mutants expressed, we found that the mutations induced structural alterations predicted by modeling that were in good agreement with kinetics/thermostability analyses. Therefore, this approach could be a reliable surrogate to predict the pathogenic role of a GCK variant.

In conclusion, in this five-year update of GCK mutations in MODY2 children from southern Italy, we have identified six new GCK variants thereby expanding the MODY2 mutation panel. Furthermore, our study, carried out by integrating DHPLC, sequencing, bioinformatics and functional analysis, provides new information about the structure-function relationship of human glucokinase mutations and MODY2.

Materials and Methods

Ethics Approval

The study was conducted according to the Helsinki II declaration and it was approved by the Ethics Committee of the School of Medicine Federico II, Naples, Italy.

Written informed consent to the study was obtained from each adult subject and from both parents of children.

Subjects

Between 2006 and 2010, 720 hyperglycemic children were monitored at the Departments of Pediatrics of the University of Naples "Federico II" and of the Second University of Naples, Italy. Sixty-six patients (mean age 109 months, 53% girls) who had fasting hyperglycemia (>5.5 mmol/L), HbA1c <7.0% and a family history of diabetes for at least two consecutive generations were enrolled in the study as suspected MODY2 individuals. The autoimmune markers of type-1 diabetes (glutamate decarboxylase, protein tyrosine phosphatase-like protein and insulin antibodies) were evaluated; the presence of more than one antibody was considered an exclusion criterion. One hundred unrelated euglycemic controls (mean age 363 months, 69% girls) were recruited at CEINGE (Advanced Biotechnologies, s.c.a.r.l. Naples) also between 2006–2010.

Patients, their mother and father, and controls provided 2 blood samples for biochemical testing and for DNA extraction. BMIz-score (Center for Disease Control normative, http://www.cdc.gov), family history of diabetes and/or other diseases, birth weight and age at admission were recorded for each patient. FPG, triglycerides (evaluated with routine methods) and HbA1c measure with HPLC (HLC-723 G7 TOSOH Bioscience Tokyo, Japan) were evaluated in each suspected MODY2 child. Genomic DNA from patients, their mother and father, and controls was extracted with the Nucleon BACC 2 kit (Amersham Biosciences Europe, Milan, Italy).

GCK Gene Analysis

The 10 exons, including their flanking intronic regions, of the *GCK* gene were amplified using primers and PCR conditions described elsewhere [11]. The amplified fragments were denatured at 95°C for 10 min and then renatured for 10 min to generate heteroduplices. Each fragment was run on the DHPLC WAVE DNA fragment analysis system (Transgenomic, Inc. Omaha, NE) using DHPLC conditions reported in Table S1. Any additional or abnormal peak shape observed in the chromatogram was further sequenced (ABI PRISM 3730; Biosystems Foster City, CA, USA). All sequences were analysed in comparison with the wild-type reference sequence (NM_000162, http://www.ncbi.nlm.nih.gov/nuccore/NM_000162) by the ABI Seqscape software v.2.5 (Applied Biosystems). The mutations and variants were then numbered according to the Human Genome Variation Society (http://www.hgvs.org/).

Analysis of *GCK* Mutations

We first evaluated each detected GCK mutation by bioinformatics (Polyphen and SIFT algorithms and Modeller programs). We also examined the enzyme function of seven mutations among the most severe found in our population in the last decade and never characterized. The mutations for the latter study mapped in the whole enzyme structure (small, large and loops connecting domains).

Bioinformatic Analysis

Two free online prediction programs, Polyphen (http://genetics.bwh.harvard.edu/pph/) and SIFT (http://sift.jcvi.org/www/SIFT_seq_submit2.html), [1] were used to predict the effect of GCK mutations on the protein. The Polyphen program [19] is a tool for the prediction of the impact of an amino acid substitution on the structure of a human protein using straight forward physical and comparative considerations. The SIFT program [20] tests a query sequence and uses multiple alignment information to predict tolerated and deleterious substitutions for every position of the query sequence. SIFT is a multistep procedure that searches for similar sequences, chooses closely related sequences that may share a function similar to that of the query sequence, obtains the alignment of these chosen sequences, and calculates normalized probabilities for all possible substitutions from the alignment. Models of all mutants of GCK were generated *in silico* with the Modeller 9v8 program using the active form of the GCK crystal structure as template [2.3 Å, Brookhaven Protein Database code (PDB code) 1v4s]. The inactive super-open form (3.4 Å, PDB code 1v4t) was also considered for comparison.

After alignment with using BODIL [21], the query and template sequences were used as input in the Modeller program [22] and 20 models were generated. The most abundant conformers of the replaced residue were selected and a simulated annealing procedure was carried out to optimize side chain conformations. The model that presented the best Modeller Discrete Optimized Protein Energy (DOPE) score was selected to be used in subsequent analyses. The initial models of selected mutants were energy minimized with the GROningen MAchine for Chemical Simulations (GROMACS) package using the GROningen MOlecular Simulation (GROMOS) 43a1 force field, to regularize the protein structure geometry. The molecules were solvated in boxes containing simple point charge water molecules. The energy minimization was obtained by 1000 steps of the steepest descent method and subsequently by 1000 steps of the conjugate gradient method. The notation used for secondary structure was taken from Kamata et al. [8].

Production of Recombinant Wild-type and Mutant Glutathionyl-S-transferase-glucokinase (GST-GCK)

Recombinant human wild-type beta cell GCK fused to GST (GST-GCK) was prepared as described previously [23]. Mutations were introduced into the GST-GCK construct by PCR using the QuikChange® II Site Directed Mutagenesis Kit (Stratagene, La Jolla, CA, USA); the oligonucleotides are reported in Table S2. Mutant constructs were checked by sequencing and digestion with specific restriction enzymes (Table S2). Fusion proteins from *E. coli* were expressed and purified as described previously [24]. Fusion proteins were stored at a concentration of about 1 mg/ml at –80°C in 30% glycerol, 50 mM glucose, 10 mM glutathione, 5 mM DTT, 200 mM KCl and 50 mM Tris/HCl, pH = 8.0. Protein concentrations were determined with the Bio-Rad Protein Assay (Bio-Rad Laboratories, GmbH München Germany), and bovine serum albumin as standard. GST-GCK purification was verified by Coomassie-stained SDS-PAGE as a single band of 75 kDa.

Enzymatic Assay

GCK activity was measured spectrophotometrically on a UVIKONxl spectrophotometer (Secoman, France), using a $NADP^+$-coupled assay with glucose-6-phosphate dehydrogenase. Determination of kinetic parameters and thermal inactivation were performed as previously described [23]. The Km for ATP was measured at a glucose concentration near the relative $S_{0.5}$

values (7, 15, 8.5, 100, 20, 5 and 11 mM respectively for wild type, p.Glu70Asp, p.His137Asp, p.Phe150Tyr, p.Val154Leu, p.Gly162Asp, p.Arg303Trp and p.Arg392Ser). Thermal inactivation experiments were assayed at a glucose concentration of 100 mM. Results are reported as means ± standard error of the mean (SEM) of three independent enzyme preparations assayed at least in duplicate.

Statistical Analysis

Variables are reported as mean±SD (continuous variables) or mean ±SEM (categorical variables). We used the Student *t* test to compare variables; significance was set at $p<0.05$. The SPSS statistical software was used.

Supporting Information

Figure S1 Close-up view of the p.Lys420Glu mutation at the inter-domain interface. The small and large domains are drawn in cyan and red, respectively. Helix 13 is shown in orange. Lys420 (red stick) forms a salt-bridge with Glu440 (yellow stick) which is located in a loop connecting the two domains.
(DOCX)

Table S1 DHPLC conditions to detect GCK variants.
(DOCX)

Table S2 Primers used for site-directed mutagenesis in GCK cDNA.
(DOCX)

Acknowledgments

We thank our diabetic patients and their families for their kind cooperation in this study.

Writing assistance: Jean Ann Gilder (Scientific Communication srl) provided writing assistance.

Provenance and peer review: Not commissioned; externally peer reviewed.

Author Contributions

Conceived and designed the experiments: LS. Performed the experiments: MC CMGH. Analyzed the data: LS MC CMGH NT MAN AZ. Contributed reagents/materials/analysis tools: DI AF CC IC VC AC. Wrote the paper: LS MC NT AZ MAN.

References

1. Ellard S, Bellanné-Chantelot C, Hattersley AT, European Molecular Genetics Quality Network (EMQN) MODY group (2008) Best practice guidelines for the molecular genetic diagnosis of maturity-onset diabetes of the young. Diabetologia 51: 546–553.
2. Incani M, Cambuli VM, Cavalot F, Congiu T, Paderi M, et al. (2010) Clinical application of best practice guidelines for the genetic diagnosis of MODY2 and MODY3. Diabet Med 27: 1331–1333.
3. Naylor R and Philipson LH (2011) Who should have genetic testing for MODY? Clin Endocrinol (Oxf) 75: 422–426.
4. Nyunt O, Wu JY, McGown IN, Harris M, Huynh T, et al. (2009) Investigating maturity onset diabetes of the young. Clin Biochem Rev 30: 67–74.
5. Iynedjian PB (2009) Molecular physiology of mammalian glucokinase. Cell Mol Life Sci 66: 27–42.
6. Massa ML, Gagliardino JJ, Francini F (2011) Liver glucokinase: An overview on the regulatory mechanisms of its activity. IUBMB Life 63: 1–6.
7. Hussain K (2010) Mutations in pancreatic ß-cell Glucokinase as a cause of hyperinsulinaemic hypoglycaemia and neonatal diabetes mellitus. Rev Endocr Metab. Disord 11: 179–183.
8. Kamata K, Mitsuya M, Nishimura T, Eiki J, Nagata Y (2004) Structural Basis for Allosteric Regulation of the Monomeric Allosteric Enzyme Human Glucokinase. Structure 12: 429–438.
9. Osbak KK, Colclough K, Saint-Martin C, Beer NL, Bellanné-Chantelot C, et al. (2009) Update on mutations in glucokinase (GCK), which cause maturity-onset diabetes of the young, permanent neonatal diabetes, and hyperinsulinemic hypoglycemia. Hum Mutat 30: 1512–1526.
10. Colom C, Corcoy R (2010) Maturity onset diabetes of the young and pregnancy. Best Pract Res Clin Endocrinol Metab 24: 605–615.
11. Tinto N, Zagari A, Capuano M, De Simone A, Capobianco V, et al. (2008) Glucokinase gene mutations: structural and genotype-phenotype analyses in MODY children from South Italy. PLoS One 3 e1870.
12. Mantovani V, Salardi S, Cerreta V, Bastia D, Cenci M, et al. (2003) Identification of eight novel glucokinase mutations in Italian children with maturity-onset diabetes of the young. Hum Mutat 22: 338.
13. Pruhova S, Dusatkova P, Sumnik Z, Kolouskova S, Pedersen O, et al. (2010) Glucokinase diabetes in 103 families from a country-based study in the Czech Republic: geographically restricted distribution of two prevalent GCK mutations. Pediatr Diabetes 11: 529–535.
14. Burke CV, Buettger CW, Davis EA, McClane SJ, Matschinsky FM, et al. (1999) Cell-biological assessment of human glucokinase mutants causing maturity-onset diabetes of the young type 2 (MODY-2) or glucokinase-linked hyperinsulinaemia (GK-HI).Biochem J 342: 345–352.
15. Davis EA, Cuesta-Muñoz A, Raoul M, Buettger C, Sweet I, et al. (1999) Mutants of glucokinase cause hypoglycaemia- and hyperglycaemia syndromes and their analysis illuminates fundamental quantitative concepts of glucose homeostasis. Diabetologia 42: 1175–1186.
16. Gidh-Jain M, Takeda J, Xu LZ, Lange AJ, Vionnet N, et al. (1993) Glucokinase mutations associated with non-insulin-dependent (type 2) diabetes mellitus have decreased enzymatic activity: implications for structure/function relationships. Proc Natl Acad Sci U S A 90: 1932–1936.
17. García-Herrero CM, Galán M, Vincent O, Flández B, Gargallo M, et al. (2007) Functional analysis of human glucokinase gene mutations causing MODY2: exploring the regulatory mechanisms of glucokinase activity. Diabetologia 50: 325–333.
18. Kesavan P, Wang L, Davis E, Cuesta A, Sweet I, et al. (1997) Structural instability of mutant beta-cell glucokinase: implications for the molecular pathogenesis of maturity-onset diabetes of the young (type-2). Biochem J 322: 57–63.
19. Zou M, Baitei EY, Alzahrani AS, Parhar RS, Al-Mohanna FA, et al. (2011) Mutation prediction by PolyPhen or functional assay, a detailed comparison of CYP27B1 missense mutations. Endocrine 40: 14–20.
20. Ng PC, Henikoff S (2003) SIFT: Predicting amino acid changes that affect protein function. Nucleic Acids Res 31: 3812–3814.
21. Lehtonen JV, Still DJ, Rantanen VV, Ekholm J, Björklund D, et al. (2004) BODIL: a molecular modeling environment for structure-function analysis and drug design. J Comput Aided Mol Des 18: 401–419.
22. Eswar N, Marti-Renom MA, Webb B, Madhusudhan MS, Eramian D, et al. (2006) Comparative Protein Structure Modeling With MODELLER. Current Protocols in Bioinformatics, John Wiley & Sons Inc. Supplement 15 5.6.1–5.6.30.
23. Galán M, Vincent O, Roncero I, Azriel S, Boix-Pallares P, et al. (2006) Effects of novel maturity-onset diabetes of the young (MODY)-associated mutations on glucokinase activity and protein stability. Biochem J 393: 389–396.
24. Liang Y, Kesavan P, Wang LQ, Niswender K, Tanizawa Y, et al. (1995) Variable effects of maturity-onset-diabetes-of-youth (MODY)-associated glucokinase mutations on substrate interactions and stability of the enzyme. Biochem J 309: 167–173.
25. Weng J, Ekelund M, Lehto M, Li H, Ekberg G, et al. (2002) Screening for MODY mutations, GAD antibodies, and type 1 diabetes-associated HLA genotypes in women with gestational diabetes mellitus. Diabetes Care 25: 68–71.
26. Stoffel M, Froguel PH, Takeda J, Zouali H, Vionnet N, et al. (1992) Human glucokinase gene: isolation, characterization, and identification of two missense mutations linked to early-onset non-insulin-dependent (type 2) diabetes mellitus. Proc Natl Acad Sci U S A 89: 7698–7702.
27. Lorini R, Klersy C, d'Annunzio G, Massa O, Minuto N, et al. (2009) Maturity-onset diabetes of the young in children with incidental hyperglycemia: a multicenter Italian study of 172 families. Diabetes Care 32: 1864–1866.
28. Matyka KA, Beards F, Appleton M, Ellard S, Hattersley A, et al. (1998) Genetic testing for maturity onset diabetes of the young in childhood hyperglycaemia. Arch Dis Child 78: 552–554.
29. Estalella I, Rica I, Perez de Nanclares G, Bilbao JR, Vazquez JA, et al. (2007) Mutations in GCK and HNF-1alpha explain the majority of cases with clinical diagnosis of MODY in Spain. Clin Endocrinol Oxf 67: 538–546.
30. Shimada F, Makino H, Hashimoto N, Taira M, Seino S, et al. (1993) Type 2 (non-insulin-dependent) diabetes mellitus associated with a mutation of the glucokinase gene in a Japanese family. Diabetologia 36: 433–437.
31. Massa O, Meschi F, Cuesta-Munoz A, Caumo A, Cerutti F, et al. (2001) High prevalence of glucokinase mutations in Italian children with MODY. Influence on glucose tolerance, first-phase insulin response, insulin sensitivity and BMI. Diabetologia 44: 898–905.

Hindawi Publishing Corporation
BioMed Research International
Volume 2013, Article ID 631082, 5 pages
http://dx.doi.org/10.1155/2013/631082

Research Article

Haplogroup T Is an Obesity Risk Factor: Mitochondrial DNA Haplotyping in a Morbid Obese Population from Southern Italy

Carmela Nardelli,[1,2] Giuseppe Labruna,[3] Rosario Liguori,[1,2] Cristina Mazzaccara,[1,2] Maddalena Ferrigno,[1] Valentina Capobianco,[1,2] Massimo Pezzuti,[1,2] Giuseppe Castaldo,[1,2] Eduardo Farinaro,[4] Franco Contaldo,[5] Pasqualina Buono,[3,6] Lucia Sacchetti,[2,7] and Fabrizio Pasanisi[5]

[1] *CEINGE Biotecnologie Avanzate S.C. a R.L., Via G. Salvatore 486, 80145 Naples, Italy*
[2] *Dipartimento di Medicina Molecolare e Biotecnologie Mediche, Università degli Studi di Napoli Federico II, Via S. Pansini 5, 80131 Naples, Italy*
[3] *IRCCS Fondazione SDN, Istituto di Ricerca Diagnostica e Nucleare, Via E. Gianturco 113, 80143 Naples, Italy*
[4] *Dipartimento di Sanità Pubblica, Università degli Studi di Napoli Federico II, Via S. Pansini 5, 80131 Naples, Italy*
[5] *CISRO, Centro Interuniversitario di Studi e Ricerche sull'Obesità e Dipartimento di Medicina Clinica e Chirurgia, Università degli Studi di Napoli Federico II, Via S. Pansini 5, 80131 Naples, Italy*
[6] *Dipartimento di Studi delle Istituzioni e dei Sistemi Territoriali, Università degli Studi "Parthenope", Via F. Acton 38, 80133 Naples, Italy*
[7] *Laboratori Misti, IRCCS Fondazione SDN-CEINGE, Via E. Gianturco 113, 80143 Naples, Italy*

Correspondence should be addressed to Lucia Sacchetti; sacchett@unina.it

Received 30 April 2013; Accepted 3 June 2013

Academic Editor: Ashraf S. Gorgey

Mitochondrial DNA (mtDNA) haplogroups have been associated with the expression of mitochondrial-related diseases and with metabolic alterations, but their role has not yet been investigated in morbid obese Caucasian subjects. Therefore, we investigated the association between mitochondrial haplogroups and morbid obesity in patients from southern Italy. The mtDNA D-loop of morbid obese patients ($n = 500$; BMI > 40 kg/m^2) and controls ($n = 216$; BMI < 25 kg/m^2) was sequenced to determine the mtDNA haplogroups. The T and J haplogroup frequencies were higher and lower, respectively, in obese subjects than in controls. Women bearing haplogroup T or J had twice or half the risk of obesity. Binomial logistic regression analysis showed that haplogroup T and systolic blood pressure are risk factors for a high degree of morbid obesity, namely, BMI > 45 kg/m^2 and in fact together account for 8% of the BMI. In conclusion, our finding that haplogroup T increases the risk of obesity by about two-fold, suggests that, besides nuclear genome variations and environmental factors, the T haplogroup plays a role in morbid obesity in our study population from southern Italy.

1. Introduction

Obesity is a multifactorial disorder caused by a combination of environmental, behavioural, and genetic factors; however, the molecular mechanisms by which these factors provoke fat mass accumulation and maintenance are not yet completely elucidated [1]. Moreover, mitochondrial dysfunctions that result in lipid accumulation and insulin resistance have been implicated in the pathogenesis of obesity [2]. Several mitochondrial DNA (mtDNA) variants have been investigated in diverse populations with obesity-related and lipid metabolism alterations [3, 4], and it was suggested that particular mtDNA haplogroups could be associated with inefficient energy expenditure [5]. A mitochondrial haplogroup (mt-haplogroup) is a collection of single nucleotide polymorphisms [6] accumulated throughout human history

in specific populations that could be attributed to genetic drift and/or climate selection [7–9]. Mitochondrial haplogroups have been associated with the expression of mitochondrial-related diseases (metabolic syndrome, type 2 diabetes, neurological disorders, infertility, and Parkinson's disease) and with various individual characteristics (aging and endurance training capacity) [3, 10–14], but, to our knowledge, their role has not yet been investigated in morbid obese Caucasian subjects. We previously reported that several DNA variants and epigenetic alterations are associated with the obese phenotype and/or with obese-related diseases [15–19]. Here, we have characterized mt-haplogroups in a large population of morbid obese adults and nonobese individuals from southern Italy to look for associations among specific mt-haplogroups and the obese phenotype.

2. Methods

2.1. Study Population. Five hundred unrelated morbid obese patients (64% females, age range 17–70 years, median; 2.5th–97.5th percentiles BMI = 45.1; 38.2–65.4 kg/m^2), and 216 non obese controls (66% females, age range 26–76 years, BMI = 22.9; 18.2–25.6 kg/m^2) were recruited from the Obesity Outpatient Clinic of the Dipartimento di Medicina Clinica e Chirurgia and from the Dipartimento di Medicina Molecolare e Biotecnologie Mediche, Federico II University Hospital, Naples (Italy), respectively. All participants were Caucasians and had lived in southern Italy for at least 3 generations. Written informed consent for participation in the study was obtained from all subjects. The research was approved by the Ethics Committee of the School of Medicine, University of Naples Federico II, and was in accordance with the principles of the Helsinki II Declaration.

2.2. Laboratory Investigations. Two blood samples (one for biochemical analysis and one for DNA extraction) were obtained after an overnight fast from each enrolled subject. Biochemical parameters were measured enzymatically with routine methods on an automated analyzer (Hitachi 747; Boehringer Mannheim, Germany). Insulin resistance was estimated in obese subjects with the homeostasis model assessment (HOMA) and the formula: fasting insulin (mU/L) X fasting glucose (mmol/L)/22.5.

The clinical and anamnestic data of each obese subject were collected, and the main metabolic parameters were evaluated. Fat mass (FM) and fat-free mass (FFM) were measured by bioimpedentiometry (Sta/BIA Akern, Florence, Italy) and respiratory quotient (RQ) and basal metabolic rate (BMR) by indirect calorimetry (Sensor Medics Vmax29, Anaheim, CA, USA). The BMI was calculated as weight (kg)/square height (m^2). Systolic and diastolic blood pressure, and cardiac frequency (beats/min) were collected by standard procedures. Metabolic syndrome (MS), which is a cluster of metabolic risk factors, namely, abdominal obesity, dyslipidemia (hypertriglyceridemia or low HDL-cholesterol concentrations), elevated blood pressure, and hyperglycemia, as defined by the American Heart Association criteria, was diagnosed if 3 out of the 5 risk factors were present [20].

2.3. Mitochondrial DNA Amplification and Sequencing. Genomic DNA was extracted from whole blood (Illustra BACC-2; GE Healthcare, UK). The D-loop region (about 1100 bp) was amplified with primers (HVI-forward: GTAAACCGGAGATGAAAACCT; HVII-reverse ACTGCATACCGCCAAAAGATA) chosen by the PRIMER 3 program (http://frodo.wi.mit.edu/) in a final volume of 25 μL containing a PCR mixture (10 μM each primer, 10x PCR buffer, 200 μM each deoxynucleotide triphosphate, and 0.5 U of Taq DNA polymerase) and 50 ng of genomic DNA. PCR consisted of an initial denaturation at 95°C for 5 min, followed by 35 cycles of 95°C for 30 s, 60°C for 1 min, and 72°C for 1 min, followed by a final extension at 72°C for 5 min. The PCR fragment was run on a 1.5% agarose gel, purified, and sequenced in both directions (BigDye Terminator v3.1 cycle sequencing method on an ABI-Prism 3730 DNA Analyzer; Applied Biosystems). Sequences were assembled with the SeqScape program v.2.5. The mtDNA nucleotide sequences were numbered according to the rCRS reference sequence (NC_012920). Haplogroups were defined by nucleotides at specific known polymorphic sites in the mtDNA [6].

2.4. Statistical Analysis. Haplogroup frequencies in patients and control subjects were compared using the χ^2 test. A $P < 0.05$ was considered the level of statistical significance. The odds ratio (OR) and 95% confidence intervals (CI) values for each haplogroup were calculated for the statistically significant haplogroup. ANOVA was performed to compare metabolic parameters in the different haplogroups. Multiple comparisons were corrected with the Bonferroni test. The Student's t-test, followed by a binomial logistic regression analysis, was used to investigate the association between the biochemical and clinical characteristics and the presence/absence of a specific haplogroup. Sample estimates were verified by bootstrapping. Statistical analyses were carried out with the PASW package for Windows (Ver.18; SPSS Inc. Headquarters, Chicago, Il, USA).

3. Results

The clinical and biochemical characteristics of the obese subjects are reported in Table 1. Metabolic syndrome was present in 41.3% of our obese subjects and was significantly more frequent in men than in women (47.9% versus 37.5%; OR/95% CI = 1.17/1.01–1.35, $P = 0.031$). Concurrent MS factors in our obese patients were hypertriglyceridemia (OR/95% CI: 16.7/10.8–26.0), hyperglycemia (OR/95% CI: 8.5/5.6–12.8), hypertension (OR/95% CI: 7.1/4.7–10.7), low serum levels of HDL cholesterol (OR/95% CI: 5.1/3.6–7.4). Haplogroup frequencies in obese and nonobese subjects are reported in Table 2. All nine common European haplogroups (H, I, J, K, T, U, V, W, and X) [21] were identified in most of our subjects (94.4%), whereas the R, L, N, B, and F haplogroups (collectively indicated as "others" in Table 2) were rare (5.6%).

European haplogroup frequencies were very similar in our obese and nonobese subjects, and the H haplogroup was the most frequent (about 40% of subjects). The T ($P = 0.004$) and J ($P = 0.02$) haplogroup frequencies were higher and lower, respectively, in obese subjects than in controls (haplogroup T: 13.2% versus 6%; haplogroup J: 5% versus 9.7%). At the χ^2 test, subjects with the T haplogroup had an increased risk of about two-fold for obesity (OR/95% CI = 1.94/1.16–3.22; $P = 0.004$), whereas subjects with the J haplogroup were less exposed to obesity (OR/95% CI = 0.63/0.45–0.89; $P = 0.02$) than subjects with the other haplogroups. These findings were confirmed by the results of bootstrap analysis based on 100 bootstrap samples.

When we divided our populations into males and females, the prevalence of the T and J haplogroups remained significantly higher and lower, respectively, in the obese females (12.4% versus 4.9%, OR/95% CI = 2.18/1.01–4.39; $P = 0.012$ for haplogroup T; 4.7% versus 11.9%, OR/95% CI = 0.55/0.38–0.78; $P = 0.009$ for haplogroup J). In addition, the T haplogroup was correlated to the degree of obesity. In fact, this haplogroup was significantly more frequent in obese subjects with a BMI higher than in those with a BMI lower than the median BMI (45 kg/m^2) (16% versus 10%, resp.; $P = 0.04$). Binomial logistic regression analysis (dependent variable: median BMI and independent variables: clinical and biochemical investigated parameters) showed that haplogroup T and systolic blood pressure are risk factors for a high degree of morbid obesity, namely, BMI > 45 kg/m^2 (OR/95% CI: 2.3/1.3–4.3 and OR/95% CI: 1.1/1.02–1.4, resp.); in fact together they account for 8% of the BMI. We did not find an association between mtDNA haplogroups and the clinical/biochemical tested variables, or in haplogroup frequencies according to MS presence/absence.

Table 1: General and biochemical characteristics of the morbid obese patients studied ($n = 500$).

	Median	Percentiles	
		2.5th	97.5th
Age (years)	32.59	17.50	57.00
Height (m)	1.66	1.51	1.85
Weight (kg)	125.54	98.00	178.40
BMI (kg/m^2)	45.10	38.20	65.40
Waist circumference (cm)	131.00	106.00	170.00
Hips circumference (cm)	134.00	114.90	158.10
W/H ratio	0.99	0.82	1.19
RQ	0.87	0.74	1.01
BMR (kcal)	2237.50	1581.38	3278.63
FFM (%)	51.40	40.28	64.11
FM (%)	48.55	35.89	59.73
SBP (mmHg)	124.45	100.00	160.00
DBP (mmHg)	80.00	60.00	100.00
Heart rate (beats/min)	80.00	60.00	100.00
Glucose (mmol/L)	5.05	3.89	7.53
Total cholesterol (mmol/L)	4.75	3.11	7.12
HDL cholesterol (mmol/L)	1.21	0.73	1.82
Triglycerides (mmol/L)	1.42	0.56	3.16
AST (U/L)	23.00	13.55	64.45
ALT (U/L)	31.00	12.00	84.45
GGT (U/L)	26.00	10.00	87.50
CHE (U/mL)	10066.37	5828.90	15084.55
Total bilirubin (μmol/L)	9.41	4.28	20.94
Uric acid (mmol/L)	0.35	0.21	0.57
Albumin (g/dL)	4.30	3.60	4.90
Total Protein (g/dL)	7.56	6.76	8.30
Creatinine (μmol/L)	70.72	44.20	106.08
Urea (mmol/L)	5.33	3.33	8.16
ALP (U/L)	76.00	42.75	247.75
C-peptide (ng/mL)	3.90	1.80	7.35
Insulin (mU/L)	19.00	6.90	53.03
HOMA	4.26	1.43	14.66

ALP: alkaline phosphatase; ALT: alanine transaminase; AST: aspartate transaminase; BMI: Body Mass Index; BMR: basal metabolic rate; CHE: cholinesterase; DBP: diastolic blood pressure; FFM: fat-free mass; FM: fat mass; GGT: γ-glutamyl transferase; HOMA: homeostatic model assessment; RQ: respiratory quotient; SBP: systolic blood pressure; W/H: waist/hip.

4. Discussion

Mitochondrial DNA haplogroups have been associated with metabolic disorders in various populations [3, 22, 23], although not yet in morbid obese Caucasians from southern Italy. The prevalence of MS in our obese patients (41%) was similar to that previously reported in a multicenter Italian study (43.6%) [24]. We found that haplogroup H was the most common haplogroup in both obese and control subjects (46.6% and 40.7%, resp.) from southern Italy, which is in agreement with the H frequency reported in other European populations (haplogroup H frequency: 13.3%–41.7%) [21]. We also show that haplogroups T and J conferred an increased and decreased risk for obesity, respectively. The J haplogroup was reported to protect against the onset of diseases related to oxidative stress and/or low inflammation grade, such as ischemic cardiomyopathy [25]. In fact, subjects bearing this haplogroup showed lower oxygen consumption (because the lower efficiency of the electron respiratory chain resulted in reduced production of radical oxygen species) than those with the H haplogroup [25].

On the other hand, subjects with haplogroup T could be intrinsically prone to develop defects in the mitochondrial oxidative phosphorylation system, which, in turn, negatively affects the performance of mitochondrial ATP production [11]. In fact, haplogroup T was reported to be more frequent in white men with fertility problems (a condition strongly dependent on ATP production) [13] and among Spanish patients affected by left ventricular hypertrophy [26]. Indeed, haplogroup T was less frequent among elite endurance athletes (possibly related to a negative effect on cardiac adaptation to endurance training) [11]. Amo et al. [27] reported that mitochondrial bioenergetic capacities and coupling efficiencies in cultured carcinoma cells did not differ between transmitochondrial cybrids harbouring mitochondria with haplogroup H and those harbouring mitochondria with haplogroup T [27]. However, the authors suggest that

Table 2: Haplogroup frequencies in morbid obese patients (n = 500) and controls (n = 216).

Haplogroup	Obese patients n (%)	Control subjects n (%)	P	OR/95% CI
H	233 (46.6)	88 (40.7)		
I	7 (1.4)	6 (2.8)		
J	25 (5.0)	21 (9.7)	0.02	0.63/0.45–0.89
K	29 (5.8)	18 (8.3)		
T	66 (13.2)	13 (6.0)	0.004	1.94/1.16–3.22
JT	0 (0)	1 (0.5)		
U	85 (17.0)	39 (18.1)		
V	13 (2.6)	4 (1.9)		
W	8 (1.6)	2 (0.9)		
X	10 (2.0)	8 (3.7)		
Others	24 (4.8)	16 (7.4)		

this result could be partially inconclusive because the effect of mitochondrial haplogroups might be too small to be detected by the procedures used [27], or they might need particular nuclear genes in order to be expressed, or they might need additional signals (nutrients and/or oxidative stress molecules) to influence oxidative phosphorylation functions, as previously described for the Uk haplogroup [28]. The foregoing studies suggest that, in our obese patients, the T haplogroup could contribute to affect the mechanisms of energy balance regulation so leading to increased fat depots.

In conclusion, our finding that haplogroup T increases the risk of obesity by about two-fold suggests that, besides nuclear genome variations and environmental factors, the T haplogroup contributes to morbid obesity in our study population from southern Italy.

Conflict of Interests

The authors have no conflict of interests to declare.

Acknowledgments

The authors thank Jean Ann Gilder (Scientific Communication srl, Naples, Italy) for text revision and editing. This work was supported by Grants Conv. CEINGE-Regione Campania (DGRC 1901/2009), IRCCS Fondazione SDN, Ministry of Health, and POR Campania FSE 2007–2013, Project CREME.

References

[1] J. S. El-Sayed Moustafa and P. Froguel, "From obesity genetics to the future of personalized obesity therapy," *Nature Reviews. Endocrinology*, vol. 9, no. 7, pp. 402–13, 2013.

[2] J. C. Bournat and C. W. Brown, "Mitochondrial dysfunction in obesity," *Current Opinion in Endocrinology, Diabetes and Obesity*, vol. 17, no. 5, pp. 446–452, 2010.

[3] T.-L. Yang, Y. Guo, H. Shen et al., "Genetic association study of common mitochondrial variants on body fat mass," *PLoS One*, vol. 6, no. 6, Article ID e21595, 2011.

[4] R. Liguori, C. Mazzaccara, F. Pasanisi et al., "The mtDNA 15497 G/A polymorphism in cytochrome b in severe obese subjects from Southern Italy," *Nutrition, Metabolism and Cardiovascular Diseases*, vol. 16, no. 7, pp. 466–470, 2006.

[5] N. Pichaud, J. W. Ballard, R. M. Tanguay, and P. U. Blier, "Naturally occurring mitochondrial DNA haplotypes exhibit metabolic differences: insight into functional properties of mitochondria," *Evolution*, vol. 66, no. 10, pp. 3189–3197, 2012.

[6] A. Torroni, K. Huoponen, P. Francalacci et al., "Classification of european mtDNAs from an analysis of three European populations," *Genetics*, vol. 144, no. 4, pp. 1835–1850, 1996.

[7] D. M. Behar, R. Villems, H. Soodyall et al., "The dawn of human matrilineal diversity," *American Journal of Human Genetics*, vol. 82, no. 5, pp. 1130–1140, 2008.

[8] D. Mishmar, E. Ruiz-Pesini, P. Golik et al., "Natural selection shaped regional mtDNA variation in humans," *Proceedings of the National Academy of Sciences of the United States of America*, vol. 100, no. 1, pp. 171–176, 2003.

[9] E. Ruiz-Pesini, D. Mishmar, M. Brandon, V. Procaccio, and D. C. Wallace, "Effects of purifying and adaptive selection on regional variation in human mtDNA," *Science*, vol. 303, no. 5655, pp. 223–226, 2004.

[10] M. A. Abdul-Ghani and R. A. DeFronzo, "Mitochondrial dysfunction, insulin resistance, and type 2 diabetes mellitus," *Current Diabetes Reports*, vol. 8, no. 3, pp. 173–178, 2008.

[11] M. G. Castro, N. Terrados, J. R. Reguero, V. Alvarez, and E. Coto, "Mitochondrial haplogroup T is negatively associated with the status of elite endurance athlete," *Mitochondrion*, vol. 7, no. 5, pp. 354–357, 2007.

[12] P. G. Ridge, T. J. Maxwell, C. D. Corcoran et al., "Mitochondrial genomic analysis of late onset Alzheimer's disease reveals protective haplogroups H6A1A/H6A1B: the Cache County Study on Memory in Aging," *PLoS One*, vol. 7, no. 9, Article ID e45134, 2012.

[13] E. Ruiz-Pesini, A. C. Lapeña, C. Díez-Sánchez et al., "Human mtDNA haplogroups associated with high or reduced spermatozoa motility," *American Journal of Human Genetics*, vol. 67, no. 3, pp. 682–696, 2000.

[14] R. Martinelli, C. Nardelli, V. Pilone et al., "MiR-519d overexpression Is associated with human obesity," *Obesity*, vol. 18, no. 11, pp. 2170–2176, 2010.

[15] V. Capobianco, C. Nardelli, M. Ferrigno et al., "MiRNA and protein expression profiles of visceral adipose tissue reveal miR-141/YWHAG and miR-520e/RAB11A as two potential miRNA/protein target pairs associated with severe obesity," *Journal of Proteome Research*, vol. 11, no. 6, pp. 3358–3369, 2012.

[16] R. Bracale, G. Labruna, C. Finelli et al., "The absence of polymorphisms in ADRB3, UCP1, PPARγ, and ADIPOQ genes protects morbid obese patients toward insulin resistance," *Journal of Endocrinological Investigation*, vol. 35, no. 1, pp. 2–4, 2012.

[17] G. Labruna, F. Pasanisi, C. Nardelli et al., "UCP1 -3826 AG+GG genotypes, adiponectin, and leptin/adiponectin ratio in severe obesity," *Journal of Endocrinological Investigation*, vol. 32, no. 6, pp. 525–529, 2009.

[18] L. Iaffaldano, C. Nardelli, M. Raia et al., "High aminopeptidase N/CD13 levels characterize human amniotic mesenchymal stem cells and drive their increased adipogenic potential in obese women," *Stem Cells and Development*, 2013.

[19] D. Ghezzi, C. Marelli, A. Achilli et al., "Mitochondrial DNA haplogroup K is associated with a lower risk of parkinson's

disease in Italians," *European Journal of Human Genetics*, vol. 13, no. 6, pp. 748–752, 2005.

[20] S. M. Grundy, J. I. Cleeman, S. R. Daniels et al., "Diagnosis and management of the metabolic syndrome: an American Heart Association/National Heart, Lung, and Blood Institute scientific statement," *Circulation*, vol. 112, no. 17, pp. 2735–2752, 2005.

[21] A. Torroni, M. Richards, V. Macaulay et al., "mtDNA haplogroups and frequency patterns in Europe," *American Journal of Human Genetics*, vol. 66, no. 3, pp. 1173–1177, 2000.

[22] L.-J. Guo, Y. Oshida, N. Fuku et al., "Mitochondrial genome polymorphisms associated with type-2 diabetes or obesity," *Mitochondrion*, vol. 5, no. 1, pp. 15–33, 2005.

[23] M. Tanaka, N. Fuku, Y. Nishigaki et al., "Women with mitochondrial haplogroup N9a are protected against metabolic syndrome," *Diabetes*, vol. 56, no. 2, pp. 518–521, 2007.

[24] G. Marchesini, N. Melchionda, G. Apolone et al., "The metabolic syndrome in treatment-seeking obese persons," *Metabolism*, vol. 53, no. 4, pp. 435–440, 2004.

[25] M. Fernández-Caggiano, J. Barallobre-Barreiro, I. Rego-Pérez et al., "Mitochondrial haplogroups H and J: risk and protective factors for ischemic cardiomyopathy," *PLoS One*, vol. 7, no. 8, Article ID e44128, 2012.

[26] M. G. Castro, C. Huerta, J. R. Reguero et al., "Mitochondrial DNA haplogroups in Spanish patients with hypertrophic cardiomyopathy," *International Journal of Cardiology*, vol. 112, no. 2, pp. 202–206, 2006.

[27] T. Amo, N. Yadava, R. Oh, D. G. Nicholls, and M. D. Brand, "Experimental assessment of bioenergetic differences caused by the common European mitochondrial DNA haplogroups H and T," *Gene*, vol. 411, no. 1-2, pp. 69–76, 2008.

[28] A. Gómez-Durán, D. Pacheu-Grau, E. López-Gallardo et al., "Unmasking the causes of multifactorial disorders: OXPHOS differences between mitochondrial haplogroups," *Human Molecular Genetics*, vol. 19, no. 17, pp. 3343–3353, 2010.

International Journal of Obesity (2013), 1–4

www.nature.com/ijo

SHORT COMMUNICATION

Characterization and predicted role of the microRNA expression profile in amnion from obese pregnant women

C Nardelli[1,2,6], L Iaffaldano[1,2,6], M Ferrigno[2], G Labruna[3], GM Maruotti[4], F Quaglia[4], V Capobianco[1,2], R Di Noto[1,2], L Del Vecchio[1,2], P Martinelli[4], L Pastore[1,2] and L Sacchetti[5]

Maternal obesity and nutrient excess *in utero* increase the risk of future metabolic diseases. The mechanisms underlying this process are poorly understood, but probably include genetic, epigenetic alterations and changes in fetal nutrient supply. We have studied the microRNA (miRNA) expression profile in amnion from obese and control women at delivery to investigate if a specific miRNA signature is associated with obesity. The expression profile of 365 human miRNAs was evaluated with the TaqMan Array in amnion from 10 obese and 5 control (prepregnancy body mass index (BMI) >30 and $<25\,kg\,m^{-2}$, respectively) women at delivery. Target genes and miRNA-regulated pathways were predicted by bioinformatics. Anthropometric and biochemical parameters were also measured in mothers and newborns. Seven miRNAs were expressed only in obese women (miR-422b, miR-219, miR-575, miR-523, miR-579, miR-618 and miR-659), whereas 13 miRNAs were expressed at a higher level and 12 miRNAs at a lower level in obese women than in controls. MicroRNAs significantly downregulated the neurotrophin, cancer/ErbB, mammalian target of rapamycin, insulin, adipocytokine, actin cytoskeleton and mitogen-activated protein kinase signaling pathways. In conclusion, we show that the miRNA profile is altered in amnion during obesity and hypothesize that this could affect pathways important for placental growth and function, thereby contributing to an increase in the newborn's risk of future metabolic diseases.

International Journal of Obesity advance online publication, 30 July 2013; doi:10.1038/ijo.2013.121

Keywords: pregnancy; miRNA; pathway

INTRODUCTION

Maternal obesity and nutrient excess *in utero* increase the risk of future metabolic diseases.[1] The mechanisms underlying this process are poorly understood, but probably include genetic, epigenetic alterations and changes in fetal nutrient supply.[1] Placenta, and particularly amnion, is the *in utero* environment that could modify fetal growth and adiposity by exerting stimulatory or inhibitory effects on fetal genome expression.[1] Examples of epigenetic mechanisms are DNA methylation, histone modifications and microRNAs (miRNAs),[1] the latter being a class of endogenous non-coding RNA molecules (18–25 nucleotides long) that exert tissue-specific regulation in a variety of biological and pathological processes.[2] The expression of placental miRNAs is altered during pregnancy in such pathological conditions as preeclampsia, small-for-gestational-age newborns[3] and fetal congenital heart defects,[4] but their role in obesity has not yet been investigated. We previously reported that miRNAs were implicated in the deregulation of metabolic pathways in subcutaneous and visceral adipose tissues in obese adults.[5,6] The aim of this study was to analyze the miRNA expression profile in amnion from obese and control women at delivery to determine if a specific miRNA signature could be associated with obesity.

MATERIALS AND METHODS

Patients and samples collection

Fifteen Caucasian pregnant women (5 controls and 10 obese subjects of a similar age (mean/s.e.m.: 29/1.3 and 31.1/1.0 years, $P=$ NS, respectively) and prepregnancy body mass index (BMI) (mean/s.e.m.: 22.8/1.4 and 38.7/1.4 $kg\,m^{-2}$, respectively)) were consecutively enrolled at the Dipartimento Neuroscienze/Scienze Riproduttive/Odontostomatologiche (University of Naples Federico II). The exclusion criteria were neoplasia, viral infection, diabetes and drug assumption. One maternal blood sample and one cord blood sample were collected at delivery. Sera and cord plasma were obtained and stored at $-80\,^{\circ}C$ until required for the measurement of biochemical parameters and leptin/adiponectin concentrations by routine methods and immunoassay (Bio-Rad, Hemel Hempstead, Herts, UK), respectively.

The term placentas, collected at delivery by cesarean section, were processed immediately. The maternal decidua was removed, the amnion was first manually separated from the chorion, washed in phosphate-buffered saline (Sigma-Aldrich, St Louis, MO, USA), mechanically minced into small pieces and immediately cryopreserved in liquid nitrogen. The newborn's weight, length, head circumference and Appearance-Pulse-Grimace-Activity-Respiration score (Apgar 1 and 5 min) were recorded at birth. All patients and controls gave their informed consent to the study and both parents gave consent for their newborns. The study was performed according to the Helsinki II Declaration and was approved by the Ethics Committee of our Faculty.

[1]Dipartimento di Medicina Molecolare e Biotecnologie Mediche, Università degli Studi di Napoli Federico II, Naples, Italy; [2]CEINGE-Biotecnologie Avanzate SCa RL, Naples, Italy; [3]IRCCS Fondazione SDN—Istituto di Ricerca Diagnostica e Nucleare, Naples, Italy; [4]Dipartimento di Neuroscienze e Scienze Riproduttive ed Odontostomatologiche, Naples, Italy and [5]Laboratori misti, IRCCS Fondazione SDN—CEINGE, CEINGE—Biotecnologie Avanzate, Naples, Italy. Correspondence: Professor L Sacchetti, Laboratori misti, IRCCS Fondazione SDN—CEINGE, CEINGE—Biotecnologie Avanzate, Via E Gianturco 113, 80143 Naples, Italy.
E-mail: lucia.sacchetti@unina.it
[6]These authors contributed equally to this work.
Received 19 April 2013; revised 7 June 2013; accepted 26 June 2013; accepted article preview online 2 July 2013

RNA isolation

Total RNA (including miRNAs) was purified from amnion (mirVana miRNA Isolation Kit; Ambion, Austin, TX, USA) and quantified by NanoDrop ND-1000 UV–Vis spectrophotometer (Thermo Fisher Scientific, Wilmington, DE, USA).

MiRNAs detection

We studied the miRNA profiles by the TaqMan low-density arrays human MicroRNA Panel v.1.0 (Applied Biosystems, Foster City, CA, USA) that contains 365 preloaded miRNAs and two endogenous controls (RNU48 and RNU44). We used 640 ng of total RNA for reverse transcription. Reverse transcription–polymerase chain reaction was performed using the 7900 HT Real-Time PCR System (Applied Biosystems). The miRNA expression values were normalized to RNU48 and to RNA isolated from controls as calibrator; relative expression values were obtained using the ΔΔCt method (relative quantification, $RQ = 2^{-\Delta\Delta Ct}$) by sequence detection system v.2.3 and RQ Manager 1.2 software (Applied Biosystems). To normalize our miRNA data further and to minimize interindividual variability, we considered the miRNAs whose mean RQ levels were <0.5 (downexpressed) or >2.0 (upexpressed) in 70% of the obese vs control women to be expressed differently. The expression levels of selected miRNAs (miR-422b, miR-23b, miR-338, miR-449b and miR-139) were also validated by single TaqMan miRNA assay (Applied Biosystems) in accordance with the manufacturer's instructions on the 7900 HT Real-Time PCR System.

Bioinformatic analysis

TargetScan Release 6.2 algorithm (http://www.targetscan.org) and the KEGG database (http://www.genome.ad.jp/kegg/) were used to predict biological targets of miRNAs and to select biological pathways, respectively.

Statistical analysis

All variables were expressed as mean and s.e.m. Student's *t*-test was used to compare groups and *P*-values <0.05 were considered statistically significant. Statistical analyses were carried out with the PASW Statistics (v. 18; SPSS Headquarters, Chicago, IL, USA).

RESULTS

Obese and control women differed in weight gain (mean/s.e.m.: 7.6/1.0 and 15.0/2.6 kg) and total cholesterol levels (mean/s.e.m.: 5.8/0.4 and 7.3/0.2 mmol l^{-1}), which were significantly lower ($P = 0.008$ and 0.016) in obese women than in controls. In addition, levels of triglycerides (mean/s.e.m.: 3.1/0.2 and 2.4/0.3 mmol l^{-1}, $P = 0.048$) and leptin (mean/s.e.m.: 47.7/10.4 and 12.4/3.9 ng ml^{-1}, $P = 0.010$) were significantly higher in obese women than in controls.

Newborns of obese and control women showed similar birth weight (mean/s.e.m.: 3.268/0.374 and 3.340/0.190 kg), length (mean/s.e.m.: 50.4/1.1 and 50.4/0.7 cm), head circumference (mean/s.e.m.: 33.9/0.7 and 34.5/0.7 cm) and Apgar scores (mean/s.e.m. (1–5 min): 7.3/0.4–8.5/0.2 and 8.0/0.3–8.8/0.2), respectively. Cord plasma adiponectin levels were significantly lower in newborns of obese women than in newborns of controls (mean/s.e.m.: 47.0/7.7 and 107.9/18.9 μg ml^{-1}, respectively, $P = 0.004$), whereas cord plasma leptin levels did not differ between the two groups.

A large percentage of the tested miRNAs, about 74% (271/365), was expressed in amnion, whereas 26% (94/365) was not. Most of the expressed miRNAs (90%, 243/271) did not differ between obese women and controls and were not further investigated. Conversely, 4.8% of miRNAs (13/271) were higher (Figure 1a) and 4.4% (12/271) were lower (Figure 1b) in obese women than in controls. Interestingly, 7/271 miRNAs (miR-422b, miR-219, miR-575, miR-523, miR-579, miR-618 and miR-659) were obesity-specific, being expressed only in amnion from obese women. Bioinformatics showed that miRNAs had a significant probability ($P < 0.01$) of deregulating several genes and metabolic pathways (Figures 1c, d and 2).

The expression levels of several miRNAs were further validated by quantitative real-time polymerase chain reaction and, except for slight differences because of the two different methodologies,

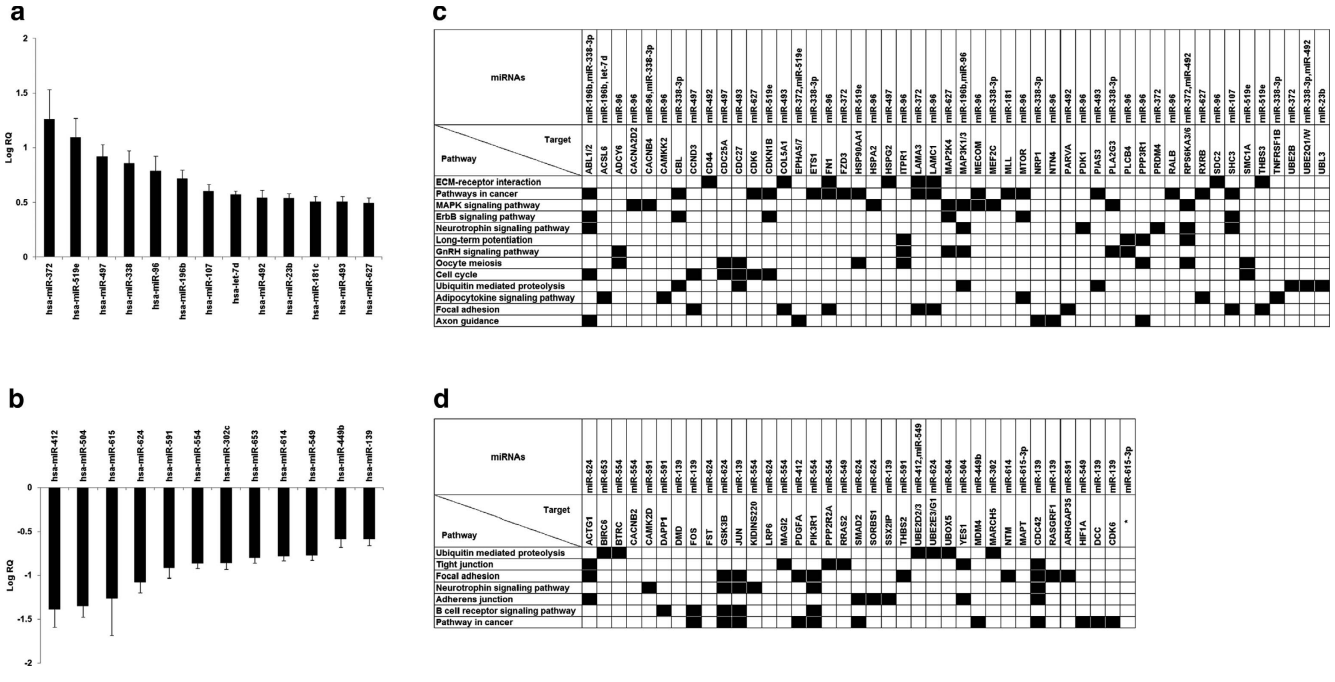

Figure 1. Differently expressed miRNAs in amnion from obese and control women. Panels (**a**) and (**b**) depict miRNAs upexpressed (13/271) and downexpressed (12/271), respectively. miRNA expression levels are shown as Log RQ mean and s.e.m. (The miRNA expression values were first normalized to RNU48, after which, the relative quantification was calculated as: $RQ = 2^{-\Delta\Delta Ct}$, where $\Delta\Delta Ct = (Ct_{obese}$ (miRNA) $- Ct_{obese}$ (RNU48)) $- (Ct_{calibrator}$ (miRNA) $- Ct_{calibrator}$ (RNU48))). Panels (**c**) and (**d**) show metabolic pathways (black squares) and genes targeted by miRNAs ($P < 0.01$) upexpressed and downexpressed, respectively. *Pathways significantly regulated by target genes of miR-615-3p were not reported by TargetScan.

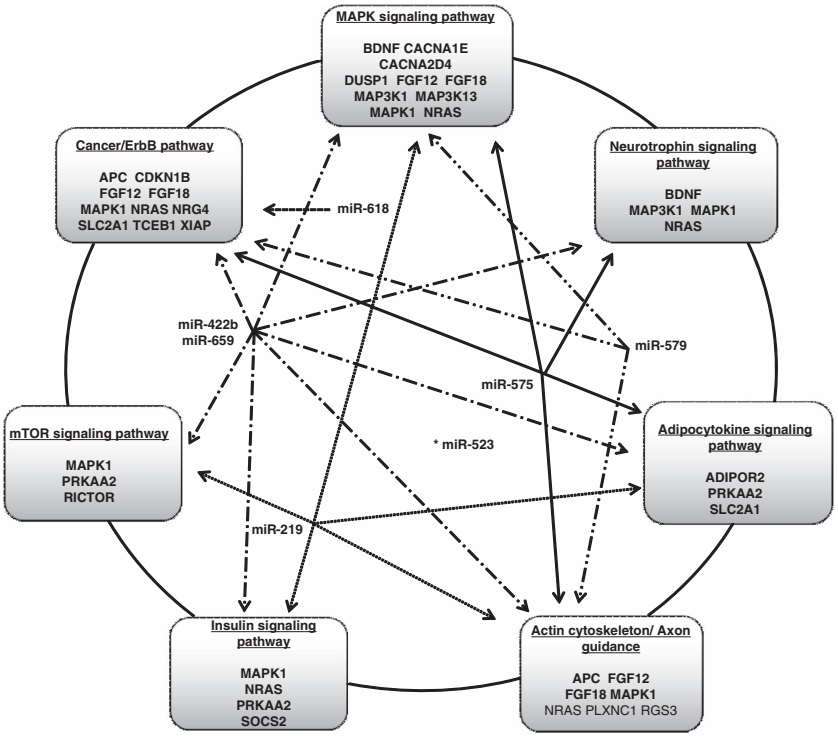

Figure 2. Pathways and genes predicted by bioinformatics to be regulated by obesity-specific miRNAs in the amnion. In boxes are reported the metabolic pathways and genes targeted by obesity-specific miRNAs (miR-422b, miR-219, miR-575, miR-579, miR-618 and miR-659) ($P < 0.01$). The arrows connect miRNAs to target genes in each pathway. *Conserved target genes of miR-523 were not predicted by TargetScan.

they were in close agreement with those obtained with TaqMan array (mean RQ values in obese vs control: miR-422b = 6.4; miR-23b = 1.19; miR-338 = 1.25; miR-139 = 0.68; miR-449b = 0.9).

DISCUSSION

It is now recognized that epigenetic modifications of the fetal genome contribute to disease development in adults.[7] Here, we show that miRNAs regulate gene expression in the amnion during obesity. In particular, we found that 25 miRNAs are differently expressed in obese with respect to control women, and have identified seven obesity-specific miRNAs.

Our differently expressed placental miRNAs include miRNAs previously associated with endometriosis (miR-196b, let-7d and miR-107),[8] preeclampsia (miR-181 and let-7d),[9,10] cancer (miR-422b)[11] or identified in sera from normal pregnancies (miR-23b, miR-372 and miR-519e).[12,13] The predicted target genes of our miRNAs belong to pathways potentially important for placental development and/or functions. In fact, the neurotrophin pathway was regulated by three obesity-specific miRNAs (miR-422b, miR-659 and miR-575), six miRNAs upexpressed (miR-196b, miR-96, miR-338-3p, miR-372, miR-492 and miR-107) and four miRNAs downexpressed (miR-591, miR-139, miR-624 and miR-554). The brain-derived neurotrophic factor was recently implicated in placental development and fetal growth in mice[14] and its placental expression was increased in intrauterine growth restriction and decreased in maternal type 1 diabetes.[14]

Obesity-specific miRNAs (miR-422b, miR-659 and miR-219) also downregulated the mammalian target of rapamycin (mTOR) and the insulin signaling pathways. mTOR is highly expressed in syncytiotrophoblasts of the human placenta and exists as two complexes with distinct regulation and function based on its association with accessory proteins: raptor in Complex 1 (mTORC1) and rictor in Complex 2 (mTORC2).[15] A multitude of upstream regulators of mTORC1, including insulin, cellular energy and oxygen levels, could affect placental size and modulate fetal growth by regulating placental nutrient transporter function.[15] Conversely, mTORC2 is involved in lipid metabolism; in fact, in *C. elegans* loss of rictor function causes developmental delay, reduced size and reproduction, and increased fat accumulation.[16] Here, we highlight a new potential mechanism based on miRNA downregulation of mTOR that could impact on fetal growth during obesity. Mammalian mTORC2 controls the actin cytoskeleton organization, as shown by the finding that its knockdown prevents actin polymerization.[17] The cytoskeleton has a crucial role in basic cellular processes and in decidualization,[18] and the downregulation of placenta actin cytoskeleton signaling was observed in preeclampsia.[19] In our study, the actin cytoskeleton pathway was predicted to be downregulated by obesity-specific miR-422b, miR-659, miR-575 and miR-579, which indicates that the placental structural organization and function are also altered in human obesity.

We also found that adiponectin levels were higher in umbilical cord plasma than in the mother's serum, and lower in obese than in control samples, in agreement with a previous report.[20] Hypoadiponectinemia might have a role in placental development and in pregnancy-related complications,[20] and also through p38 mitogen-activated protein kinase signaling activation. In this study, both the adipocytokine and mitogen-activated protein kinase signaling pathways were downregulated by obesity-specific miR-422b, miR-659, miR-579, miR-575 and miR-219, which supports the concept that epigenetic regulation of placental adiponectin and of its signaling could be involved in the pathophysiology of obesity during pregnancy.

In conclusion, we show that the miRNA profile is altered in amnion during obesity and hypothesize that this could affect pathways important for placental growth and function, thereby contributing to an increase in the newborn's risk of future metabolic diseases.

CONFLICT OF INTEREST

The authors declare no conflict of interest.

ACKNOWLEDGEMENTS

This work was supported by grants from CEINGE Regione Campania (DGRC 1901/2009), IRCCS Fondazione SDN, Ministry of Health and POR Campania FSE 2007–2013 and Project CREME. We thank Jean Ann Gilder (Scientific Communication srl, Naples, Italy) for revising and editing the manuscript.

REFERENCES

1 Lillycrop KA, Burdge GC. Epigenetic changes in early life and future risk of obesity. *Int J Obes* 2011; **35**: 72–83.
2 Heneghan HM, Miller N, Kerin MJ. Role of microRNAs in obesity and the metabolic syndrome. *Obes Rev* 2010; **11**: 354–361.
3 Pineles BL, Romero R, Montenegro D, Tarca AL, Han YM, Kim YM *et al.* Distinct subsets of microRNAs are expressed differentially in the human placentas of patients with preeclampsia. *Am J Obstet Gynecol* 2007; **196**: e1–261.e6.
4 Yu Z, Han S, Hu P, Zhu C, Wang X, Qian L *et al.* Potential role of maternal serum microRNAs as a biomarker for fetal congenital heart defects. *Med Hypotheses* 2011; **76**: 424–426.
5 Martinelli R, Nardelli C, Pilone V, Buonomo T, Liguori R, Castanò I *et al.* miR-519d overexpression is associated with human obesity. *Obesity (Silver Spring, MD)* 2010; **18**: 2170–2176.
6 Capobianco V, Nardelli C, Ferrigno M, laffaldano L, Pilone V, Forestieri P *et al.* miRNA and protein expression profiles of visceral adipose tissue reveal miR-141/YWHAG and miR-520e/RAB11A as two potential miRNA/protein target pairs associated with severe obesity. *J Proteome Res* 2012; **11**: 3358–3369.
7 Fowden AL, Forhead AJ, Coan PM, Burton GJ. The placenta and intrauterine programming. *J Neuroendocrinol* 2008; **20**: 439–450.
8 Hawkins SM, Creighton CJ, Han DY, Zariff A, Anderson ML, Gunaratne PH *et al.* Functional microRNA involved in endometriosis. *Mol Endocrinol* 2011; **25**: 821–832.
9 Mayor-Lynn K, Toloubeydokhti T, Cruz AC, Chegini N. Expression profile of microRNAs and mRNAs in human placentas from pregnancies complicated by preeclampsia and preterm labor. *Reprod Sci* 2011; **18**: 46–56.
10 Yang Q, Lu J, Wang S, Li H, Ge Q, Lu Z. Application of next-generation sequencing technology to profile the circulating microRNAs in the serum of preeclampsia versus normal pregnant women. *Clin Chim Acta* 2011; **412**: 2167–2173.
11 Lee CH, Subramanian S, Beck AH, Espinosa I, Senz J, Zhu SX *et al.* MicroRNA profiling of BRCA1/2 mutation-carrying and non-mutation-carrying high-grade serous carcinomas of ovary. *PLoS One* 2009; **4**: e7314.
12 Li H, Guo L, Wu Q, Lu J, Ge Q, Lu Z. A comprehensive survey of maternal plasma miRNAs expression profiles using high-throughput sequencing. *Clin Chim Acta* 2012; **413**: 568–576.
13 Kotlabova K, Doucha J, Hromadnikova I. Placental-specific microRNA in maternal circulation—identification of appropriate pregnancy-associated microRNAs with diagnostic potential. *J Reprod Immunol* 2011; **89**: 185–191.
14 Mayeur S, Silhol M, Moitrot E, Barbaux S, Breton C, Gabory A *et al.* Placental BDNF/TrkB signaling system is modulated by fetal growth disturbances in rat and human. *Placenta* 2010; **31**: 785–791.
15 Jansson T, ILMH Aye, DCI Goberdhan. The emerging role of mTORC1 signaling in placental nutrient-sensing. *Placenta* 2012; **33**(Suppl 2): e23–e29.
16 Jones KT, Greer ER, Pearce D, Ashrafi K. Rictor/TORC2 regulates *Caenorhabditis elegans* fat storage, body size, and development through sgk-1. *PLoS Biol* 2009; **7**: e60.
17 Jacinto E, Loewith R, Schmidt A, Lin S, Rüegg MA, Hall A *et al.* Mammalian TOR complex 2 controls the actin cytoskeleton and is rapamycin insensitive. *Nat Cell Biol* 2004; **6**: 1122–1128.
18 Ihnatovych I, Livak M, Reed J, de Lanerolle P, Strakova Z. Manipulating actin dynamics affects human *in vitro* decidualization. *Biol Reprod* 2009; **81**: 222–230.
19 Kang JH, Song H, Yoon JA, Park DY, Kim SH, Lee KJ *et al.* Preeclampsia leads to dysregulation of various signaling pathways in placenta. *J Hypertens* 2011; **29**: 928–936.
20 Palin MF, Bordignon VV, Murphy BD. Adiponectin and the control of female reproductive functions. *Vitam Horm* 2012; **90**: 239–287.

STEM CELLS AND DEVELOPMENT
Volume 22, Number 16, 2013

DOI: 10.1089/scd.2012.0499

High Aminopeptidase N/CD13 Levels Characterize Human Amniotic Mesenchymal Stem Cells and Drive Their Increased Adipogenic Potential in Obese Women

Laura Iaffaldano,[1,2,*] Carmela Nardelli,[1,2,*] Maddalena Raia,[1] Elisabetta Mariotti,[1] Maddalena Ferrigno,[1] Filomena Quaglia,[3] Giuseppe Labruna,[4] Valentina Capobianco,[1,2] Angela Capone,[3] Giuseppe Maria Maruotti,[3] Lucio Pastore,[1,2] Rosa Di Noto,[1,2] Pasquale Martinelli,[3] Lucia Sacchetti,[1,2] and Luigi Del Vecchio[1,2]

Maternal obesity is associated to increased fetal risk of obesity and other metabolic diseases. Human amniotic mesenchymal stem cells (hA-MSCs) have not been characterized in obese women. The aim of this study was to isolate and compare hA-MSC immunophenotypes from obese (Ob-) and normal weight control (Co-) women, to identify alterations possibly predisposing the fetus to obesity. We enrolled 16 Ob- and 7 Co-women at delivery (mean/SEM prepregnancy body mass index: 40.3/1.8 and 22.4/1.0 kg/m^2, respectively), and 32 not pregnant women. hA-MSCs were phenotyped by flow cytometry; several maternal and newborn clinical and biochemical parameters were also measured. The expression of membrane antigen CD13 was higher on Ob-hA-MSCs than on Co-hA-MSCs ($P < 0.005$). Also, serum levels of CD13 at delivery were higher in Ob- versus Co-pregnant women and correlated with CD13 antigen expression on Ob-hA-MSCs ($r^2 = 0.84$, $P < 0.0001$). Adipogenesis induction experiments revealed that Ob-hA-MSCs had a higher adipogenic potential than Co-hA-MSCs as witnessed by higher peroxisome proliferator-activated receptor gamma and aP2 mRNA levels ($P < 0.05$ and $P < 0.05$, respectively), at postinduction day 14 associated with increased CD13 mRNA levels from baseline to day 4 postinduction ($P < 0.05$). Adipogenesis was similar in the two sets of hA-MSCs after CD13 silencing, whereas it was increased in Co-hA-MSCs after CD13 overexpression. CD13 expression was high also in Ob-h-MSCs from umbilical cords or visceral adipose tissue of not pregnant women. In conclusion, antigen CD13, by influencing the adipogenic potential of hA-MSCs, could be an in utero risk factor for obesity. Our data strengthen the hypothesis that high levels of serum and MSC CD13 are obesity markers.

Introduction

The increase in the incidence of obesity in pregnant women in the last two decades has paralleled that observed in the general population [1–3]. Although maternal fat stores increase in all pregnant women, irrespective of prepregnancy weight [4], the storage capacity of subcutaneous adipose tissue is impaired, and fat predominantly accumulates in the visceral adipose tissue (VAT) in obeses [5]. VAT is an important risk factor for metabolic imbalance in human subjects, also during pregnancy [6–8]. In fact, maternal obesity is related to offspring obesity [9], and there is an increased risk of adverse outcomes for both mother and child [10–13]. Moreover, the risk of childhood obesity was quadrupled if the mother was obese before pregnancy [14], which suggests that the in utero environment is obesogenic. In mammals, the placenta is the main interface between the fetus and the mother; it regulates intrauterine development and modulates adaptive responses to suboptimal in utero conditions [15,16].

Placenta is also an important source of stem/progenitor cells [17–19]. In particular, human amniotic mesenchymal stem cells (hA-MSCs) have been shown to differentiate into cell types of mesenchymal origin such as chondrocytes, adipocytes, and osteocytes [20–22]. The phenotype of hA-MSCs from normal pregnant women has been characterized and found to differ in terms of cytokine expression from that of pregnant women affected by pre-eclampsia [23].

[1]CEINGE-Biotecnologie Avanzate S.C.a R.L., Naples, Italy.
[2]Dipartimento di Medicina Molecolare e Biotecnologie Mediche, Università degli Studi di Napoli Federico II, Naples, Italy.
[3]Dipartimento di Neuroscienze e Scienze Riproduttive ed Odontostomatologiche, Naples, Italy.
[4]Fondazione IRCCS SDN–Istituto di Ricerca Diagnostica e Nucleare, Naples, Italy.
*These two authors contributed equally to this work.

Thus far, little is known about hA-MSCs from obese women.

The aim of this study was to characterize hA-MSCs from term placenta of obese (Ob-) women and to test their adipogenic potential with respect to that of normal weight control (Co-) women. We also measured several maternal and newborn clinical and biochemical parameters, and looked for correlations between these parameters with the hA-MSC immunophenotype. We found that the Ob-hA-MSC immunophenotype was characterized by increased expression levels of the CD13 surface antigen that correlated with maternal CD13 serum levels. Adipogenesis was higher in Ob-hA-MSCs than in Co-hA-MSCs, and returned to the control value after CD13 silencing. On the other hand, CD13 overexpression increased the adipogenic potential of Co-hA-MSCs. Our findings suggest that CD13 could contribute to obesity programming in the fetus and indicate that maternal serum CD13 is an obesity risk marker.

Materials and Methods

Patients and controls

Sixteen Ob- (age range: 26–39 years) and seven Co-pregnant women, (age range: 26–38 years), prepregnancy body mass index (BMI) (mean/SEM) 40.3/1.8 and 22.4/1.0 kg/m^2, respectively, and thirty-two not pregnant women (16 obese and 16 normal weight, BMI > 30 kg/m^2 and < 25 kg/m^2, respectively), were recruited at the Dipartimento di Neuroscienze e Scienze Riproduttive ed Odontostomatologiche, University of Naples "Federico II." The clinical, personal, and family history of the 23 women was recorded during a medical interview conducted by an expert upon hospitalization. Data relative to each pregnancy follow-up and delivery were also recorded. The general characteristics of the newborn and clinical data (birth weight, length, head circumference, Apgar score) were recorded at birth.

Sample collection

Two fasting peripheral blood samples were collected in the morning from not pregnant women and from Ob- and Co-pregnant women, immediately before delivery. One sample was used for DNA extraction, whereas the other was centrifuged at 2,500 rpm for 15 min and serum was stored at −80°C until further processing. At delivery, placentas were collected by the C-section from each enrolled woman and immediately processed. Bioptic samples of VAT were also collected from not pregnant obese and control women during obstetric surgery (ovarian cysts). All patients and controls gave their informed consent to the study and both parents gave consent for their newborns. The study was performed according to the Helsinki II Declaration and was approved by the Ethics Committee of our Faculty.

Biochemical evaluations

The main serum biochemical parameters were evaluated by routine assays. Leptin and adiponectin were measured in maternal serum with Luminex xMAP Technology on a BioRad Multiplex Suspension Array System (Bio-Rad), according to the manufacturer's instructions. The ratio leptin/adiponectin (L/A) was also calculated.

Aminopeptidase N/CD13 ELISA assay

Aminopeptidase N (APN)/CD13 serum levels were measured by ELISA (Life Science). Briefly, the microtiter plate was precoated with a specific anti-CD13 antibody. Standards or samples were then added to the appropriate microtiter plate wells with a biotin-conjugated polyclonal antibody preparation specific for CD13. Next, avidin conjugated to horseradish peroxidase was added to each microplate well and incubated for 15 min at room temperature. A TMB substrate solution (3,3′,5,5′-tetramethylbenzidine) was then added to each well. The enzyme-substrate reaction was terminated by the addition of a sulfuric acid solution and the color change was measured spectrophotometrically at a wavelength of 450 nm. The amount of CD13 in each sample was determined by comparing the absorbance of the sample to a standard curve.

Cell isolation from placenta tissue

Placentas were collected and immediately processed, according to Parolini et al. [24]. After removal of the maternal decidua, the amnion was manually separated from the chorion and extensively washed 5 times in 40 mL of phosphate-buffered saline (PBS) containing 100 U/mL penicillin, 100 μg/mL streptomycin, and 250 μg/mL amphotericin B (all from Sigma-Aldrich), after which, it was mechanically minced into small pieces [24]. Amnion fragments were digested overnight at 4°C in the ACCUMAX® reagent (Innovative Cell Technology), a combination of DNase, protease, and collagenolytic enzymes [25], containing 100 U/mL penicillin, 100 μg/mL streptomycin, and 250 μg/mL amphotericin B. The next day, digestion enzymes were inactivated with a complete culture medium constituted by the low-glucose DMEM (Sigma-Aldrich) supplemented with 10% of heat-inactivated bovine serum (FBS), 1% of nonessential amino acids, and 2% of ultraglutamine (all from Lonza). After centrifugation at 300 *g* for 10 min, cell pellets and digested tissue fragments were seeded in a cell culture dish (BD Falcon) in the complete culture medium and incubated at 37°C in 5% CO_2. One week later, digested tissue pieces were removed from the dish and discarded, and isolated cells formed distinct fibroblast colony-forming units. When the colonies reached 70% confluence, they were washed with PBS and detached with trypsin/EDTA (Sigma-Aldrich), counted, and reseeded in the complete medium for expansion at a concentration of about 5,000/cm^2 [24].

Cell preparation

hA-MSCs were expanded for several passages. The absence of mycoplasma contamination was assessed as described previously [26]. The population doubling level was calculated for each subcultivation with the following equation: population doubling = $[\log_{10}(N_H) - \log_{10}(N_I)]/\log_{10}(2)$, where N_I is the cell inoculum number and N_H is the cell harvest number [27]. The increase in population doubling was added to the population doubling levels of the previous passages to yield the cumulative population doubling level. When 70%–80% confluent cultures reached about 4 population doublings, they were detached with trypsin/EDTA, resuspended in PBS with 10% FBS, and processed for flow cytometry, DNA, and RNA extraction. Cellular viability was

Table 1. Surface Immunophenotypic Profile Investigated in Human Amniotic Mesenchymal Stem Cells by Flow Cytometry

Fluorochrome	*CD antigen*	*Other names*	*Molecular weight (kDa)*	*Cell expression*	*Function*
FITC	CD9	Tspan-29	24–26	Platelets, pre-B cells, activated T cells	Adhesion, migration, platelet activation
APC	CD10	CALLA	100	B/T precursors, stromal cells	Endopeptidase
PE	CD13	APN	150	Granulocytes, monocytes and their precursors, endothelial cells, epithelial cells, mesenchymal stem cells	Metalloproteinase
PE	CD14	LPS-R	53–55	Monocytes, macrophages	Receptor for LPS/LPB complex
APC	CD15	Lewis X	_	Granulocyte, monocyte, epithelial cells	Cell adhesion
PE	CD16	FCγRIIIa	50–65	Neutrophils, NK, macrophages	Low affinity with FCγ receptor, mediates phagocytosis
APC	CD19	Bgp95	95	B cells, not on plasma cells	Signal transduction
FITC	CD26	DPP IV	110	Mature thymocytes, T, B, NK cells	Exoprotease, costimulation
APC	CD28	Tp44	44	Most T cells, thymocytes, NK and plasma cells	Costimulation
APC	CD29	VLA β1-chain	130	T, B, granulocytes, monocytes, fibroblasts, endothelial cells, NKs, platelet	Adhesion activation, embryogenesis, and development
FITC	CD31	ECAM-1	130–140	Monocytes, platelets, granulocytes, and endothelial cells	Cell adhesion
APC	CD33	My9	67	Monocytes, granulocytes, mastocytes, and myeloid progenitors	Cell adhesion
APC	CD34	My10	105–120	Hematopoietic stem cells and progenitors, endothelial cells	Cell adhesion
APC	CD36	Platelet GPIV	85	Platelets, monocytes, macrophages, endothelial cells, erythroid precursors	Adhesion and phagocytosis
FITC	CD40	Bp50	48	Monocytes, macrophages, B cells, endothelial cells, fibroblasts, keratinocytes	Costimulation to B cells, growth, differentiation, and isotype switching
APC	CD44	H-CAM	90	Leukocytes, erythrocytes, and epithelial cells	Rolling, homing, and aggregation
Per Cp	CD45	LCA	180–220	Hematopoietic cells, except erythrocytes and platelets	Critical for T and B cell receptor-mediated activation
FITC	CD47	IAP I	50–55	Hematopoietic, epithelial, endothelial, and brain mesenchymal cells	Adhesion
FITC	CD49d	VLA-4	150	B cells, T cells, monocytes, eosinophils, basophils, NKs, dendritic cells	Adhesion, migration, homing, activation
APC	CD54	ICAM-1	80–114	Epithelial and endothelial cells monocytes. Low on resting lymphocytes, upregulate on activated	T cell activation
PE	CD56	NCAM	175–220	Neural, tumors, embryonic tissue, NK	Homophilic and heterophilic adhesion
PE	CD58	LFA-3	40–70	Leucocytes, erythrocytes, epithelial endothelial cells, and fibroblasts	Costimulation
FITC	CD71	Transferrin recepor	95	Reticulocytes, erythroid precursor	Controls iron intake during cell proliferation
APC	CD81	TAPA-1	26	B and T cells, monocytes, endothelial cells	Signal transduction

(*continued*)

Table 1. (Continued)

Fluorochrome	CD antigen	Other names	Molecular weight (kDa)	Cell expression	Function
FITC	CD90	Thy-1	25–35	Hematopoietic stem cells, neurons, mesenchymal stem cells	Inhibition of hematopoietic stem cells and neuron differentiation
PE	CD99	MIC2	32	Leucocyte, NK, monocytes, endothelial and epithelial cells	Leucocyte migration, T cell activation, cell adhesion
PE	CD105	Endoglin	90	Endothelial and mesenchymal stem cells, erythroid precursors, monocytes	Angiogenesis, modulates cellular response to TGFβ1
PE	CD117	c-kit	145	Hematopoietic stem cells and progenitors	Crucial for hematopoietic stem cells
PE	CD133	Prominin-1	120	Hematopoietic stem cell, endothelial, epithelial, and neural precursors	Unknown function, stem cell marker
PE	CD151	PETA-3	32	Endothelial and epithelial cells, megakaryocytes, platelets	Adhesion
PE	CD166	ALCAM	100–105	Neurons, activated T cells, epithelial cells, mesenchymal stem cells	Adhesion, T cell activation
PE	CD200	OX-2	33	B cells, activated T cells, thymocytes, neurons, endothelium	Downregulatory signal for myeloid cell functions
FITC	CD243	MDR-1	170	Stem cells, multidrug-resistant tumors	Influences the uptake, distribution, elimination of drugs
APC	CD271	NGFR	75	Neurons, stromal and dendritic follicular cells	Low affinity for NGF receptor
APC	CD324	E-cadherin	120	Epithelial, keratinocytes, platelet	Adhesion, growth, differentiation
APC	CD338	ABCG-2	72	Hematopoietic stem cells, liver, kidney, intestine, side population of stem cells	Absorption and excretion of xenobiotics
FITC	HLA-ABC	Class I MHC	46	All nucleated cells and platelets	Antigen presentation
FITC	HLA-DR	Class II MHC	30	B cells, monocytes, myeloid progenitors, activated T and dendritic cells	Antigen presentation

assessed by both Trypan blue dye exclusion and the analysis of light scatter proprieties in flow cytometry, and it was never lower than 90%.

Using the above cell isolation and preparation procedures, h-MSCs were also isolated from the umbilical cord (hUC-MSCs) of one obese and one control pregnant woman.

Isolation of hVAT-MSCs

Briefly, VAT bioptic samples were washed with PBS containing 100 U/mL penicillin, 100 μg/mL streptomycin, and 250 μg/mL amphotericin B (all from Sigma-Aldrich), minced into small pieces, and digested with 1.5 mg/mL collagenase type I (GIBCO) at 37°C. The digestion enzymes were inactivated with FBS. After centrifugation at 1500 *g* for 5 min, cell pellets and digested tissue fragments were washed and seeded in a cell culture dish (BD Falcon) in the complete culture medium and incubated at 37°C in 5% CO_2. When the colonies reached 60%–70% confluence, they were washed with PBS and detached with trypsin/EDTA (Sigma-Aldrich), counted, and reseeded in the complete medium for expansion at a concentration of about 5,000/cm^2 [28].

DNA typing

The fetal origin of both amnion and hA-MSCs was verified by DNA typing. Genomic DNA was extracted from the mother's peripheral blood, from amnion samples, and from hA-MSCs using the Nucleon BACC2 extraction kit (Illustra DNA Extraction Kit BACC2; GE Healthcare). The DNA concentration was evaluated using the NanoDrop® ND-1000 UV-Vis spectrophotometer (NanoDrop Technologies). Genomic DNA (1 ng) was amplified in a final volume of 25 μL using the AmpFlSTR® Identifiler™ PCR Amplification Kit (Applied Biosystems). The AmpFlSTR Identifiler PCR Amplification Kit is a short tandem repeat (STR) multiplex assay that amplifies 15 repeat loci and the Amelogenin gender determining marker in a single polymerase chain reaction (PCR) amplification using a primer set labeled with four fluorescent molecules. The amplification was performed with the GeneAmp PCR System 9700 (Applied Biosystems) instrument. PCR products were then analyzed by capillary electrophoresis on the ABI Prism 3130 Genetic Analyzer (Applied Biosystems) together with an allelic ladder, which contained all the most common alleles for the analyzed loci

that were present in Caucasian populations and both a negative- and a positive-quality control sample. Typically, 1μL of each sample was diluted in 18.7μL of deionized formamide; each sample was supplemented with 0.3 μL of an internal size standard (LIZ 500 Applied Biosystems) labeled with an additional fluorophore. The samples were denatured at 95°C for 4 min, and then placed in the auto sampler tray (maximum of 96 samples) on the ABI Prism 3130 for automatic injection in the capillaries. The data were analyzed by Gene Mapper Software (Applied Biosystems).

Immunophenotyping of h-MSCs by flow cytometry

We analyzed the expression of 38 hematopoietic, mesenchymal, endothelial, epithelial, and no-lineage membrane antigens on the surface of hA-MSCs, hUC-MSCs, and hVAT-MSCs by four-color flow cytometry (Table 1). The antibody cocktails contained in each tube are detailed in Supplementary Table S1 (Supplementary Data are available online at www.liebertpub.com/scd). All monoclonal antibodies (MoAbs) were from Becton Dickinson (San Jose) except anti-CD338-APC, which was from R&D (Minneapolis), anti-CD-133-PE and anti-CD271-APC MoAbs, which were from Milenyi Biotec (Bergisch Gladbach). For all antibody staining experiments, at least 1×10^5 hA-MSCs isolated from each placenta sample were incubated at 4°C for 20 min with the appropriate amount of MoAbs, washed twice with PBS, and finally analyzed with an unmodified Becton-Dickinson FACSCanto II flow cytometer (Becton-Dickinson), that was set up according to published guidelines [29]. For each sample, the respective control was prepared to determine the level of background cellular autofluorescence without antibody staining.

CaliBRITE beads (Becton-Dickinson, catalog no. 340486) were used as quality controls across the study as described elsewhere [30,31], according to the manufacturer's instructions. Daily control of CaliBRITE intensity showed no change in instrument sensitivity throughout the study. The relative voltage range for each detector was assessed *una tantum* using the eight-peak technology (Rainbow Calibration Particles, Becton-Dickinson, catalog no. 559123) at the beginning of the study.

Compensation was set in the FACS-DiVa (Becton-Dickinson) software, and compensated samples were analyzed. Samples were acquired immediately after staining using the FACSCanto II instrument, and at least 10,000 events were recorded for each monoclonal combination. Levels of CD antigen expression were displayed as median fluorescence intensity (MFI). The FACS-DiVa software (Becton-Dickinson) was used for cytometric analysis.

Differentiation potential toward the adipogenic lineage

hA-MSCs and hVAT-MSCs were cultured in the low-glucose DMEM (Sigma-Aldrich) supplemented with 10% of FBS, 2% of ultraglutamine, and 1% of nonessential amino acids at 37°C in 5% CO_2 (all from Lonza). The cells were passaged twice before the addition of the differentiation medium composed of the DMEM with the addition of 10% FBS, 1 μM dexamethasone, 0.5 mM 3-isobutyl-1-methylxhantine, 200 μM indomethacin, and 10 μg/mL insulin. Media were changed every 2 days and cells were either stained or collected for RNA extraction.

CD13 RNA interference and overexpression

hA-MSCs plated at a density of 5,000 cells/cm^2 were transfected using 20 μL Lipofectamine 2000 according to the manufacturer's instructions (Invitrogen) with 8 μg short hairpin RNAs (shRNAs) expressing plasmids (Open Biosystem) or with an 8 μg pCMV-Sport 6 Vector (Invitrogen), to silence or to overexpress CD13 mRNA, respectively. Transfected cells were induced to differentiate toward the adipogenic lineage up to 4 days.

Effect of interferon-γ on the expression of CD13 on the surface of h-MSCs

The expression of CD13 on the surface of Co- and of Ob-h-MSCs isolated from the amnion, umbilical cord, and VAT was measured after exposure of cells to 0.8 and 12.5 ng/mL interferon (IFN)-γ at 37°C for 24 h, using untreated Co- and Ob-h-MSCs as controls. At the end of incubation, the cells were

Table 2. Clinical and Biochemical Characteristics of Obese and Normal Weight Control Pregnant Women at Delivery and Their Newborns

A

Mother's parameters	*Ob-pregnant women (n = 16)*	*Co-pregnant women (n = 7)*
Age (years)	32.6 (0.9)	30.7 (1.5)
Weight (kg)[a]	110.1 (5.4)	65.2 (3.6)
Height (m)	163.3 (1.6)	169.0 (1.7)
BMI prepregnancy (kg/m^2)[a]	40.3 (1.8)	22.4 (1.0)
Weight gain in pregnancy[b]	8.4 (1.3)	14.3 (1.8)
Systolic blood pressure (mmHg)	124.3 (2.7)	117.1 (5.1)
Diastolic blood pressure (mmHg)[c]	82.5 (2.2)	74.2 (2.0)
Frequency cardiac	79.6 (1.7)	79.0 (3.7)
Gestational age	38.4 (0.3)	38.7 (0.2)
Glucose (mmol/L)	4.3 (0.1)	4.0 (0.3)
Total cholesterol (mmol/L)	6.9 (0.4)	7.3 (0.1)
Triglycerides (mmol/L)	2.8 (0.2)	2.3 (0.3)
AST (U/L)	15[d] (12.2–26.5[d])	14.8 (0.7)
ALT (U/L)	13[d] (9.2–17.7[d])	12.1 (1.1)
ALP (U/L)	124.2 (11.1)	115.0 (12.6)
GGT (U/L)	11.0 (1.7)	8.8 (1.5)
Leptin (L) (ng/mL)[a]	38.5 (2.2)	15.2 (3.3)
Adiponectin (A) (μg/mL)	6.0 (0.7)	7.5 (1.4)
L/A[a]	7.7 (0.6)	2.6 (0.5)

B

Newborn features	*Ob-newborns (n = 16)*	*Co-newborns (n = 7)*
Birth weight (kg)	3162 (0.1)	3401 (0.1)
Length (cm)	49.6 (0.7)	50.8 (0.7)
Head circumference (cm)	34.0 (0.4)	34.8 (0.3)
Apgar 1′	7.0[d] (7.0–8.0[d])	7.8 (0.2)
Apgar 5′	9.0[d] (8.5–9.0[d])	8.7 (0.1)

Data are expressed as mean (SEM) (parametric distributions).
Statistically significant difference at the Student *t* test.
[a]$P < 0.0001$.
[b]$P < 0.05$.
[c]$P < 0.05$.
[d]Median value and 25th–75th percentiles (nonparametric distributions).

harvested by trypsin, washed in PBS, counted, and adjusted to the same concentrations of 1×10^5 h-MSCs. Subsequently, their immunophenotype was examined by flow cytometry.

Adipocyte staining

After 14 days of differentiation, the adipocyte cultures were stained for lipid droplets, which are an index of differentiation. The cells were washed in PBS and fixed in 10% formalin for 1 h. Then, they were washed in PBS and the lipids were stained for 15 min with Oil Red O prepared by mixing vigorously three parts of a stock solution (0.5% Oil Red O in 98% isopropanol) with two parts of water, and then eliminating undissolved particles with a 0.4-μm filter. Cells were then washed with water and the number of adipocytes was evaluated with a microscope. Relative lipid levels were assessed

Table 3. Immunophenotyping of Human Amniotic Mesenchymal Stem Cells Isolated from Obese and Control Pregnant Women

		Ob-hA-MSCs		*Co-hA-MSCs*		
Fluorochrome	*Antigen*	*MFI*	*25th-75th Percentiles*	*MFI*	*25th-75th Percentiles*	*P value*
Not expressed antigens						
FITC	CD31	364.0	278.3–511.3	306.5	286.8–368.0	0.3254
	CD40	444.0	336.5–568.3	388.0	357.0–457.8	0.4824
	CD243	363.0	292.3–528.3	307.5	274.0–378.3	0.2061
	HLA-DR	355.0	283.8–530.0	297.0	272.5–374.8	0.2415
	NC	325.0	250.0–516.3	279.0	218.8–418.8	0.4260
PE	CD14	166.5	125.5–197.8	134.5	124.5–157.8	0.2815
	CD16	36.0	11.5–71.7	65.5	50.5–72.0	0.2407
	CD117	142.5	109.5–189.3	121.0	116.0–176.8	0.6065
	CD133	95.5	80.5–112.8	87.5	76.50–110.5	0.5423
	NC	115.5	91.75–181.5	102.5	93.25–135.0	0.5427
APC	CD15	122.0	91.0–283.5	122.5	80.0–162.5	0.6065
	CD36	241.5	194.0–388.5	200.5	145.5–267.3	0.2417
	CD271	208.0	127.0–296.5	170.0	127.5–233.3	0.6065
	CD338	200.5	106.5–373.0	107.5	101.8–146.8	0.1223
	CD19	192.0	154.0–241.3	144.0	120.3–182.2	0.1012
	CD28	91.0	5.2–228.5	85.5	0–122.0	0.1722
	CD33	147.5	10.0–189.5	105.5	90.0–132.3	0.6734
	CD34	186.5	105.0–241.5	133.0	17.5–206.0	0.4250
	NC	169.0	99.5–244.8	92.0	64.0–204.0	0.2061
Per Cp	CD45	215.5	133.8–251.3	167.0	146.0–208.0	0.6734
	NC	305.0	252.0–483.3	288.5	261.3–348.8	0.7431
Expressed antigens						
FITC	CD9	3,538.0	2,172.0–6,871.0	2,156.0	1,743.0–3,495.0	0.2417
	CD26	1,287.0	651.8–3,235.0	1,308.0	742.3–1,920.0	0.9626
	CD47	1,339.0	980.3–2,312.0	1,287.0	1,106.0–1,344.0	0.4824
	CD49d	1,185.0	946.8–1,393.0	941.0	708.3–1,140.0	0.2061
	CD71	1,271.0	796.5–2,147.0	1,093.0	897.0–1,538.0	0.7431
	CD90	37,140.0	22,740.0–52,690.0	36,210.0	21,640.0–50,260.0	0.8149
	CD324	517.0	463.0–551.0	436.0	375.0–545.0	0.3027
	HLA-ABC	9,363.0	4,033.0–14,180.0	5,424.0	3,987.0–6,539.0	0.1223
	NC	325.0	250.0–516.3	279.0	218.8–418.8	0.4260
PE	CD13	9,802.0	6,786.0–17,130.0	3,950.0	3,634.0–4,961.0	0.0043[a]
	CD56	496.0	293.8–711.0	528.0	151.0–1,048.0	0.9626
	CD58	2,432.0	1,723.0–2,792.0	2,009.0	1,798.0–2,459.0	0.5427
	CD99	405.0	296.5–586.3	467.5	360.5–651.0	0.3736
	CD105	652.0	507.0–1,329.0	790.0	746.0–847.8	0.6734
	CD151	16,010.0	10,970.0–21,430.0	19,410.0	11,090.0–23,690.0	0.4260
	CD166	5,215.0	3,551.0–7,382.0	4,634.0	3,962.0–5,608.0	0.6734
	CD200	722.5	205.8–1,699.0	1,137.0	631.5–1,444.0	0.3736
	NC	115.5	91.7–181.5	102.5	93.2–135.0	0.5427
APC	CD10	1,247.0	999.3–2,319.0	1,890.0	1,122.0–3,031.0	0.3736
	CD29	45,150.0	25,130.0–54,610.0	24,240.0	17,660.0–40,000.0	0.0832
	CD44	11,440.0	8,186.0–16,290.0	7,259.0	6,613.0–9,753.0	0.0678
	CD54	9,910.0	5,404.0–14,260.0	10,660.0	9,486.0–24,670.0	0.3736
	CD81	31,240.0	19,110.0–55,050.0	38,890.0	24,500.0–44,640.0	0.8149
	NC	169.0	99.5–244.8	92.0	64.0–204.0	0.2061

[a]Significant *P* value at the Mann–Whitney test.
hA-MSC, human amniotic mesenchymal stem cells; MFI, median fluorescence intensity.

by redissolving the Oil Red O present in stained cells in 98% isopropanol, and then determining absorbance at 550 nm.

RNA isolation

Total RNA was purified from hA-MSCs isolated from term placentas of Co- and of Ob-pregnant women using the mirVana™ miRNA isolation kit (Ambion) and its concentration was evaluated with the NanoDrop ND-1000 UV-Vis spectrophotometer (NanoDrop Technologies).

Quantitative real-time PCR of mRNAs

Real-time quantitative PCR (qRT-PCR) was carried out on the Applied Biosystems 7900HT Sequence Detection system (Applied Biosystems). cDNAs were synthesized from 2 μg of total RNA using hexamer random primers and M-MuLV Reverse Transcriptase (New England BioLabs). The PCR was performed in a 20 μL final volume containing cDNA, 1 × SYBR Green PCR mix, and 10 μM of each specific primer. Supplementary Table S2 lists the oligonucleotide primers used for PCR of selected genes: peroxisome proliferator-activated receptor gamma (PPARγ), CD13, protein homologous to myelin P2 (aP2), and glyceraldehyde-3-phosphate dehydrogenase (GAPDH). The PCR conditions for reverse transcription were stage 1: 50°C, 2 min; stage 2: 95°C, 10 min; stage 3: 95°C, 15 s; 60°C, 1 min/40 cycles; and stage 4: 95°C, 15 s; 60°C, 1 min. Levels of target genes were quantified using specific oligonucleotide primers and normalized for GAPDH expression.

Statistical analysis

The parameters investigated were expressed as mean and standard error of the mean (SEM) (parametric distributions) or as the median value and 25th and 75th percentiles (nonparametric distributions). The Student's *t* and Mann–Whitney tests were used to compare parametric and nonparametric data, respectively. *P* values < 0.05 were considered statistically significant. Correlation analysis was performed with the SPSS package for Windows (ver. 18; SPSS, Inc.).

Results

The clinical and biochemical characteristics of the mothers and their newborns are reported in Table 2 (A and B, respectively). Weight gain was lower ($P < 0.05$) and diastolic blood pressure was higher ($P < 0.05$) in Ob- than in Co-pregnant women. Both the leptin concentration ($P < 0.0001$) and the L/A ratio ($P < 0.0001$) were higher in Ob- than in Co-pregnant women at delivery. Biometric characteristics did not differ significantly between Ob- and Co-newborns.

Isolation of hA-MSCs

We isolated hA-MSCs from the mesenchymal layer of amniotic membranes obtained from our Ob- and Co-pregnant women at delivery. The fetal origin of all isolated hA-MSCs was confirmed by STR typing of DNA of the mother and of the hA-MSCs. Mycoplasma contamination of cultures was checked and excluded (data not shown). All isolated hA-MSCs were characterized by a high proliferation potential and collected after four population doublings. Morphologically, cultured Ob- and Co-hA-MSCs showed a similar fibroblastic-like morphology after four population doublings (Supplementary Fig. S1).

Immunophenotyping of h-MSCs

The antigenic mosaic displayed by Ob- and Co-hA-MSCs is shown in Table 3. Seventeen of the 38 antigens investigated were not expressed on the surface of hA-MSCs (hematopoietic antigens: CD14, CD15, CD16, CD19, CD28, CD33, CD34, CD45, and CD117; the endothelial marker PECAM-1/CD31; and no-lineage markers: thrombospondin receptor/CD36, Bp50/CD40, Prominin-1/CD133, MDR-1/CD243, NGFR/CD271, ABCG-2/CD338, and HLA-DR). Both Ob- and Co-hA-MSCs were positive for the following mesenchymal markers: CD9, CD10, CD13, CD26, CD29, CD44, CD47, CD49d, CD54, CD56, CD58, CD71, CD81, CD90, CD99, CD105, CD151, CD166, CD200, and HLA-ABC. A very weak positivity for the epithelial antigen E-cadherin/CD324 was

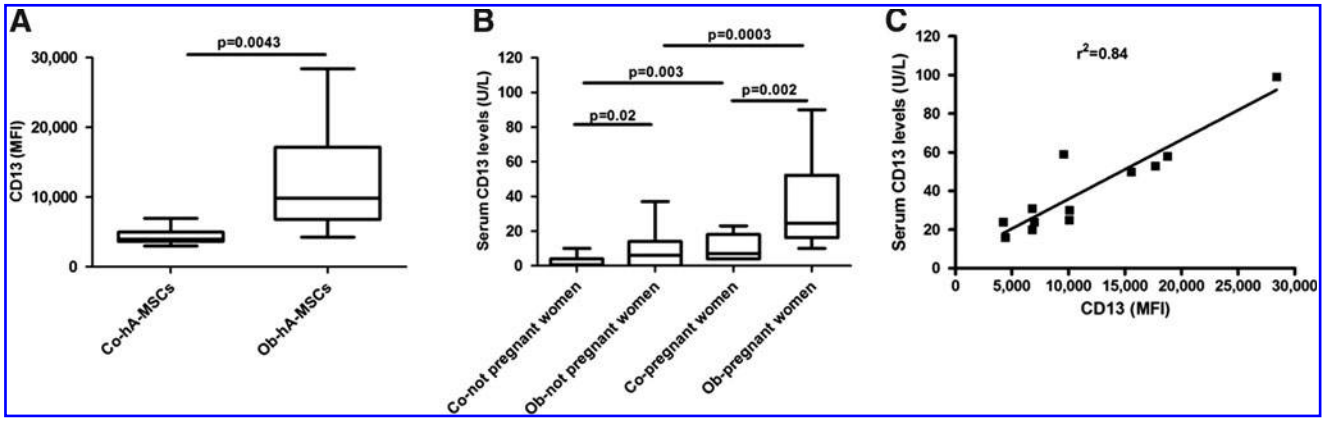

FIG. 1. Expression of CD13 antigen in control (Co-) and obese (Ob-) pregnant women. **(A)** Ob-Human amniotic mesenchymal stem cells (hA-MSCs) expressed significantly higher amounts (at Mann–Whitney test) of CD13 surface antigen compared with Co-hA-MSCs ($P < 0.005$); **(B)** serum levels of CD13 were significantly higher both in Ob- than in Co-not pregnant women ($P < 0.05$) and in Ob- than in Co-women at delivery ($P < 0.005$); **(C)** serum CD13 levels were correlated with CD13 surface expression levels in Ob-pregnant women ($r^2 = 0,84$; $P < 0.0001$). The box plots provide a vertical view of the data expressed as median, 25th percentile, 75th percentile, and extreme values.

also observed. Interestingly, CD13 expression was significantly higher in Ob-hA-MSCs than in Co-hA-MSCs, that is, MFI: 9,802.0 and 3,950.0, respectively ($P < 0.005$) (Table 3 and Fig. 1A). The immunophenotype characterization confirmed the mesenchymal origin and the higher CD13 expression in hVAT-MSCs and hUC-MSCs from Ob- than from Co-women (hVAT-MSCs - MFI: 8,200.0 vs. 1,100.0 and hUC-MSCs - MFI: 4,965.0 vs. 3,155.0, respectively).

APN/CD13 serum levels

We first measured baseline serum levels of CD13 in a small group of not pregnant obese and normal weight women and found significantly higher values in the obese subset (medians: 6.00 and 1.00 U/L, $P < 0.05$, respectively) (Fig. 1B). The serum levels of CD13 were also significantly higher in Ob- than in Co-pregnant women at delivery (medians: 24.00 and 7 U/L, $P < 0.005$, respectively), (Fig. 1B). CD13 levels were significantly higher in Ob- and Co-pregnant women than in not pregnant Ob- and Co-women: four ($P < 0.0005$) and seven times ($P < 0.005$), respectively. Furthermore, in Ob-pregnant women, serum CD13 levels were significantly correlated to the levels of CD13 on the surface of hA-MSCs ($r^2 = 0.84$; $P < 0.0001$) (Fig. 1C).

CD13 h-MSC expression and adipogenic differentiation

To investigate whether CD13 is involved in adipogenesis, we cultured Ob- and Co-hA-MSCs for 14 days in the adipogenic induction medium. At the end of incubation, the adipogenic potential, as measured by PPARγ and aP2 mRNA levels, was higher in Ob- than in Co-hA-MSCs. In fact, as shown in Fig. 2A and B, the mean RQs at day 14 were 0.04 and 0.02, respectively, for PPARγ ($P < 0.05$), and 0.02 and 0.01, respectively, for aP2 ($P < 0.05$). The same results were obtained with Oil Red staining; in fact, staining was more intense in Ob- than in Co-hA-MSCs at day 14 of differentiation [Abs (550 nm) = 0.6 and 0.4, $P < 0.05$, respectively] (Fig. 2C). During adipogenesis, CD13 mRNA levels remained higher in Ob- than in Co-hA-MSCs. CD13 silencing by shRNA in Ob-hA-MSCs resulted in a switch-off of CD13 mRNA expression, as evaluated by RT-PCR (Fig. 3A), and at the same time, the adipogenic potential of these cells did not differ from that observed in Co-hA-MSCs, as shown by similar PPARγ mRNA levels measured in silenced Ob-hA-MSCs and in Co-hA-MSCs ($P = 0.71$) (Fig. 3B). In agreement to CD13 involvement in adipogenesis, we overexpressed CD13 in Co-hA-MSCs (mRNA CD13 mean RQ = 7.23) and observed at day 4 of differentiation that PPARγ mRNA levels were higher in treated (mean RQ = 0.015) than in untreated (mean RQ = 0.001) Co-hA-MSCs. The adipogenic potential at day 14 was also higher in Ob- than in Co-hVAT-MSCs isolated from not pregnant women [aP2: RQs were 0.050 and 0.036; Oil Red O Abs (550 nm): 0.559 and 0.437, respectively].

Upregulation of CD13 h-MSC expression by IFN-γ

We next evaluated if CD13 expression could be upregulated in h-MSCs by IFN-γ as occurs in murine cellular models [32]. To this aim, we treated the Co- and Ob-hA-MSCs with 0.8 ng/mL or 12.5 ng/mL IFN-γ for 24 h. We found that CD13 expression was significantly higher on membranes of

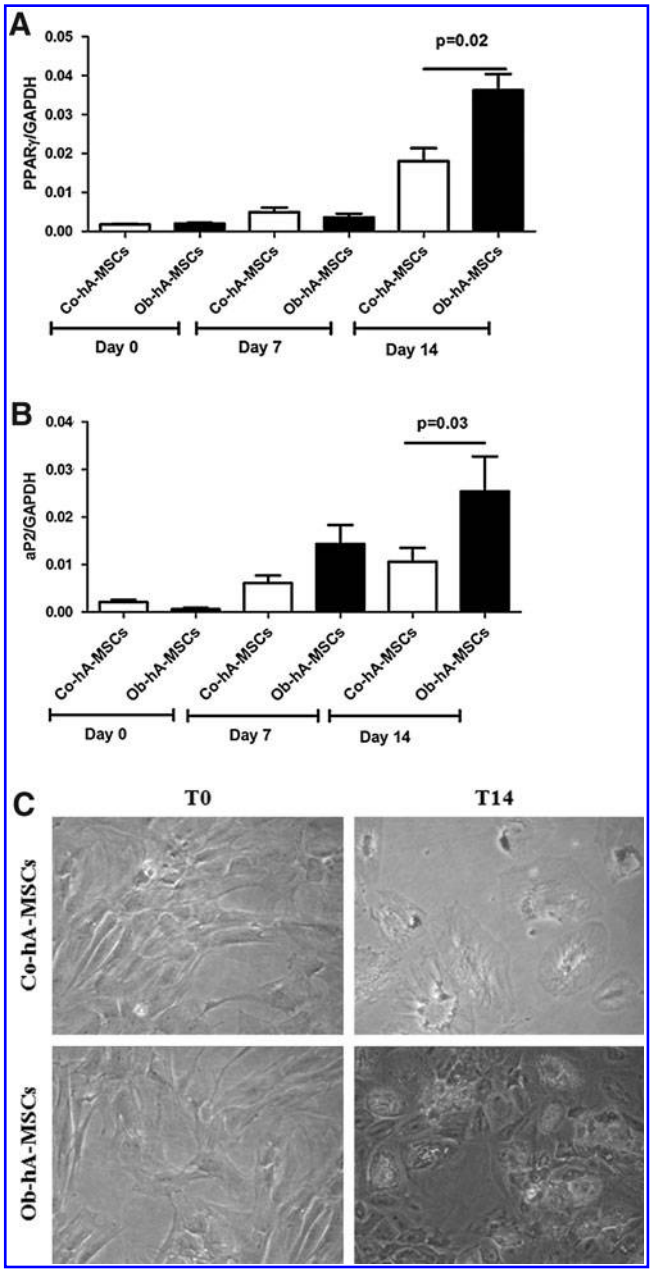

FIG. 2. Adipogenic potential in Ob-hA-MSCs and in Co-hA-MSCs. The statistically significant higher mRNA expression levels of PPARγ ($P < 0.05$) **(A)** and of aP2 ($P < 0.05$) **(B)** measured 14 days after the adipogenic induction, indicated increased adipogenesis in Ob- versus Co-hA-MSCs. **(C)** The higher adipogenesis in Ob- than in Co-hA-MSCs was also confirmed by Oil Red staining [Abs (550 nm) = 0.6 and 0.4, $P < 0.05$, respectively].

Co-hA-MSCs treated with 12.5 ng/mL IFN-γ ($P < 0.05$) than in untreated cells, whereas there was a slight, not significant, increase in treated Ob-hA-MSCs (Supplementary Fig. S2) versus the untreated counterpart cells. In addition, IFN-γ treatment (12.5 ng/mL at 37°C for 24 h) induced the increase of CD13 membrane expression in hVAT-MSCs (Ob- and Co-MSCs: 39% and 8%, respectively), and in Co-hUC-MSCs (4%) versus the untreated counterpart cells, but not in Ob-hUC-MSCs. Our results suggest that high levels of INF-γ drive

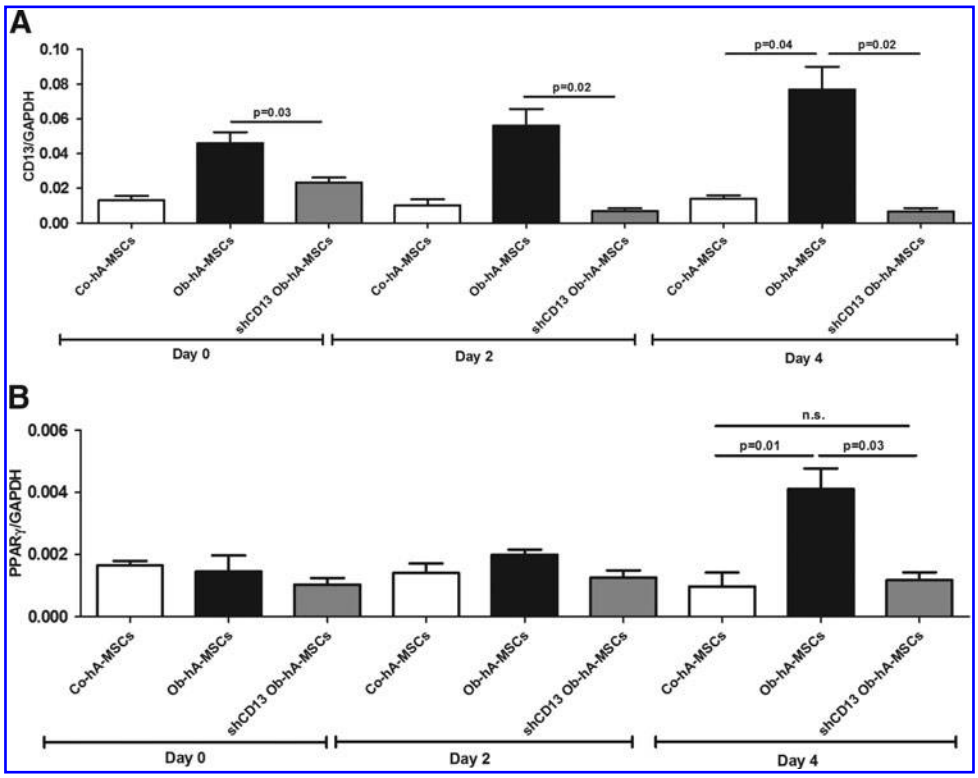

FIG. 3. Role of CD13 in adipogenesis. **(A)** mRNA expression levels of CD13 were significantly higher in Ob- than in Co-hA-MSCs at day 0 ($P < 0.05$), day 2 ($P < 0.05$), and day 4 ($P < 0.05$) when cultured with the adipogenic medium. CD13 mRNA expression was switched-off in Ob-hA-MSCs after CD13 silencing with shRNA. **(B)** At day 4 of adipogenic induction, PPARγ mRNA expression levels that were significantly higher in Ob-hA-MSCs than in Co-hA-MSCs ($P < 0.02$), decreased to the levels detected in Co-hA-MSCs after CD13 silencing ($P = 0.71$), which indicates that CD13 enhances adipogenesis in hA-MSCs. n.s.: not statistically significant difference.

the upregulation of CD13 expression in Co-h-MSCs, irrespective of their source and of pregnancy, whereas its effect on Ob-h-MSC CD13 expression during obesity is ambiguous.

Discussion

Human amniotic membrane is a readily available source of abundant fetal MSCs that are free from ethical concerns [33]. hA-MSCs isolated from normal weight healthy women at delivery have been characterized [24,34,35], but, to our knowledge, the features of hA-MSCs from obese women are largely unknown. In this study, we used flow cytometry to characterize hA-MSCs isolated at delivery from two groups of women: prepregnancy normal weight and prepregnancy severely obese women. The immunophenotypic characterization confirmed the mesenchymal origin of the isolated cells [36]. In particular, the distribution of CD56 was in agreement with the placental origin of the isolated hA-MSCs. In fact, this marker is absent from bone marrow [34] and from adipose tissue-derived mesenchymal stem cells [37]. Similarly, the endothelial marker PECAM-1/CD31, and the hematopoietic antigens CD14, CD15, CD16, CD19, CD28, CD33, CD34, CD45, and CD117 were absent from isolated Ob- and Co-hA-MSCs. Staining for the E-cadherin/CD324 epithelial antigen was very weak in our Ob- and Co-hA-MSC preparations; the coexpression of epithelial, although at a low intensity, and mesenchymal markers on our hA-MSCs was in agreement with previous findings [38,39]. Overall, our results are similar to those reported by Parolini et al. [24] and/or Roubelakis [35] regarding the expressed (CD49d, CD90, HLA-ABC, CD13, CD56, CD105, CD166, CD10, CD29, CD44, and CD54) and not expressed (PECAM-1/CD31, HLA-DR, CD14, Prominin-1/CD133, NGFR/CD271, CD34, and CD45) membrane-bound antigens in hA-MSCs. We found that the Ob-hA-MSC immunophenotype is characterized by a significantly higher expression of the APN/CD13 antigen with respect to the Co-hA-MSC phenotype. Besides amnion, CD13 was overexpressed in h-MSCs isolated from the umbilical cord in obese women and in those isolated from VAT in not pregnant obese women.

Type II metalloprotease APN/CD13 (EC. 3.4.11.2) is a heavily glycosylated membrane-bound protein (~960aa, ~150 kDa) that is encoded by the human ANPEP gene located on chromosome 15 (q25-q26) [40]. This protein exists also in a soluble form. APN/CD13 is a ubiquitous enzyme present in a wide variety of human organs, tissues, and cell types, including the placenta, human umbilical vein endothelial cells, monocytes, lymphocytes T, hypothalamus, and epithelial intestinal cells [41]. It has various mechanisms of action: enzymatic cleavage of peptides, endocytosis, and signal transduction [42]. APN/CD13 is involved in inflammation, cellular differentiation and proliferation, apoptosis, cell adhesion, and motility [42]. Dysregulated expression of membrane and/or soluble forms of APN/CD13 has been observed in many diseases [43], but until now, it has never been associated with obesity. Here we provide the first demonstration that the CD13 antigen is increased on hA-MSCs during obesity and could play a role in adipogenesis. In fact, we first detected a higher adipogenic potential in Ob- than in Co-hA-MSCs after 14 days of adipogenic differentiation, and then observed that the adipogenic potential of Ob-hA-MSCs was comparable to that of Co-hA-MSCs after CD13 silencing. Conversely, the adipogenic potential increased in Co-hA-MSCs after CD13 overexpression. Furthermore, we provide evidence that INFγ upregulated CD13 expression in Co-hA-MSCs.

Intriguingly, in Ob-pregnant women, APN/CD13 serum levels at delivery were higher than in Co-pregnant women and correlated with CD13 surface Ob-hA-MSC expression ($r^2 = 0.84$, $P < 0.0001$), which support the hypothesis that the placenta is the major source of the high CD13 levels measured in maternal serum [44]. We also found that the leptin concentration and the L/A ratio were increased in Ob-maternal serum at delivery. This finding confirms the concept that these two parameters are obesity risk markers [45,46].

In conclusion, this characterization of Ob-hA-MSCs shows that antigen CD13, by influencing the adipogenic potential of these cells, could be an in utero risk factor for obesity. Our data strengthen the hypothesis that high serum CD13 and mesenchymal stem cell CD13 are markers of obesity.

Acknowledgments

The present work was supported by grants from CEINGE Regione Campania (DGRC 1901/2009) and by MIUR-PRIN 2008. We thank Jean Ann Gilder (Scientific Communication srl, Naples, Italy) for revising and editing the manuscript.

Author Disclosure Statement

The authors declare no financial conflict of interests.

References

1. Guelinckx I, Devlieger R, Beckers K and Vansant G. (2008). Maternal obesity: pregnancy complications, gestational weight gain and nutrition. Obes Rev 9:140–150.
2. Heslehurst N, Ells LJ, Simpson H, Batterham A, Wilkinson J and Summerbell CD. (2007). Trends in maternal obesity incidence rates, demographic predictors, and health inequalities in 36,821 women over a 15-year period. BJOG 114: 187–194.
3. Kim SY, Dietz PM, England L, Morrow B and Callaghan WM. (2007). Trends in pre-pregnancy obesity in nine states, 1993–2003. Obesity (Silver Spring) 15:986–993.
4. Pipe NG, Smith T, Halliday D, Edmonds CJ, Williams C and Coltart TM. (1979). Changes in fat, fat-free mass and body water in human normal pregnancy. Br J Obstet Gynaecol 86:929–940.
5. Ehrenberg HM, Huston-Presley L and Catalano PM. (2003). The influence of obesity and gestational diabetes mellitus on accretion and the distribution of adipose tissue in pregnancy. Am J Obstet Gynecol 189:944–948.
6. Capobianco V, Nardelli C, Ferrigno M, Iaffaldano L, Pilone V, Forestieri P, Zambrano N and Sacchetti L. (2012). miRNA and protein expression profiles of visceral adipose tissue reveal miR-141/YWHAG and miR-520e/RAB11A as two potential miRNA/protein target pairs associated with severe obesity. J Proteome Res 11:3358–3369.
7. Drolet R, Richard C, Sniderman AD, Mailloux J, Fortier M, Huot C, Rhéaume C and Tchernof A. (2008). Hypertrophy and hyperplasia of abdominal adipose tissues in women. Int J Obes (Lond) 32:283–291.
8. Bartha JL, Marín-Segura P, González-González NL, Wagner F, Aguilar-Diosdado M and Hervias-Vivancos B. (2007). Ultrasound evaluation of visceral fat and metabolic risk factors during early pregnancy. Obesity (Silver Spring) 15:2233–2239.
9. Harvey NC, Poole JR, Javaid MK, Dennison EM, Robinson S, Inskip HM, Godfrey KM, Cooper C and Sayer AA; SWS Study Group. (2007). Parental determinants of neonatal body composition. J Clin Endocrinol Metab 92:523–526.
10. Chu SY, Callaghan WM, Kim SY, Schmid CH, Lau J, England LJ and Dietz PM. (2007). Maternal obesity and risk of gestational diabetes mellitus. Diabetes Care 30:2070–2076.
11. O'Brien TE, Ray JG and Chan WS. (2003). Maternal body mass index and the risk of preeclampsia: a systematic overview. Epidemiology 14:368–374.
12. Metwally M, Ong KJ, Ledger WL and Li TC. (2008). Does high body mass index increase the risk of miscarriage after spontaneous and assisted conception? A meta-analysis of the evidence. Fertil Steril 90:714–726.
13. Sattar N, Clark P, Holmes A, Lean ME, Walker I and Greer IA. (2001). Antenatal waist circumference and hypertension risk. Obstet Gynecol 97:268–271.
14. Li C, Kaur H, Choi WS, Huang TT, Lee RE and Ahluwalia JS. (2005). Additive interactions of maternal prepregnancy BMI and breast-feeding on childhood overweight. Obes Res 13:362–371.
15. Fowden AL and Forhead AJ. (2004). Endocrine mechanisms of intrauterine programming. Reproduction 127:515–526.
16. Fowden AL, Forhead AJ, Coan PM and Burton GJ. (2008). The placenta and intrauterine programming. J Neuroendocrinol 20:439–450.
17. Okawa H, Okuda O, Arai H, Sakuragawa N and Sato K. (2001). Amniotic epithelial cells transform into neuron-like cells in the ischemic brain. Neuroreport 12:4003–4007.
18. Zeigler BM, Sugiyama D, Chen M, Guo Y, Downs KM and Speck NA. (2006). The allantois and chorion, when isolated before circulation or chorio-allantoic fusion, have hematopoietic potential. Development 133:4183–4192.
19. Fukuchi Y, Nakajima H, Sugiyama D, Hirose I, Kitamura T and Tsuji K. (2004). Human placenta-derived cells have mesenchymal stem/progenitor cell potential. Stem Cells 22:649–658.
20. Pittenger MF, Mackay AM, Beck SC, Jaiswal RK, Douglas R, Mosca JD, Moorman MA, Simonetti DW, Craig S and Marshak DR. (1999). Multilineage potential of adult human mesenchymal stem cells. Science 284:143–147.
21. In 't Anker PS, Scherjon SA, Kleijburg-van der Keur C, de Groot-Swings GM, Claas FH, Fibbe WE and Kanhai HH. (2004). Isolation of mesenchymal stem cells of fetal or maternal origin from human placenta. Stem Cells 22:1338–1345.
22. Katz AJ, Tholpady A, Tholpady SS, Shang H and Ogle RC. (2005). Cell surface and transcriptional characterization of human adipose-derived adherent stromal (hADAS) cells. Stem Cells 23:412–423.
23. Hwang JH, Lee MJ, Seok OS, Paek YC, Cho GJ, Seol HJ, Lee JK and Oh MJ. (2010). Cytokine expression in placenta-derived mesenchymal stem cells in patients with pre-eclampsia and normal pregnancies. Cytokine 49:95–101.
24. Parolini O, Alviano F, Bagnara GP, Bilic G, Bühring HJ, Evangelista M, Hennerbichler S, Liu B, Magatti M, et al. (2008). Concise review: isolation and characterization of cells from human term placenta: outcome of the first international Workshop on Placenta Derived Stem Cells. Stem Cells 26:300–311.
25. Grant A, Palzer S, Hartnett C, Bailey T, Tsang M and Kalyuzhny AE. (2005). A cell-detachment solution can reduce background staining in the ELISPOT assay. Methods Mol Biol 302:87–94.
26. Mariotti E, Mirabelli P, Di Noto R, Fortunato G and Salvatore F. (2008). Rapid detection of mycoplasma in continuous cell lines using a selective biochemical test. Leuk Res 32:323–326.

27. Bieback K, Kern S, Klüter H and Eichler H. (2004). Critical parameters for the isolation of mesenchymal stem cells from umbilical cord blood. Stem Cells 22:625–634.
28. Schäffler A and Büchler C. (2007). Concise review: adipose tissue-derived stromal cells—basic and clinical implications for novel cell-based therapies. Stem Cells 25:818–827.
29. Perfetto SP, Ambrozak D, Nguyen R, Chattopadhyay P and Roederer M. (2006). Quality assurance for polychromatic flow cytometry. Nat Protocols 1:1522–1530.
30. Lamoreaux L, Roederer M and Koup R. (2006). Intracellular cytokine optimization and standard operating procedure. Nat Protocols 1:1507–1516.
31. Maeker HT and Trotter J. (2006). Flow cytometry controls, instrument setup, and the determination of positivity. Cytometry Part A 69A:1037–1042.
32. Gabrilovac J, Cupić B, Zivković E, Horvat L and Majhen D. (2011). Expression, regulation and functional activities of aminopeptidase N (EC 3.4.11.2; APN; CD13) on murine macrophage J774 cell line. Immunobiology 216:132–144.
33. Miki T, Lehmann T, Cai H, Stolz DB and Stromk SC. (2005). Stem cell characteristics of amniotic epithelial cells. Stem Cells 23:1549–1559.
34. Mariotti E, Mirabelli P, Abate G, Schiattarella M, Martinelli P, Fortunato G, Di Noto R and Del Vecchio L. (2008). Comparative characteristics of mesenchymal stem cells from human bone marrow and placenta: CD10, CD49d, and CD56 make a difference. Stem Cells Dev 17:1039–1041.
35. Roubelakis MG, Trohatou O and Anagnou NP. (2012) Amniotic fluid and amniotic membrane stem cells: marker discovery. Stem Cells Int 2012:107836.
36. Delorme B, Ringe J, Gallay N, Le Vern Y, Kerboeuf D, Jorgensen C, Rosset P, Sensebé L, Layrolle P, Häupl T and Charbord P. (2008). Specific plasma membrane protein phenotype of culture-amplified and native human bone marrow mesenchymal stem cells. Blood 111:2631–2635.
37. Gronthos S, Franklin DM, Leddy HA, Robey PG, Storms RW and Gimble JM. (2001). Surface protein characterization of human adipose tissue-derived stromal cells. J Cell Physiol 189:54–63.
38. Sakuragawa N, Kakinuma K, Kikuchi A, Okano H, Uchida S, Kamo I, Kobayashi M and Yokoyama Y. (2004). Human amnion mesenchyme cells express phenotypes of neuroglial progenitor cells. J Neurosci Res 78:208–214.
39. Soncini M, Vertua E, Gibelli L, Zorzi F, Denegri M, Albertini A, Wengler GS and Parolini O. (2007). Isolation and characterization of mesenchymal cells from human fetal membranes. J Tissue Eng Regen Med 1:296–305.
40. Watt VM and Willard HF. (1990). The human aminopeptidase N gene: isolation, chromosome localization, and DNA polymorphism analysis. Hum Genet 85:651–654.
41. Lai A, Ghaffari A and Ghahary A. (2010). Inhibitory effect of anti-aminopeptidase N/CD13 antibodies on fibroblast migration. Mol Cell Biochem 343:191–199.
42. Mina-Osorio P. (2008). The moonlighting enzyme CD13: old and new functions to target. Trends Mol Med 14:361–371.
43. Luan Y and Xu W. (2007). The structure and main functions of aminopeptidase N. Curr Med Chem 14:639–647.
44. Kawai M, Araragi K, Shimizu Y and Hara Y. (2009). Identification of placental leucine aminopeptidase and triton-slowed aminopeptidase N in serum of pregnant women. Clin Chim Acta 400:37–41.
45. Labruna G, Pasanisi F, Nardelli C, Tarantino G, Vitale DF, Bracale R, Finelli C, Genua MP, Contaldo F and Sacchetti L. (2009). UCP1-3826 AG+GG genotypes, adiponectin, and leptin/adiponectin ratio in severe obesity. J Endocrinol Invest 32:525–529.
46. Labruna G, Pasanisi F, Nardelli C, Caso R, Vitale DF, Contaldo F and Sacchetti L. (2011). High leptin/adiponectin ratio and serum triglycerides are associated with an "at-risk" phenotype in young severely obese patients. Obesity (Silver Spring) 19:1492–1496.

Address correspondence to:
Dr. Lucia Sacchetti
CEINGE-Biotecnologie Avanzate S.C.a R.L.
Via G. Salvatore
Naples 486-80145
Italy

E-mail: sacchett@unina.it

Received for publication September 12, 2012
Accepted after revision March 12, 2013
Prepublished on Liebert Instant Online March 14, 2013

This article has been cited by:

1. Carmela Nardelli, Giuseppe Labruna, Rosario Liguori, Cristina Mazzaccara, Maddalena Ferrigno, Valentina Capobianco, Massimo Pezzuti, Giuseppe Castaldo, Eduardo Farinaro, Franco Contaldo, Pasqualina Buono, Lucia Sacchetti, Fabrizio Pasanisi. 2013. Haplogroup T Is an Obesity Risk Factor: Mitochondrial DNA Haplotyping in a Morbid Obese Population from Southern Italy. *BioMed Research International* **2013**, 1-5. [CrossRef]